MUSCLE STEM CELLS REGULATE THE BIOENERGETIC FUNCTION OF MYOFIBERS IN MITOCHONDRIAL MYOPATHIES

A Dissertation
Presented to
The Academic Faculty

by

Mahir Mohiuddin

In Partial Fulfillment
of the Requirements for the Degree
Doctor of Philosophy in the
Wallace H. Coulter Department of Biomedical Engineering

Georgia Institute of Technology & Emory University
August 2021

MUSCLE STEM CELLS REGULATE THE BIOENERGETIC FUNCTION OF MYOFIBERS IN MITOCHONDRIAL MYOPATHIES

Approved by:

Dr. Young C. Jang, PhD, Advisor
School of Biological Sciences
Georgia Institute of Technology

Dr. Luke P. Brewster, MD, PhD
Department of Surgery
Emory University

Dr. Nick J. Willett, PhD
Department of Orthopedics
Emory University

Dr. Carlos A. Aguilar, PhD
Department of Biomedical Engineering
University of Michigan

Dr. Hee Cheol Cho, PhD
Department of Biomedical Engineering
Georgia Institute of Technology & Emory University

Date Approved: June 24, 2021

To my father, for inspiring me to discover my potential.

ACKNOWLEDGEMENTS

A PhD is more than just a degree; it's a conduit of professional and personal growth that allow you to discover what you're capable of as a researcher, a colleague, and a friend. I have been blessed to be surrounded by so many impactful people who have facilitated my growth, and I could not reach my potential without them.

First and foremost, I would like to express gratitude toward my dad, whose life story has been my underlying inspiration to be the best person I can be. Dad, in every stage of your life, you aspired to not only make yourself stand out, but the people around you too. You told me to "make everyone else's lives easier" to become stronger as a group, and I've carried that philosophy with me to this day. I've also noticed the many skills you acquired during your PhD, and that drove me to get my own. Even on the days I struggled with my doctoral work, you reminded me that one day I will look back and appreciate how much I've grown throughout my PhD. As I inch closer to the finish line, I can say you were right, and I cannot thank you enough for giving me the motivation to push forward whenever I needed it. I also want to thank the rest of my family for standing by my side through this journey. Mom, I could not be here without you. You've shown me how to have fun and make time for the things I enjoy. It's important to set aside time to develop relationships and personal skills that I was able to apply to my work, so thank you for providing those lessons. Samer and Maymun, I've always been able to count on you to share and discuss our similar interests and show me that I'm never alone in them. You have also both taught me how to become a leader, and for that I am eternally grateful.

I also could not have completed my PhD without the guidance and expertise of my advisor, Young Jang. Young, I want to especially thank you for pushing me to be my best self and rekindling my flame whenever I started to fall behind. You regularly reminded me that we are in this together and you won't let me fail, and I am grateful for your support every step of the way. You have showed me what it means to be a hard worker and a team player, and those skills are critical for a doctoral thesis project. Although you have claimed that I am always confident about my experiments, my confidence stems from your mentorship, knowing that I will always have you to help me troubleshoot and determine the next best step with your expertise.

Next, I wish to express gratitude to my labmates in the Jang lab that have assisted me in my project. Shannon, I cannot express how grateful I am for having you by my side at the start, finish, and every stage in between. With the deep knowledge we have about each other's projects, bouncing various ideas off of each other has been incredibly valuable to getting me to where I am today. Woojin, I've always looked up to you as a secondary mentor and I have modeled so much of my approach towards the completion of my project after you. Jeongmoon, we have been through the thick and thin of our projects together, spending late nights together in lab, and helping each other out in every way possible. Particularly, I wish to express my deepest gratitude for the countless times you've brought me snacks and given me the energy to finish my day. I would also like to pay special regards to our "lab mom," Eunjung, who created the foundation of the Jang lab and taught us so many essential skills to get our projects off the ground. Berna, thank you for giving me the opportunity to learn how to be a mentor and putting in the time and effort to facilitate this project. It has been incredibly rewarding to watch you grow and develop as your own

independent researcher over the years. Gunjae, your creativity has not gone unnoticed, and I want to thank you for coming up with so many clever solutions to so many research questions and technical issues. Nanhee, I want to express gratitude for not only providing us with a laugh whenever we needed it, but also your valiant effort in maintaining the Jang lab and our mouse colony. Finally, I want to thank our lab members Mira, Utku, Melody, and Henry for all your support these last few years.

I am also indebted to my thesis committee members, whose expert perspectives have generously contributed to this work. Carlos Aguilar, I could not have asked for a better "sister lab" due to your strong understanding of genetic regulation of muscle stem cells. Thank you for showing me a great time and teaching me so much each time I visited University of Michigan. Nick Willett, your expertise in musculoskeletal injuries has proved invaluable to my project and I am grateful to hear your opinions about not only my, but also other trainees' projects in our Muscle Group Meetings. Luke Brewster, I am grateful for your deep clinical knowledge in peripheral artery disease, providing me with a thorough understanding of patients' needs and limitations, how to address these limitations from a therapeutic outlook, and thoughtfully correcting me when I'm wrong about the various manifestations of PAD. Hee Cheol Cho, thank you for your expertise in stem/progenitor cells, your passionate view of my project, and for asking insightful questions that allowed me to reflect on stem cell physiology.

Furthermore, I would like to thank those who I have developed personal relationships with over the years for your motivation and support through my graduate school career. First, I wish to express my deepest gratitude to my girlfriend, Megan, who has seen me at my best and at my worst, yet still sticks with me through it all. Thank you

for letting me practice my presentations on you and coming up with insights from an outside perspective. I am grateful for all of the times you let me lecture you on how fascinating muscle stem cells and mitochondria can be, but also for providing a distraction whenever I needed one. Next, I want to acknowledge my closest undergraduate group of friends, which we termed “The Swamp,” for helping me develop both my interpersonal skills and engineering skills. Luke, Brandyn, Lurski, Avi, Tyler, Johnny, Sean H, Sean K, Mac, Dan, Carlos, Weingarten, Adam, and Drew, you have all been a crucial part of my support system and played an essential role in making me who I am today. I also want to thank the friends I made in Atlanta. Ben, Andy, Mary, and Steph, thank you for all of the game nights, pool times, or countless hours watching TV together to unwind after a long day, but also providing inspiration in each other’s doctoral projects. My other graduate student friends, including Meghan, Gilad, Joe, Gio, and Casey, also deserve credit for supporting me through my PhD, but I am also grateful for all of the connections I have made during my time here.

Of course, I also need to thank the Biomedical Engineering department at Georgia Institute of Technology and Emory University for giving me the opportunity to pursue my dreams and supporting such a captivating project. The academics, research opportunities, and collaborative nature of the program brings out the best in all of the trainees. The department also provided countless social gatherings to engender collaborations and develop connections with our peers. Specifically, special thanks to Kyla Ross and Ella Chamis, who provided unparalleled guidance to graduate students in various aspects of our academic and personal lives. Moreover, I want to thank the Physiological Research Laboratory (PRL) staff, particularly Dr. Richard Noel, Dr. Laura O’Farrell, Ogeda, Altair,

Andrea, and Josh for ensuring our animals received the absolute best care. Dr. Richard Noel and Dr. Laura O'Farrell, thank you for your thoughtful advice regarding surgical models and post-operative care. Additionally, I want to express gratitude to Richard and Ogeda for your regular conversations with me about professional and personal plans, which helped me refine my own research and career paths.

Finally, I owe the city of Atlanta my appreciation for not just providing a home, but really making it feel like a home. The city encompasses so many bright individuals and never fails to maintain a common ground to meet these individuals. Thank you, Atlanta, for encompassing so many reputable universities and never running out of activities to pursue or places to explore.

TABLE OF CONTENTS

LIST OF FIGURES

LIST OF SYMBOLS AND ABBREVIATIONS

ACh	Acetylcholine
AChR	Acetylcholine Receptor
ADP	Adenosine Diphosphate
AMPK	Adenosine Monophosphate-Activated Protein Kinase
ANOVA	Analysis of Variance
aPKC	Atypical Protein Kinase C
ApoE	Apolipoprotein E
ATP	Adenosine Triphosphate
BAK	BCL2-Antagonist/Killer 1
BAX	BCL2-Associated X
BCA	Bicinchoninic Acid Assay
BDNF	Brain-Derived Neurotrophic Factor
bFGF	Basic Fibroblast Growth Factor
Ca^{2+}	Calcium Ion
CCCP	Carbonyl Cyanide 3-Chlorophenylhydrazone
ChR2	Channelrhodopsin-2
CLI	Critical Limb Ischemia
COX	Cytochrome C Oxidase
DAPI	4′,6-diamidino-2-phenylindole
DBS	Donor Bovine Serum
dKO	Double Knockout
DMD	Duchenne Muscular Dystrophy
DMEM	Dulbecco's Modified Eagle Medium
DMSO	Dimethyl Sulfoxide
Drp1	Dynamin-Related Protein 1
DTA	Diphtheria Toxin A
ECAR	Extracellular Acidification Rate
ECM	Extracellular Matrix
EDL	Extensor Digitorum Longus
EGTA	Ethylene Glycol-bis(β-aminoethyl ether)-N,N,N',N'-tetraacetic acid
eMHC	Embryonic Myosin Heavy Chain
ETC	Electron Transport Chain
FACS	Fluorescence Activated Cell Sorting
FBS	Fetal Bovine Serum
FGF	Fibroblast Growth Factor
FGF21	Fibroblast Growth Factor 21
Fis1	Mitochondrial Fission 1

FMO	Fluorescence Minus One
FoxO	Forkhead Box O
FOXO3	Forkhead Box O3
G	Glutamate
GFP	Green Fluorescent Protein
GM	Glutamate + Malate
GPS2	G-protein Pathway Suppressor 2
H&E	Hematoxylin and Eosin
H+ND	Hypoxia plus Nutrient Deprivation
H_2O_2	Hydrogen Peroxide
HBSS	Hank's Balanced Salt Solution
HGF	Hepatocyte Growth Factor
HIF-1	Hypoxia-Inducible Factor 1
HLI	Hindlimb Ischemia
IACUC	International Animal Care and Use Committee
IGF-1	Insulin-like Growth Factor 1
IHC	Immunohistochemistry
IL-6	Interleukin-6
iPSC	Induced Pluripotent Stem Cells
LDPI	Laser Doppler Perfusion Imaging
M	Malate
MAPK	Mitogen-Activated Protein Kinase
MARK2	Microtubule Affinity-Regulating Kinase 2
Mfn1	Mitofusin 1
Mfn2	Mitofusin 2
MHC	Myosin Heavy Chain
MOTS-c	Mitochondrial ORF of the 12S rRNA Type-C
mtDNA	Mitochondrial DNA
mTORC1	Mechanistic Target of Rapamycin Complex 1
MuSC	Muscle Stem Cell
Myf5	Myogenic Factor 5
MyoD	Myoblast Determination Protein 1
MyoG	Myogenin
NMJ	Neuromuscular Junction
O_2	Dioxygen
OCR	Oxygen Consumption Rate
Opa1	Optic Atrophy 1
PAD	Peripheral Artery Disease
Pax7	Paired box protein 7
PBS	Phosphate Buffered Saline
PDGF	Platelet-Derived Growth Factor

PEG	Poly(Ethylene Glycol)
PEGDA	Poly(Ethylene Glycol) Diacrylate
PGC-1α	Peroxisome Proliferator-Activated Receptor Gamma Coactivator 1α
Phb	Prohibitin
PINK1	PTEN-Induced Kinase 1
PLAGA	Poly(Lactic-Co-Glycolic Acid)
PPARα	Peroxisome Proliferator-Activated Receptor α
PRL	Physiological Research Laboratory
PTP	Permeability Transition Pore
PV	Parvalbumin
qPCR	Quantitative Polymerase Chain Reaction
ROS	Reactive Oxygen Species
S	Succinate
SDH	Succinate Dehydrogenase
SIRT1	Sirtuin 1
SNT	Sciatic Nerve Transection
SOD	Superoxide Dismutate
SPADE	Spanning Tree Progression of Density Normalized Events
SRSF1	Serine/Arginine-Rich Splicing Factor 1
TA	Tibialis Anterior
TCA	Tricarboxylic Acid
TGFβ	Transforming Growth Factor β
TNFα	Tumor Necrosis Factor α
VEGF	Vascular Endothelial Growth Factor
WT	Wildtype
YFP	Yellow Fluorescent Protein
α-BTX	α-bungarotoxin

SUMMARY

Skeletal muscle tissue exhibits a high degree of plasticity due to their muscle stem cells, which are indispensable for muscle fiber repair, and the unique architecture of their mitochondria, which provide the energy for muscle fiber function, maintenance, and regeneration. In response to injury, quiescent muscle stem cells (MuSCs) undergo myogenesis to activate, differentiate, and fuse into the muscle fiber as new myonuclei that regulate myofiber repair. To meet the high energy demands of muscle regeneration, MuSCs increase in mitochondrial content through the various phases of myogenesis. However, when muscle mitochondria become dysfunctional, such as in peripheral artery disease (PAD) and Duchenne muscular dystrophy (DMD), MuSCs are debilitated and myofiber mitochondria remain defective, resulting in mitochondrial myopathy. Despite the characterization of mitochondrial dysfunction in these two disease models, the relationship between MuSC mitochondria and the bioenergetic function of the myofiber has not been investigated. To address this, the overarching objective of this thesis was to explore the role of MuSCs in remodeling the mitochondrial network and function of the myofiber in mitochondrial myopathies. We first correlated the MuSC response with the stages of mitochondrial network remodeling following a murine hindlimb ischemia (HLI) model of PAD and discovered that MuSC-derived myonuclei drive mitochondrial biogenesis. As direct evidence of MuSC-mediated remodeling of mitochondria, we then revealed that mitochondrial dysfunction in the MuSC yields deficient bioenergetic function of the dystrophic myofiber, which can be rescued by transplantation of MuSCs with healthy mitochondria. We tested this further in ischemic muscle after aging, which exacerbated the

mitochondrial dysfunction, and again observed significant improvements in bioenergetic function following transplantation of healthy MuSCs. Overall, this thesis established that MuSC mitochondria play a consequential role on myofiber bioenergetic function, identified a source of mitochondrial dysfunction in dystrophic muscle, developed a model of age-associated PAD, and provided a conceptual framework for MuSC transplantation as a therapeutic approach for mitochondrial myopathies.

CHAPTER 1. INTRODUCTION

1.1 Motivation

Skeletal muscle is one of the largest organs in the body and exhibits a high degree of plasticity that allows it to adapt to various stressors, diseases, or injuries. This plasticity arises from the shared volume of various niche components within the skeletal muscle that provides robust cell-cell signaling and modulation of the tissue. The crosstalk between myofibers, muscle stem cells that repair damaged myofibers, motor neurons that innervate myofibers, and the vasculature that provides oxygen and nutrients for myofiber function is critical to skeletal muscle homeostasis. Moreover, the mitochondria within these niche components, particularly within the myofiber, present a unique, striated morphology different than any other cell type and are vital for providing the energy required to maintain skeletal muscle functions and regeneration upon injury. However, in some disease models where the mitochondria are debilitated, the organized network of myofiber mitochondria becomes disordered, crosstalk between the skeletal muscle niche components is disrupted, and myofiber regeneration is significantly debilitated, underscoring the importance of skeletal muscle mitochondria. Although the accumulation of mitochondrial dysfunction in injury or disease has been shown to impair skeletal muscle regeneration, herein referred to as mitochondrial myopathy, the role of muscle stem cell mitochondria on myofiber regeneration has not been thoroughly studied. In fact, in two common mitochondrial myopathies, peripheral artery disease (PAD) where there is an occlusion of a blood vessel in the extremities resulting in ischemia-induced myofiber atrophy and Duchenne muscular dystrophy (DMD) where a mutation in the dystrophin gene destabilizes the myofiber

membrane to invoke myofiber degeneration, several niche components of the muscle are also impaired. Though there is currently no cure for either of these disease models, their muscle stem cells and mitochondria have recently been explored as therapeutic targets to enhance regeneration of the skeletal muscle tissues and restore the function of the mitochondria upon onset of the disease.

To this end, the overarching objective of this dissertation is to explore the role of muscle stem cells in remodeling the mitochondrial network and the function of mitochondrial myopathies. We hypothesized that in these mitochondrial myopathies, namely peripheral artery disease and Duchenne muscular dystrophy, muscle stem cells and muscle stem cell-derived myonuclei of the myofiber play critical roles in restoring the mitochondrial reticula and bioenergetic function of the pathological skeletal muscle. We tested this hypothesis through three different specific aims.

1.2 Specific Aims

Specific Aim 1: Correlate the temporal response of the muscle stem cell to remodeling of the mitochondrial network in ischemic myofibers. The primary objective of this aim was to identify the temporal muscle stem cell response to blood vessel occlusion and correlate it to remodeling of the myofiber's mitochondrial network. We hypothesized significant MuSC-mediated alterations to the myonuclear number, mitochondrial content, and bioenergetic function of the myofiber during muscle regeneration in a surgical hindlimb ischemia (HLI) model of PAD. To visualize recovery of the myofiber at various timepoints up to 56 days following ischemic injury, we quantified myonuclei in isolated single fibers

and used multiple transgenic reporter mice for MuSCs (*Pax7-tdTomato*) and mitochondria (*mitoDendra2*). Biochemical analyses, such as mtDNA copy number, and functional mitochondrial assays, such as ATP production, O_2 consumption rate, and H_2O_2 generation, were also performed to determine changes in mitochondrial content and bioenergetics. We also tested alterations to MuSC niche components of the skeletal muscle, such as the vasculature and neuromuscular junction. Revascularization following HLI was assessed through laser Doppler perfusion imaging and another transgenic reporter mouse model (*Thy1-YFP*) was utilized to characterize the reorganization of the motor neuron.

Specific Aim 2: Demonstrate that transplanted muscle stem cells remodel the mitochondria of dystrophic host skeletal muscle. The primary objectives of this aim were to assess the relationship between endogenous dystrophic muscle stem cell mitochondria and myofiber mitochondria, and to test whether muscle stem cell transplantation can enhance the bioenergetic function of the dystrophic myofiber. We hypothesized that dystrophic muscle stem cells, derived from the *mdx* mouse model of Duchenne muscular dystrophy, harbor defective mitochondria that propagate to the myofiber through myogenesis, but transplantation of muscle stem cells with healthy mitochondria to *mdx* muscle can improve the bioenergetic function of the dystrophic myofiber. We first performed extensive characterization of muscle stem cell mitochondrial content, gene expression, and function at various stages of myogenesis using FACS-purified muscle stem cells from *mdx*/*mitoDendra2* muscles. We then ectopically transplanted healthy muscle stem cells to visualize the mitochondrial network and quantify the bioenergetic function of engrafted dystrophic myofibers. To establish the causal relationship between transplanted muscle

stem cell mitochondria and bioenergetic function of the engrafted myofiber, we also transplanted muscle stem cells with dysfunctional mitochondria into *mdx* muscle as a loss-of-function experiment.

Specific Aim 3: Investigate mitochondrial remodeling following muscle stem cell transplantation into aged ischemic skeletal muscle. Because PAD is an age-associated disease, the primary objectives of this aim were to identify age-dependent changes of the muscle stem cell response and mitochondrial remodeling to ischemic injury, and to rescue the age-related decline in muscle regenerative capacity and bioenergetic function with muscle stem cell transplantation. Due to the muscle stem cell exhaustion observed in age, we hypothesized that aged mice exhibit attenuated myonuclear accretion and mitochondrial function following HLI, which can be improved through the transplantation of healthy muscle stem cells. We quantified age-related changes in myonuclear number and mitochondrial content/morphology by isolating and imaging single myofibers from ischemic *mitoDendra2* muscles. Mitochondrial function and gene expression were also tested in young and aged ischemic muscles through respirometers and quantitative polymerase chain reaction (qPCR). To assess age-dependent changes to other skeletal muscle components, we performed laser Doppler perfusion imaging for revascularization kinetics and employed the *Thy1-YFP* transgenic mouse model to investigate alterations to the neuromuscular junction. Finally, after transplantation of healthy muscle stem cells to aged ischemic muscle, we investigated changes to the mitochondrial network through imaging, mitochondrial function with a respirometer, and mitochondrial gene expression through qPCR.

1.3 Significance

Aim 1 was performed to inform the regeneration kinetics of skeletal muscle components following hindlimb ischemia, particularly of the relationship between the muscle stem cell and the myofiber's mitochondrial network to demonstrate muscle stem cell-driven modulation of the mitochondria. Because muscle stem cell transplantation has been investigated to improve muscle regeneration, we then tested the ability of exogenous muscle stem cells to remodel the host mitochondria and enhance bioenergetic function in a less severe, dystrophic mitochondrial myopathy that models DMD in Aim 2. Once we provided evidence that transplanted muscle stem cells can transfer their mitochondria into dystrophic myofibers through myogenic fusion in order to improve bioenergetic function, we then utilized this muscle stem cell transplantation technique to revitalize skeletal muscle regeneration and mitochondrial function in an aged hindlimb ischemia mouse model, which resembled a similar pathological manifestation to severe human PAD. Taken together, the outcomes and knowledge gained from this project highlight the role of muscle stem cells on moderating the mitochondrial network and provide insight into the capabilities of muscle stem cell transplantation. These findings serve as a basis to further develop multi-scale muscle stem cell-based therapies for complex mitochondrial myopathies.

CHAPTER 2. BACKGROUND AND LITERATURE REVIEW

2.1 Skeletal Muscle, Stem Cells, and Mitochondria

2.1.1 Skeletal Muscle Physiology

2.1.1.1 Functions of Skeletal Muscle

Skeletal muscles are one of the largest organs of the body by mass (40% of total body weight), and therefore requires many of the resources and nutrients within the body (30-50% of whole-body protein turnover). Although skeletal muscles are composed mostly of water (75%), 20% of muscle mass is constituted by structural, contractile, and regulatory proteins while the remaining 5% includes fat, minerals, and carbohydrates. Moreover, skeletal muscle is highly complex due to numerous cell types that make up the muscle that must all interact with each other to maintain skeletal muscle homeostasis, but this complexity also gives rise to the high degree of muscle plasticity. Myofibers, muscle stem cells, endothelial cells that make up the vasculature, pericytes surrounding the blood vessels, fibro-adipogenic progenitor cells, motor neurons, Schwann cells that direct motor neurons, and immune cells like macrophages, neutrophils, and leukocytes are some of the cells that find a home in skeletal muscle. Even mitochondria, which were once their own cells prior to the evolutionary endosymbiosis into eukaryotic cells, play vital roles in the communication between these skeletal muscle cells. This shared volume allows close cell-cell signaling among these various cell types and can provide compensatory mechanisms for the overall tissue to adapt to stress. However, when stress or injury overwhelms one of

these components and results in aberrant cellular responses, cell-cell interactions become debilitated, the entire "home" collapses, and skeletal muscle functions are impaired.

Traditionally, the primary functions of skeletal muscle are to provide movement (locomotion), maintain posture, and protect/support vital organs within various parts of the body, all accomplished by converting chemical energy (in the form of ATP produced by mitochondria) into mechanical energy. However, skeletal muscle is involved in several other functions too. For example, not only does skeletal muscle generate energy for these classical functions, but it can also store this energy long-term through glycogen synthesis, after which glycogen can be consumed for energy production during high intensity exercise[1,2]. Interestingly, this is achieved by the uptake of glucose from the blood and then conversion from glucose into glycogen in the muscle, allowing muscle to store this energy metabolite as well as regulate blood glucose levels, thereby demonstrating a link between skeletal muscle and the vasculature[3,4]. Along with skeletal muscle's ability to regulate biochemical energy, it can also control thermal energy by producing heat for the maintenance of core temperature. Furthermore, in terms of storage, muscles can act as a reservoir for amino acids that can be transported to other tissues like the skin, brain, and heart for the synthesis of organ-specific proteins[5-7]. Additionally, recent findings have now established skeletal muscle's role as an endocrine organ due to the release of myokines (muscle-derived cytokines) that can exert paracrine and endocrine signalling to other organs[8,9], or even autocrine effects that allow muscle to maintain the metabolic homeostasis of lipids and proteins[10]. The list of myokines produced in muscle is ever-growing, but includes signalling factors such as PGC-1α (peroxisome-proliferator activated receptor γ coactivator 1α), BDNF (brain-derived neurotrophic factor), VEGF (vascular endothelial

growth factor), FGF21 (fibroblast growth factor 21), IL-6 (interleukin-6), and many more[11-15]. Together, the complexity and numerous functions of skeletal muscle highlight the importance of this organ in maintaining healthy body physiology and homeostasis.

2.1.1.2 Myofibers

In order the conduct the skeletal muscle's primary function of locomotion, individual myofibers within the muscle contract and relax to shorten or lengthen the entire muscle that is connected to different skeletal bones at each end with a tendon. Anatomically, each muscle is comprised of thousands of myofibers that are wrapped together with a connective tissue sheath (perimysium) into fiber bundles called fascicles[16]. Contraction of these individual myofibers is controlled by myofilaments assembled together in an orderly and characteristic arrangement (giving muscles a striated pattern) and occurs within the sarcomere, which is the fundamental contractile unit of myofibers. The two most abundant myofilaments are actin filaments and myosin heads, which bind together and result in a conformational change in the myosin heads for the energy-demanding myofiber contraction upon calcium ion release from the sarcoplasmic reticulum. In order to unbind, ATP must be produced and bound to this complex to release the myosin head from the actin filament, signifying the high energy requirements for this binding/unbinding cycle (called the cross-bridge cycle)[17]. The synthesis of these actin and myosin proteins, as well as several thousand other contractile, structural, and regulatory proteins are dictated by nearby myonuclei within the myofiber.

Skeletal myofibers are post-mitotic and multinucleated, so myofibers cannot undergo cell division and, instead, form syncytia of many nuclei that each regulate a

discrete volume of myofiber surrounding it. While this feature remains consistent across all myofibers, muscle fibers also exhibit a high degree of variability and heterogeneity within the muscle. Myofibers can range in diameter from 20 μm to over 100 μm, which has been shown to be inversely related to the oxidative capacity of the fiber type, distinguished by the various isoforms of myosin heavy chain (MHC)[18]. There are slow-twitch myofibers that rely on oxidative metabolism for fatigue resistance, but tend to be smaller in width and generate low contractile force. Conversely, fast-twitch myofibers utilize glycolytic metabolism, which makes these fibers susceptible to fatigue, but allows for increased force generation per contraction. Typically, postural muscles like the soleus are composed of primarily slow-twitch fibers while phasic muscles like the extensor digitorum longus (EDL) contain mostly fast-twitch muscles. Other muscles, like the tibialis anterior (TA) have a mixture of both fiber types, with slow-twitch myofibers towards the periphery of the muscle and fast-twitch myofibers deeper within the muscle[19]. There are several underlying mechanisms that determine the type of a myofiber, and evidence shows that the fiber type of a myofiber can switch under various stressors like exercise[20]. Some of these key contributors include metabolic activity of the myofiber and the type of motor neuron that innervates the myofiber.

2.1.1.3 Motor Neurons

In order for myofibers to contract, they require innervation from a motor neuron that can induce excitation-contraction initiated at the neuromuscular junction (NMJ). In fact, a decline in innervation and loss of excitation-contraction coupling are known causes of muscle degeneration[21]. During excitation-contraction, an action potential is transmitted through the motor neuron and its axon terminal releases the neurotransmitter acetylcholine

(ACh) at the NMJ. The acetylcholine receptors (AChR) on the post-synaptic endplate on the myofiber bind to the ACh from the motor neuron to depolarize voltage-gated calcium ion (Ca^{2+}) channels of the T-tubules in the myofiber, which in turn triggers the release of Ca^{2+} from the sarcoplasmic reticulum. Ca^{2+} ions can then bind to troponin, causing a conformational change that allows it to move tropomyosin away from the myosin-binding sites on actin so that the cross-bridge between actin and myosin can form for contraction.

There are two major regions of the NMJ that are critical for excitation-contraction coupling: the pre-synaptic motor neuron and the post-synaptic endplate. The pre-synaptic motor neuron is guided to the NMJ by terminal Schwann cells, which can be identified by the canonical marker S100β[22]. At the NMJ, axon terminals release ACh in synaptic vesicles. These vesicles are produced in the cell body and contain vacuolar-type H^+ pumps that use ATP to move protons into the vesicle. Neurotransmitter transport proteins exchange the protons for ACh, and the v-SNAREs on the vesicle bind to t-SNARES on the axon terminal to bind the vesicle to the membrane and prepare for release[23]. After release, the vesicle is transported back to the cell body to be reloaded with more ACh[24]. Importantly, these processes involved with neurotransmitter release, as well as maintenance of the motor neuron's membrane potential, require high amounts of energy. Accordingly, motor neurons and their axon terminals contain high densities of mitochondria to meet these energy demands[25], though the mitochondrial content varies depending on the type of motor unit. Type I motor units utilize oxidative metabolism to generate energy while type II motor units use glycolytic metabolism, and both types have been shown to influence the myofiber type that they innervate by directing the metabolic machinery and expression of protein isoforms of the myofiber[26]. However, bidirectional

communication between myofibers and motor neurons has recently been emphasized as an important interaction for the maintenance of the neuromuscular system, particularly through retrograde signalling pathways from the myofiber to the motor neuron[27,28].

On the post-synaptic side of the NMJ on the myofiber, the endplate contains a massive concentration of AChR grouped together in a pretzel-like morphology. Because each myofiber only has one NMJ, it is critical for the pre-synaptic axon terminal to overlap efficiently with the post-synaptic endplate for excitation-contraction to occur[29]. However, if the post-synaptic NMJ degenerates, the overlap between the axon terminal and endplate is lost and the post-synaptic receptors become fragmented rather than displaying a convoluted, pretzel-like shape. During post-synaptic endplate regeneration, driven and regulated by subsynaptic nuclei located on the myofiber just beneath the AChR, the receptors exhibit a more donut-shaped morphology, typically with an elongated oval invagination[30]. These subsynaptic nuclei are crucial for repairing the post-synaptic NMJ by controlling the expression of important neurotrophic factors such as agrin, various neuregulins, Wnt ligands, and more to facilitate the formation of a regenerating NMJ[31-33].

2.1.1.4 Vasculature

Located in close proximity to motor neurons due to neurovascular congruency[34], blood vessels are another imperative component to skeletal muscle physiology. The vasculature of skeletal muscle comes from primary arteries that branch into smaller arterioles and capillaries that course parallel to motor neurons and myofibers in order to supply the oxygen and nutrients required for cellular and mitochondrial function[35]. Although skeletal muscles as a whole account for approximately 25% of the total cardiac

output to meet basal metabolic needs, the capillary density within the muscle varies dramatically based upon fiber type[36]. Because of the greater oxygen needs in slow-twitch, oxidative myofibers compared to fast-twitch, glycolytic myofibers, oxidative myofibers contain a greater capillary density and number of interconnections between adjacent capillaries to cater to the increased metabolic requirements[37].

Not only is the vasculature required for skeletal muscle homeostasis, but healthy muscles also provide biomechanical and biochemical support for endothelial cell-driven capillary growth, sprouting, and angiogenesis[38]. For example, β1 integrin, a type of cell adhesion molecule found in skeletal muscle, is necessary for endothelial cell differentiation and capillary tube formation, and loss of these integrins resulted in impairments of angiogenesis[39-41]. Similarly, laminin, a structural protein that constitutes the myofiber membrane, directly impacts endothelial cell morphology, differentiation, and migration during neovascularization[42,43]. From a biochemical standpoint, skeletal muscle expresses vascular endothelial growth factor (VEGF), a potent inducer of angiogenesis that stimulates endothelial cell migration, proliferation, and differentiation into vessel structures, further exemplifying the reciprocal interactions between skeletal muscle and the vasculature[44,45].

2.1.1.5 Muscle Stem Cells

Skeletal muscle possesses a remarkable regenerative capacity and plasticity due to the presence of endogenous resident muscle stem cells (MuSCs), also known as satellite cells[46]. These MuSCs, identified by the expression of the canonical marker, paired box protein 7 (Pax7), reside between the basal lamina and the sarcolemma of the myofiber and

are indispensable to muscle regeneration[46]. Normally in a quiescent state under physiological conditions (G0 phase), MuSCs can rapidly enter the cell cycle upon injury to the myofiber to initiate myogenesis for myofiber repair. Interestingly, recent evidence has also shown that MuSCs are critical to maintenance of other skeletal muscle components like the NMJ and vasculature[47]. MuSCs are found in close proximity to and with higher activity near the NMJ, and depletion of MuSCs disrupted regeneration of the NMJ following a denervation injury due to diminished numbers of subsynaptic nuclei[48]. Moreover, quiescent MuSCs have exhibited a propensity to localize near capillaries, attributed to the reciprocal cross-talk between MuSCs and endothelial cells through Dll4 signaling of the Notch pathway[49]. VEGF has also been heavily implicated in this cross-talk because of the high VEGF expression of MuSCs that promotes capillary formation[50]. Reciprocally, endothelial cells exhibit high expression of a panel of growth factors (IGF-1, HGF, FGF, PDGF, VEGF) that also maintain MuSC viability and proliferation[51]. Thus, the MuSC niche is not only crucial for myofiber repair, but for growth and maintenance of various other skeletal muscle components too.

2.1.2 Muscle Stem Cells in Skeletal Muscle Regeneration

Skeletal muscle regeneration is driven by adult myogenesis, the biological process of repairing skeletal muscle tissue post-development, and is tightly regulated by the muscle stem cell (MuSC) following stress or injury. Because mature myofibers are post-mitotic, multinucleated syncytia formed by the fusion of differentiated MuSC-derived myoblasts, MuSCs are required for myofiber formation, maintenance, and growth[52]. Typically quiescent in a homeostatic state, the MuSC enters the cell cycle and activates a set of transcriptional factors in order to self-renew or asymmetrically differentiate following

damage to the myofiber. Some of the MuSC progeny proliferate and self-renew to replenish the quiescent stem cell pool for future rounds of regeneration. Meanwhile, other populations of committed MuSC progeny (myoblasts), marked by expression of myogenic regulatory factors like MyoD, MyoG, and Myf5[53], can either form *de novo* myofibers to generate new fibers, or differentiate and fuse with existing myofibers to increase the number of myonuclei and volume of regenerating fibers. Prior to fusion into the myofiber, differentiated MuSC progeny migrate to the site of injury driven by chemoattractants like VEGF and bFGF, damage-associated molecular patterns controlled by Toll-like receptor-mediated signaling, and TNFα and TGFβ cytokines[51,54-57].

Interestingly, MuSCs exhibit significant heterogeneity based on the expression of various transcription factors or cell surface markers that dictate the fate of the cell. For example, relative expression of the Pax7 transcription factor determines whether a MuSC is fated for self-renewal or myogenic differentiation. MuSCs with low Pax7 expression are primed for myogenic commitment and display elevated metabolic activity compared to MuSCs with high Pax7 expression[58]. It has been suggested that microRNAs, such as miR-431, mediate MuSC heterogeneity by regulating the Pax7 levels within the cells during regeneration[59]. Other microRNAs like miR-1 and miR-133a have also been implicated as mediators of MuSC heterogeneity by controlling the content and biogenesis of mitochondria in quiescent muscle stem cells through Dlk1-Dio3 gene cluster signaling, which influences the metabolic capacity of MuSCs[60]. Not only do transcription factors determine the fate of MuSCs, but cell surface markers like CD34 can also distinguish subpopulations of MuSCs[61]. Indeed, MuSCs with high CD34 expression maintained stemness properties due to FoxO inhibition while CD34-low MuSCs were primed for

myogenic differentiation[62]. Moreover, in these committed MuSCs that are fated for myogenesis, the cells exhibit polarity of intracellular signaling proteins and cell adhesion molecules during asymmetric division to determine the fate of each daughter cell, which are then retained in the progeny[63-65]. The heterogeneity of MuSCs also extends beyond self-renewal versus myogenic cell fates, and niche-directed MuSCs have been previously described. A subset of MuSCs are located in close proximity to the neuromuscular junction and assist with NMJ regeneration, and they have recently been identified by expression of SRSF1[66]. Another subpopulation of MuSCs is destined to reside near the vasculature through VEGF and Notch signaling, and can facilitate angiogenesis through interactions with endothelial cells[49,51]. Because of these functional heterogeneities of MuSCs, it is important to consider these differences in MuSC response during muscle regeneration on a cell-to-cell basis following various modes of injury.

2.1.3 Myonuclear Domain

Several studies have indicated that muscle stem cells play a critical role in determining the myofiber's myonuclear domain, defined as the discrete cytoplasmic volume surrounding each myonucleus that the nucleus transcriptionally regulates. When myonuclear domain was first defined in 1989, it was thought to be a fixed property of myofibers, with loss of myonuclei accompanied by myofiber atrophy and MuSC-derived myonuclear accretion associated with hypertrophy in order to keep the myonuclear domain constant[67,68]. This concept was based on the foundation of post-natal developmental growth of myofibers where the number of myonuclei scaled linearly with myofiber size in uninjured EDL and diaphragm muscles from 2 to 6 weeks of age in mice, though the myonuclear domain size becomes significantly larger at 5 months of age[69,70]. Since then,

many studies have further challenged this hypothesis through a variety of injury-induced atrophy and exercise-induced hypertrophy models[71]. In a denervation model involving transection of the peroneal nerve, investigators noted myofiber atrophy without the loss of myonuclei, thereby decreasing the size of the myonuclear domain[70]. Likewise, acute ischemia/reperfusion induced by a tourniquet led to myofiber atrophy without any changes in myonuclear number[72]. Moreover, through hindlimb suspension for 14-56 days and subsequent mechanical unloading-induced atrophy, myonuclei were not lost in atrophied myofibers[73-75], though decreased myonuclear number was reported for long-term (90 days) unloading[76]. Importantly, however, after depletion of MuSCs in a Pax7-DTA transgenic mouse model, the lack of muscle stem cell-mediated myonuclear accretion during mechanical reloading inhibited myofiber regrowth despite the conserved myonuclear number during atrophy, indicating that the MuSC plays a significant role in myofiber hypertrophy[77].

By inducing myofiber hypertrophy through both resistance training and endurance exercise, concomitant increases in myofiber size and myonuclear number were observed[78]. Hypertrophy following testosterone supplementation in both humans and mice further validated this relationship between increased myofiber size and myonuclear number, and again, MuSC depletion inhibited myofiber atrophy[79,80]. Conversely, some reports claim that hypertrophy can occur independent of MuSC myogenic fusion following denervation, resistance training, and mechanical overloading, where increased myofiber sizes were observed prior to or even in the absence of myonuclear accretion[81-83]. These findings imply that resident myonuclei also play a role in myofiber hypertrophy and can compensate for the lack of myonuclear accretion by upregulating their own transcriptional output. The

plasticity of the transcriptional regulation of these myonuclei can be attributed to "muscle memory" at the cellular level, initiated by the muscle stem cell. Recent investigations revealed that myonuclei acquired from MuSCs during exercise overload training are retained during disuse (detraining), and these MuSC-derived myonuclei can drive myofiber hypertrophy during a subsequent bout of exercise re-training[84,85]. This same phenomenon was reported by subjecting sedentary mice to anabolic steroids to induce hypertrophy, followed by a period of inactivity, then another round of steroid injection[86]. The authors suggest that epigenetic changes in the MuSC in response to exercise or steroids are propagated to their downstream myonuclei, which allow these MuSC-derived myonuclei to transcriptionally promote myofiber hypertrophy within their myonuclear domain upon secondary exposure to the same stress. These reports further highlight the importance and the role of MuSCs in regulating the myonuclei that dictate myofiber size by governing their individual domains.

2.1.4 Nuclear-Mitochondrial Genome Communication

Within the domain that each myonucleus modulates, a critically important component of the cytoplasm that nuclei regulate are the mitochondria. In order to maintain and remodel the myofiber's mitochondrial network, nuclei must express both signaling transcription factors to promote the synthesis of new mitochondria and proteins that constitute the structure of mitochondria. While 13 proteins of the mitochondrial electron transport chain complexes are encoded by mtDNA, thousands of mitochondrial proteins are nuclear-encoded and need to be imported into the mitochondria, illustrated by the proximity of mitochondrial reticula to the nucleus[87]. Not only does the nucleus direct synthesis of proteins involved in the mitochondrial structure, but it also codes for master

regulators of mitochondrial biogenesis and dynamics. For example, PGC-1α, PPARα, SIRT1, FOXO3, and AMPK are all expressed in the nucleus, but act as transcription factors that induce mitochondrial biogenesis[88-90]. Similarly, Drp1, Opa1, Mfn1, Mfn2, Fis1, and many more are also nuclear-encoded and play crucial roles in both mitochondrial fission and fusion dynamics[91]. Furthermore, several molecules and proteins have been implicated in the crosstalk between nuclei and mitochondria. Proteins such as the prohibitin isoforms, which have been shown to possess both a mitochondrial- and nuclear-targeting sequence to assist in the import of mitochondrial proteins, allow the mitochondrial genome and the nuclear genome to communicate[92-94]. Since prohibitin is translocated to the mitochondria dependent on the mitochondrial membrane potential, the protein can also inform the nucleus about the polarity and quality of the mitochondria[92]. If the mitochondria are indeed impaired, for example double-strand breaks in the mtDNA, the nucleus senses mitochondrial RNA in the cytoplasm released by BAX and BAK in order to initiate apoptosis and trigger an immune response[95]. Other proteins, such as the transcription factor G-protein Pathway Suppressor 2 (GPS2) have further demonstrated nuclear-mitochondrial crosstalk by promoting mitochondrial biogenesis following GPS2 translocation from the mitochondria to the nucleus[96]. Small molecules such as vitamin B or even the mtDNA-encoded signaling peptide MOTS-c have also displayed important roles in the nuclear-mitochondrial relationship. Several different vitamins (vitamin B1, B2, B3, B5, and B8) act as nutritional cofactors or coenzymes for TCA cycle metabolites that are directly involved in methylation or acetylation modifications to nuclear histones[97]. The mtDNA-encoded MOTS-c inhibits the folate cycle and purine biosynthesis in the nucleus, consequently activating the AMPK metabolic pathway[98]. A more thorough understanding

of how these proteins and molecules facilitate the communication between myonuclei and mitochondria, and how myonuclei regulate the mitochondria within its domain, will provide a basis for exploring the relationship between MuSCs, MuSC-derived myonuclei, and mitochondria during skeletal muscle regeneration.

2.1.5 Mitochondrial Domain

While MuSCs (and other mononuclear cells) exhibit a distinct relationship with their mitochondria, the post-mitotic and multinucleated myofiber displays a more unique mitochondrial network that is organized into columns of mitochondrial reticula along the z-line of the contractile apparatus. Each of these columnar reticula can be compared to an electric battery, both of which generate energy from chemical reactions. Thus, the mitochondrial network, which allows efficient exchange of energy and metabolites between reticula, is similar to an array of batteries in series, much like those found in electric car battery packs that provide synergistically more power than the sum of the individual battery cells, emphasizing the importance of an organized mitochondrial network. However, when these reticula become disorganized and overlap, the myofiber loses its ability to generate large amounts of energy. Moreover, skeletal muscle contains one of the highest densities of mitochondria relative to other cells in the body, and the value of mitochondria cannot be understated. Because of their responsibility in generating the energy required for most of life's functions, mitochondria have even been compared to the traditional Asian medicine concept of "chi," or the vital life force[99]. From a philosophical standpoint, mitochondria harness and produce the energy of life itself, and with so many of these mitochondria residing within myofibers, skeletal muscle can be observed as a key

player in maintaining the force of life. In this vein, when skeletal muscle mitochondria become defective, so does the ability to sustain life.

As a repair mechanism for defective mitochondria in mononuclear cells, the cells can segregate healthy and dysfunctional mitochondria during mitosis based upon the quality of the mtDNA in order for one daughter cell to harbor the healthy mitochondria while the other daughter cell retains the defective mitochondria and undergoes apoptosis[100]. In contrast, because myofibers are post-mitotic, they are unable to accomplish this replication-based mitochondrial segregation. Instead, similar to the idea of the myonuclear domain, the mitochondria of the myofiber are compartmentalized into discrete domains centered around their myonucleus of origin, herein referred to as the mitochondrial domain[101]. These mitochondria of the myofiber can even be further classified as either interfibrillar mitochondria, which provide the energy for contraction, or subsarcolemmal, which provide energy for maintaining the membrane potential and integrity[102]. Following injury, however, defective interfibrillar mitochondria have revealed altered networks that span several sarcomeres, likely due to the highly dynamic nature of mitochondria regulated by fission and fusion events to remove damaged portions of the reticulum[103]. These dynamic events are coordinated by GTPases including Drp1, OPA1, Mfn1, Mfn2, and many others[91]. To remove damaged fragments of mitochondria, fission events pinch off the dysfunctional portion of the mitochondria to be selectively degraded and eliminated through PINK1- and Parkin-mediated mitochondrial autophagy (mitophagy)[104,105]. Alternatively, dysfunctional mitochondria can also fuse together with healthy mitochondria to dilute the effects of the deficient mitochondria.

If enough defective mitochondria are present, the myofiber will fail to maintain its health and consequently degenerate, thereby activating muscle stem cells to initiate skeletal muscle regeneration. To meet the high energy demands required for muscle regeneration, the mitochondrial content of the MuSC changes during adult myogenesis. While quiescent MuSCs have few active mitochondria (in order to protect the reserve stem cell pool from oxidative stress to ensure longevity) and rely on glycolytic metabolism[106,107], activated MuSCs transiently depend more on fatty acid oxidation[108]. As myogenesis progresses, differentiated MuSCs increase their mitochondrial content and again shift their metabolism towards oxidative phosphorylation to provide the energy for myogenic fusion[107]. Through fusion, MuSCs also deposit their newly synthesized mitochondria into the regenerating myofiber. However, when the shift from initial glycolysis to oxidative phosphorylation is precluded by limiting oxygen availability or dysregulating electron transport chain activity, differentiation of MuSCs and their myogenic fusion potential are significantly reduced[109-111], indicating that these phases of metabolic switching are required to meet the energy demands of myofiber formation and regeneration.

2.2 Mitochondrial Myopathies

In this section, we describe several forms of mitochondrial myopathies, which we define as a myopathy (pathological muscle due to disease, injury, or stress) associated with mitochondrial dysfunction within the myofiber. The most commonly described mitochondrial myopathies are caused by mutations in mtDNA that cause deficiencies in complex activity of the electron transport chain, such complex I deficiencies. In these models, the etiology of the disease stems directly from mitochondrial dysfunction that leads to impairments in muscle function. Here, however, we outline forms of mitochondrial

myopathies where mitochondrial dysfunction is a consequence of factors other than mtDNA-based deficiencies, such as oxidative stress or calcium overload. In these diseases, the ensuing mitochondrial dysfunction is also chronic, similar to traditional mitochondrial myopathies, which exacerbates the pathophysiology of the disease and subsequently further deteriorates skeletal muscle function.

2.2.1 Sarcopenia

Sarcopenia is defined as the age-related loss of skeletal muscle mass and strength. There are several commonly described hallmarks of aging that may result in sarcopenia, including stem cell exhaustion, mitochondrial dysfunction, loss of proteostasis, cellular senescence, genomic instability, epigenetic alterations, altered intercellular communication, deregulated nutrient sensing, and telomere attrition. While this list of potential contributions towards sarcopenia is extensive, here we will focus on stem cell exhaustion and mitochondrial dysfunction for the purpose of this thesis. However, it is important to note that limited protein synthesis[112,113], diminished myokine expression[114], impaired angiogenesis due to senescent endothelial cells[115,116], and degenerated motor neurons leading to denervation of the myofiber[117-119] also play major roles in the age-related loss of muscle mass and function.

However, one of the key factors that leads to sarcopenia is the reduced MuSC number and function of aged skeletal muscle. Thus far, several studies have reported the depletion of MuSCs as an effect of age due to a reduced ability to maintain muscle stem cell quiescence and self-renew to replenish the reserve MuSC pool[120-122]. This is, in part, caused by multiple rounds of skeletal muscle regeneration over the lifetime of the

individual, which results in a gradual decline of quiescent MuSC number, but other studies elaborate on this depletion by indicating that aged MuSCs also shift towards a myogenic lineage rather than self-renewal[123]. This functional deficiency of aged muscle stem cells has been attributed to quiescent MuSC senescence and apoptosis[124]. As expected, when MuSCs were genetically ablated in aged mice, skeletal muscle exhibited a more severe impairment in myofiber regeneration compared to younger mice, likely due to decreted myonuclear number[125,126]. Similarly, ablated MuSCs in aged muscles also exacerbated neuromuscular degeneration and fibrotic deposition, indicating that MuSCs have profound effects on maintaining neuromuscular health and preventing fibrosis[125,127], but are unable to do so in old age when MuSCs are depleted and lose function. Even without genetic MuSC ablation, aged muscle stem cells exhibited decreased VEGF gene expression and, consequently, reduced MuSC-mediated angiogenic stimulation that impaired aged muscle repair[128]. Though the underlying mechanism for aged MuSC dysfunction has yet to be identified, numerous studies have pointed towards altered Notch and Wnt signaling in quiescent aged MuSCs and their progeny[129-132]. Interestingly, the effect of age on MuSC number and dysfunction is fiber type-dependent, with type II glycolytic myofibers losing MuSCs with age while type I oxidative myofibers exhibited no change with age[133], suggesting that there may be a metabolic influence on aged MuSC number and function.

In the context of metabolism, mitochondrial dysfunction has a profound effect on tissue bioenergetics, or the ability of cells to transform oxygen and organic substrates into usable energy in the form of ATP through respiration[134,135]. In fact, mitochondrial health plays a consequential role in sarcopenia due to the elevated oxidative stress in age, commonly referred to as the mitochondrial theory of aging[136]. Mitochondria can become

dysfunctional when electrons leak from damaged complexes and react with oxygen to create reactive oxygen species (ROS) such as superoxide, which can induce oxidative stress that damages the mitochondrial membranes, mtDNA, or mitochondrial enzymes, as well as a slew of other cellular components. These defects in the mitochondria can accumulate over age, resulting in greater ROS generation and, therefore, even more mitochondrial damage[136,137]. While scavenging antioxidant enzymes, such as superoxide dismutase (SOD), can regulate oxidative stress by converting the highly reactive superoxide into the signaling molecule hydrogen peroxide (H_2O_2), an imbalance between ROS and antioxidants can overwhelm the defense system and further damage the mitochondria, resulting in a vicious cycle of ROS production and oxidative damage. Because mitochondria are one of the primary sources for ROS such as superoxide, hydrogen peroxide, and hydroxyl radical, it is critical to eliminate dysfunctional mitochondria and remodel the network to restore bioenergetic function. Though the removal of dysfunctional mitochondria typically occurs through mitochondrial dynamics and mitophagy, these quality control mechanisms are debilitated in age[138,139], further leading to accumulation of mitochondrial defects and impairing the ability of myofibers to remodel their mitochondrial network. While it has been shown that sarcopenia is associated with MuSC dysfunction, mitochondrial damage, and oxidative stress in the myofiber[140], the relationship and interactions between these abnormalities, particularly in conjunction with other disease models, remain unknown.

2.2.2 Peripheral Artery Disease

2.2.2.1 Pathophysiology

Chronic age-related diseases affect nearly half of all Americans and can lead to hospitalization, long-term disability, reduced quality of life, and death[141,142]. Specifically, cardiovascular diseases, such as age-associated peripheral artery disease, remain the leading cause of death and disability in the United States and are anticipated to magnify with the nation's aging population if not effectively addressed now[143,144].

Peripheral artery disease (PAD) is a progressive cardiovascular disease characterized by abnormal perfusion to the extremities due to blockage of the blood vessels, most commonly the femoral artery or popliteal artery[145]. 12% of all Americans, but 20% of Americans over the age of 60, are affected by PAD, delineating the age-dependent prevalence of the disease. While some cases of PAD remain asymptomatic, many patients progress to painful intermittent claudication or to the more severe critical limb ischemia, where blood flow is insufficient to maintain tissue viability, thereby resulting in amputation rates reaching 50% of patients[146-149]. The ischemia not only leads to reduced viability and atrophy of the myofiber[150], but also induces degeneration of other skeletal muscle niche components like the motor neuron and neuromuscular junction due to their reliance of oxygen and nutrients provided by the blood[151]. Furthermore, PAD has been shown to be comorbid with other cardiovascular diseases, diabetes, renal artery stenosis, hypertension, and obesity, exacerbating the pain and poor quality of life associated with the disease[145,152].

Through partial stenotic blockage or full occlusive blockage of the blood vessels[148], PAD manifests varying degrees of ischemic injury to the skeletal muscle, where the lack of oxygen and nutrients leads to extensive tissue damage and consequent remodeling. Along with alterations to the vascular network, ischemia has been shown to cause

degeneration of the myofiber and dysfunction of the mitochondria due to unregulated oxidative stress[140,150,151,153]. Interestingly, several large clinical studies in PAD patients have demonstrated that muscle function/oxidative capacity is the strongest predictor of morbidity/mortality[154-160]. Previous reports have also documented evidence of skeletal muscle myopathies in PAD patients[161,162], although the mechanistic link between myofibers and their mitochondria in ischemic muscle is incompletely understood. Over the past several years, there have been reports that targeting skeletal muscle metabolism (delivery of MTP-131/elampretide – a cardiolipin targeting compound; as well as expression of a mitochondrial-targeted catalase) can reduce/prevent muscle necrosis, improve muscle contractile function, and enhance limb perfusion recovery in mice subjected to hindlimb ischemia, exemplifying the clear relationship between ischemic myofibers and the quality of their mitochondria[163-165]. Moreover, another clinical study discovered a novel 'mitochondrial signature', characterized by depression of mitochondrial gene expression and respiratory function in skeletal muscle that associated with limb amputation in PAD patients[166]. This growing body of evidence[140,158,167-174] establishes the importance of skeletal muscle mitochondria to PAD pathophysiology. In order to develop a successful treatment for PAD, it is necessary to understand the highly orchestrated regenerative process of the skeletal muscle components following an ischemic injury to provide a basis for a multi-scale therapeutic regimen.

Another potential therapeutic target for PAD is the MuSC, which is required for myofiber repair. In PAD, MuSCs have demonstrated a marked reduction in myogenic potential, although it is not clear whether it is due to a decreased number of MuSCs or their impaired function[150]. Through chronic rounds of regeneration, as observed after ischemic

injury, persistent stress may exhaust the endogenous MuSC reserve pool and diminish the regenerative capacity of the ischemic muscle[120,126,175]. Alternatively, ischemia-induced oxidative stress, characterized by high levels of reactive oxygen species (ROS), can oxidatively damage critical components of the MuSC required for activation and differentiation, such as their mitochondria. Indeed, researchers have demonstrated that ROS dramatically reduce the viability, proliferation, and differentiation of MuSCs due to impaired mitochondrial function[176,177]. Conversely, protecting the mitochondria of the MuSC by enhancing the expression of mitochondrial protein S-nitrosation attenuates both myofiber damage and ischemia-induced denervation by allowing the ischemic MuSC to generate more myonuclei and subsynaptic nuclei[151]. However, the precise mechanism through which MuSCs communicate with their mitochondria following ischemia has not been fully investigated and further studies are required to elucidate the interactions between MuSCs and their mitochondria during adult myogenesis in PAD.

2.2.2.2 Animals Models

Although there are numerous animal models to test the cell/tissue responses, biomolecular mechanisms, and therapeutic interventions for PAD, none of these models have tested the age-related effects of the disease. Preclinical models for PAD include mice, rats, pigs, cats, dogs, rats, rabbits, and even various species of primates, though current research is performed overwhelmingly on rodents and pigs since they most closely resemble human vascular anatomy[178]. Because of the varying degrees of PAD in humans (asymptomatic, intermittent claudication, critical limb ischemia), various modes of ischemic injury have been induced in mice to represent the degree of ischemia. Some studies have performed transient ischemia/reperfusion injuries by using a tourniquet on the

hindlimb in order to model intermittent claudication[151,179-183]. More commonly, however, surgical hindlimb ischemia procedures have been performed to represent more severe models of PAD. These procedures are typically referred to as subacute and acute hindlimb ischemia, where subacute ischemia ligates the femoral artery without removal of the artery, and acute ischemia both ligates and excises a portion of the artery[184-187]. Among variations in procedural or surgical protocols, strains of mice also exhibit vastly different sensitivities to ischemic injury[188]. *BALB/c* and *129S2/Sv* mice both present severe grades of necrosis to hindlimb ischemia compared to *C57BL/6J* mice, and this has been attributed to fewer pre-existing collateral vessels, reduced angiogenic potential, decreased oxidative capacity, and worse myogenic potential[188-192]. Another mouse model that closely resembles human PAD is the ApoE knockout mouse that develops a form of diabetes similar to humans with Type 1 diabetes mellitus, a frequent comorbidity with PAD[193,194]. Nonetheless, similar species-to-species variations in the sensitivity to ischemic injury have also been observed in pigs, rats, and dogs[195-197]. Although the vast majority of these investigations have been conducted on young animals rather than aged animals that represent the pathophysiology of aging associated with PAD, these findings emphasize the importance to consider the mode of injury, strain, and genetic background of the animal model when testing cellular responses to PAD and therapeutic approaches.

2.2.2.3 Current Treatments and Recent Advances

While treatments are available to manage the symptoms of PAD and slow the progression of the disease, there is currently no cure. Based on the stage of PAD, treatments can range from physical rehabilitation, like walking/exercise programs, to medications that prevent blood clots and lower blood pressure to invasive surgical procedures such as

angioplasty or bypass surgery[198]. However, even with early intervention, many patients will still progress to the more severe critical limb ischemia and require amputation[199]. Recent regenerative medicine approaches have made attempts to address the cause of PAD non-invasively through collateral vessel formation, but have had limited success. Various growth factor treatments using vascular endothelial growth factor, fibroblast growth factor, hypoxia-inducible factor-1α, and/or hepatocyte growth factor, as well as cell-based therapies using delivery of bone marrow-derived mononuclear cells, peripheral blood-derived mononuclear cells, and mesenchymal stromal cells to promote angiogenesis have been explored with inconsistent outcomes[200-202]. In fact, recent evidence suggests that the ischemia-induced loss of viable muscle tissue, which acts as an indispensable matrix of growth factors and biomechanical support, may be the cause of failure for current revascularization techniques[38,41]. Furthermore, research has demonstrated that similar degrees of stenosis in the blood vessels may present diverse degrees of symptoms, indicating that perfusion alone does not dictate the underlying progression of the disease[203]. Rather, skeletal muscle degeneration and the dysfunction of its mitochondria have also been implicated in determining the prognosis of PAD[166,188,189]. This paradox further demonstrates the need to elucidate the skeletal muscle regeneration mechanism in complex musculoskeletal diseases such as PAD in order to develop a multi-disciplinary approach to treat ischemia-induced myopathy.

2.2.3 Duchenne Muscular Dystrophy

2.2.3.1 Pathophysiology

Another progressive degenerative mitochondrial myopathy that affects 1 in 3500 newborn males is Duchenne muscular dystrophy (DMD), where there is a slow atrophy of skeletal muscle as the child ages. Although it is currently characterized as a genetic disease due to an X-linked recessive mutation in the dystrophin gene, DMD was originally considered a metabolic disease[204]. Though the altered metabolism in the pathogenesis of DMD has since been overlooked and considered a secondary phenomenon to dystrophinopathy, numerous studies in the last few years have brought the mitochondrial dysfunction in DMD patients back to light[205,206].

In patients afflicted with DMD, symptoms typically appear within 3 to 5 years after birth, leading to muscle atrophy and the need for a wheelchair or other mobility aids after the age of 10, and mortality before the age of 30 due to respiratory failure (usually of the diaphragm muscle)[207-209]. The etiology of the disease is based on a multitude of different mutations in the dystrophin gene that leads to total or partial loss of dystrophin function, with 1 in 3 new cases resulting in a novel mutation[207,210]. Considered one of the largest known human genes (2.5 Mb and 79 different exons), dystrophin is highly prone to different mutations[211]. Physiologically, dystrophin is a protein that connects the cytoskeleton of the myofiber to the membrane and extracellular matrix. Without functional dystrophin, it has been hypothesized that the myofiber membrane becomes unstable and the ensuing sarcolemmal tears allows an influx of extracellular calcium ions (Ca^{2+}) into the myofiber[212]. Because mitochondria are responsible for buffering intracellular Ca^{2+} ions through the permeability transition pore, the Ca^{2+} overload results in uptake of the ions and, therefore, mitochondrial swelling[213-215]. The swelling of mitochondria directly leads to damage of the mitochondrial membranes, disrupted mitochondrial membrane potential,

and eventual loss of function[207,212]. As a consequence, the mitochondria then induce activation of apoptosis and necrosis of the dystrophic myofiber[208], though the precise mechanisms of Ca^{2+}-induced mitochondrial dysfunction in dystrophic cells and tissues have not yet been fully elucidated.

Some studies suggest that the altered metabolism in DMD is a result of dysregulated oxidative stress due to the Ca^{2+} overload of dystrophic mitochondria. While healthy mitochondria generate a low level of reactive oxygen species (ROS) required for cell-cell signalling pathways, the disrupted mitochondrial membranes in dystrophic tissues result in overproduction of ROS that lead to cycles of myofiber degeneration and regeneration[216,217]. Using nuclear magnetic resonance spectroscopy and mitochondrial functional analyses, the damaged mitochondrial membrane and elevated ROS production have also been shown to be associated with diminished oxidative capacity and ATP generation of human and mouse dystrophic mitochondria[218-221]. Indeed, by treating dystrophic mitochondria with oligomycin, an ATP synthase inhibitor, no change in ATP production was observed, insinuating that these mitochondria harbor impaired electron transport chain complexes required for oxidative phosphorylation[216]. Moreover, dystrophic muscles seem to retain these defective mitochondria rather than selectively removing them through autophagy, likely due to impaired mitochondrial dynamics[222], and stimulating mitochondrial autophagy (mitophagy) through urolithin A treatment or AMPK activation demonstrated marked improvements in dystrophic myofiber function[223,224]. Interestingly, however, these deficiencies in mitochondrial function extend beyond dystrophic myofibers and have been also been observed in myoblasts and epidermal melanocytes that do not require dystrophin for cell membrane integrity, indicating that there may be intrinsic mitochondrial

dysfunction in dystrophic cells regardless of dystrophin expression, and that Ca^{2+} overload due to sarcolemmal tears may not be the only contributing factor to the impaired energy metabolism[216,225-227]. Rather, the mitochondrial dysfunction may originate during development or in progenitor cells via mtDNA mutations[228], which is then exacerbated by Ca^{2+} overload in the myofiber. Potentially, muscle stem cells may also possess dysfunctional mitochondria, and through the cycles of degeneration and regeneration of the dystrophic myofiber (and the resulting myogenic fusion of the MuSC into the myofiber), the mitochondrial defects could accumulate over time.

Dystrophic muscle has been shown to not only exhibit deficiencies in mitochondrial function, but muscle stem cell function too. In fact, recent findings have revealed that MuSCs play a direct role in contributing to the etiology and progression of DMD, leading to impaired myogenic capacity of dystrophic muscle[229]. This is, in part, due to MuSC depletion through repeated rounds of degeneration and regeneration in dystrophic mice[227,230]. More recent studies, however, have also pointed towards aberrant asymmetric division of MuSCs that result in an imbalance between self-renewing and myogenic MuSCs that impairs MuSC function as well as number[231]. To compensate for the stem cell exhaustion, dystrophic MuSCs are more primed to self-renew and repopulate the reserve MuSC pool rather than asymmetrically divide to generate committed myogenic progenitors, leading to deficits in myofiber repair[65]. The impaired asymmetric division is thought to be an effect of dysregulated polarity during MuSC division. There are several regulatory factors that control polarity during asymmetric division, including Notch signalling, phosphorylated Par-6 interactions with aPKC (atypical protein kinase C) and Numb, Par-1 binding to MARK2 (microtubule affinity-regulating kinase 2), and more[232-

[236]. Importantly, however, RNA sequencing data have revealed that MuSCs highly express dystrophin, which interacts with MARK2 to regulate cell polarity during asymmetric MuSC division[65]. Without functional dystrophin, MuSCs are unable to effectively undergo asymmetric division and the committed progeny are lost over time. Interestingly, although these dystrophic muscle-forming progeny are diminished, this subpopulation still retains similar myogenic capacity compared to healthy committed MuSCs[237,238]. Nonetheless, the clear dysregulation in MuSC number, function, and asymmetric division rationalize the MuSC as a promising therapeutic target to restore myogenic capacity in dystrophic muscles.

2.2.3.2 Animal Models

There are several different animal models of muscular dystrophy that represent the varying manifestations of the disorder based on the partial or total loss of dystrophin[239]. The most commonly used animal model for DMD is the *mdx* mouse, which was first discovered spontaneously in a colony of *C57BL/10ScSn* mice and found to have a nonsense point mutation in exon 23 of dystrophin that aborted full-length dystrophin expression[240,241]. Since then, several chemical variant *mdx* strains were crossed with *C57BL/6* mice to generate *mdx*^{2cv}, *mdx*^{3cv}, *mdx*^{4cv}, and *mdx*^{5cv}, which each carry a different point mutation and manifest similar clinical presentations to each other[242-244]. Although these mice only exhibit a 25% reduction in lifespan, compared to the 75% reduction in DMD patients, these mice model the phenotype of early DMD before the onset of severe symptoms, such as myofiber necrosis, cellular infiltration, high variability in myofiber sizes, and numerous centrally nucleated myofibers[245]. Thus, this model allows the testing of therapeutic interventions applicable to young DMD patients. To represent more severe

manifestations of DMD, double knockout mice (dKO) have also been generated. Namely, utrophin/dystrophin and α7-integrin/dystrophin dKO mice have exhibited marked reductions in lifespan and increased myofiber degeneration compared to traditional *mdx* mice, though they are also more difficult to generate and care for[246-249]. Furthermore, because utrophin and α7-integrin are expressed in a wide variety of tissues other than muscle, there are deficits in various organs that may confound the impacts of muscular dystrophy. More recently, another dystrophic mouse model was generated through double knockout of dystrophin and telomerase, which also show more severe muscle wasting, but may also have off-target effects that are not exhibited by human DMD patients[230,250]. While each of these mouse lines present their own benefits and limitations, it is important to consider using the appropriate strain to address each individual research goal.

2.2.3.3 Current Treatments and Recent Advances

Currently, there is no universal cure for Duchenne muscular dystrophy. Rather, the majority of treatment options include physical therapy, exercise, mobility aids (wheelchairs and walkers), and medication such as corticosteroids to improve muscle regeneration. Because DMD is a genetic disorder, recent therapeutic approaches have focused overwhelmingly on gene therapies to restore the function of dystrophin. There is only one gene-based therapy on the market (Exondys 51) that allows exon skipping to restore the reading frame of exon 51 in the dystrophin gene[251]. However, due to the thousands of different mutant variants in the dystrophin gene, this approach is only applicable for a small subset of DMD patients[210]. Other advances in gene therapy have demonstrated great therapeutic potential, but have so far only led to mild dystrophin restoration and poor improvement in muscle phenotype due to lack of specificity, poor delivery, and low

efficiency[252,253]. For example, adeno-associated virus delivery of CRISPR-Cas9 with guided RNAs to remove exon 23 in *mdx* muscle and restore "mini dystrophin" has shown some benefits, but with limited efficiency[254,255]. Although AAV-mediated approaches have not been effective for MuSCs, lentiviral-mediated gene delivery of mini dystrophin into MuSCs were shown to be sustained for years, implying that MuSCs can be a primary target to improve the long-term efficacy of gene therapy due to their ability to self-renew[256]. Again, however, this approach is confined by a specific mutation in the dystrophin gene and was only effective in a small subset of dystrophic MuSCs, but this can be overcome by transplanting MuSCs with a normal dystrophin gene to restore dystrophin in the engrafted myofiber following myogenic fusion[252].

2.3 Therapeutic Transplantation Models

2.3.1 Muscle Stem Cell Transplantation

Due to the limitations of the current treatments and recent therapeutic approaches for PAD and DMD, researchers have investigated transplantation strategies to functionally repair muscles affected by mitochondrial myopathies. Because MuSCs are critical to skeletal muscle regeneration, they have become a main therapeutic target in the treatment of chronic musculoskeletal disorders that lead to the exhaustion or dysfunction of MuSCs over time. To address the depletion, transplantation of freshly isolated, $Pax7^+$ MuSCs have shown great therapeutic potential to replenish the myogenic pool in ischemic muscles[257]. While direct injection of MuSCs shows promise, major limitations include low cell survival and poor engraftment efficiency despite only requiring a small number of transplanted MuSCs to generate thousands of myonuclei for efficient myofiber repair[258,259].

Furthermore, hypoxic environments and oxidative stress *in vivo*, such as those found in the tissue following ischemic injury, contribute to the cell death of transplanted MuSCs[260]. On the other hand, MuSC transplantation into dystrophic muscles have shown much higher efficiency, contributing to the regeneration of up to 94% of myofibers, restoring dystrophin, and increasing contractile function. These transplanted MuSCs not only remarkably improved myofiber stability and function, but also repopulated the quiescent stem cell pool to facilitate regeneration following subsequent rounds of injury[258]. However, these transplanted MuSCs are confined to the injection sites due to their inability to migrate over long distances. To address this, investigators have used PEG hydrogels as a delivery vehicle for MuSCs to mimic the biomechanics of the MuSC niche and noted significantly enhanced propagation of transplanted MuSCs[261]. By co-delivering MuSCs with Wnt7a in a similar PEG hydrogel, migration of transplanted muscle stem cells was remarkably enhanced to facilitate regeneration in deeper portions of the dystrophic muscle[262]. Moreover, preconditioning of the MuSCs either *in vivo* or *in vitro* has recently been explored to further improve the therapeutic impacts of MuSC transplantation.

Because MuSCs are highly adaptive to stress, preconditioning MuSCs to mild stress may induce epigenetic changes in gene expression to protect against a more severe stress. When the MuSC is exposed to stress, the chromatin of its nucleus is remodeled through histone methylation/acetylation to allow accessibility of transcription factors and DNA binding proteins to various genes that regulate its stress response[263]. For example, preconditioning MuSCs in hypoxic culture (*in vitro* model of ischemic preconditioning) has been shown to improve self-renewal and engraftment efficiency of transplanted cells in ischemic hindlimb muscle[106,264], although the epigenetic changes following

preconditioning have not yet been characterized. Other stem cell types, such as mesenchymal stromal cells, neural stem cells, and cardiac progenitor cells, have also responded positively to ischemic preconditioning in terms of stem cell survival and transplantation efficiency, with HIF-1, heat shock proteins, and mitochondria implicated as important mediators of preconditioning-induced changes[265,266]. Exercise preconditioning is another form of enhancing MuSC transplant efficiency by enriching the mitochondrial content of transplanted cells through the PGC-1α pathway and priming the MuSC to readily activate through the mTORC1 pathway[267,268]. Mitochondria specifically play a critical role in the protection of cells through regulation of reactive oxygen species (ROS) and antioxidant enzymes like SOD1[266,269,270]. Appropriate ROS regulation in mitochondria can effectively protect mesenchymal stem cells and cardiac progenitor cells against consequent injurious oxidative stress induced by severe hypoxia[271,272].

In dystrophic muscle, hypoxic preconditioning is likely not needed due to more effectively regulated oxidative stress compared to ischemic injuries. Rather, correcting the polarity of MuSCs during asymmetric division is a priority. In one study, cells were treated with a MAPK pharmacological inhibitor prior to transplantation to restore the polarity of the engrafted cells during asymmetric division[273]. Another pharmacological agent that could benefit transplanted cells is forskolin, which increases MuSC proliferation and mitochondrial content, improving the number of transplantable MuSCs and allowing pre-treated muscle stem cells to transfer more mitochondria to the engrafted myofiber[274]. Recent breakthroughs in stem cell research also provide another method to maximize the number of transplantable MuSCs. MuSCs derived from embryonic stem cells have demonstrated the ability to engraft effectively in dystrophic muscles to restore dystrophin

and improve contractility[275,276]. To minimize the risk of rejection, autologous transplantation of MuSCs derived from induced pluripotent stem cells (iPSC) has also been explored[275]. Importantly, these iPSCs can be genetically modified to repair the dystrophin gene prior to conversion into MuSCs and transplantation into the muscle, allowing these transplanted cells to simultaneously improve muscle regeneration and restore dystrophin in the engrafted myofiber[253]. Overall, there are several approaches to optimize MuSC transplantation that show therapeutic potential, although more studies need to be conducted to uncover the correct method for each disease model.

2.3.2 Mitochondrial Transplantation and Cell-Based Transfer

In many chronic illnesses where mitochondrial dysfunction is persistent, synthesizing new dysfunctional mitochondria will not compensate for the stress-induced mitochondriopathy. Therefore, transplantation of whole mitochondria into affected tissues to replace or augment damaged mitochondria and restore tissue bioenergetics would be a revolutionary approach when conventional therapies are unsuccessful. While the phenomenon of mitochondrial transplantation dates back to 1982, little research into its therapeutic value has been conducted[277]. In recent years, however, direct injection of isolated mitochondria to ischemic skeletal or cardiac muscle has shown promise in its ability to engraft into the tissue through macropinocytosis and improve functional outcomes by restoring gait patterns, decreasing infarct size, and improving cardiac output[179,278-280]. In stark contrast, other groups have presented opposing results where only few mitochondria were internalized and did not exhibit any change in bioenergetics[281], possibly due to poor quality of the transplanted mitochondria, which demonstrates the need to further investigate mitochondrial transplantation as a potential therapy for mitochondrial

myopathies[281]. Another mechanism through which mitochondria can be transplanted is through cell-based horizontal transfer from one cell to another[282]. Mesenchymal stromal cells, endothelial cells, macrophages, cardiomyocytes, and even muscle stem cells have all exhibited intercellular transfer of their mitochondria to another cell through tunneling nanotubes[283-287]. Intercellular transfer of mitochondria from muscle stem cells into myofibers are distinct from the mitochondrial transfer of other cells though. While most cells transfer mitochondria through tunneling nanotubes between two different individual cells that remain separate, MuSCs transfer their mitochondria to myofiber through cell-cell fusion. However, the role of MuSC-mediated mitochondrial transfer following transplantation has not been investigated. Because of the significant mitochondrial dysfunction in endogenous cells due to high oxidative stress in PAD and calcium overload in DMD, transferring damaged mitochondria from one damaged cell to another is not likely to enrich bioenergetics. However, by transplanting MuSCs with healthy mitochondria into diseased muscle, it is possible to engineer the mitochondrial network of the recipient myofiber by enhancing both myogenic potential and mitochondrial transfer to optimize functional recovery of the tissue.

CHAPTER 3. MUSCLE STEM CELLS INITIATE MITOCHONDRIAL REMODELING OF ISCHEMIC SKELETAL MUSCLE[1]

3.1 Abstract

Ischemic injury as a result of peripheral artery disease leads to extensive damage and alterations to skeletal muscle homeostasis. Although recent research has investigated the tissue-specific responses to ischemia, the role of the muscle stem cell in the regeneration of its niche components within skeletal muscle has been limited. To elucidate the regenerative mechanism of the muscle stem cell in response to ischemic insults, we explored cellular interactions between the vasculature, neural network, and muscle fiber within the muscle stem cell niche. Using a surgical murine hindlimb ischemia model, we first discovered a significant increase in subsynaptic nuclei and remodeling of the neuromuscular junction following ischemia-induced denervation. In addition, ischemic injury causes significant alterations to the myofiber through a muscle stem cell-mediated accumulation of total myonuclei and a concomitant decrease in myonuclear domain size, possibly to enhance the transcriptional and translation output and restore muscle mass. Results also revealed an accumulation of total mitochondrial content per myonucleus in ischemic myofibers to compensate for impaired mitochondrial function and high turnover rate. Taken together, the findings from this study suggest that the muscle stem cell plays a

[1] Adapted from Mohiuddin M, et al. Critical Limb Ischemia Induces Remodeling of Skeletal Muscle Motor Unit, Myonuclear-, and Mitochondrial-Domains. Sci Rep. 2019 Jul 2;9(1):9551. doi: 10.1038/s41598-019-45923-4.

role in motor neuron reinnervation, myonuclear accretion, and mitochondrial biogenesis for skeletal muscle regeneration following ischemic injury.

3.2 Introduction

Peripheral artery disease (PAD) is an age-associated degenerative vascular disease characterized by abnormal perfusion in the limbs due to occlusions of the blood vessels. In its most severe form, referred to as critical limb ischemia (CLI), where blood flow is insufficient to maintain tissue viability, amputation rates can reach up to 50%[288]. While recent regenerative medicine approaches on collateral vessel formation have made some progress, the dysregulation of the skeletal muscle in PAD and the subsequent tissue remodeling have not been thoroughly investigated[202,289,290]. Recent evidence suggests that the ischemia-induced loss of viable muscle tissue, which acts as an indispensable matrix of growth factors and biomechanical support for new vessel formation, may be the cause of failure for current revascularization therapies[41,291]. This paradox emphasizes the importance to elucidate the skeletal muscle regeneration mechanism in complex injuries such as PAD.

Skeletal muscles possess a remarkable regenerative capacity due to the presence of endogenous resident muscle stem cells (MuSCs), also known as satellite cells[46]. Upon injury, $Pax7^+$ quiescent MuSCs, which reside adjacent to basal lamina and sarcolemma of the multinucleated myofiber, undergo asymmetric division in which some committed progenies can either form *de novo* myofibers to generate additional myofibers or proliferate, differentiate, and fuse with existing myofibers to increase the number of myonuclei and volume in regenerating fibers. Meanwhile, other populations of MuSC

progeny self-renew to replenish the quiescent stem cell pool for future rounds of regeneration[52]. Emerging evidence suggests that MuSC function and regenerative capacity are dictated by cellular and acellular interactions with its surrounding microenvironment, or niche, such as the vasculature, neuromuscular junction (NMJ) of a neural network, myofibers, interstitial stromal cells of the extracellular matrix, as well as various infiltrating immune cells[53]. Of these niche components, the vasculature and microvessels are located close to MuSCs and provide necessary nutrients and growth factors required for MuSC function and muscle homeostasis[49]. Blood vessels also carry oxygen and carbon dioxide that are essential for oxidative metabolism throughout the myofibers and within MuSCs to generate energy and regulate redox signaling[292,293]. In addition, vascular networks near MuSCs play a crucial role in recruiting circulating stem cells and transporting immune cells during the initial phase of muscle repair[294,295]. Thus, the lack of functional blood perfusion to skeletal muscle not only disrupts cellular function and respiration by limiting nutrient and oxygen delivery but also compromises muscle regeneration[150].

It has been well documented that motor neuron innervation maintains muscle homeostasis by regulating excitation-contraction coupling as well as controlling the gene expression pattern of myofibers[296]. Denervation of the muscle fiber due to injury or neuromuscular disease results in muscle wasting and remodeling of motor units[297,298]. Anatomically, peripheral nerves, such as lower motor neurons, are located close in contact with the vasculature (neurovascular congruency)[34] and exhibit functional interdependency. In support of this notion, some of the axonal guidance factors are known to possess angiogenic properties[299], and other well-known angiogenic factors, such as vascular endothelial growth factor (VEGF), guide terminal Schwann cell-mediated peripheral nerve

regeneration[300]. As such, when blood flow is restricted in ischemic injury, motor neurons undergo rapid Wallerian degeneration, and their regenerative response is activated[151,153]. Moreover, a recent report showed that the regeneration of the motor neuron and its corresponding neuromuscular synapses are in part linked to an increase in activation of MuSC and myogenesis, supported by the proximity of the MuSC to the NMJ[301]. Conversely, genetic depletion of MuSCs diminishes the regenerative response of the NMJ[48], demonstrating crosstalk between the MuSC and the NMJ. Furthermore, it has been revealed that synaptic mitochondria also play a role in maintaining NMJ[302,303]. While ischemic injury has been linked to excessive generation of the deleterious mitochondrial-derived reactive oxygen species (ROS) that oxidize the NMJ and other niche components of the MuSC, protecting mitochondria against oxidative stress attenuates ischemia-induced denervation and muscle atrophy[151]. Yet, the majority of previous studies have reported tissue-specific interactions in response to ischemic insults (i.e., ischemia – muscle stem cell, ischemia – muscle fiber, ischemia – motor neuron), and a comprehensive investigation elucidating the mechanistic crosstalk between collateral vascularization, motor unit formation, muscle stem cell activation, muscle fiber regeneration, and the mitochondria that drive these energy-demanding processes altogether has not been conducted.

To address this gap in knowledge, we characterized the remodeling of the MuSC niche components, notably the vasculature, NMJ, and myofiber, at various time points to elucidate the sequential regenerative response following ischemia/reperfusion injury. Using the murine hindlimb ischemia (HLI) model that manifests similar pathophysiology as human PAD, here we demonstrate ischemia-induced early necrotic degeneration of muscle fibers and denervation of the NMJ. First, we show that an increase in subsynaptic

nuclei and myonuclei throughout the muscle fiber are driven by proliferation and activation of MuSCs, which facilitate the regeneration of these tissues. Second, the accretion of myonuclei produces a smaller myonuclear domain, or cytoplasmic volume of myofiber transcriptionally governed by each myonucleus, as a regenerative response to ischemia. In parallel, the increased myogenesis and myonuclear number are coupled with an increase in mitochondrial content that is compartmentalized into discrete domains around each myonucleus. Moreover, we show that the high turnover rate of mitochondria through autophagy at early stages of regeneration resets the mitochondrial domain, or the mitochondrial network surrounding each myonucleus. Collectively, this study highlights the highly orchestrated remodeling of the MuSC and its niche components following hindlimb ischemia and provides a basis to investigate multi-scale therapies for complex skeletal muscle injuries.

3.3 Methods

3.3.1 Animal Models

All animal procedures were conducted under the approval of the Institutional Animal Care and Use Committee (IACUC) of the Georgia Institute of Technology and performed in accordance with all relevant guidelines and regulations. All mice in this study were either *C57BL/6J* genetic background or backcrossed with *C57BL/6J* for more than 6 generations and were initially purchased from Jackson Laboratory. Mice were bred and maintained in pathogen-free conditions with a 12-12 light/dark cycle in the Physiological Research Laboratory (PRL) at Georgia Institute of Technology. For muscle stem/satellite cell reporter, mice expressing a tamoxifen-inducible *Cre* from the endogenous Pax7

promoter were bred with mice carrying a loxP-flanked STOP cassette followed by TdTomato in the ROSA26 locus. Alternatively, to deplete muscle stem cells, mice expressing a tamoxifen-inducible *Cre* from the *Pax7* promoter were bred with mice carrying a loxP-flanked STOP cassette followed by diphtheria toxin-A (DTA) in the ROSA26 locus. We also crossed this $Pax7^{Cre}$ transgenic mouse with a mitochondrial reporter, $Rosa26^{HA\text{-}MITO}$, to trace the lineage of muscle stem cell-derived mitochondria through myogenesis and fusion into the myofiber. Other transgenic reporter mice include: *Thy1-EYFP (line 16)* for motor neuron[304], *mitoDendra2* for mitochondria[101,305], *mtKeima* for mitochondrial autophagy[306,307], and $PV\ Cre^{ER}$*; ChR2-EYFP* (tamoxifen-inducible Cre recombinase inserted into PV locus bred with mice carrying a loxP-flanked STOP cassette followed by ChR2-EYFP) for expression of EYFP driven by calcium-binding protein parvalbumin to detect type IIB and IIX fast-twitch fibers[308]. Both males and females aged between 3 and 6 months, considered young adults, were used in a randomized manner for all experiments in this study. No differences in muscle regeneration were observed in response to ischemic injury between 3-month old and 6-month old mice.

3.3.2 Surgical Procedure

To study the effects of peripheral artery disease, we employed a well-characterized murine hindlimb ischemia (HLI) surgical ligation model[309]. Briefly, a small unilateral incision (1 cm long) was made from the ankle to the medial thigh to expose the femoral vessels. The femoral artery and vein were then ligated with 5-0 sutures between the superficial epigastric artery and profunda femoris artery. A second ligation was made proximal to the branching of the tibial arteries, and the segment of vessels between the two ligations was excised. The skin was then closed using both sutures and wound clips. The

sham surgery, where the femoral artery and vein were exposed similar to the method above without ligation or excision, was performed on the contralateral leg. Animals were maintained in single-housed cages for 3-56 days following HLI. Laser Doppler Perfusion Imaging (LDPI) was performed on a MoorLDI Imager at a scan resolution of 210x160 pixels and a height of 21 cm before euthanization by CO_2 inhalation. Perfusion was quantified in the lower hindlimb using MoorLDI Software V5.3.

3.3.3 Histochemistry and Immunostaining

Immediately following euthanization of animals, the tibialis anterior (TA) muscles were either snap frozen in 2-methylbutane cooled by liquid nitrogen for cryosectioning or fixed in 4% paraformaldehyde for single myofiber isolation. Frozen TA muscles were sliced into 10 μm sections while fixed TA was mechanically separated into 20-30 single myofibers per sample from random areas of the muscle. The gastrocnemius was frozen in liquid nitrogen for Western blot analysis while the extensor digitorum longus (EDL) was fixed for immunostaining. Hematoxylin and eosin (H&E) and immunofluorescence were performed as previously described[310]. Materials and antibodies can be found in the appendix for dilution factors, vendors, and catalog numbers of materials. All images were taken on either Zeiss Axio Observer D1 or Zeiss 700 Laser Scanning Confocal microscopes and quantified using ImageJ. Z-stack images were taken to obtain a 3D rendering of myofibers in ImageJ and myofiber volume was approximated as the volume of a cylinder using the average radius along a 500 μm length of the myofiber.

3.3.4 Western Blot Analysis

Gastrocnemii were homogenized with 25 strokes using a 5 mL PTFE tissue grinder with clearance 0.15-0.25 mm (VWR 89026-392, 89026-404) at 3,000 rpm in RIPA lysis buffer (VWR 97063-270) supplemented with Roche cOmplete Mini Protease Inhibitors (Roche 04693124001) and PhosSTOP Phosphatase Inhibitors (Roche 04906837001). Following 3 freeze-thaw cycles in liquid nitrogen and on ice, the samples were centrifuged at 18,400 *g* for 10 minutes, and the supernatants (homogenates) were normalized to total protein concentration using a BCA protein assay kit (Thermo 23225). 50 µg of protein were run through 4-20% Criterion TGX Gels (Bio-Rad 5671093) at 150 V for 185 minutes and transferred to a PVDF membrane using a Trans-Blot Turbo System at 2.5 A for 7 minutes. Ponceau staining (Sigma P7170) was used as a loading control. Antibodies used can be found in the appendix. Membranes were imaged on Li-Cor Odyssey CLx-1050 Infrared Imaging System and bands were quantified on Li-Cor Image Studio V5.2.

3.3.5 RNA Isolation and Quantitative Polymerase Chain Reaction

Using the normalized tissue homogenate prepared for western blot analysis, 50 µL of homogenate was added to 300 µL of RLT buffer supplied in the RNeasy® Mini Kit (Qiagen 74104) supplemented with 1% β-mercaptoethanol to inactivate RNases. The protocol according to Qiagen RNeasy® kit was followed for the remaining RNA isolation steps. The RNA concentration was measured by a NanoDrop One while A260/230 and A260/280 ratios were calculated for quality control. RNA content was then calculated by normalizing the RNA concentration to total muscle mass. To reverse transcribe the RNA to copy DNA, RNA concentrations were normalized to each other and the protocol according to Applied Biosystems High-Capacity cDNA Reverse Transcription Kit (Applied Biosystems 4368814) was followed, and the samples were run in a thermal cycler

according to the recommended conditions. Finally, the Applied Biosystems PowerUp SYBR Green Master Mix (Applied Biosystems A25742) was used with the primers listed in the appendix using an Applied Biosystems StepOnePlus Real-Time PCR system to perform the qPCR reactions. β-actin and B2M, which were found to be stably expressed following ischemia, were used housekeeping genes to quantify relative fold induction.

3.3.6 Mitochondrial Functional Testing

Mitochondria were isolated from lower limb muscles distal to the knee by differential centrifugation. Muscles from each leg were digested with 5 mL dispase II (100 µg/mL) and trypsin (1 mg/mL) in Chappel-Perry buffer (see appendix for detail). The digested tissue was then homogenized, centrifuged at 12,000 *g* for 10 minutes, and resuspended in 5 mL Chappel-Perry buffer II (appendix). The suspensions were then centrifuged at 600 *g* for 10 minutes, and the supernatants subsequently centrifuged at 7,000 *g* to pellet the mitochondria. 300 µg of mitochondria resuspended in respiration buffer (appendix) was used immediately in the Oroboros Oxygraph-2k high-resolution respirometer for basal (state 1) oxygen consumption rate and H_2O_2 generation detected with the Amplex Red assay kit.

3.3.7 Statistical Analyses

Sample sizes were chosen on the basis of preliminary experiments to ensure adequate statistical power using G*Power. All statistical analyses in this study were performed on GraphPad Prism 7 and data is presented as mean ± standard deviation (SD). Data from the contralateral controls did not change over time; therefore, multiple comparison tests for significance were performed between the mean of control and each time point. Normality

of data was tested with the Shapiro-Wilk test. For experiments in which data was collected from different mice over time, a one-way ANOVA with Tukey's *post hoc* test or Kruskal-Wallis test with Dunn's *post hoc* test were used based on whether or not normality can be assumed. A paired two-tailed t-test or Mann-Whitney U test was used to compare the injured hindlimbs to their contralateral controls based on normality. A two-way ANOVA with Tukey's *post hoc* test was performed for experiments with various time points where each ischemic sample was compared to its contralateral control. A *p*-value of less than 0.05 was considered statistically significant.

3.4 Results

3.4.1 Hindlimb Ischemia Induces Skeletal Muscle Regeneration

To investigate morphological changes to the skeletal muscle fibers and muscle stem cell niche following chronic hindlimb ischemia (HLI), we aimed to correlate blood perfusion to muscle regeneration. First, laser Doppler perfusion imaging (LDPI) was used to quantify the abnormal perfusion in the ischemic limb (right-hand side of each scan) to demonstrate a significant decrease in perfusion to the ischemic limb compared to its contralateral control (left-hand side of each scan) at all time points up to 56 days following HLI (Fig. 1A, 1B, 1C). Perfusion did not significantly improve in the ischemic limb until 14 days after injury (Fig. 1C).

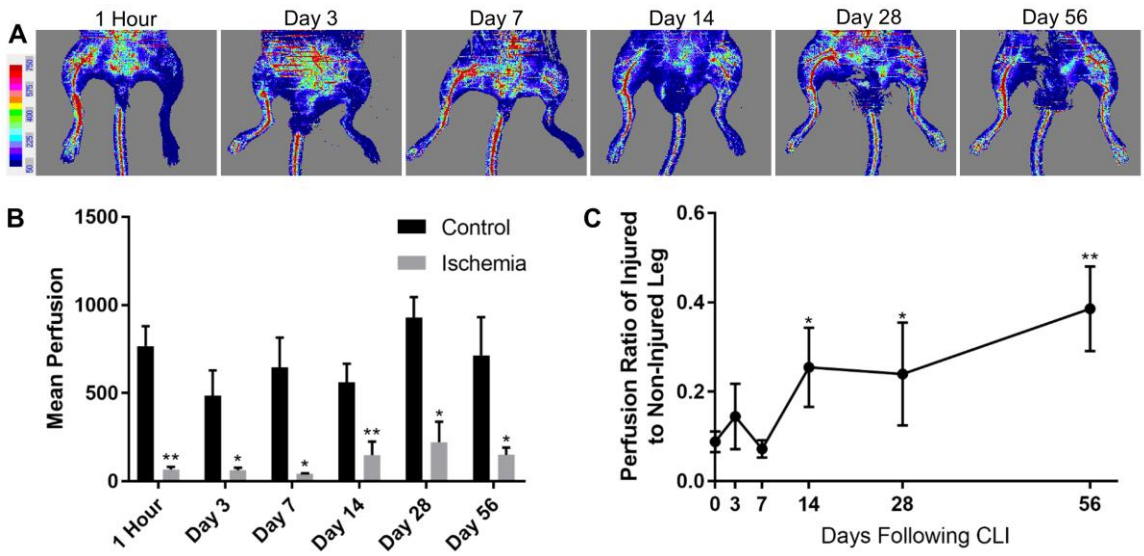

Figure 1. Laser Doppler perfusion imaging following hindlimb ischemia. (A) LDPI of ventral mouse hindlimbs 1 hour, 3 days, 7 days, 14 days, 28 days, and 56 days following CLI. Control leg on left, ischemic leg on right. Scale bar represents blood flow perfusion by color. (B) Mean perfusion to hindlimb distal to the knee in ischemic leg and contralateral control over 56 days. n=6, *p<0.05, **p<0.01 using two-way ANOVA with Tukey's *post hoc* test. (C) Ratio of perfusion in ischemic leg to control over 56 days. n=6, *p<0.05, **p<0.01 compared to day 0 using one-way ANOVA with Tukey's *post hoc* test.

Next, we assessed various parameters of skeletal muscle regeneration to correlate to the perfusion. By first analyzing gross morphology of ischemic muscles, we noted that only the soleus muscle, comprised of primarily slow-twitch myofibers, was decreased at day 7 when normalized to overall body weight, which did not change over 56 days post-HLI compared to initial body weight (Fig. 2A, 2B). We did not observe any other changes in muscle wet weight over 56 days following injury. However, hematoxylin-eosin (Fig. 2C) and immunofluorescent staining (Fig. 2D) of cross-sections from the tibialis anterior muscle (TA) showed extensive myofiber damage, and presence of necrotic fibers markedly increased at days 3 and 7. A high number of nuclei within the interstitial space was also observed at 7 days following HLI, implying immune cell infiltration required for clearance of dead or damaged myofibers[295]. Interestingly, when reperfusion to the ischemic limb

improved at day 14, we found a coinciding peak in embryonic myosin heavy chain (eMHC) positive myofibers (Fig. 2E), a marker for early stages of regeneration[311]. This suggests that sufficient perfusion through collateral vascularization parallels activation and myogenesis of muscle stem cells for muscle regeneration. To further assess myofiber regeneration, we noted a substantial increase in the percentage of centrally nucleated fibers, characteristic of regenerating myofibers, at day 14 that persisted for up to 56 days (Fig. 2F). Furthermore, even though muscle fibers were regenerating, muscle atrophy, as measured by overall fiber cross-sectional area, did not fully recover through at least day 56, suggesting that the functional deficiency may be prolonged following ischemic myopathy (Fig. 2G). Plots of cross-sectional myofiber area distributions for days 14 and 28 following ischemia also demonstrated leftward shifts in the distribution, further indicating atrophied myofibers (Fig. 2H). By measuring the cross-sectional area of only centrally nucleated myofibers, we report a decrease in area of regenerating muscle fibers at days 14 and 28 followed by a subsequent increase in the area by day 56 that is still not fully healed compared to control (Fig. 2I). In accordance with other models of ischemia[150], we observed a delayed regenerative response to ischemia compared to chemical modes of injury such as cardiotoxin and barium chloride, where immune cell infiltration was seen at days 3-4 and both $eMHC^{+}$ and centrally nucleated fibers were decreased by day 14 following injury[312,313]. These data show a delayed ischemia-induced regenerative response of skeletal muscle tissue, dependent on reperfusion to the hindlimb, which continues for at least 56 days.

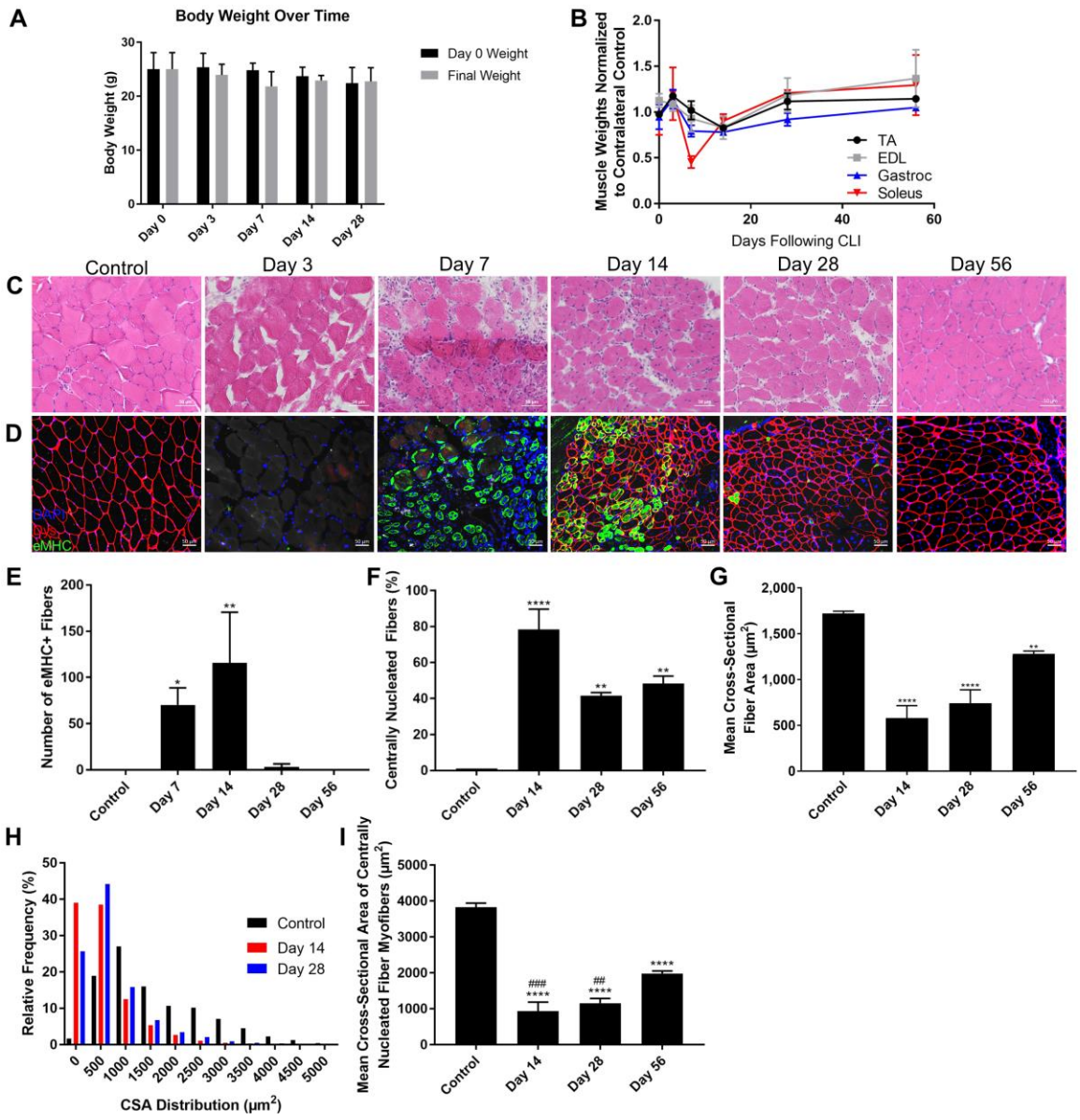

Figure 2. Skeletal muscle regeneration following hindlimb ischemia. (A) Mean body weights of mice before and after HLI at various endpoints. (B) Wet weights of various hindlimb muscles normalized to endpoint body weight over 56 days following ischemic injury. (C) H&E staining of TA cross-sections in control, and 3 days, 7 days, 14 days, 28 days, and 56 days following HLI. (D) Immunohistochemistry of TA cross-sections in control, and 3 days, 7 days, 14 days, 28 days, and 56 days following HLI. Dystrophin pseudo-colored in red, eMHC in green, nuclei in blue. Scale bars on cross-sections represent 50 μm. (E) Total number of eMHC+ fibers within a 0.33 mm^2 field of view for control, 7 days, 14 days, 28 days, and 56 days following HLI. (F) Percentage of centrally nucleated fibers in control, 14 days, 28 days, and 56 days following surgery. (G) Mean cross-sectional fiber area of 4 random 0.33 mm^2 fields of view of the TA using dystrophin in control, 14 days, 28 days, and 56 days following HLI. n=3, $^{*}p<0.05$, $^{**}p<0.01$, $^{***}p<0.001$, $^{****}p<0.0001$ using one-way ANOVA compared to control for all figures.

(H) Distribution of cross-sectional fiber areas in control, 14 days, and 28 days following HLI. (I) Mean cross-sectional area of centrally nucleated myofibers of the TA. n=3, ****p<0.0001 compared to control. $^{\#\#}p$<0.01, $^{\#\#\#}p$<0.001 compared to day 56.

3.4.2 Hindlimb Ischemia Induces Motor Unit Remodeling

In the next set of experiments, we examined the effects of ischemia on motor neuron disruption and subsequent denervation at the neuromuscular junction (NMJ). Given that a decline in innervation and loss of motor units are known causes of muscle degeneration[21], we tested whether denervation plays a role in the ischemia-induced atrophic process. Using a well-established motor neuron reporter mice, in which YFP expression is driven by the *Thy1* regulatory element[304], we observed marked alterations in NMJs in the ischemic extensor digitorum longus muscle (EDL) compared to control (Fig. 3A). Notably, at day 3 and day 7, presynaptic terminals of the motor axons exhibited abnormal thinning and signs of Wallerian degeneration while the postsynaptic endplates were severely fragmented compared to the normal pretzel-like morphology seen at day 0. When muscle fibers are innervated, the presynaptic nerve terminal and postsynaptic acetylcholine receptors (AChR) of the NMJ overlay each other. Hence, to quantify innervation states of the muscle fibers, NMJs of each group were categorized as normal NMJ morphology (pretzel-like, convoluted folding structure with more than 75% overlay), partially denervated (fragmented AChR with between 25% and 75% overlay), or completely denervated (fragmented AChR with less than 25% overlay). Representative images of denervation states are shown in Fig. 3C. Following HLI, we report a decrease in NMJs with normal morphology and an increase in complete denervation in ischemia-affected muscle compared to day 0, with peak denervation observed on day 3. Interestingly, the loss of normal NMJ morphology lasted until at least day 56 (Fig. 3D, 3E). By observing the post-

synaptic endplates (acetylcholine receptors – AchR) on single myofibers randomly isolated from the (TA) muscle, comprised of almost all fast-twitch oxidative-glycolytic (type IIA) and fast-twitch glycolytic (types IIB/X) with few slow-twitch oxidative (type I) fibers[19], we can also investigate the subsynaptic nuclei that are responsible for maintaining and remodeling the NMJ following denervation (Fig. 3B). Despite a transient decrease in subsynaptic nuclei per NMJ at days 3 and 7, which may be attributed to smaller, fragmented NMJs in denervated myofibers[117], we observed a significant increase in the number of subsynaptic nuclei 28 and 56 days following HLI compared to day 0 (Fig. 3F). Intriguingly, the accumulation of subsynaptic nuclei precedes the increase in NMJ area. The increased subsynaptic nuclei also coincide with the regeneration of the NMJ, indicating a dependence of NMJ restoration on the number of subsynaptic nuclei. These data further suggest a persistent functional deficiency in myofiber excitation-contraction coupling and corroborates the continued regeneration of skeletal muscle tissues up to 56 days.

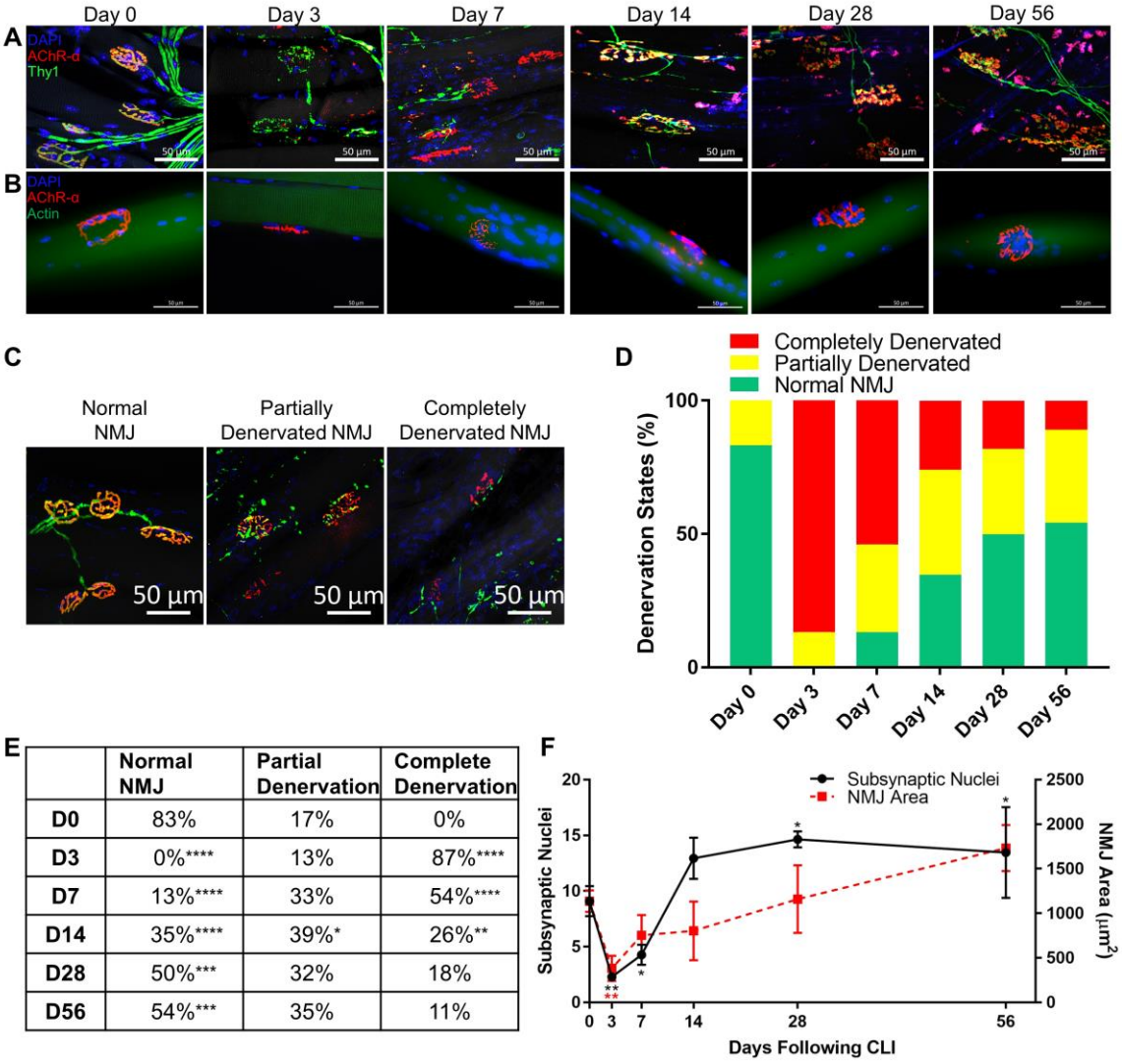

	Normal NMJ	Partial Denervation	Complete Denervation
D0	83%	17%	0%
D3	0%****	13%	87%****
D7	13%****	33%	54%****
D14	35%****	39%*	26%**
D28	50%***	32%	18%
D56	54%***	35%	11%

Figure 3. Remodeling of the motor unit following hindlimb ischemia. (A) NMJ in EDL 1 hour (day 0), 3 days, 7 days, 14 days, 28 days, and 56 days following HLI. Nuclei pseudo-colored in blue, α-bungarotoxin (for acetylcholine receptor-α subunit) in red, Thy1 (for motor neuron axon terminal) in green. Maximum intensity projection was performed on images from confocal microscopy. (B) NMJ on single myofibers from TA from 1 hour (day 0), 3 days, 7 days, 14 days, 28 days, and 56 days following HLI. Nuclei pseudo-colored in blue, acetylcholine receptor-α subunit in red, actin in green. (C) Representative images of normal, partially denervated, and completely denervated NMJ. Acetylcholine receptor-α subunit (α-bungarotoxin) pseudo-colored in red, Thy1 in green. (D) Percentages of normal, partially denervated, and completely denervated NMJ in EDL (at least 20 NMJs per sample) 1 hour (day 0), 3 days, 7 days, 14 days, 28 days, and 56 days following CLI. (E) Average data values of NMJ denervation states as shown in Fig. 2c with significant differences compared to day 0 denoted by asterisks using two-way ANOVA. (F) Number of subsynaptic myonuclei within each NMJ (at least 15 NMJ's per sample) and their associated NMJ areas of single myofibers from the TA. All scale bars represent 50 µm.

n=3, *p<0.05, **p<0.01, ***p<0.001, ****p<0.0001 using one-way ANOVA compared to day 0 for all figures.

It is also worth noting that since fiber type is in part determined by innervation from a specific motor neuron type, alteration in the motor unit organization may lead to a shift in fiber type[26]. Indeed, we observed an ischemia-induced loss of slow-twitch type I fibers 14- and 28-days following injury while percentages of fast-twitch type IIA and types IIB/X fibers were unchanged (Fig. 4A, 4B, 4C). Slow-twitch type I fibers rely on oxidative metabolism and are high in mitochondrial content. Thus, the loss of these fibers indicate that these oxidative fibers and their mitochondria that govern oxidative phosphorylation are particularly susceptible to ischemia-induced damage. Together, these results suggest that ischemia-induced denervation plays a role in muscle atrophy, and the generation of subsynaptic nuclei assists in the repair of denervated NMJs and remodeling of the motor unit for up to 56 days following HLI.

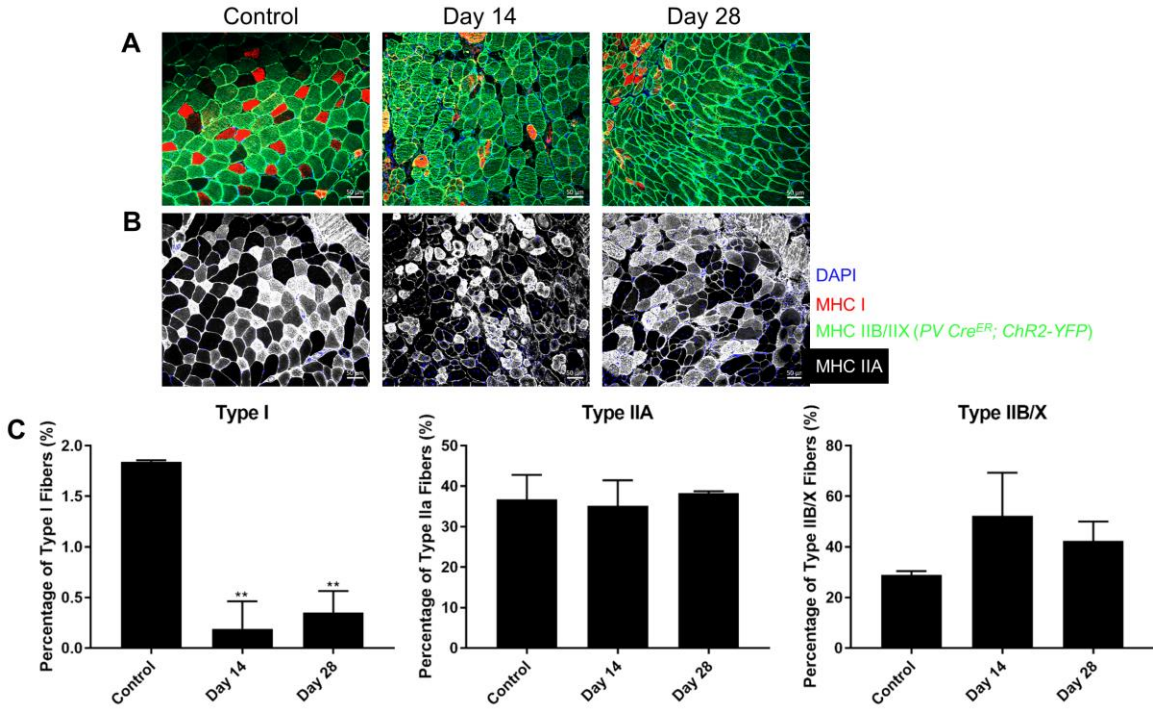

Figure 4. Fiber type shifting following hindlimb ischemia. (A) TA cross-sections of *PV-Cre; ChR2-YFP* mice for expression of fiber type IIB/IIX (MHC IIB/IIX) and stained for fiber type I (MHC I) in control, 14 days, and 28 days following HLI. Nuclei pseudo-colored in blue, MHC I in red, and MHC IIB/IIX in green. (B) TA cross-sections of wildtype mice stained for fiber type IIA (MHC IIA) in control, 14 days, and 28 days following HLI. Nuclei pseudo-colored in blue, MHC IIA in white. Scale bars represent 50 μm. (C) Percentages of type I, IIA, and IIB/X fibers, respectively. n=3, $^{**}p<0.01$ using one-way ANOVA compared to control.

3.4.3 Muscle Stem Cells Decrease Myonuclear Domain Following Hindlimb Ischemia

To further elucidate the role of MuSCs, myogenesis, and myonuclear number in the regenerative process of the ischemic myopathy, we examined changes to myonuclear content throughout the entire myofiber after ischemia. To achieve this, single myofibers were isolated (Fig. 5A) and as seen in immunohistochemistry images, ischemic fibers were centrally nucleated. Myonuclei were assembled into longitudinal rows along the center of the myofiber, notably at days 7 and 14, characteristic of newly fused myonuclei originating from differentiated MuSCs[314]. Surprisingly, despite the degeneration of muscle tissue following ischemic injury, a substantial increase in myonuclei number was observed at day 7 that prevails for at least 56 days (Fig. 5B). In addition, we assessed alterations in the myonuclear domain, defined as the cytoplasmic volume of myofiber transcriptionally governed by each myonucleus. By taking z-stack images on a confocal microscope and finding the average radius of the myofiber, the myofiber volume can be approximated as a cylinder. The myonuclear domain is then quantified as the total volume of the myofiber divided by the number of myonuclei within the myofiber. Interestingly, the size of the myonuclear domain was significantly decreased at 7- and 14-days following injury (Fig. 5C), likely as a regenerative response to ischemia in order to enhance transcriptional

regulation of the myofiber cytoplasm within its domain, but returns to normal after the tissue perfusion had improved. Consistent with these data, the total amount of RNA isolated from ischemic muscle homogenate was significantly higher at days 7 and 14 compared to control (Fig. 5D).

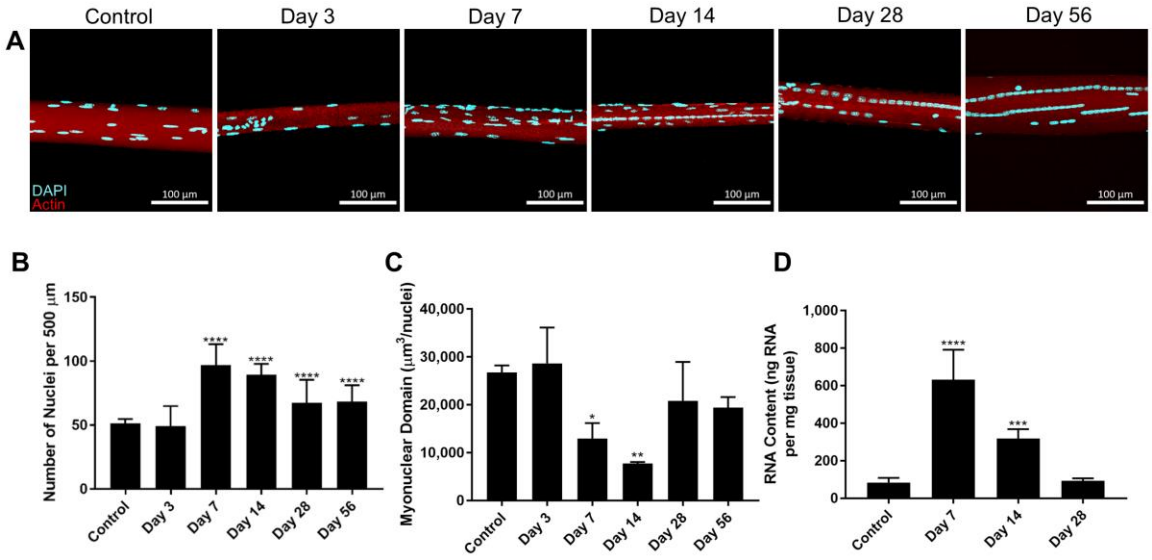

Figure 5. Changes in myonuclear domain following hindlimb ischemia. (A) Z-stack confocal imaging of single myofibers from TA of control, 3 days, 7 days, 14 days, 28 days, and 56 days following HLI. Nuclei pseudo-colored in light blue, actin in red. (B) Number of myonuclei per 500 µm of myofiber (at least 20 fibers per sample) at various timepoints (n=6). (C) Myonuclear domain of at least 20 single myofibers per sample over 500 µm at various timepoints, calculated as myofiber volume divided by number of myonuclei. Myofiber volume was approximated as the volume of a cylinder using the average radius along a 500 µm length of myofiber (n=6). (D) Total isolated RNA levels in gastrocnemius homogenate normalized to muscle mass. All data is presented as mean ± standard deviation. $^{*}p<0.05$, $^{**}p<0.01$, $^{***}p<0.001$, $^{****}p<0.0001$ using one-way ANOVA compared to control for all figures.

Since myofibers are multinucleated syncytia formed by the fusion of the differentiated myotubes[52], we then investigated the frequency of MuSCs following ischemia to ascertain the origin of the accreted myonuclei in the MuSC niche. To explore MuSC frequency, we isolated single myofibers from a tamoxifen-inducible MuSC reporter mouse we generated by crossing *Pax7 Cre^{ER}* with *ROSA26-tdTomato* mice (Fig. 6A). As

hypothesized, we observed a substantial increase in quiescent $Pax7^+$ MuSC content at days 7 and 14 following ischemia, with a peak at day 7 that accompanies the accretion of myonuclei and a concomitant decrease in the myonuclear domain (Fig. 6B). Because Pax7 is a canonical marker for quiescent MuSC[52], the greater frequency of $Pax7^+$ cells implies that MuSCs have undergone adult myogenesis and asymmetric division to increase self-renewal of MuSCs following ischemia to replenish the pool of quiescent MuSCs to continue regenerating and for future rounds of regeneration. Furthermore, the increased number of myonuclei also indicates active differentiation and fusion events of MuSCs into the myofiber following claudication of muscle, further supported by the augmented embryonic myosin heavy chain expression at day 14. Taken together (Fig. 6C), these data demonstrate that HLI muscle exhibit considerable MuSC-dependent remodeling of the myonuclear domain to enhance the transcriptional and translation output of the newly formed myofiber and restore muscle mass following injury.

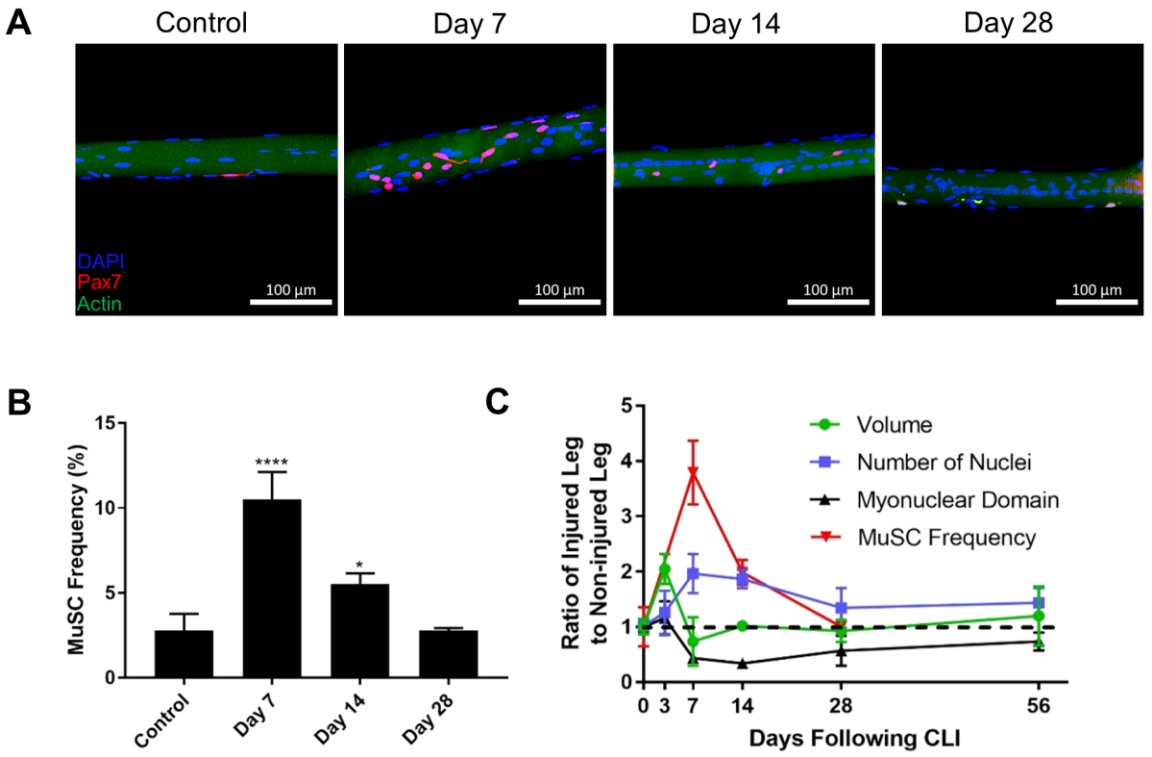

Figure 6. Ischemic muscle stem cells proliferate to increase myonuclear number. (A) Z-stack confocal imaging of single myofibers from TA of Pax7-TdTomato mice control, 7 days, 14 days, and 28 days following HLI. Nuclei pseudo-colored in blue, Pax7 in red, actin in green. All scale bars represent 100 µm. Maximum intensity projection performed on all z-stack images (n=3). (B) MuSC frequency of at least 20 single myofibers per sample at various timepoints reported as percentage of $Pax7^+$ cells out of total myonuclei (n=3). $^*p<0.05$, $^{****}p<0.0001$ using one-way ANOVA compared to control for all figures. (C) Myofiber volume, myonuclei number, myonuclear domain, and MuSC frequency as a ratio of ischemic to control myofiber. Dashed line represents a ratio of 1.

The *Pax7-tdTomato* transgenic mouse model also allows detection of MuSCs undergoing myogenesis to fuse with existing myofibers or form *de novo* myofibers by quantifying the number of $tdTomato^+$ myofibers[49]. Indeed, we observed substantial MuSC fusion into myofibers at day 14 following ischemia (Fig. 7A, 7B). Interestingly, all centrally nucleated myofibers were $tdTomato^+$, consistent with previous literature that has demonstrated that centrally located myonuclei are derived from differentiated MuSCs[314]. Conversely, to deplete MuSCs before the ischemic injury, we generated a different

tamoxifen-inducible mouse model by crossing *Pax7 Cre*^{ER} with *ROSA26-diphtheria toxin-A*. Without MuSCs, the soleus muscle, predominantly composed of slow-twitch type I myofibers[19], was unable to regenerate 28 days following injury (Fig. 7C), suggesting that proliferation and fusion of MuSCs into the ischemic myofiber as new myonuclei are required for effective muscle regeneration following HLI.

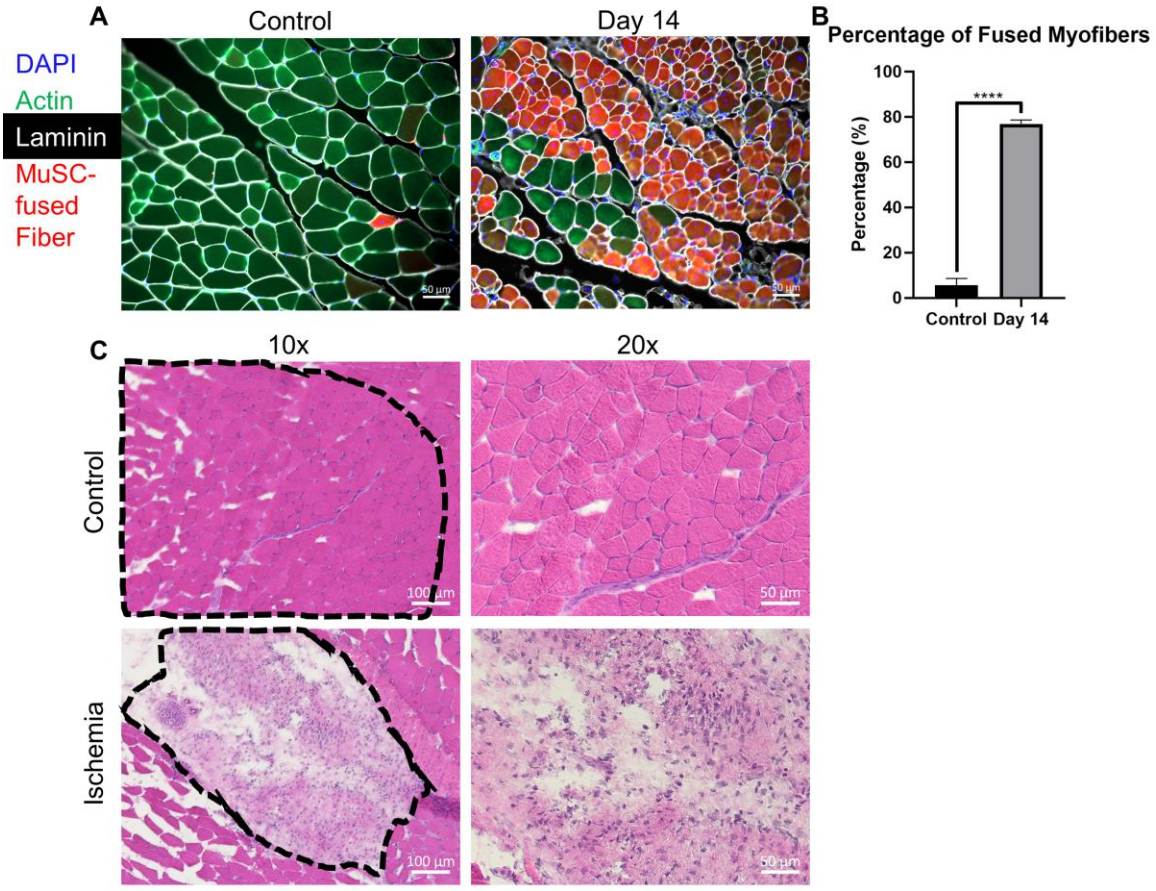

Figure 7. Muscle stem cell fusion following hindlimb ischemia and myofiber damage in soleus of muscle stem cell depleted transgenic mice. (A) Representative images of immunostained gastrocnemius muscle in *Pax7-tdTomato* transgenic mice 14 days following ischemic injury. Nuclei pseudo-colored in blue, actin in green, laminin in white, and MuSC-fused myofibers in red. (B) Quantification of the number of MuSC-fused myofibers 14 days following ischemic injury. n=3, ****p<0.0001 using a t-test compared to control. (C) Representative images of hematoxylin and eosin staining of soleus of *Pax7-DTA* transgenic mice, in which muscle stem cells are depleted. Soleus muscle is demarcated by the dashed outline and shows extensive myofiber damage following ischemic injury without muscle stem cells.

3.4.4 Mitochondrial Network Remodels Following Hindlimb Ischemia

Another critical component of muscle repair is the bioenergetics of regenerating myofibers[315]. Muscle regeneration is a highly energy-dependent process, and an increase in mitochondrial content usually couples with adult myogenesis[88,316,317]. Moreover, since mitochondrial DNA accounts for only 13 of the proteins that constitute mitochondria while over 99% of mitochondrial proteins are nuclear-encoded[87], we examined changes in mitochondrial to myonuclear ratio. To this end, we isolated single myofibers from reporter mice expressing a mitochondrial-targeted fluorescent protein (Dendra2)[305] and imaged the myofibers on a confocal microscope with a constant gain and laser power to delineate relative mitochondrial content of the myofiber (Fig. 8A). In control samples, we noted local mitochondrial networks as punctate and segregated into columns along the Z-line of the myofiber contractile apparatus. At 7 days post-HLI, however, mitochondrial networks in ischemic myofibers spanned several sarcomeres (Fig. 8A)[101]. The reticulum of mitochondria is observed again at 14 and 28 days following HLI. Surprisingly, we found high mitochondrial densities found between the centralized nuclei at later time points, indicated by the red arrowheads (Fig. 8A), suggesting that the new mitochondria are synthesized by the MuSC-derived myonuclei. Because mitochondria are typically compartmentalized to discrete domains centered around their nuclei of origin[101], we then quantified mitochondrial domain, or relative mitochondrial volume per myonucleus, as a metric to describe changes in the mitochondrial network surrounding each myonucleus. Although there is no change in mitochondrial domain detected at 7- and 14-days following ischemia when the myonuclear domain is at its smallest, we observed an ensuing dramatic

increase in mitochondrial domain 28 days following HLI, after myonuclear domain size has returned to normal, but myonuclei number is still elevated (Fig. 8E). Furthermore, to support this striking increase in mitochondrial content, we also quantified relative mtDNA copy number, which correlates with mitochondrial biogenesis[318]. To measure mtDNA copy number[319,320], we determined the mtDNA/nDNA ratio by quantifying the expression of an mtDNA-encoded mitochondrial gene, *mt-Co1*, relative to a nuclear-encoded mitochondrial gene, *Sdha*[321]. In parallel with the increased mitochondrial content observed in single myofibers isolated from *mitoDendra2* transgenic mice, mtDNA copy number is significantly upregulated 28 days following ischemic injury (Fig. 8F). This increased mitochondrial content and mtDNA expression at 28 days insinuate greater mitochondrial biogenesis in regenerating myofibers, particularly near the MuSC-derived centrally located myonuclei. To directly track mitochondria stemming from MuSCs, we generated a transgenic mouse model for lineage tracing of mitochondria derived from Pax7-expressing MuSCs (*Pax7*$^{Cre\text{-}ER}$ crossed with *Rosa26*$^{HA\text{-}MITO}$)[322]. 28 days following ischemic injury, isolated myofibers portrayed the interfibrillar MuSC-derived mitochondria as a landscape similar to the total mitochondria seen in our mitoDendra2 transgenic model with distinguishable mitochondrial densities between centrally located myonuclei (Fig. 8G), indicating that MuSCs and MuSC-derived myonuclei are responsible for restoring the mitochondrial network following hindlimb ischemia.

To test whether this increase in mitochondria was a compensatory response to prior mitochondrial damage, we employed the mitochondrial-targeted Keima (mtKeima) transgenic mouse model to delineate mitochondrial autophagy or mitophagy. Keima is a pH-dependent fluorescent protein that when targeted to the mitochondria can be used to

assess relative quantities of healthy and dysfunctional mitochondria[307]. At the healthy, physiological pH of mitochondria (pH 7.4), the Keima protein exhibits fluorescence with an excitation wavelength of 488 nm and depicts a green signal (Fig. 8B). However, when mitochondria are dysfunctional and selectively degraded by the lysosome through mitophagy, the acidic environment (pH 4.5) shifts the excitation wavelength of the Keima protein to 555 nm to display a red signal (Fig. 8C)[307]. By merging the two channels after confocal imaging of isolated myofibers, relative levels of healthy and autophagic mitochondria within the skeletal muscle after an ischemic injury can be observed by quantifying the mean fluorescent intensity of each signal (Fig. 8D). Consistent with mitoDendra2 data, isolated myofibers from mtKeima mice 14 days following HLI demonstrate high autophagic mitochondrial density between centrally located myonuclei, demarcated by the white arrowheads, implying that the newly synthesized mitochondria are dysfunctional and degraded through mitophagy. However, 28-day samples exhibit increased healthy mitochondrial density between centrally located myonuclei, indicating that most of these newly synthesized mitochondria are functional. Compared to the relative levels of mitophagy and healthy mitochondria in uninjured control (red:green ratio), there is a dramatic increase in mitophagy up to 14 days after ischemic injury while the relative number of healthy mitochondria remains unchanged (Fig. 4g, h). However, by day 28, mitophagy decreases, and there is a substantial accumulation of healthy mitochondria in order to restore the physiological ratio of autophagic to healthy mitochondria (Fig. 4g, h). These results suggest high rates of mitochondrial turnover in conjunction with increased mitochondrial biogenesis through 28 days following hindlimb ischemia.

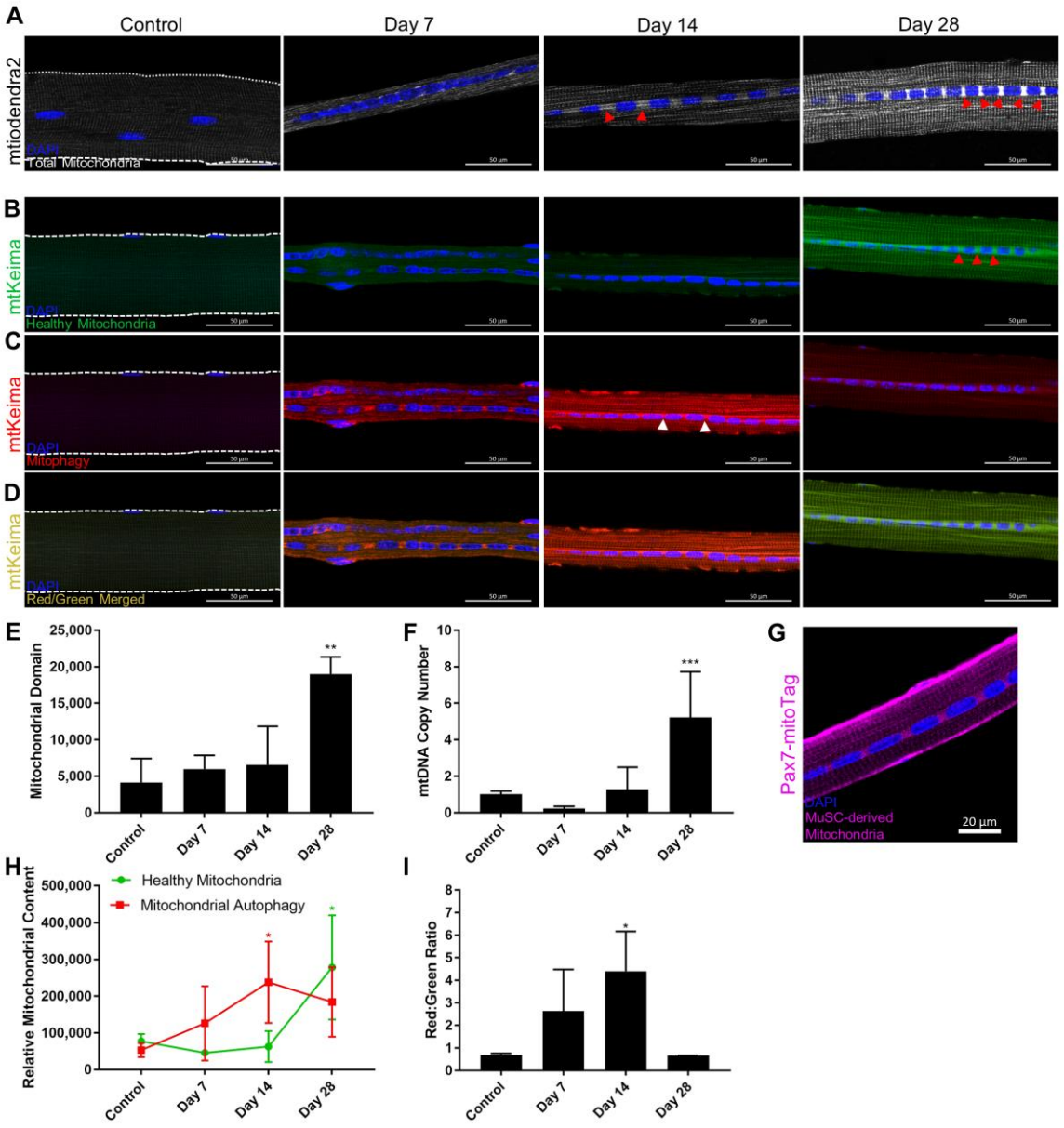

Figure 8. Changes in mitochondrial domain following hindlimb ischemia. (A) Confocal imaging of single myofibers from TA of mitoDendra2 mice control, 7 days, 14 days, and 28 days following HLI using constant gain and laser power. Nuclei pseudo-colored in blue, mitochondria in white. Red arrowheads indicate areas of high mitochondrial density. (B) Confocal imaging of single myofibers from TA of mtKeima mice in 488nm channel to delineate healthy mitochondria. (C) Confocal imaging of single myofibers from TA of mtKeima mice in 555nm channel to delineate Mitophagy. (D) Merged images of mtKeima myofibers in green (B) and red (C) channels to portray relative levels of healthy to autophagic mitochondria. Scale bars represent 50 µm. (E) Mitochondrial domain of at least 20 single myofibers per sample at various timepoints calculated as relative integrated fluorescent density of total mitochondria in mitoDendra2 mice divided by the number of myonuclei (n=3). (F) Relative mtDNA copy number

quantified as expression of mitochondrial-encoded *mt-Co1* normalized by expression of nuclear-encoded *Sdha* (n=3). (G) Representative confocal image of single myofiber from TA of Pax7-mitoTag mice to delineate myonuclei (blue) and MuSC-derived mitochondria (purple). Scale bar represents 20 μm. (H) Relative mitochondrial content of healthy and autophagic mitochondria of at least 20 myofibers per sample in mtKeima mice calculated as mean fluorescent intensity of each fiber (n=3). (I) Red to green ratio of myofibers in mtKeima mice to represent mitochondrial autophagy to healthy mitochondria (n=3). *p<0.05, **p<0.01, ***p<0.001 using one-way ANOVA compared to control for all figures.

3.4.5 Mitochondrial Membrane is Altered Following Hindlimb Ischemia

In order to determine a potential mechanistic link between high mitochondrial turnover and muscle stem cell-derived mitochondrial network remodeling, we next investigated protein expression of OPA1, a nuclear-encoded dynamin-like GTPase that plays an imperative role in the fusion of the inner mitochondrial membrane and stabilization of the cristae ultrastructure[323-325]. An OPA1 precursor containing a mitochondrial targeting sequence is imported into the mitochondrion and proteolytically cleaved into the long (L-OPA1) isoform and anchored to the inner membrane[326]. While L-OPA1 is then subsequently processed into the short (S-OPA1) isoform in the matrix and translocated to the intermembrane space[327], a critical balance of both isoforms is necessary for functional mitochondrial fusion dynamics[328]. Western blot analyses demonstrated considerably diminished protein expression levels of both L-OPA1 (Fig. 9A, 9D, 9E) and S-OPA1 (Fig. 9B, 9D, 9E) at 7 and 14 days post-HLI. The decreased OPA1 content of both isoforms at days 7 and 14, coinciding with high levels of mitophagy at these time points, suggests that OPA1 plays a role in the elevated mitochondrial turnover due to impaired mitochondrial dynamics. Interestingly, when *Opa1* gene expression is substantially

upregulated by day 28 (Fig. 9C), OPA1 protein levels recover, and the ratio of mitophagy to healthy mitochondria is restored. Furthermore, prohibitin 2 (PHB2), a multi-functional mitochondrial scaffolding protein localized in the inner membrane, is essential for proper cleavage of OPA1 into the L-OPA1 isoform[92]. We observed PHB2 protein significantly elevated at day 14 (Fig. 9F, 9I, 9J), while *Phb2* gene expression is downregulated (Fig. 9G). Since PHB2 import into the mitochondria is dependent upon the maintenance of mitochondrial membrane potential, in severely damaged muscle, PHB2 is unable to target depolarized mitochondria and regulate the cleavage of OPA1 appropriately[92], further suggesting that ischemia induces damage to mitochondria. Intriguingly, prohibitin 1 (PHB1), which is known to modulate mitophagy following oxidative stress[329], exhibited a striking upregulation in gene expression at 14 and 28 days after ischemic injury (Fig. 9H), indicating that PHB1 may contribute to the functional cleavage of OPA1 by day 28 to compensate for the altered PHB2 expression. Overall, these findings indicate that OPA1, PHB2, and PHB1 are key processes that resolve mitochondrial dysfunction and augment mitochondrial dynamics following HLI.

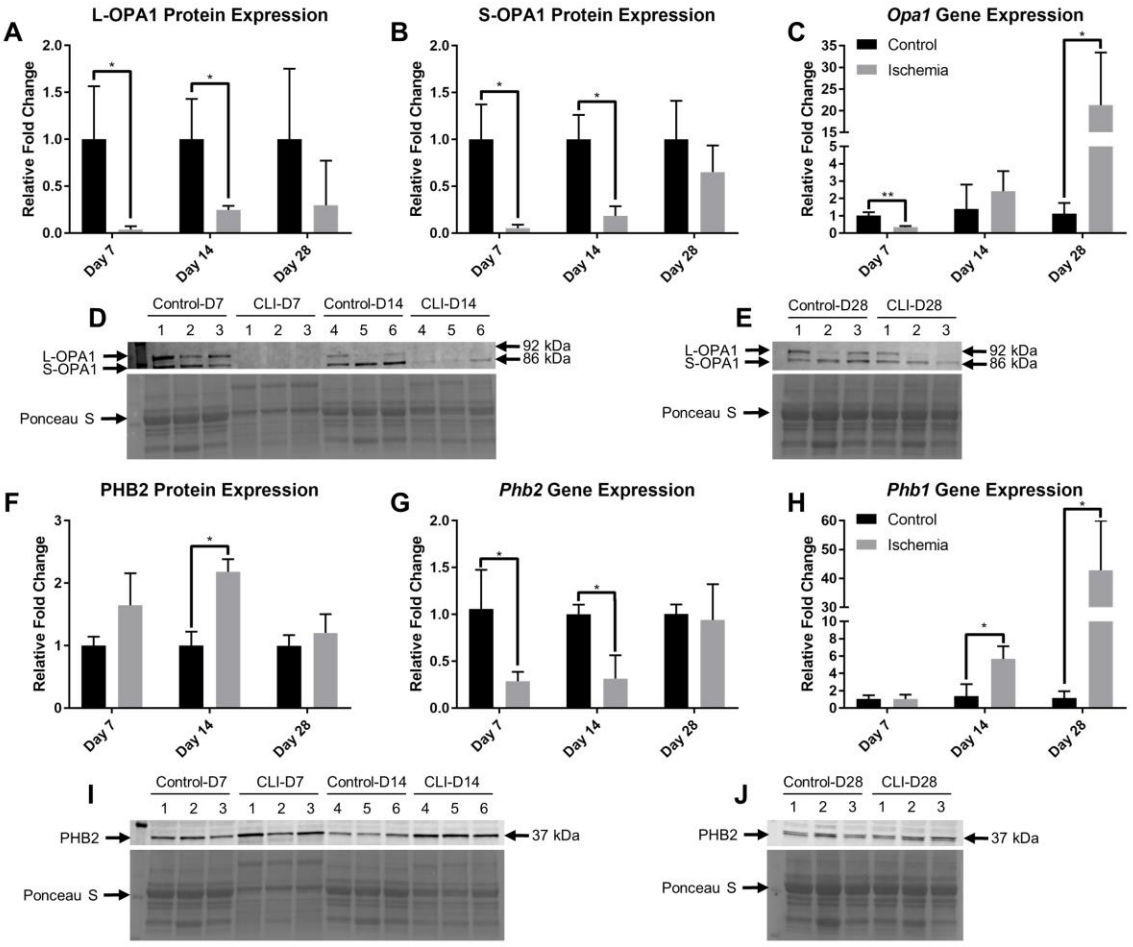

Figure 9. Altered mitochondrial membrane protein expression after hindlimb ischemia. (A) Quantified Western blot analyses 7, 14, and 28 days following CLI for the long isoform of OPA1 protein expression (n=3). (B) Quantified Western blot analyses 7, 14, and 28 days following HLI for the short isoform of OPA1 protein expression (n=3). (C) Relative gene expression of *Opa1* 7, 14, and 28 days following critical limb ischemia (n=3). (D) Western blot analyses 7 days and 14 days following HLI for long (L-) and short (S-) isoforms of OPA1 and Ponceau S as loading control (n=3). (E) Western blot analyses 28 days following HLI for long (L-) and short (S-) isoforms of OPA1 and Ponceau S as loading control (n=3). (F) Quantified Western blot analyses 7, 14, and 28 days following HLI for prohibitin 2 protein expression (n=3). (G) Relative gene expression of *prohibitin 2* 7, 14, and 28 days following HLI (n=3). (H) Relative gene expression of *prohibitin 1* 7, 14, and 28 days following HLI (n=3). (I) Western blot analyses 7 days and 14 days following HLI for PHB2 and Ponceau S as loading control (n=3). (J) Western blot analyses 28 days following HLI for PHB2 and Ponceau S as loading control (n=3). *$p<0.05$, **$p<0.01$ using multiple t-tests compared to control for all figures. Black bars represent control and gray bars represent hindlimb ischemia for all figures.

3.4.6 Mitochondrial Function is Impaired after Hindlimb Ischemia

Because mitochondrial dynamics are regulated by redox state[330], we next investigated alterations to mitochondrial oxidative phosphorylation and ROS generation by performing functional analyses and measuring levels of various proteins associated with mitochondria at days 7, 14, and 28. We analyzed the bioenergetic function of isolated mitochondria at day 7 by measuring basal (State 1) respiration. The basal oxygen consumption did not reach a statistical difference. However, in State 1, mitochondrial emission of H_2O_2 was ~3-fold higher in ischemic muscle compared to contralateral control (Fig. 10A)[140]. To further assess mitochondrial function, Western blot analyses (Fig. 10B, 10C, 10D) for the electron transport chain complexes also revealed that subunits of complexes I, II, and IV at day 7 and complex II at day 14 were significantly declined, suggesting a potential disruption in mitochondrial bioenergetics and concomitant release of ROS following ischemia and reperfusion. However, by day 28, the expression of all electron transport chain complexes returned to control (Fig. 10B, 10D). Furthermore, the protein levels of key antioxidant enzymes that convert the highly reactive superoxide into the H_2O_2 signaling molecule, SOD2 (MnSOD) in the mitochondrial matrix and SOD1 (CuZnSOD) in the intermembrane space and cytosol, exhibited no change in SOD2 content, but a significant decrease in SOD1 content on day 14 (Fig. 10E, 10F, 10G). Finally, the amount of the oxygen-binding protein myoglobin, typically correlated with mitochondria content[331], was decreased at day 14, supporting the loss of myoglobin-rich type I fibers following ischemia and suggesting decreased oxygen utilization and high mitochondrial turnover in the ischemic muscle (Fig. 10E, 10H). Taken together, these results demonstrate a novel finding that an ischemia-induced mitochondrial dysfunction is

strongly coupled with MuSC-induced mitochondrial domain remodeling and mitochondrial biogenesis to restore skeletal muscle bioenergetic function in the newly regenerated myofibers.

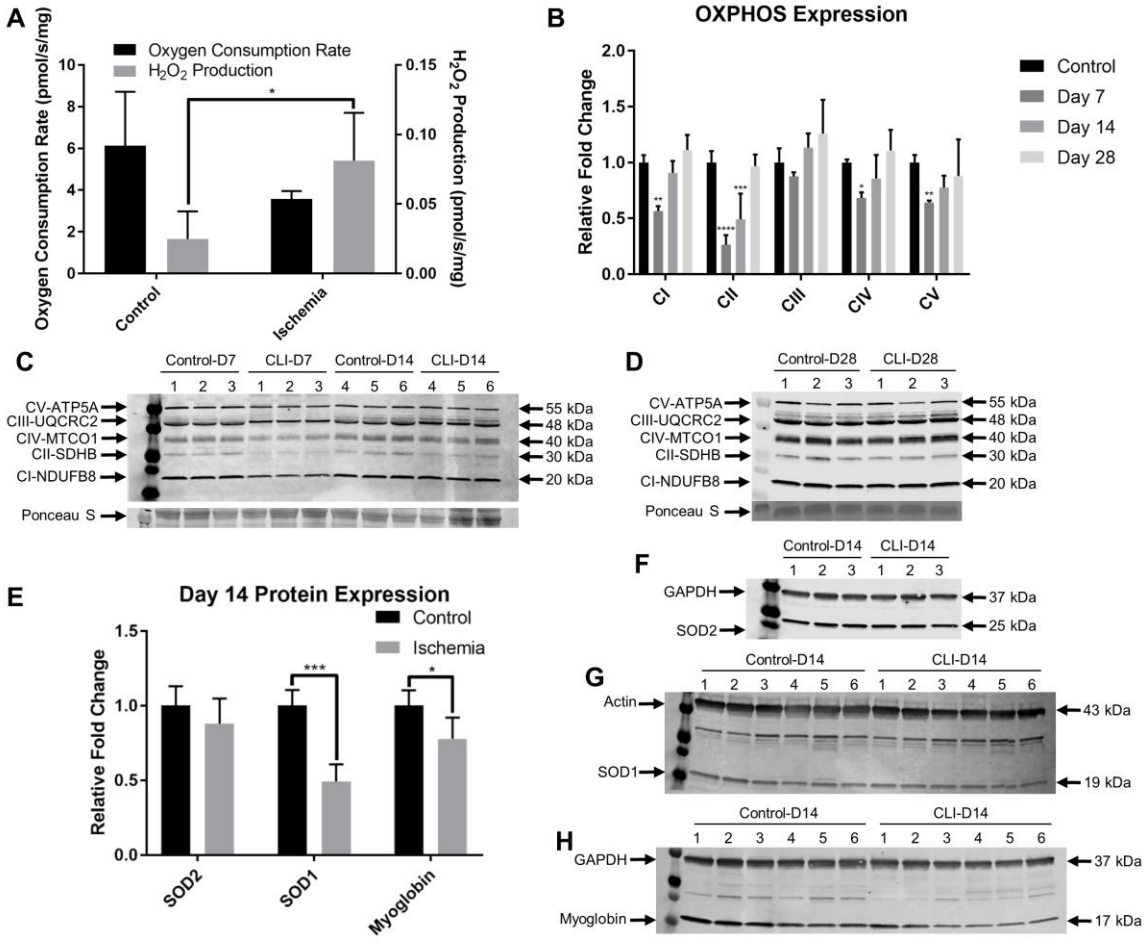

Figure 10. Impaired mitochondrial function following hindlimb ischemia. (A) Basal (state 1 respiration) oxygen consumption rate and mitochondrial hydrogen peroxide (H_2O_2) production from hindlimb skeletal muscles 7 days following HLI using Oroboros Oxygraph-2k (n=3). (B) Quantified Western blot analyses 7, 14, and 28 days following CLI for mitochondrial ETC complex I (NDUFB8-subunit), complex II (SDHB-subunit), complex III (UQCRC2-subunit), complex IV (MTCO1-subunit), and complex V (ATP5A-subunit) relative protein expression (n=3). (C) Western blot analyses 7 days and 14 days following HLI for mitochondrial ETC complexes and Ponceau S for loading control (n=3). (D) Western blot analyses 28 days following CLI for mitochondrial ETC complexes and Ponceau S for loading control (n=3). (E) Quantified Western blot analyses 14 days following HLI for SOD2 (n=3), SOD1 (n=6), and myoglobin (n=6) protein expression. (F) Western blot analyses 14 days following HLI for SOD2 and GAPDH as loading control (n=3). (G) Western blot analyses 14 days following HLI for SOD1 and actin as loading

control (n=6). (H) Western blot analyses 14 days following HLI for myoglobin and GAPDH as loading control (n=6). 3 or 6 representative biological samples for each blotted protein are shown and each protein blot was conducted on the same gel and membrane. *p<0.05, **p<0.01, ***p<0.001, ****p<0.0001 using multiple t-tests for panels A and E, one-way ANOVA for individual complexes in panel B compared to control for all figures.

3.5 Discussion

In the present study, we report hindlimb ischemia-induced remodeling of various niche components of the MuSC, particularly the neuromuscular junction of the motor unit, myonuclear number, and mitochondrial content of the myofiber. Due to the delayed regenerative response of skeletal muscle as a result of the abnormal perfusion to the tissues, we observed incomplete regeneration of the MuSC niche components for up to 56 days. Specifically, myofibers were still centrally nucleated while NMJs were incompletely reinnervated for at least 56 days. Ischemia-induced denervation at early time points resulted in a subsequent reorganization of the motor units that were associated with a loss of slow-twitch, type I fibers at days 14 and 28. Moreover, the increase in subsynaptic nuclei that maintain the NMJ synaptic transmission following ischemia supports the notion that MuSCs play a role in the repair of the NMJ[301]. In parallel, the MuSC-mediated increase in number of the myonuclei within a muscle fiber and its concomitant decrease in myonuclear domain, or cytoplasmic volume governed by each myonucleus, are likely a part of the repair mechanism of skeletal muscle in order to restore the transcriptional and translational output of contractile and structural components of regenerating myofibers. The smaller myonuclear domain following an ischemia-induced fusion of MuSCs into damaged fibers also allows enhanced expression of transcripts required for mitochondrial and myofibrillar

network remodeling. We also demonstrate for the first time that ischemia/reperfusion-induced changes in the myonuclear remodeling are significantly correlated with the mitochondrial content adjacent to centrally located myonuclei, known as the mitochondrial domain, to potentially support the high energy demands of the regenerating tissues and remodel the mitochondrial reticulum of the myofibers.

In order to gain a more comprehensive understanding of mitochondrial biogenesis during ischemia/reperfusion-induced skeletal muscle regeneration, it is necessary to determine the origin of the accumulated mitochondria. While 13 proteins of the mitochondrial electron transport chain are encoded by mtDNA, thousands of mitochondrial proteins are nuclear-encoded and need to be imported into the mitochondria[87], illustrated by the high mitochondrial density localized adjacent to myonuclei. For example, a scaffold protein known as OPA1, which is encoded in the nuclear genome but contains a mitochondrial targeting sequence, maintains the cristae organization and plays a major role in mitochondrial dynamics by regulating fusion of the inner membrane[323-325]. Based on the findings from this study, there are several possible explanations for the increase in mitochondrial content. First, oxidative stress and ROS may directly upregulate the genes required for mitochondrial dynamics (fusion and fission)[332]. Because mitochondrial fission of damaged fragments is a requirement of mitochondrial autophagy[104], there may be an increase of fission events in myofibers following hindlimb ischemia. However, the diminished levels of OPA1, required for mitochondrial fusion[323-325], and the sensitivity of OPA1 to high levels of ROS generated after an ischemic injury[330], indicate that mitochondrial fusion is debilitated. Therefore, it is unlikely that mitochondrial dynamics dictate increased mitochondrial content.

A second possible explanation for the increased mitochondrial content is that due to the mitochondrial dysfunction and impaired bioenergetics[333], myonuclei may respond as an adaptive measure to upregulate expression of the genes required to produce functional mitochondria and meet the high energy demands of skeletal muscle. This is accomplished by MuSCs fusing with degenerating myofibers to increase the number of myonuclei that can more generate transcripts for the biogenesis of their surrounding mitochondria. While we observe an increase in quiescent $Pax7^{+}$ MuSCs that have few active mitochondria and rely on glycolytic metabolism at day 7 following injury[106], this is accompanied by an increase in differentiating myogenic progenies through the asymmetric division of MuSCs that can fuse into multinucleated myotubes[334]. The myotubes then undergo a late fusion into regenerating myofibers to produce mature myonuclei that migrate to the center of the myofiber[314], supported by the accretion of myonuclei and their locations after an ischemic insult. These MuSC-derived myonuclei may also produce genes such as SIRT1, PGC-1α, FOXO3, or AMPK in order to initiate mitochondrial biogenesis[90,335,336]. Due to the ischemia-induced damage to the mitochondria, it is likely that these myonuclei synthesize new mitochondria to remodel the mitochondrial network within its domain. To corroborate this hypothesis, our findings display remarkably high mitochondrial densities located between the centrally positioned myonuclei as a mechanism to reset its mitochondrial domain. Proteins such as the prohibitin isoforms, which have been shown to possess both the mitochondrial- and nuclear-targeting sequence to assist in the import of nuclear-encoded mitochondrial proteins such as OPA1[92-94], allow the mitochondrial genome and the nuclear genome to communicate during muscle regeneration. Signified by the elevated levels of prohibitin 2 and the close proximity of mitochondria to the myonuclei following

ischemia, we suggest for the first time that MuSC-derived myonuclei drive biogenesis of mitochondria to restore the compartmentalized architecture of the mitochondrial reticula within a regenerating myofiber. To further elucidate the mechanism behind the mitochondrial biogenesis, we plan to examine the roles of master regulators involved in mitochondrial formation and dynamics and conduct a loss-of-function study by analyzing myonuclei number and mitochondrial content in transgenic mice with depleted MuSCs.

While we establish a notable increase in mitochondrial content by day 28 following ischemia, our data also contributes insight into the preceding ischemia-induced mitochondrial dysfunction. While ROS, such as hydrogen peroxide (H_2O_2), is required for redox signaling and regulation of transcription factors, imbalanced homeostasis resulting in excess H_2O_2 production can oxidize lipids, proteins, and nucleic acids of the MuSC niche[337]. Mitochondria are one of the major sources of ROS and generate H_2O_2 by converting the highly reactive superoxide into the more stable H_2O_2, catalyzed by the antioxidant enzyme superoxide dismutase (SOD). To elucidate the precise origin of increased H_2O_2 production in ischemic mitochondria, the enzymatic activity of the mitochondrial membrane complexes and isoforms of SOD as well as quantification of superoxide levels are required. Although complex I releases ROS into the mitochondrial matrix, complex III releases ROS to both sides of the inner membrane[338]. Since the content of SOD2 (MnSOD), primarily localized in the matrix, is unchanged while the contents of SOD1 (CuZnSOD) and OPA1, both found in the intermembrane space and along the inner membrane, are decreased, we postulate that ROS are present in the intermembrane space due to complex III-mediated electron leak. So, to fully characterize the mitochondrial dysfunction following ischemia, we can analyze complex III activity to test this hypothesis.

Finally, because the vasculature is required in biological tissues to supply key nutrients, growth factors, chemokines, oxygen, and immune cells that initiate tissue regeneration and regulate mitochondrial function[292-295,339], it is evident that functional perfusion to the tissues is a key determinant in regeneration kinetics. It is noteworthy, however, that our studies were conducted on *C57BL/6J* mice, which have been shown to exhibit more pre-existing collateral vessels[190], greater angiogenic potential, higher revascularization rates[189], increased mitochondrial respiration[191], and enhanced skeletal muscle regeneration compared to other strains of mice (i.e., *BALB/c*, *129S2/Sv*)[192]. While beyond the scope of this current study, similar genetic polymorphisms may manifest in the population of human PAD patients and thus, it is worthwhile to study the effects of ischemia in various mouse strains to provide a more representative animal model of PAD despite genetic differences.

In summary, we demonstrate remodeling of MuSC niche components following ischemic injury, notably through neuromuscular junction repair by subsynaptic nuclei, increased myonuclei number, decreased myonuclear domain, and greater mitochondria content per nucleus of skeletal muscle fibers. These data also indicate that HLI resets the myonuclear and mitochondrial domains, coordinated by the muscle stem cell, as part of the regenerative mechanism in ischemic conditions. The findings from this study illustrate the complex regenerative response of the MuSC niche following critical limb ischemia and serve as a basis to further explore mechanisms of mitochondrial biogenesis in skeletal muscle regeneration.

CHAPTER 4. MUSCLE STEM CELLS DICTATE BIOENERGETIC FUNCTION OF DYSTROPHIC SKELETAL MUSCLE

4.1 Abstract

Mitochondrial dysfunction has been implicated in various pathologies, including muscular dystrophies, though the underlying source of these defective mitochondria remains unclear. During muscle regeneration, resident muscle stem cells (MuSCs) undergo adult myogenesis to form *de novo* myofibers or fuse to existing syncytia. Leveraging this cell-cell fusion process, we postulated that mitochondria stemming from MuSCs could be transferred to myofibers during muscle regeneration to remodel the mitochondrial network and restore bioenergetic function. In this study, using FACS-purified MuSCs from wildtype *C57BL6/J* and dystrophic *mdx* mice, we assessed the myogenic capacity and bioenergetic function of these MuSCs *in vitro*. MuSCs were tested for gene expression, differentiation potential, and oxygen consumption rate through the course of myogenic progression. To test the ability of MuSCs to remodel the mitochondria in mature myofibers, we then performed ectopic transplantation of MuSCs with mitochondrial fluorescent reporters via intramuscular injections. Engrafted myofibers were identified and isolated based on fluorescent markers. MuSC-engrafted myofibers were imaged for changes in mitochondrial morphology, gene expression, and mitochondrial bioenergetic function. First, the myogenic capacity of dystrophic MuSCs to form myotubes was significantly impaired (77% reduction in myotube number, $p<0.001$). Along with altered mitochondrial gene expression and content, MuSCs from *mdx* mice also manifested a significant

reduction in mitochondrial respiration (28% decrease in basal respiration, $p<0.01$; 25% decrease in ATP production, $p<0.01$). Furthermore, mitochondria stemming from dystrophic MuSCs were shown to fuse with existing dystrophic myofibers to propagate mitochondrial dysfunction (23% decline in ADP-stimulated respiration, $p<0.01$). Conversely, by transplanting healthy donor MuSCs into dystrophic host muscle, the organization of the mitochondrial network was restored, mitochondrial biogenesis was improved (84% upregulation of mtDNA copy number, $p<0.05$; 41% upregulation of PGC-1α *(ppargc1)*, $p<0.05$), and the bioenergetic function was rejuvenated (51% increase in ADP-stimulated respiration, $p<0.05$). Similarly, when bioenergetically-compromised donor MuSCs were transplanted, improvements in mitochondrial organization and bioenergetic function were ablated in the dystrophic recipients. Overall, these findings reveal a unique role of muscle stem cells as an essential regulator of myofiber mitochondrial homeostasis and provide insight into a potential therapeutic target against various mitochondrial myopathies.

4.2 Introduction

Duchenne muscular dystrophy (DMD) is a debilitating skeletal muscle disorder characterized by a loss-of-function mutation in dystrophin, a structural protein that connects the membrane and cytoskeleton of the myofiber to its surrounding extracellular matrix[210,340]. As a consequence, unstable sarcolemmal membranes cause dystrophic myofibers to become susceptible to contraction-induced injuries, invoking progressive muscle wasting[341]. To repair damaged muscle, quiescent muscle stem cells (MuSCs), also referred to as satellite cells, commit to the myogenic lineage and initiate adult myogenesis through activation of distinct transcriptional factors, followed by differentiation and fusion

into *de novo* syncytia or existing multinucleated myofibers[46]. Proliferating MuSCs can also self-renew to replenish the quiescent stem cell pool. However, in DMD, repeated rounds of degeneration and regeneration impair the myogenic progression of MuSCs and eventually deplete the muscle-forming stem cell pool[65,205]. These pathological features exacerbate the regenerative capacity of DMD myofibers and ultimately lead to loss of ambulatory function and early death caused by the failure of vital respiratory muscles[227]. Hence, considerable research effort has been directed towards developing cell-based therapies to restore dystrophin and regenerative function in pre-clinical and clinical models of DMD[342].

Prior to discovery of dystrophin, DMD was considered a metabolic disorder[204]. Recent studies reconfirmed that the loss of dystrophin is indeed accompanied by myofiber mitochondrial dysfunction and a concomitant increase in oxidative stress[221,343-345]. Moreover, pre-clinical studies reported that restoration of mitochondrial bioenergetic function ameliorates pathological progression in the animal models of DMD[223,346]. Several investigators have reported correlative evidence that the unstable sarcolemmal membrane and contraction-induced injuries cause an overwhelming influx of extracellular Ca^{2+} that alters mitochondrial buffering capacity and this, in turn, leads to mitochondrial swelling, loss of mitochondrial membrane potential, a decline in oxidative phosphorylation, an increase in reactive oxygen species (ROS) production, permeability transition pore (PTP) opening, and apoptotic or necrotic death of myofibers[345-348]. Recently, we demonstrated that during muscle regeneration, damaged mitochondria are removed by macro-autophagy (mitophagy), and newly synthesized mitochondria stemming from satellite cells reconstitute mitochondrial networks to reestablish mitochondrial-nuclear genome

communication in regenerating myofibers[103]. Since myofibers are both multinucleated and post-mitotic, and because of the short half-life of mitochondria relative to the myofiber[349], the reciprocal interactions between myonuclei and the mitochondrial network are crucial in maintaining the mitochondrial domains (distinct regions of mitochondria surrounding and regulated by each myonucleus) within mature skeletal myofibers. Approximately 99% of mitochondrial proteins are nuclear-encoded and must be transported from myonuclei into mitochondria[350]. Thus, without competent accretion of new myonuclei derived from MuSCs, mitochondrial homeostasis and bioenergetic function are severely compromised[117,351]. In addition, muscle mitochondria form myofibrillar- and subsarcolemmal-mitochondrial networks, allowing an efficient exchange of nascent proteins encoded by different myonuclei[352]. Furthermore, despite their confined locations within myofibers, muscle mitochondria readily regulate their size, shape, and volume through mitochondrial dynamics (fission, fusion, and mitophagy) to maintain plasticity[101]. Yet, very little is known on whether recurring degeneration and impaired asymmetric division of MuSCs impact the formation of the mitochondrial network and whether putative mitochondrial dysfunction found in DMD myofibers arise directly from MuSCs as a consequence of repetitive rounds of adult myogenesis.

Herein, we demonstrate that MuSC mitochondria play a causal role in the bioenergetic function of mature myofibers. In dystrophin-deficient MuSCs, which embody defective mitochondria, bioenergetically-compromised mitochondria are transferred to myofibers during muscle regeneration. Consequently, in DMD muscle, repeated degeneration and myogenic fusion of MuSC-derived myotubes during muscle repair lead to accumulation of bioenergetically-impaired mitochondria from muscle stem cells and

cause chronic mitochondrial dysfunction in dystrophic myofibers. By leveraging ectopic MuSC transplantation, we demonstrate that healthy donor MuSCs can reconstitute the mitochondrial network of dystrophic host muscle and ameliorate mitochondrial function. Conversely, the transplantation of MuSCs with damaged mitochondria abolishes this metabolic enrichment, verifying that high quality of donor MuSC mitochondria is critical in boosting the oxidative capacity of the diseased muscle during muscle regeneration. These findings provide a conceptual foundation for using MuSC-derived mitochondrial transplantation as a therapeutic tool that can be applied to numerous skeletal muscle disorders, including mitochondrial myopathies.

4.3 Methods

4.3.1 Animal Models

Young (2-4 months) and aged (20-24 months) *C57BL/6J* mice, as well as *mitoDendra2*, *H2B-EGFP*, *Rosa26-tdTomato*, *β-actin-GFP*, *Pax7-tdTomato* and *DMD-mdx4CV* mice, all with *C57BL/6J* genetic background, were purchased at Jackson Laboratory. $Pax7^{Cre}$ mice were crossed with $Rosa26^{HA\text{-}MITO}$ mice to generate a reporter mouse for lineage tracing mitochondria derived from Pax7-expressing MuSCs. *SOD1* knockout mice were provided by Dr. Holly Van Remmen (Oklahoma Medical Research Foundation). All mice were housed, aged, and/or bred in pathogen free conditions in the Jang lab mouse colony of the Physiological Research Laboratory (PRL) at Georgia Institute of Technology. All procedures were performed in accordance with the Institutional Animal Care and Use Committee (IACUC) at Georgia Institute of Technology.

4.3.2 Muscle Stem Cell Isolation and Transplantation

MuSCs were isolated through a cell sorting procedure as previously performed[353,354]. Briefly, hindlimb muscle tissues were harvested from young (2-4 months of age) and aged (20-24 months of age) mice, and then they were incubated in 20 mL of DMEM media containing 0.2% collagenase type II (Worthington Biochemical Corporation) and 2.5 U/ mL dispase (Gibco) for 90 min. at 37 °C. After tissue digestion, the resulting media were mixed with same volume of stop media (20% FBS in F10), filtered using a cell strainer with a pore size of 70 μm, and then centrifuged (300 *g* for 5 min. at 4 °C) (Allegra X-30R Centrifuge, Beckman Coulter, USA) to obtain the myofiber-associated cell pellet. The cell pellets were washed with Hank's balanced salt solution (HBSS) containing 2% donor bovine serum (DBS), and the cells were incubated with primary antibodies. For MuSC sorting, a cocktail mixture containing the following antibodies was used: (1) APC conjugated anti-mouse CD11b (1:200; BioLegend), CD31 (1:200; BioLegend), CD45 (1:200; BioLegend), Sca-1 (1:200; BioLegend), and Ter119 (1:200; BioLegend), (2) PE conjugated anti-mouse CD29 (1:100; BioLegend), and (3) biotinylated anti-mouse CD184 (1:100; BD Biosciences). After incubation for 30 min. at 4 °C, the primary antibodies-treated cells were washed, centrifuged (300 *g* for 5 min. at 4 °C), and then treated with a secondary antibody (Streptavidin PE-Cy7) (1:50; Invitrogen) for 20 min. at 4 °C. Following propidium iodine (PI) treatment and strainer filtration (70 μm), the MuSCs (PI, CD11b, CD45, Sca-1, and Ter119; negative selection, CD29 and CD184; positive selection) were subsequently isolated by fluorescence activated cell sorting (FACS) (BD FACS Aria III, BD Biosciences, USA). 24 hours after $BaCl_2$ (1.2% w/v) injury to the tibialis anterior muscle (TA) of the recipient mouse to induce regeneration, 200,000 freshly sorted MuSCs suspended in 10 µl HBSS with 2% donor bovine serum

were injected intramuscularly into the TA muscle with a Hamilton syringe. Donor MuSCs were collected from *β-actin-GFP* mice to track transplanted cells following engraftment and myogenic fusion into the myofiber. 4 weeks following MuSC transplantation, mice were euthanized and the TAs were dissected for tissue analysis. Sham injury with $BaCl_2$ injection but no MuSC transplantation was used as the contralateral control. No differences in mitochondrial content or myofiber respiration were observed between naive *mdx* muscle and $BaCl_2$-injured muscle 28 days after injection.

4.3.3 SPADE Tree Analysis

Using β1-integrin (CD29) and CXCR4 (CD184) as stemness markers of MuSCs from FACS sorting data, we clustered purified MuSCs from wildtype and *mdx* mice based on CD29 and CD184 expression using SPADE (spanning tree progression of density normalized events) tree analysis to delineate the heterogeneity of the MuSC population in 2 dimensions. Each node represents a set of MuSCs clustered together based on expression of all surface markers (CD11b, CD45, Sca-1, Ter119, CD29, and CD184). The size and color of each node represents the relative number of cells and median marker expression. SPADE was performed on MATLAB using a source code found at **http://pengqiu.gatech.edu/software/SPADE/**. The following parameters were used to generate the SPADE trees: apply compensation matrix in FCS header, Arcsinh transformation with a cofactor of 150, neighborhood size of 5, local density approximation factor of 1.5, maximum allowable cells in pooled downsampled data of 50,000, target density of 20,000 cells remaining, and number of desired clusters of 15. Within the SPADE tree, nodes were then manually grouped to congregate nodes with high CD29/high CD184 expression, high CD29/low CD184 expression, low CD29/high CD184 expression, and

low CD29/low CD184 expression. The total number of cells within each of these groups were then counted and compared between wildtype and *mdx* MuSC populations.

4.3.4 Muscle Stem Cell Culture and Immunostaining

Following MuSC isolation, 8,000 purified cells were seeded into an ibidi 96 well glass bottom plate in F10 media supplemented with 20% horse serum, 1% glutaMAX, 1% penicillin/streptomycin, and 25 ng/mL basic fibroblast growth factor (bFGF). For quiescent MuSCs, cells were fixed with 4% paraformaldehyde after 12 hours to allow cells to adhere to bottom of the plate. To proliferate MuSCs while inhibiting differentiation, 25 ng/mL bFGF was supplemented daily. To differentiate MuSCs and facilitate fusion into myotubes, MuSCs were first treated with 25 ng/mL bFGF for 4 days and then allowed to differentiate and fuse for another 6 days before fixation. Fixed cells were then stained by treating cells with Hoechst 33342 (1:1000 dilution) for DAPI and phalloidin-iFluor 555 (1:500 dilution) for F-actin, diluted in blocking buffer (2% BSA, 0.5% goat serum, 0.5% Triton X-100 in PBS). After staining, z-stack images of cells were taken on a Zeiss 700 Laser Scanning Confocal microscope. Mitochondrial content was quantified by measuring relative fluorescent intensity of *Dendra2* signal in maximum intensity projections.

4.3.5 Mitochondrial Isolation and Transplantation

Mitochondria were first isolated by mincing and digesting mouse skeletal tissue with 0.1 mg/ml dispase, 1 mg/ml trypsin in Chappell-Perry buffer (100 mM KCl, 50 mM MOPS, 10 mM $MgSO_4$-$7H_2O$, 10 mM ATP, pH 7.4). Isolated mitochondria were obtained from digested tissue through differential centrifugation and a BCA assay was performed to determine protein concentration. Recipient tibialis anterior muscles were injected with 2

mg/ml hyaluronidase 1 hour before transplantation of 250 µg isolated mitochondria using an insulin syringe. Transplanted muscles were dissected and fixed for cryosectioning 2 and 7 days following injection to visualize uptake of isolated mitochondria.

4.3.6 Myoblast Isolation

Myoblasts were isolated as previously described with some modifications[355]. Whole hindlimb muscles were collected from euthanized mouse to isolate myoblasts. Collected muscles were minced finely with surgical scissors and added to digestion solution (0.2% type 2 collagenase in DMEM). Tissues were digested for 1 hour at 37 °C followed by passing the tissue slurry through a 20G needle for several times to break the remaining chunks. To stop the reaction, 40 mL PBS was added to the slurry. Single cells were collected by using 40 µm nylon mesh filter and the cell pellets were plated on collagen coated dish with growth media (30% FBS, 1% Pen/Strep, 1% non-essential amino acids, 10 ng/mL FGF-2 in DMEM). After a 16-hour attachment, the cells in the supernatant were transferred and attached to a new collagen-coated dish for 3 hours at 37 °C. Again, the supernatant was collected to be transferred to a Matrigel-coated dish. After 24 hours, media was changed to remove unattached cells. After another 24 hours, attached cells were trypsinized and re-plated on a new collagen-coated dish that was shaken every 5 minutes for 10 times. The isolated primary myoblasts in the supernatant were relocated onto a new Matrigel-coated dish for further experiments.

4.3.7 Mitochondrial Respiration of Stem Cells and Myoblasts

Using the Lucid Scientific RESIPHER device on a 96-well plate, oxygen flux of the cell monolayer can be quantified real-time throughout MuSC culture and myogenesis.

Oxygen flux was quantified in wells with 8,000 seeded MuSCs during the first 4 days with 25 ng/mL bFGF supplementation to proliferate MuSCs and during the next 6 days without bFGF to allow MuSC differentiation and fusion. For comprehensive analysis of mitochondrial respiration in MuSCs, 8,000 cells per well in a Seahorse XFp miniplate were supplemented with 25 ng/mL for 8 days until confluent. Myoblasts, validated through lineage tracing (Pax7-tdTomato) as MuSC progenies, were also isolated via pre-plating[355] for Seahorse mitochondrial analysis. Prior to running the Seahorse assay, media was changed to XF Base DMEM with 1 mM pyruvate, 2 mM glutamine, and 10 mM glucose. Sensor cartridges were loaded for sequential injections to result in final concentrations of 1 µM oligomycin, 1 µM carbonyl cyanide 3-chlorophenylhydrazone, and 0.5 µM rotenone. MuSCs and the cartridge were placed in a Seahorse XFp Analyzer to test mitochondrial function at various stress conditions.

4.3.8 Skeletal Muscle Immunofluorescent Imaging

Following euthanasia, mouse hindlimbs were fixed in 4% PFA and the tibialis anterior muscles were dissected. For cross-sectional images, muscles were prepared as previously described[310] where muscles were cryopreserved with 20% sucrose overnight then frozen in liquid nitrogen-cooled 2-methylbutane. Muscles were sectioned at 10 µm in a cryostat and stained with phalloidin (for F-actin) (Thermo A22287), SOD2 (Enzo ADI-SOD-100-F), and DAPI (Vector Labs H-1200) for fluorescent imaging on a Zeiss 700 Laser Scanning Confocal microscope. For single fiber images, fixed muscle fiber bundles were first stained with phalloidin and DAPI, then mechanically separated into single muscle fibers as previously described[103]. Isolated muscle fibers were mounted on slides for imaging on a confocal microscope.

4.3.9 Biochemical Analyses

For Western blot analyses to quantify protein contents, tibialis anterior muscles were homogenized in BioMasher homogenization tubes (VWR KT749625-0030) in RIPA lysis buffer (VWR 97063-270) supplemented with Roche cOmplete Mini Protease Inhibitors (Roche 04693124001) and PhosSTOP Phosphatase Inhibitors (Roche 04906837001) at 1 mL lysis buffer per 100 mg muscle tissue. After 3 freeze-thaw cycles, muscle homogenates were centrifuged at 18,400 *g* for 10 minutes and the supernatants were collected. The supernatants were normalized for protein concentration using a BCA assay kit (Thermo 23225) and mixed with Laemmli buffer (Bio-Rad 161-0737). 50 µg of the protein mix were run through a 4-20% Criterion TGX gel (Bio-Rad 5671093) at 150 V for 85 minutes and transferred to a PVDF membrane using the Trans-Blot Turbo System at 2.5 A for 7 minutes. Following antibody staining, membranes were imaged on Li-Cor Odyssey CLx-1050 Infrared Imaging System and bands were quantified on Li-Cor Image Studio V5.2. Membranes were subsequently stained with Ponceau solution (Sigma P7170) as a loading control and imaged on Amersham.

For quantitative real-time polymerase chain reaction, muscles were homogenized in a similar method to Western blot preparation with the exception of RLT buffer supplied in the RNeasy® Mini Kit (Qiagen 74104) supplemented with 1% β-mercaptoethanol (Sigma M6250) instead of RIPA lysis buffer. Following collection of the supernatant, RNA was isolated according to the protocol provided by Qiagen RNeasy® kit. RNA concentration was measured in a NanoDrop One and samples were normalized according to RNA content. The Applied Biosystems High Capacity cDNA Reverse Transcription Kit (4368814) was used to reverse transcribe the isolated RNA into cDNA. The cDNA was

combined with Applied Biosystems PowerUp SYBR Green Master Mix (A25742) and corresponding primers in 96-well plates and run in an Applied Biosystems StepOnePlus Real-Time PCR system to perform the qPCR reactions. β-actin and B2m, which we found to be stably expressed in our muscle samples, were used as housekeeping genes to quantify relative fold induction. For the PCR array data, cDNA was mixed with PowerUp SYBR Green Master Mix, loaded into the Qiagen Mouse Mitochondria RT^2 Profiler PCR Array (330231), and run in an Applied Biosystems StepOnePlus to quantify the data.

4.3.10 Mitochondrial Respiration of Permeabilized Myofibers

Immediately following euthanasia and dissection of the tibialis anterior, fresh muscles were places in cold buffer X (7.23 mM K_2EGTA, 2.77 Ca K_2EGTA, 20 mM imidazole, 20 mM taurine, 5.7 mM ATP, 14.3 mM phosphocreatine, 6.56 mM $MgCl_2$-$6H_2O$, 50 mM K-MES) as previously described[356]. Fiber bundles with approximate wet weights of 4 mg were mechanically separated under a dissecting scope with fine forceps and permeabilized with 30 µg/ml saponin for 40 minutes. For transplanted muscles, a NIGHTSEA Stereo Microscope Fluorescence Adapter (Electron Microscopy Sciences SFA-LFS-RB, SFA-LFS-GR) was used to locate and isolate fluorescent engrafted fibers. Following permeabilization, fiber bundles were washed in cold buffer Z (105 mM K-MES, 30 mM KCl, 10 mM KH_2PO_4, 5 mM $MgCl_2$-$6H_2O$, 0.5 mg/ml BSA, 1 mM EGTA) for 15 minutes to remove any residual saponin.

Following permeabilization of fiber bundles, samples were loaded into an Oroboros O2k Oxygraph with 2 mL buffer Z without $MgCl_2$ and supplemented with 2.5 mM Magnesium Green (Thermo M3733) in order to simultaneously measure oxygen

consumption and relative ATP production rates. Prior to loading samples in the chamber, the system was calibrated using various titrations of ATP to ADP ratios to determine relative ATP production due to the higher binding affinity of Magnesium Green to ATP compared to ADP. After loading samples, the chamber was equilibrated for 15 minutes to reach basal (State 1) respiration rates. Glutamate (10 mM) and malate (2 mM) were then added to the chambers for complex I-linked State 2 respiration rates, followed by the addition of ADP (5 mM) to initiate State 3 respiration. Oxygen consumption rates were expressed as pmol/sec/mg fiber wet weight while relative ATP production rate was measured as changes in the ATP to ADP ratio. All measurements were conducted at 37 °C and a working [O_2] range ~250 to 175 µM.

4.3.11 SDH and COX Activity Staining

SDH (succinate dehydrogenase) activity staining was performed on 10 µm thick frozen sections of fresh (unfixed) TA muscles to observe oxidative fibers. The cross-sections were incubated in 50 mM phosphate buffer containing 50 mM sodium succinate and 0.5 mg/ml nitro blue tetrazoliumand (Sigma-Aldrich, N5514) for 50 minutes at 37 °C. The SDH staining solution was made fresh before staining. Then, the sections were washed with distilled H_2O 3 times. Completely dried slides were then mounted with glycerol containing mounting media.

For COX (cytochrome c oxidase) activity staining, the tissue section was prepared the same way as the tissue section used for SDH staining. The COX staining solution contains 75 mg/mL sucrose (Sigma-Aldrich, S9378), 2.3 µM 3,3'-diaminobenzidine (Sigma-Aldrich, D8001), 0.1 mg/mL cytochrome c (Sigma-Aldrich, C2506), and 2 µg/mL

catalase (Sigma-Aldrich, C1345) in 50 mM phosphate buffer and it was made fresh before the incubation. The tissue sections were incubated with the COX staining media for 1 hour at 37 °C followed by three times of wash with distilled H_2O. Then, the slides were dipped in ascending concentrations of ethanol (50%, 70%, 95%, and 100%) to dehydrate the tissue. Finally, slides were cleared with xylene solution and mounted with acrytol mounting media.

4.3.12 mRNA Sequencing and Differentially Expressed Gene Analysis

For mRNA sequencing, mRNA isolation and preparation were conducted as previously described[357]. Briefly, sorted MuSCs were collected in Trizol (Thermo) and total RNA was purified with miRNeasy Micro kit (Qiagen) following the manufacturer's instruction. The quality of RNA and its concentration were measured by a spectrophotometer (Nanodrop 2000c) and Bioanalyzer (Agilent 2100). cDNA libraries were produced using SmartSeq4 protocol (Clontech) using 10 ng of total RNA following the manufacturer's instructions. We sequenced individual library using 76 paired-end reads with an average depth of 50M reads per sample. RNA sequencing reads were then processed with Trimmomatics (ver. 0.38)[358] to remove potential adapter sequences and to trim low quality sequences. Trimmed RNA-Seq reads were then mapped to Mus musculus genome (GRCm38) and gene expression quantified using RSEM (ver. 1.2.28)[359]. We used tximport (ver. 1.8) to import expected read counts into DESeq2 (ver. 1.2) Bioconductor package[360]. We removed genes with FPKM < 1 across all samples to exclude lowly expressed genes. Differential gene expression analysis was performed using DESeq2. Genes were determined to be significantly differentially expressed if an absolute average expression fold change between WT and mdx groups was greater than 2 with P-value

below 0.01 after multiple corrections. Gene Set Enrichment Analysis (GSEA) was performed to determine significantly enriched GO terms and pathways[361].

4.3.13 Endurance Exercise

Endurance-exercised donor mice were run on a 4-lane rodent motor-driven treadmill (Omnitech, USA). For proper adaptation to the treadmill, mice were pre-trained for one week at 5-10 meters/minute for 10-20 minutes each day. Following pre-training, each training session for the main exercise was progressively increased from 5-10 m/min to 15-20 m/min over 50-60 minutes each day. The mice underwent a warm-up session (2-3 m/min) and a cool-down session (3-5 m/min) before and after the main exercise, respectively. These exercises continued for 8 weeks at 5 sessions each week. After completion of the exercise protocol, MuSCs were purified from exercised donor mice one week after the last session to allow metabolic changes of the MuSC and skeletal muscle to occur.

4.3.14 Statistical Analyses

All statistical analyses were performed on GraphPad Prism 7 and data is presented as mean ± standard deviation (SD). Samples sizes were chosen using G*Power based on preliminary experiments to ensure adequate statistical power. Normality of data was tested with Shapiro-Wilk test. For all experiments comparing 2 different groups of animals (wildtype vs. *mdx*, young vs. aged, wildtype vs. *SOD1KO*), unpaired two-tailed t-tests assuming Gaussian distribution were used to determine statistical differences. For experiments comparing experimental conditions from the same animal with a treatment group and contralateral control group (control *mdx* vs. transplanted *mdx*, control *SOD1KO*

vs. transplanted *SOD1KO*), paired two-tailed t-tests assuming Gaussian distribution were used to test statistical differences. For permeabilized fiber experiments comparing a control group and transplanted group with various states of respiration measured for each sample, multiple paired t-tests with Holm-Sidak correction was performed. *p*-value was computed without the assumption of consistent scatter (standard deviation). For experiments with 3 different groups (wildtype vs. *mdx* vs. *mdx* + MuSC transplantation), ordinary one-way ANOVA was performed using Tukey's *post hoc* test for multiple comparisons. Gaussian distribution was assumed, but Geisser-Greenhouse correction was performed because sphericity was not assumed. A *p*-value of less than 0.05 was considered statistically significant for all experiments.

4.4 Results

4.4.1 MuSCs from Dystrophin-Deficient mdx *Mice Exhibit Mitochondrial Dysfunction*

Studies have reported that muscles from *mdx* mice, an animal model of Duchenne muscular dystrophy (DMD), show significant deficits in mitochondrial function[221,344,346]. To determine whether mitochondrial dysfunction in *mdx* myofibers originates from MuSCs, as opposed to later in the myogenic progression of myofiber formation, FACS-purified quiescent MuSCs from young wildtype and *mdx* mice were compared. First, to examine morphological differences, mitochondrial reporter (*mitoDendra2*) mice, in which the fluorescent protein *Dendra2* is targeted to the mitochondrial matrix[305], were cross-bred with *mdx* mice and their MuSCs were compared to MuSCs isolated from *mitoDendra2* (referred to as WT). Prior to analyses of the mitochondrial fluorescent protein, *Dendra2*, we first validated our mitochondrial reporter by comparing it to a commonly used

mitochondrial stain, MitoTracker[362]. Interestingly, in both MuSCs and mature myofibers, the *Dendra2* fluorescent signal was retained following treatment of a mitochondrial membrane uncoupler, CCCP, while MitoTracker was not (Fig. 11A). Thus, this allowed us to track total mitochondria of cells and tissues using the *mitoDendra2* system regardless of mitochondrial membrane potential. Following FACS-purification of muscle stem cells, overall MuSC yield was not different (Fig. 11B). However, the distribution of MuSC diameter and mitochondrial content per MuSC, as measured by fluorescent pixel intensity per cell, was shifted towards the right, displaying that quiescent MuSCs from *mdx* mice possess greater mitochondrial content compared to WT controls (Figure 11C, 11D, 11E).

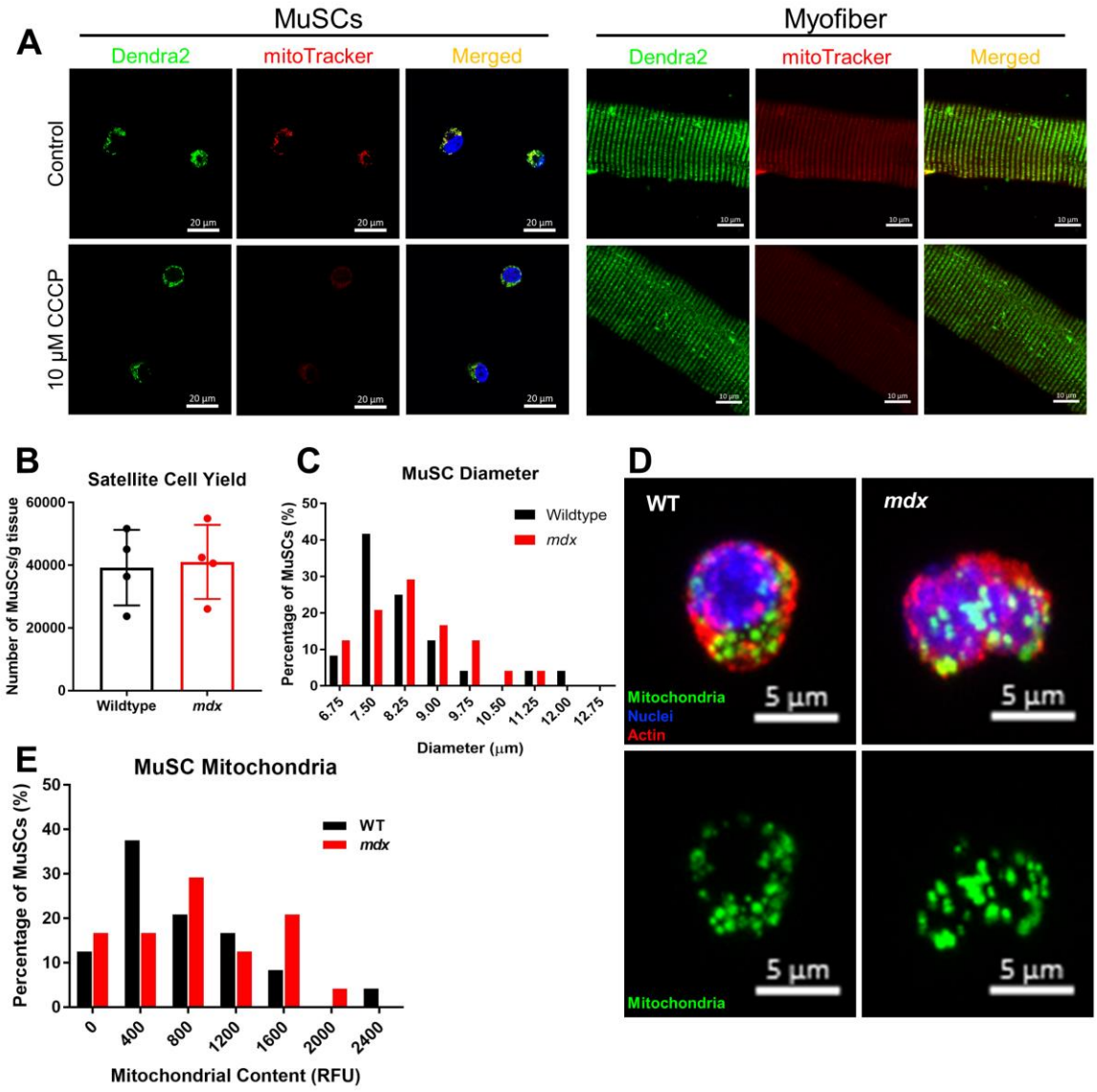

Figure 11. Dystrophic MuSCs possess greater mitochondrial content. (A) Comparison of mitoDendra2 fluorescent signal to mitoTracker staining from live MuSCS (left) and myofibers from FDB muscle (right) with or without CCCP treatment. mitoDendra2 in green, MitoTracker in red, nuclei in blue. (B) MuSC yield per gram of tissue from wildtype and *mdx* skeletal muscle (n=4). (C) Histogram of diameter of 25 MuSCs from mitoDendra2 and mdx/mitoDendra2 muscle. (D) Representative maximum intensity projection of confocal images of quiescent MuSCs purified from wildtype (WT)/*mitoDendra2* and *mdx*/*mitoDendra2*. Mitochondria are depicted in green, nuclei in blue, F-actin in red. (E) Histogram of mitochondrial content (pixel intensity) of 25 MuSCs.

Next, to assess differences in mitochondrial molecular signature and metabolism, we assessed bulk RNA sequencing on freshly isolated MuSCs from WT and *mdx* mice.

The transcriptome profile revealed that gene sets regulating mitochondrial protein complex and mitochondrial inner membrane were among the most differentially enriched pathways in quiescent *mdx* MuSCs compared to WT control cells (Figure 12A). Running mRNA samples through a mitochondrial PCR array further demonstrated substantial upregulation of mitochondrial genes in *mdx* MuSCs (Figure 12B, 12D). Specifically, in *mdx* MuSCs, the majority of the nuclear-encoded mitochondrial electron transport chain (ETC) genes were upregulated, supporting the notion that dystrophic MuSCs comprise of higher mitochondrial content than WT MuSCs. In stark contrast, all 13 ETC genes encoded by mitochondrial DNA were dramatically downregulated in *mdx* MuSCs as shown by RNA sequencing and RT-PCR validation (Figure 12C, 12D), suggesting a potential disruption in nuclear and mitochondrial genome communication.

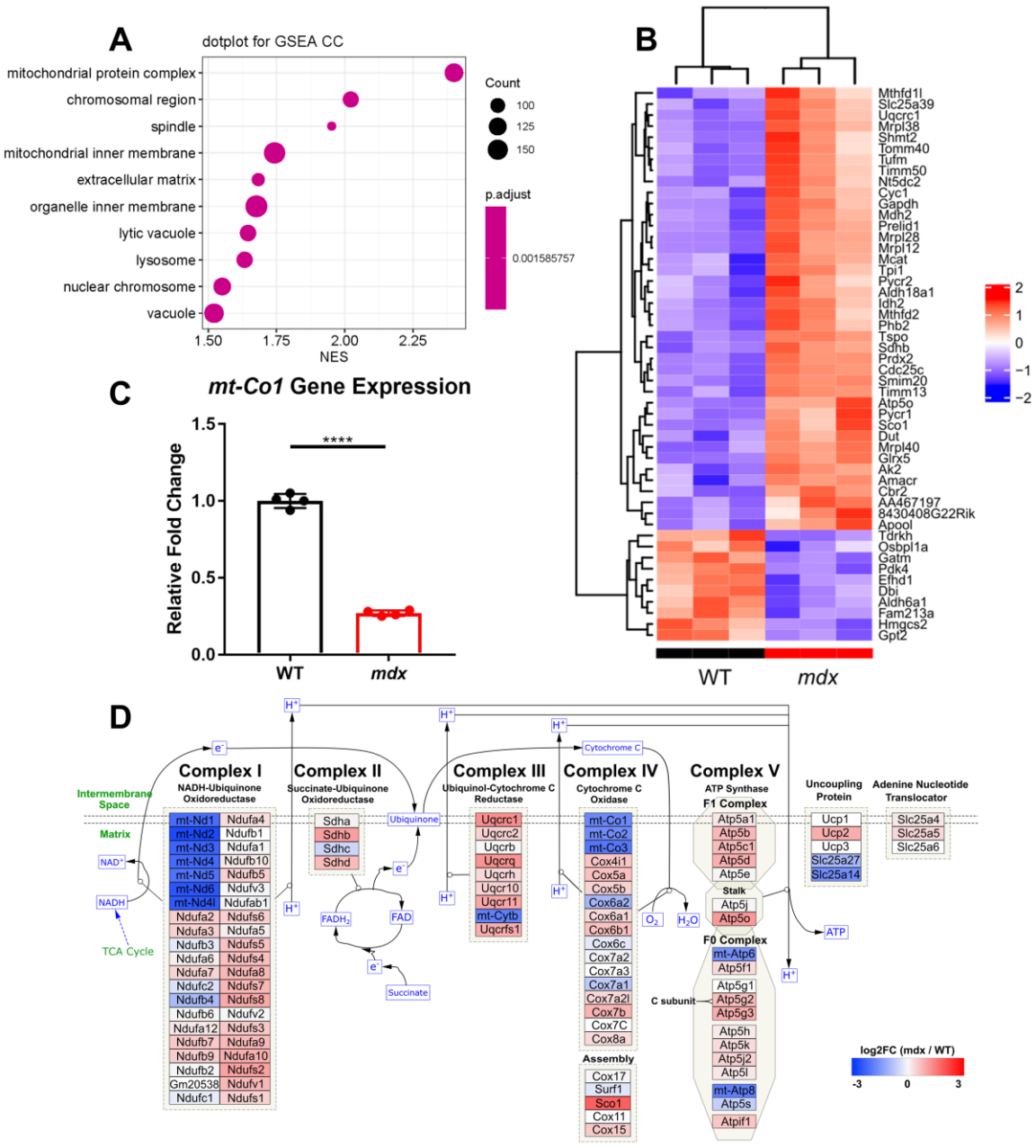

Figure 12. Dystrophic MuSCs upregulate nuclear-encoded mitochondrial gene expression. (A) Gene set enrichment pathway analysis of mdx MuSCs compared to wildtype MuSCs. (B) Hierarchical clustering and heatmap of top fifty differentially regulated mitochondrial gene expression. (C) *mt-Co1* (mitochondrial-encoded cytochrome c oxidase I) qPCR validation of RNA-seq data. (D) Diagram and changes in gene expression of mitochondrial electron transport chain and oxidative phosphorylation using RNA seq. data. Gene expression changes between mdx and WT MuSCs for ETC pathway were illustrated using Cytoscape, Wikipathways plug-in (http://www.wikipathways.org). Mean ± SD, ****p<0.0001 using t-test compared to wildtype control for all figures.

Recent investigations showed that MuSCs from *mdx* muscle exhibit significant deficits in myogenesis *ex vivo*[65,274]. Specifically, dystrophic MuSCs lose their polarity during asymmetric division that leads to a reduction of muscle-forming MuSC progeny. The remaining quiescent MuSCs also tend to become senescent over time. Thus, we assessed the relative expression of surface markers associated with stemness in WT compared to *mdx* MuSCs and clustered similar subpopulations from each together via SPADE tree analysis. Interestingly, dystrophic muscles *in vivo* partially lost the MuSC subpopulation that co-expressed low levels of β1-integrin and CXCR4, stemness markers which are required to maintain and produce viable quiescent cells[363,364] (Fig. 13A, 13B). These β1-integrin^{Lo}/CXCR4^{Lo} MuSCs likely differentiate into committed progeny due to their low stemness marker expression, and the reduction of this subpopulation further elucidates the mechanism by which dystrophic muscle may lose these muscle-forming MuSCs and supports the observation of an abnormal balance between self-renewing and committed MuSCs claimed by Dumont *et al.*[65].

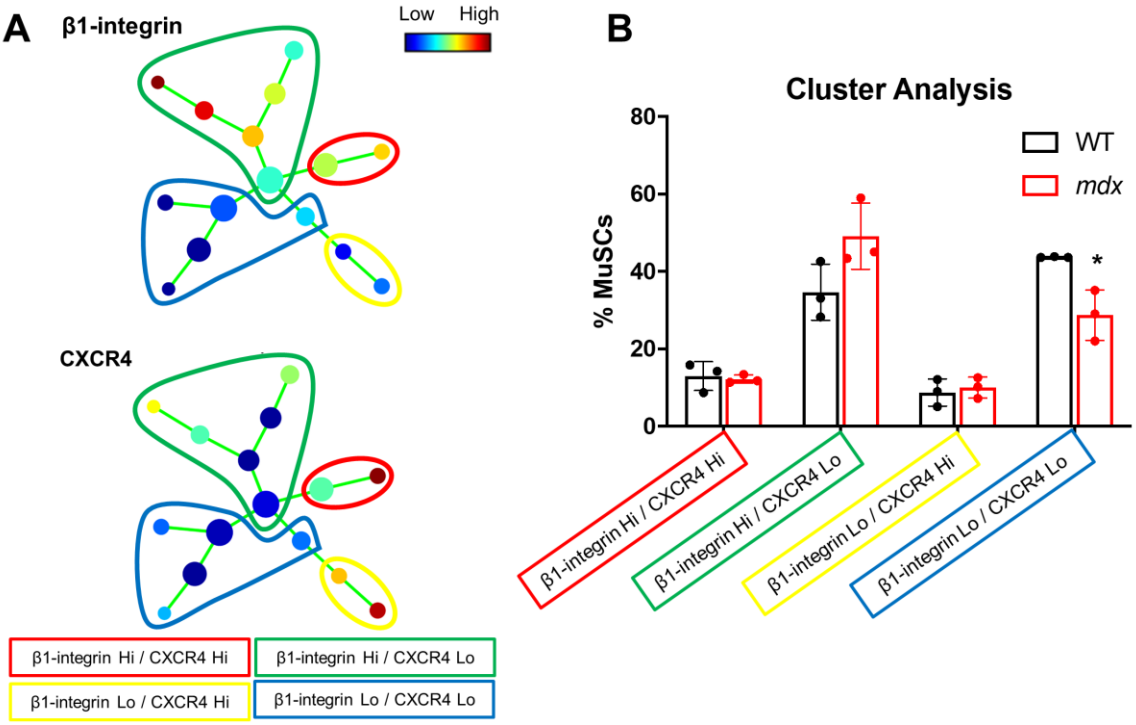

Figure 13. SPADE tree analysis of FACS-purified MuSCs. (A) Cluster analysis of wildtype and *mdx* MuSCs using SPADE tree analysis of β1-integrin and CXCR4 surface marker expression. (B) Quantification of the percentage of MuSCs within each cluster (n=3 biological replicates). Mean ± SD, **p*<0.05 using multiple t-tests compared to wildtype control for all figures.

To test whether the altered myogenic capability is linked to mitochondrial bioenergetic function, we measured mitochondrial content and kinetic oxygen flux, a metric for mitochondrial oxidative respiration, from all subpopulations of cultured MuSCs through myogenic activation, proliferation, and differentiation into myotubes. Although WT MuSCs have been shown to remarkably increase in respiration to cope with the high energy demands of myotube formation[103,107], the ability of *mdx* MuSCs to fuse into myotubes was significantly compromised (Figure 14A, 14B), corroborating the observation of diminished muscle-forming MuSC progeny. Interestingly, even in cells that formed multinucleated myotubes expressing myosin heavy chain (MHC), dystrophic myotubes harbored fewer mitochondria quantified by mitoDendra2 fluorescent pixel

intensity per myotube (Figure 14C, 14D), implying that mitochondria may play a role in this aberrant balance during asymmetric division.

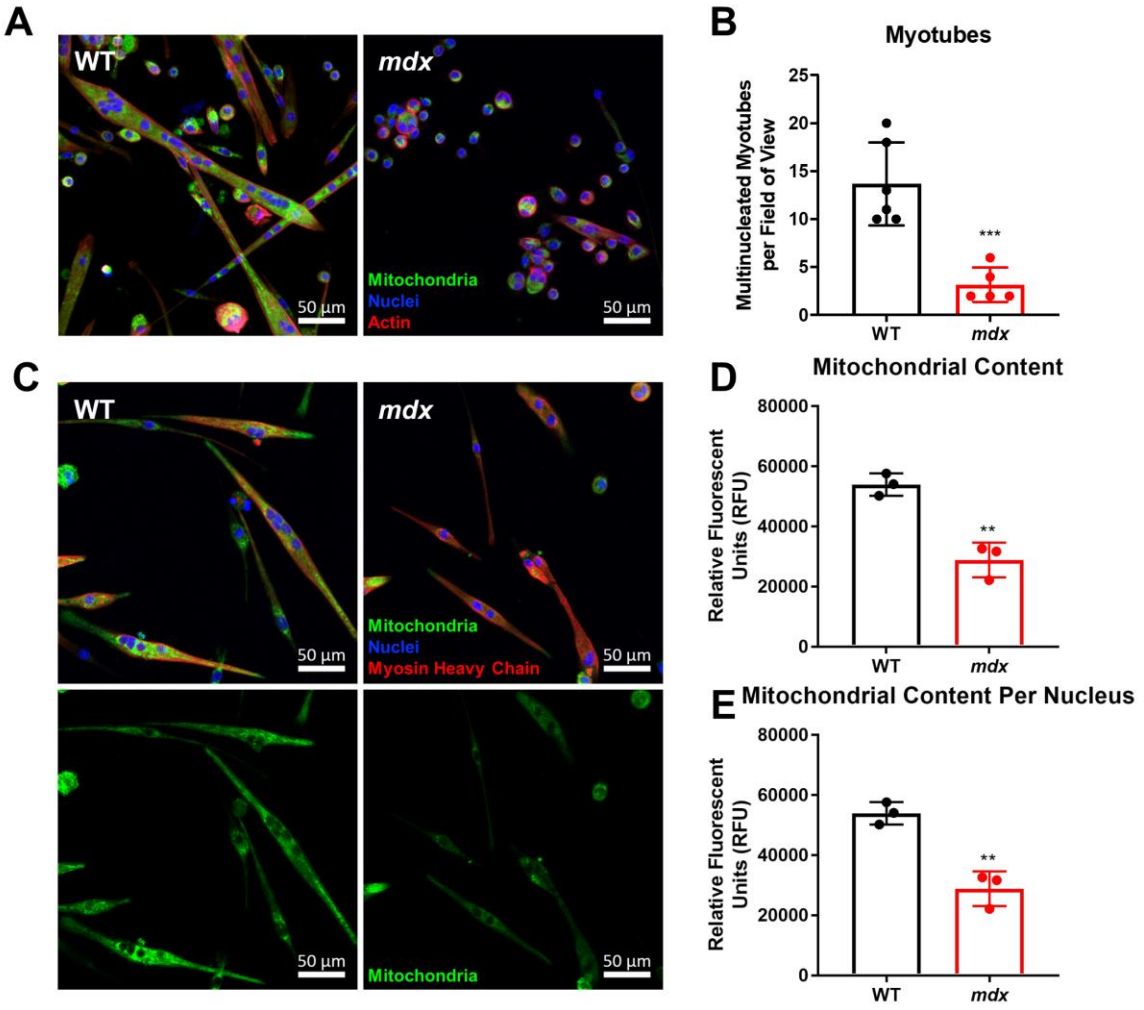

Figure 14. Dystrophic MuSCs have limited myogenic capacity and ability to form new mitochondria. (A) Representative confocal images of MuSCs following differentiation from WT/*mitoDendra2* and *mdx*/*mitoDendra2* mice. Mitochondria in green, nuclei in blue, actin in red. (B) Quantification of number of multinucleated myotubes within each field of view. Each sample represents biological replicates (n=6). (C) Representative confocal images of myosin heavy chain (MHC)-positive MuSC-derived myotubes from WT/*mitoDendra2* and *mdx*/*mitoDendra2* mice. Mitochondria in green, nuclei in blue, MHC in red. (D) Quantification of total mitochondrial content (pixel intensity) from 20 MHC^+ myotubes per biological replicate. (E) Quantification of total mitochondrial content normalized to the number of nuclei within myotubes. Each sample represents the mean pixel intensity from n=3 biological replicates. Mean ± SD, $^{**}p<0.01$, $^{***}p<0.001$ using t-tests compared to contralateral control for all figures.

Next, we directly measured mitochondrial function at various stages of MuSC culture and found that oxidative capacity was attenuated throughout myogenesis (Figure 15A), indicating a diminished ability to synthesize new mitochondria during differentiation and fusion of muscle-forming MuSC progeny. To further assess this reduction in bioenergetics seen in *mdx* MuSCs, we quantified oxygen flux of undifferentiated MuSCs normalized to total protein content after administering mitochondrial ETC inhibitors to test whether the altered mitochondrial function originates in the MuSCs prior to differentiation. The basal oxygen consumption rate (OCR) of dystrophic MuSCs was decreased compared to WT cells, even when normalized to total protein content (Figure 15B, 15D). When MuSC mitochondria were stimulated with ATP synthase inhibitor (oligomycin) and mitochondrial membrane potential uncoupler (CCCP) to allow free electron flow through the ETC, *mdx* MuSCs also displayed deficiencies in ATP production, measured by the difference in respiration before and after addition of oligomycin (Fig. 15E) and maximal respiration, measured by the difference in respiration before and after addition of CCCP (Fig. 15F). Following addition of a mitochondrial ETC complex I inhibitor, rotenone, to stop ETC activity, we can measure non-mitochondrial respiration (Fig. 15L) and proton leak, defined as the respiration due to protons leaking into the mitochondrial matrix through ETC complexes other than ATP synthase and quantified as the difference in respiration after oligomycin compared to rotenone, which was found to be diminished in *mdx* MuSCs (Figure 15G). Seahorse analysis also allows quantification of coupling efficiency, or the ability for cells to produce ATP per pmol of oxygen consumed, which was surprisingly increased in dystrophic MuSCs (Fig. 15H), likely as a compensatory response to impaired mitochondrial health. Spare capacity, or the difference between maximal mitochondrial

respiration ability and resting basal state, did not change between WT and *mdx* MuSCs (Fig. 15I, 15J). Finally, the ratio between oxidative phosphorylation, measured by basal OCR, and glycolysis, measured by basal ECAR, was also significantly reduced in *mdx* MuSCs (Fig. 15K), despite dystrophic MuSCs also having decreased non-mitochondrial respiration (Fig. 15L). Collectively, these data support the notion that dystrophic MuSCs possess impaired mitochondria that limit the cells' abilities to meet the energy demands of myogenic progression.

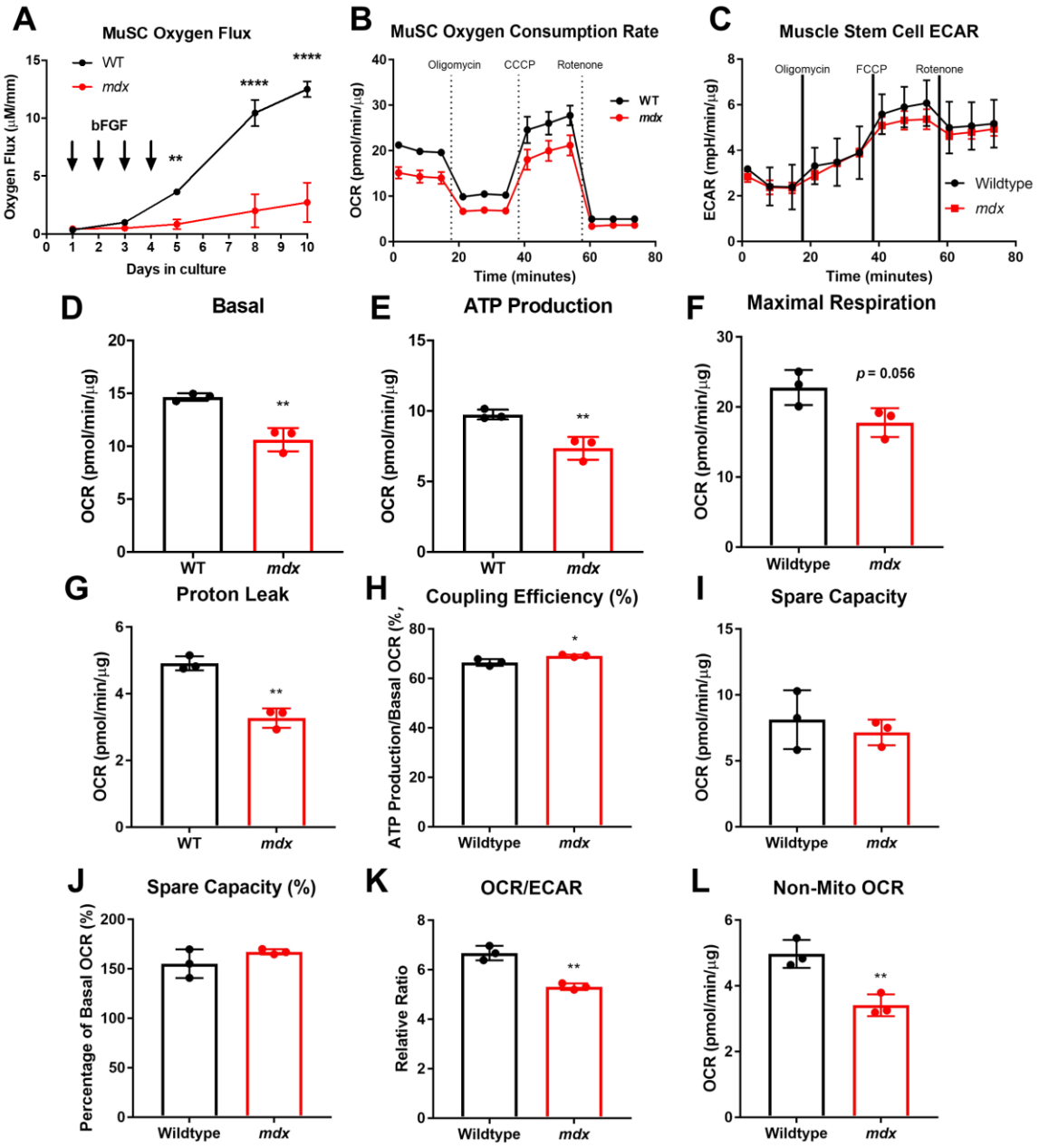

Figure 15. MuSC mitochondria in *mdx* mice have impaired bioenergetic function. (A) Comparison of muscle stem cell oxygen flux rate *in vitro*. FACS-purified MuSCs from WT and *mdx* were supplemented with 25 ng/ml bFGF for the first 4 days and monitored for 10 days. (B-L) Oxygen consumption rates (OCR) at various states of respiration, extracellular acidification rate (ECAR), ATP production, proton leak, and coupling efficiency of MuSCs cultured for 8 days with daily 25 ng/ml bFGF supplementation using a Seahorse XFp Analyzer (n=3). Mean ± SD, **p*<0.05, ***p*<0.01, *****p*<0.0001 using t-tests compared to wildtype control for all figures.

4.4.2 Dysfunctional Mitochondria Propagate from Dystrophic MuSCs into Mature Myofibers

During muscle regeneration, MuSC-derived myotubes form mature myofibers by fusing their intracellular components, including mitochondria. Under homeostatic conditions, myonuclei within the healthy, multinucleated myofiber each regulates a discrete volumetric "domain" of mitochondria around it[101]. However, following damage to the myofiber, myonuclei may be lost through apoptosis and the mitochondrial domain is reorganized via MuSC fusion into the myofiber to generate more myonuclei that each regulate a new mitochondrial domain. Indeed, using a transgenic mouse model for lineage tracing of mitochondria derived from Pax7-expressing MuSCs (*Pax7 Cre*^{ER} crossed with *Rosa26*$^{HA\text{-}MITO}$)[322], we can visualize the mitochondrial domain of MuSC-derived myonuclei (Fig. 16A). We hypothesized that if dystrophic MuSCs contain dysfunctional mitochondria, fusion of these MuSCs and their mitochondria-regulating nuclei will transmit their defective mitochondria into the myofiber. Thus, we analyzed the mitochondrial morphology of mature myofibers isolated from mitoDendra2 control (WT) and *mdx*/mitoDendra2 (*mdx*) muscles. Since bioenergetic function relies on the mitochondrial morphology within the cell[352], we assessed the mitochondrial organization of the myofibers. While myofibers from control mice display a healthy mitochondrial network that is segregated into compartmentalized reticula along the contractile apparatus[101], dystrophic myofibers portrayed a highly disordered mitochondrial morphology (Fig. 16B), particularly near the subsarcolemmal region of the myofiber which may be more susceptible to contraction-induced membrane instability[348]. Next, using permeabilized myofiber bundles loaded into a high-resolution respirometer, we measured

the oxygen consumption rate of isolated myofibers normalized to wet weight at basal respiration without exogenous substrates (state 1), mitochondrial ETC complex I-linked respiration with the addition of glutamate and malate (state 2)[365], and ATP-converting respiration by addition of ADP (state 3). Although there was no statistical difference in OCR between WT and *mdx* myofibers at state 1 or state 2 respiration, state 3 respiration of *mdx* myofibers was significantly reduced (Fig. 16C). Moreover, by assessing these various states of respiration in isolated mitochondria derived from WT and *mdx* skeletal muscle, we found diminished state 2 and state 3 respirations (Fig. 16D), though these mitochondria may be derived from components of skeletal muscle other than myofibers, such as motor neurons and vascular-associated cells and tissues. Together, these data are indicative of disrupted bioenergetic function of dystrophic muscle, consistent with previous studies[221].

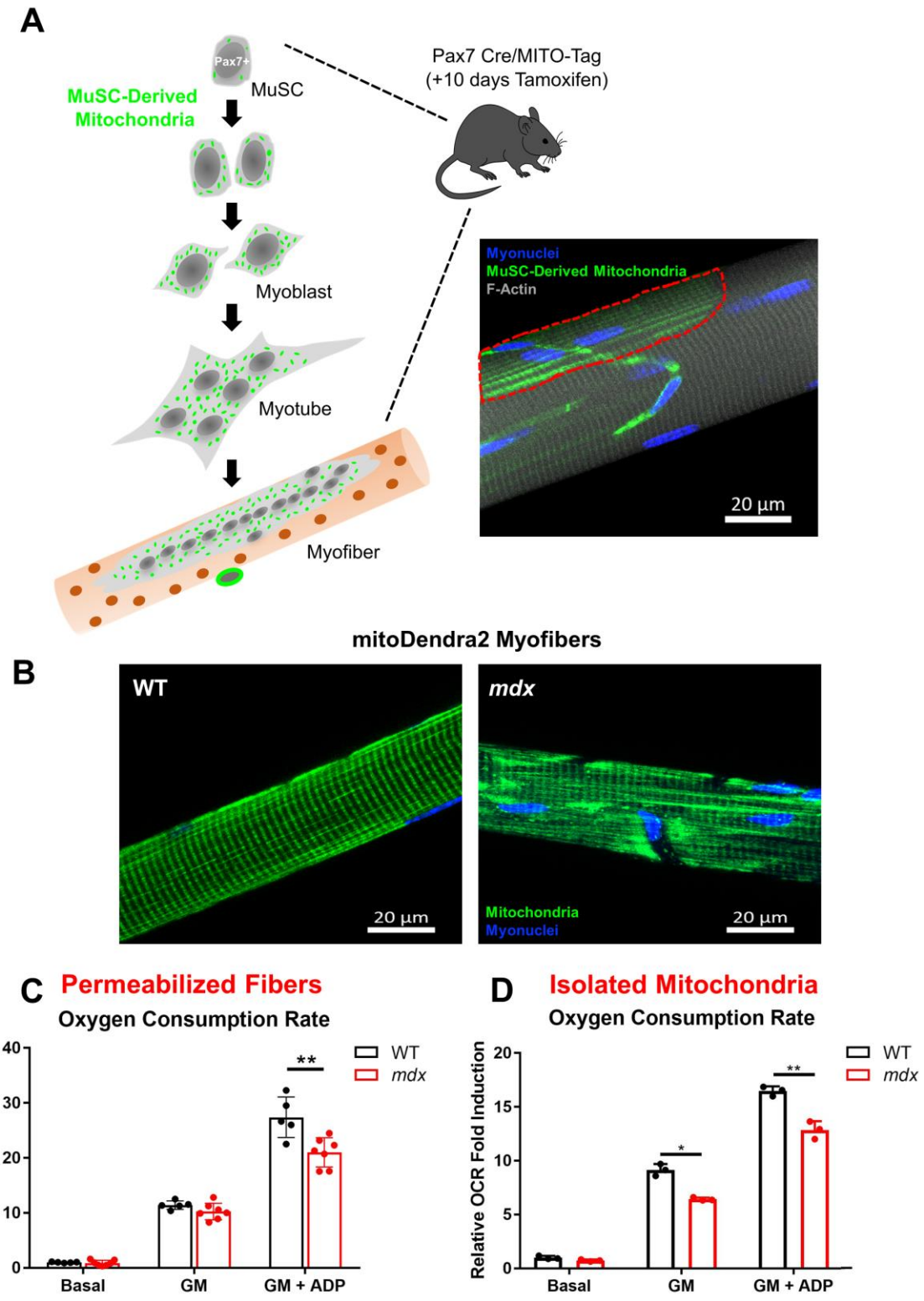

Figure 16. Dystrophic skeletal muscle myofibers harbor dysfunctional mitochondria. (A) Graphical representation of mitochondrial domain of MuSC-derived myonuclei and representative image of mitochondrial domain of MuSC-derived myonuclei using lineage

tracing of mitochondria from MuSCs (myofiber from transgenic Pax7-mitoTag muscle). Myonuclei in blue, MuSC-derived mitochondria in green, F-actin in gray. (B) Representative confocal images of isolated single myofiber from WT/*mitoDendra2* and *mdx*/*mitoDendra2* tibialis anterior muscle. Mitochondria in green, myonuclei in blue. (C) Bioenergetic functional measurement of permeabilized myofibers from wildtype and *mdx* tibialis anterior muscle. Basal (no substrate), state 2 (Complex I-linked substrates glutamate and malate) (GM), and state 3 (GM+ADP) respiration of ($n \geq 5$), all normalized to basal WT respiration. (D) Basal, state 2, and state 3 respiration of isolated mitochondria from homogenized skeletal muscles, normalized to basal WT respiration. Mean ± SD, $*p<0.05$, $**p<0.01$ using multiple t-tests compared to wildtype for all figures.

Due to the impaired bioenergetic function observed in both myofibers and isolated mitochondria from whole muscle tissue, we then assessed functional parameters of skeletal muscle health. Cytochrome c oxidase (COX) and succinate dehydrogenase (SDH) are mitochondrial ETC enzymes critical for oxidative phosphorylation that generates energy for skeletal muscle functions. Although overall enzymatic activities and frequency of COX and SDH were not statistically different, *mdx* muscles displayed clustering of COX^+ and SDH^+ myofibers, an attribute of motor unit remodeling following the pathological denervation of dystrophic myofibers (Fig. 17A, 17B)[366]. To directly investigate innervation of motor neurons, we employed a transgenic mouse model to visualize the Thy1 regulatory element of the pre-synaptic axon (*Thy1-YFP*) and crossed it with *mdx* mice to generate dystrophic motor neuron reporter mice (*mdx*/*Thy1-YFP*). Following staining of the post-synaptic endplates with α-bungarotoxin (BTX) to visualize the α-subunit of acetylcholine receptors (AChR) (Fig. 17C), we observed degeneration and thinning of the motor neuron as well as fragmentation of the post-synaptic NMJ endplate (Fig. 17D). Taken together, these data indicate that dystrophic MuSCs harbor defective mitochondria that limit their myogenic capacity and not only contribute to the mitochondrial dysfunction of dystrophic myofibers following myogenic fusion, but may also play a role in the deficiencies of MuSC

niche components like the motor neuron. Therefore, our findings highlight the MuSC as a source of mitochondrial dysfunction in pathological DMD muscle.

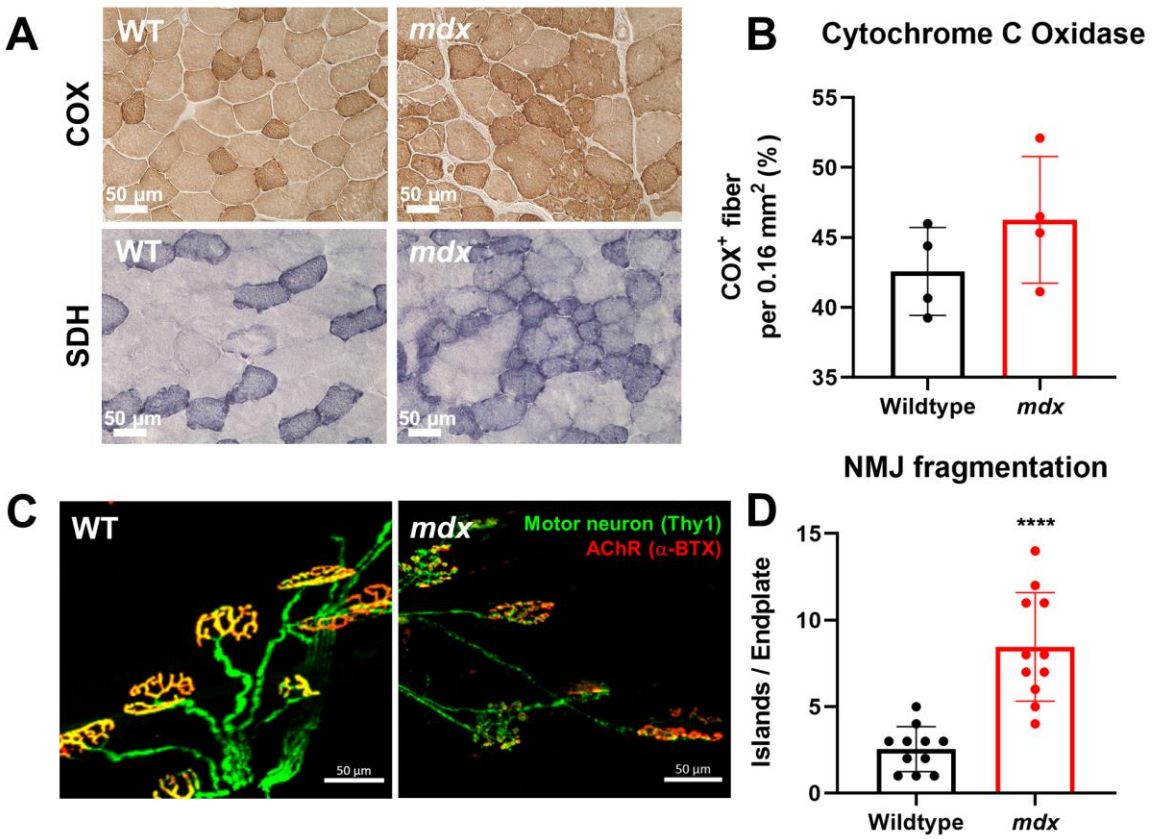

Figure 17. Motor unit remodeling of dystrophic muscle. (A) Representative images of COX activity and SDH activity staining of tibialis anterior muscles from WT and *mdx* mice. (B) Quantification of COX^+ fibers per field of view. (C) Neuromuscular junctions from WT/Thy1-YFP and *mdx*/Thy1-YFP transgenic mice expressing YFP in the Thy1 regulatory element of the pre-synaptic motor neuron. Thy1 in green, AChR in red (stained by α-bungarotoxin). (D) Quantification of NMJ fragmentation as measured by the number of islands per post-synaptic endplate. Mean ± SD, ****p<0.0001 using t-test compared to wildtype control (n=3).

4.4.3 Transplanted MuSCs Transfer their Mitochondria to Myofibers

Since dystrophin-deficient MuSCs embody defective mitochondria that convey to the mature myofiber through myogenic fusion, we interrogated the ability of healthy, transplanted MuSCs to remodel the mitochondrial domain of dystrophic myofibers, generate myonuclei that effectively regulate mitochondrial homeostasis, and improve the bioenergetic function of the myofibers. Because mitochondria are located in the cytoplasm of the cell, and the vast majority of mitochondrial proteins (~99%) are nuclear-encoded[350], we isolated purified quiescent MuSCs through FACS (Fig. 18A) from transgenic reporter mice with fluorescent proteins expressed in either cytosolic or nuclear compartments and transplanted them into *mdx* muscle to delineate successful transfer of MuSC-derived cytosol and myonuclei to dystrophic myofibers (Fig. 18B). Interestingly, centrally located myonuclei, a spatial characteristic of myonuclei within regenerating myofibers, expressed the nuclear fluorescence marker of transplanted MuSCs, suggesting that these centrally located myonuclei were derived from the transplanted MuSCs.

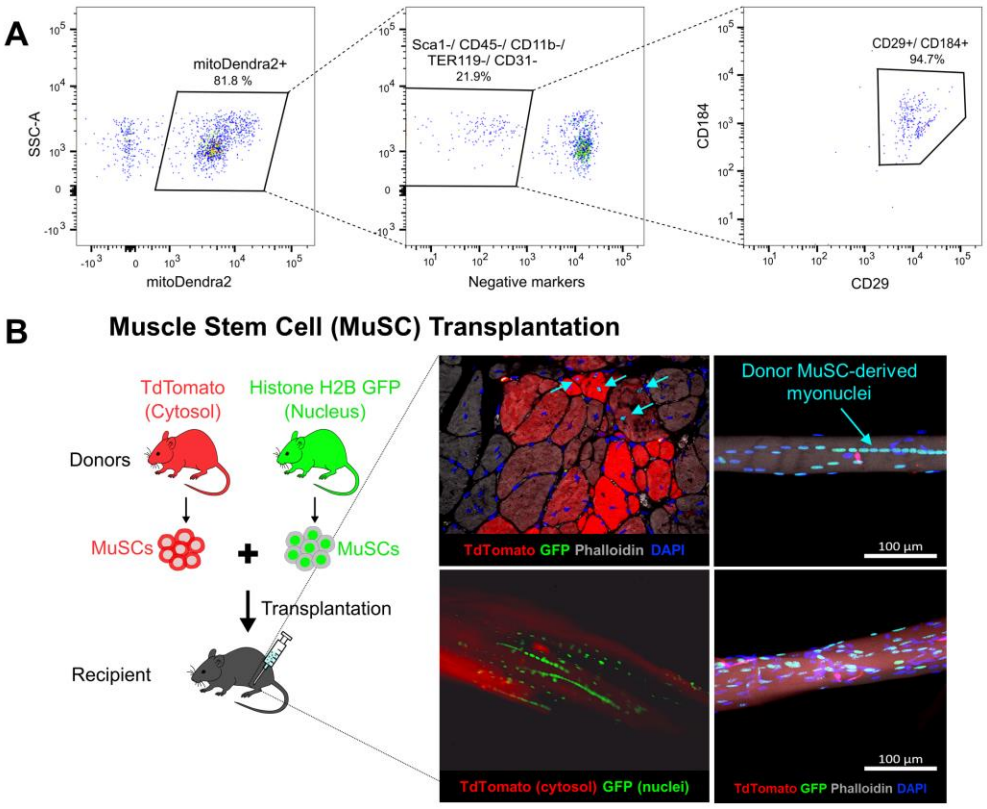

Figure 18. Transplanted MuSCs transfer cytosol and nuclei to engrafted myofibers. (A) Representative gating of quiescent MuSCs using fluorescence-activated cell sorting (FACS). (B) Schematic diagram and representative images of MuSC transplantation. An equal number of TdTomato (cytoplasm) expressing MuSCs and H2B-EGFP (nuclear) expressing MuSCs were transplanted into *mdx* TA. Representative images of cross-section and single fiber of transplanted muscles are shown. TdTomato in red, H2B in green, actin in gray, myonuclei in blue. Scale bar: 100 µm.

Next, to directly visualize MuSC-driven transfer of mitochondria into dystrophic myofibers, we transplanted MuSCs isolated from mitochondrial reporter mice, *mitoDendra2*, into *mdx* recipients (Fig. 19A) and indeed found that transplanted MuSC mitochondria were engrafted into recipient myofibers, demonstrated by cross-sectional imaging, single fiber imaging (Fig. 19B) and Western blotting of the whole muscle homogenate (Fig. 19C). While most of the transplanted mitochondria formed an organized interfibrillar mitochondrial network at 28 days following transplantation, we also observed

high densities of mitochondria in newly regenerating fibers demarked by centrally located myonuclei (Fig. 19B, *bottom*), implying that MuSC-derived myonuclei and newly synthesized mitochondria form a nuclear-mitochondrial genome network and integrate into the existing mitochondrial reticula of the recipient muscle. As an alternative approach, we also tested whether transplantation of freshly isolated mitochondria into the dystrophic muscle would provide similar bioenergetic improvements (Fig. 19D)[179]. However, donor naked mitochondria failed to incorporate into host myofibers and we observed a significant increase in interstitial infiltration of mononuclear cells and myofiber necrosis (Fig. 19E). These observations exemplify the need for MuSCs as delivery vehicles for mitochondrial delivery via cell-cell fusion and the necessity for nuclei to communicate with and functionally regulate the transplanted mitochondria.

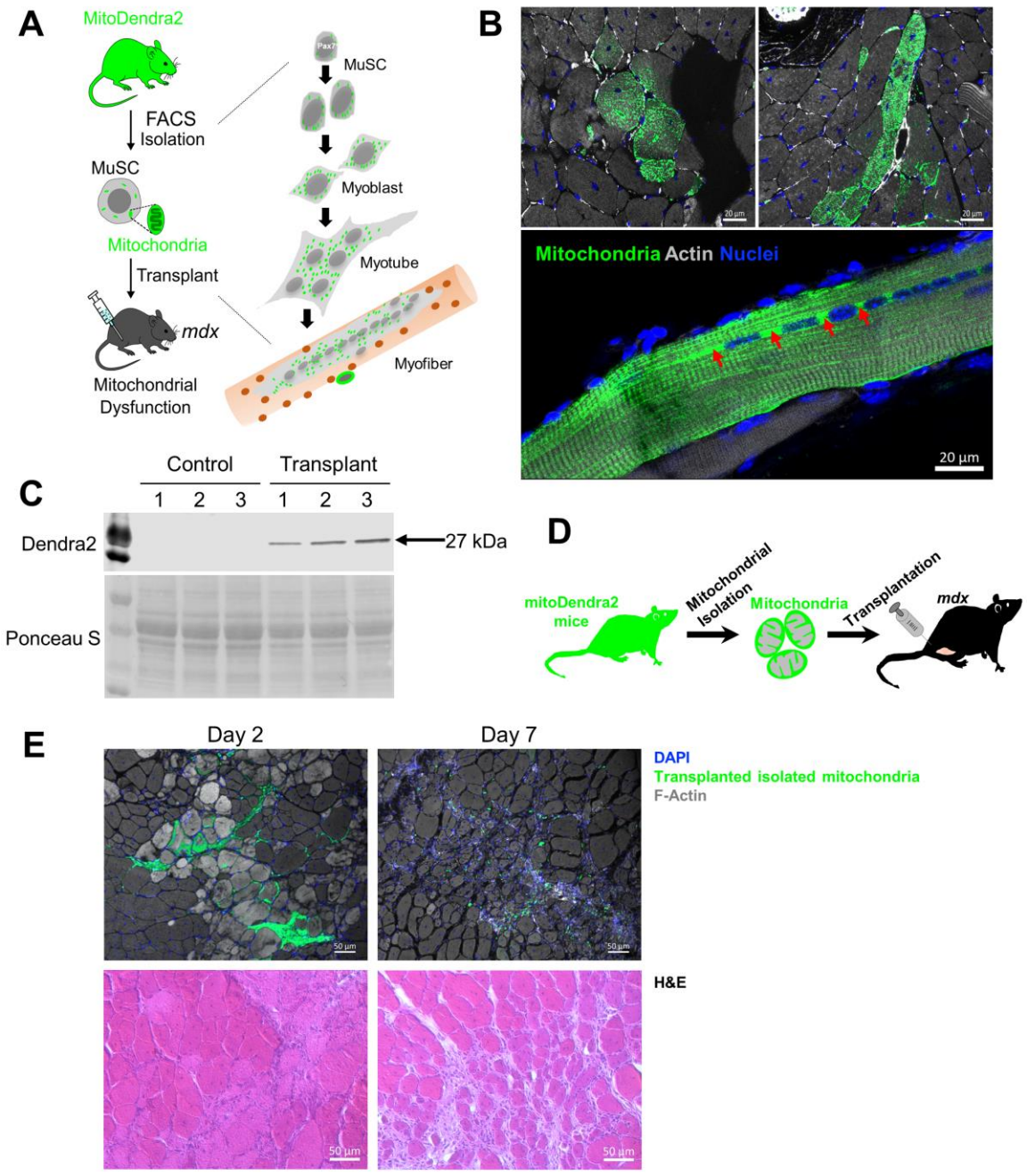

Figure 19. Transplanted MuSCs transfer mitochondria to engrafted myofibers. (A) Schematic diagram of *mitoDendra2* MuSC transplantation into *mdx* tibialis anterior (TA) muscle. (B) Representative images of mitochondrial transfer. Cross-section of TA (top) and isolated myofiber (bottom) from TA 28 days following transplantation. Mitochondria in green, actin in gray, myonuclei in blue. Red arrows depict muscle stem cell-derived mitochondria. (C) Dendra2 Western blot of muscle homogenate from *mdx* control and MuSC transplanted *mdx* muscle (n=3). (D) Schematic diagram of *mitoDendra2* isolated mitochondria transplantation into *mdx* TA muscle. (E) Cross-sections of TA muscle 2 days

and 7 days following transplantation of isolated mitochondria. Nuclei in blue, transplanted isolated mitochondria in green, F-actin in gray.

Next, to further validate efficient MuSC-based mitochondrial transfer, we measured relative mtDNA copy number of muscle homogenates from *mdx* control and transplanted *mdx* muscle and noted an elevated mtDNA copy number in transplanted muscle, corroborating the mitochondrial synthesis driven by MuSC-derived myonuclei in the recipient muscle (Fig. 20A). Furthermore, following mitochondrial transplantation, the overall mitochondrial gene expression was drastically upregulated in the recipient muscle (Fig. 20B). Among differentially regulated mitochondrial genes in the transplanted muscle, the Slc25 family of proteins showed the most striking changes (Fig. 20B). Slc25 is a family of nuclear-encoded mitochondrial proteins that are responsible for transporting substrates and metabolites involved in the TCA cycle into the mitochondria[367]. We verified this finding of increased mitochondrial content by measuring elevated protein content of a key mitochondrial electron transport chain component, complex I (NDUFB8 subunit) in MuSC transplanted muscles (Fig. 20C, 20E), though we found no differences in TCA cycle enzyme citrate synthase (Fig. 20D, 20F). It is also worth noting that after examining relative mitochondrial content of engrafted myofibers by immunostaining for SOD2, an antioxidant enzyme localized in the mitochondrial matrix, we discerned that MuSCs fused without discrimination into both high mitochondrial, oxidative type fibers and low mitochondrial, glycolytic type fibers (Fig. 20G). Altogether, these data indicate that donor MuSCs transfer functional mitochondria to various host myofiber types, and a relative increase in healthy mitochondria could lead to bioenergetic enhancements following transplantation.

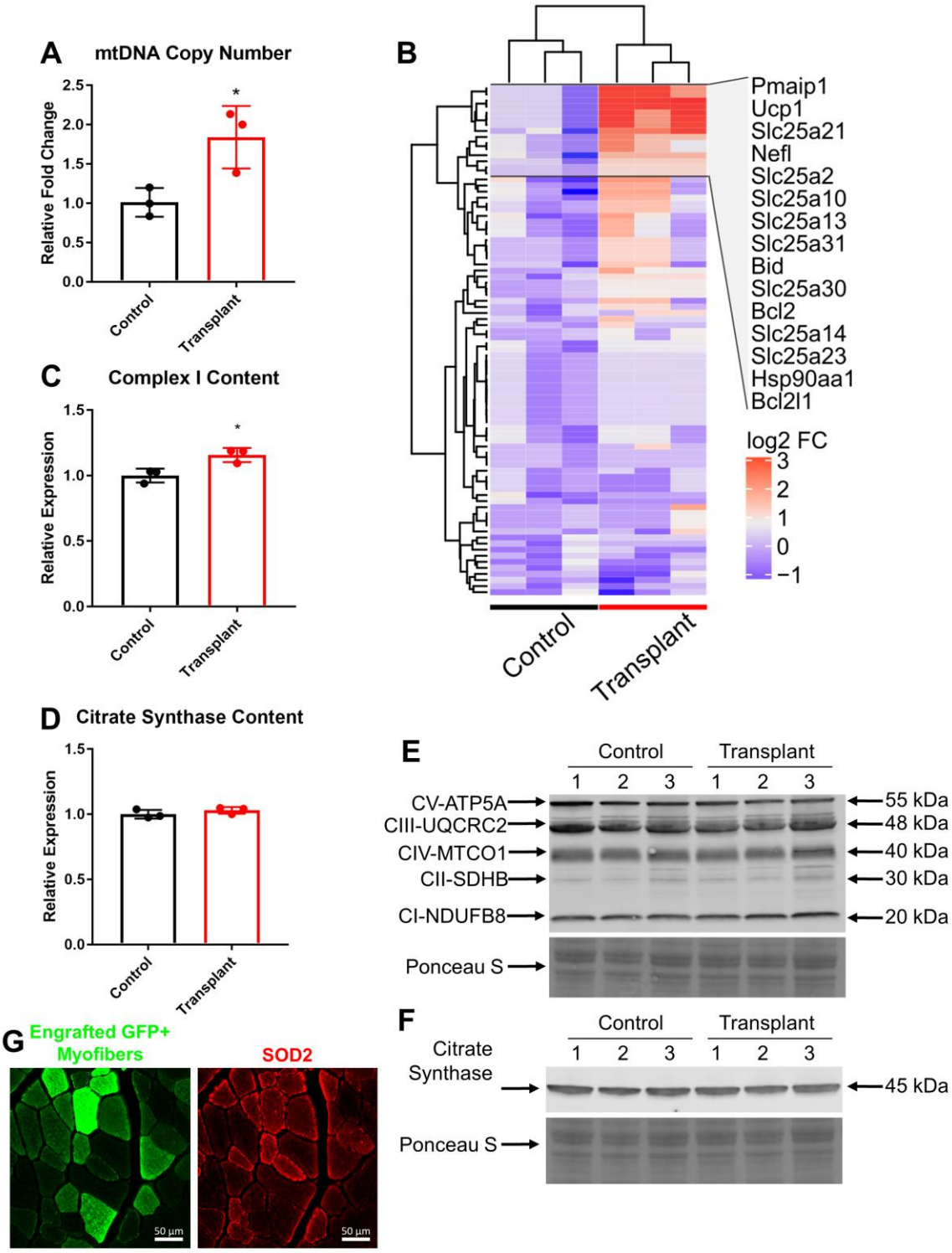

Figure 20. MuSC transplantation improves mitochondrial gene and protein expression. (A) mtDNA copy number of *mdx* control and MuSC transplanted TA of *mdx* mice (n=3). (B) Hierarchical clustering of mitochondrial gene expression from *mdx* control and MuSC transplanted *mdx* muscle using PCR array (n=3). (C) Complex I (NDUFB8-

subunit) Western blot analysis of muscle homogenate from *mdx* control and MuSC transplanted *mdx* muscle (n=3). (D) Citrate synthase content following transplantation of young MuSCs into *mdx* (n=3). (E) Western blot image of *mdx* control and transplanted muscle homogenates for OXPHOS complexes. (F) Western blot image of *mdx* control and transplanted muscle homogenates for citrate synthase content. (G) Mitochondrial content (SOD2 immunostaining) of transplanted MuSC-engrafted myofibers. Engrafted myofibers in green, SOD2 in red. Mean ± SD, *$p<0.05$ compared to *mdx* control using t-test for all figures.

4.4.4 MuSC-Derived Mitochondrial Transplantation Improves Bioenergetic Function

In the next set of experiments, we examined whether enhanced mitochondrial content via healthy MuSC transplantation resulted in functional bioenergetic improvements of the dystrophic host muscle. To address this, we assessed the morphology and bioenergetic function of the transplanted mitochondria relative to the endogenous *mdx* mitochondria. In multinucleated skeletal muscle, mitochondria form reticula in distinct locations[101,352]. This morphological arrangement of mitochondrial reticula is tightly correlated to the cell's ability to generate energy[352], so we first compared the various spatial configurations of myofiber mitochondria. Whereas the segregated architecture of endogenous mitochondrial reticula was lost in *mdx/mitoDendra2* myofibers, transplanted MuSC-derived mitochondria from young *mitoDendra2* mice into standard *mdx* mice restored the structural integrity of the mitochondrial network, similar to that of endogenous mitochondria from WT/*mitoDendra2* myofibers, and centrally located myonuclei were surrounded by high densities of exogenous mitochondria (Fig. 21A, 21B, 21C). In support of the high perinuclear mitochondrial density of transplanted myofibers, gene expression of PGC-1α, a master regulator of mitochondrial biogenesis, was upregulated (Fig. 21D),

demonstrating that transplanted MuSCs remodel the mitochondrial network within the dystrophic myofiber.

Because mitochondria must form an organized network in order to efficiently distribute ATP to the regenerating myofibers[352], we next performed direct functional analyses of MuSC-derived mitochondria following transplantation to ascertain whether the transferred mitochondria could improve the oxidative phosphorylation activity of dystrophic myofibers. Although there was no statistical difference in oxygen consumption rate between *mdx* controls and isolated transplanted myofibers with their own endogenous substrates at basal respiration, the addition of complex I-linked substrate, glutamate and malate (state 2), as well as supplementation of ADP (state 3) showed significant improvements in oxidative phosphorylation of the engrafted myofibers (Fig. 21E). ATP measurements from transplanted myofibers also exhibited increased ATP production at state 3 respiration (Fig. 21F). In contrast, when *mdx* donor MuSCs were transplanted into *mdx* recipient muscle (Fig. 21G), no improvements in mitochondrial biogenesis or oxidative capacity were observed (Fig. 21H, 21I, 21J), reaffirming our hypothesis that mitochondria of transplanted MuSCs must be healthy to drive rejuvenation of the host muscle.

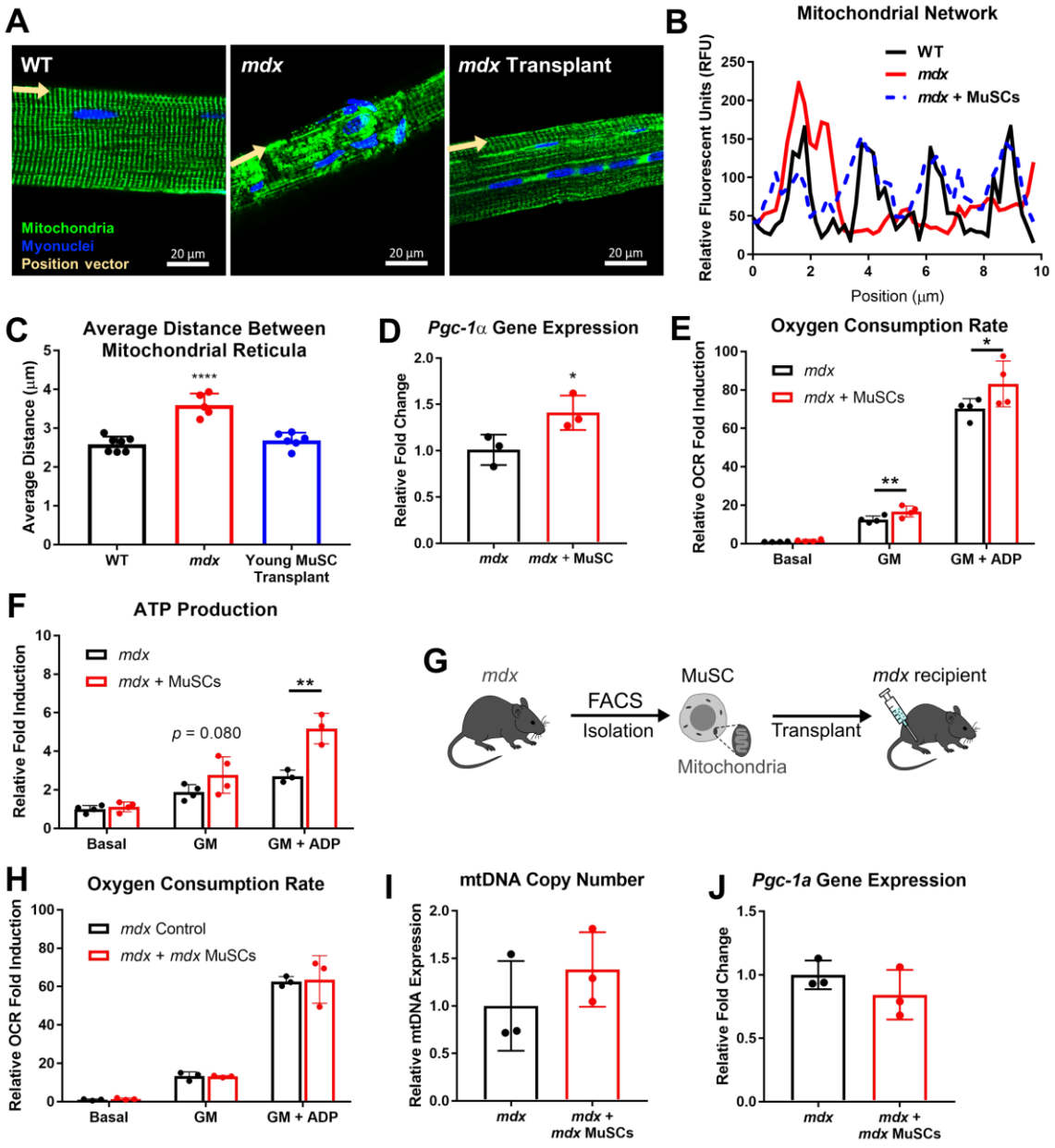

Figure 21. Transplantation of healthy MuSCs improves bioenergetic function in *mdx* mice. (A) Representative z-stacked images of single fibers from TA of WT/mitoDendra2, *mdx*/mitoDendra2, and *mdx* transplanted with young mitoDendra2 MuSCs. Mitochondria in green, myonuclei in blue, and position vectors along the myofibers in yellow. (B) Quantification of mitochondrial network organization (relative fluorescent units) along 10 μm of fiber length (position vector) to portray segregation of reticula. (C) Average distance between mitochondrial reticula along 100 μm of fiber length (n≥5). (D) Pgc-1α gene expression of contralateral mdx control and young MuSC transplanted TA in mdx (n=3). (E) States 1, 2, and 3 OCR (normalized to *mdx* control state 1 respiration) of permeabilized myofibers from mdx control and healthy MuSC transplanted TA in mdx (n=4). (F) ATP production in states 1, 2, and 3 respiration (normalized to *mdx* control state 1 ATP

production) of mdx control and young MuSC transplanted TA in mdx (n≥3). (G) Schematic diagram of transplantation of *mdx* MuSC donor into *mdx* host. (H) OCR of permeabilized fibers (normalized to *mdx* control state 1 respiration) following transplantation of *mdx* MuSCs into *mdx* host (n=3). (I) mtDNA copy number following transplantation of *mdx* MuSCs into *mdx* host (n=3). (J) *Pgc-1α* gene expression following transplantation of *mdx* MuSCs into *mdx* recipients (n=3). Mean ± SD, **p*<0.05, ***p*<0.01, *****p*<0.0001 compared to contralateral control using one-way ANOVA for panel C, t-test for panels D, I, and J, and multiple t-tests for panels E, F, and H.

The beneficial effects of endurance exercise training on skeletal muscle mitochondrial biogenesis and mitochondrial function have been well characterized[267]. Likewise, endurance exercise has been shown to promote myogenesis and myonuclear accretion[368]. Although the transplantation efficiency of exercised MuSC mitochondria has not yet been studied, we postulated that transplantation of bioenergetically-enriched mitochondria from exercise-trained donor MuSCs would propagate to dystrophic myofibers during myogenesis. Indeed, when we transplanted 8-week endurance-exercised MuSCs as donors (Fig. 22A), we observed significantly upregulated mtDNA copy number and PGC-1α expression compared to control (Fig. 22B, 22C), implying increased mitochondrial biogenesis in these muscles. To test whether this increased mitochondrial content was associated with improved mitochondrial function, exercised-MuSC-fused *mdx* myofibers were tested in a respirometer. We observed an elevated basal oxygen consumption rate compared to *mdx* control (Fig. 22D), substantiating the increased mitochondrial content demonstrated by mtDNA copy number data. Indicative of improved oxidative function, these transplanted mitochondria also manifested higher state 2 and state 3 oxygen consumption rate than *mdx* control (Fig. 22D), demonstrating that transplanted MuSCs from endurance exercise-trained MuSCs fuse their mitochondria to dystrophic myofibers to promote mitochondrial biogenesis and restore bioenergetic function.

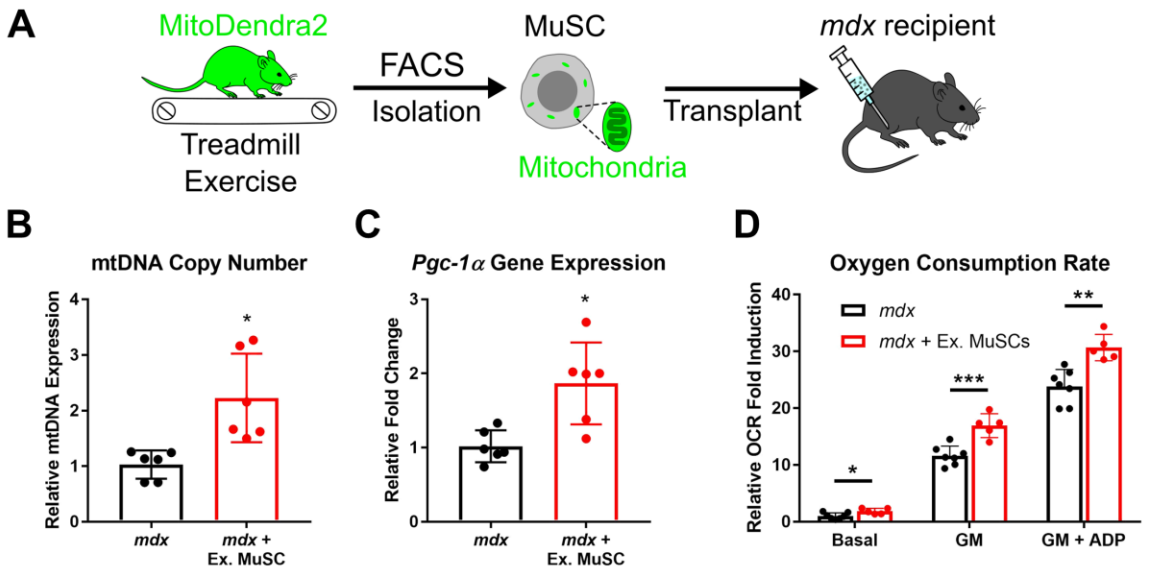

Figure 22. Transplantation of exercised MuSCs improves bioenergetic function in *mdx* mice. (A) Schematic of exercise-trained donor MuSCs transplanted into *mdx* host muscle. (B) mtDNA copy number of *mdx* control and exercised MuSC transplanted TA in *mdx* (n=6). (C) *Pgc-1α* gene expression of *mdx* control and exercised MuSC transplanted TA in *mdx* (n=6). (D) States 1, 2, and 3 OCR (normalized to *mdx* control state 1 respiration) of *mdx* control and exercised MuSC transplanted TA in *mdx* (n=6). Mean ± SD, **p*<0.05, ***p*<0.01, ****p*<0.001 compared to contralateral control using t-tests for panels B and C, and multiple t-tests for panel D.

4.4.5 Transplantation of MuSCs with Dysfunctional Mitochondria Does Not Improve Bioenergetic Function

To verify that the functional restoration of mitochondria following transplantation depends on the fusion of healthy donor MuSC-derived mitochondria, we performed a complementary analysis by transplanting MuSCs with defective mitochondria and assessing their effect on the bioenergetics of engrafted myofibers. Mitochondrial dysfunction is a hallmark of aging that has been thoroughly studied and linked to a number of age-related diseases[117]. To verify this, we characterized the mitochondrial function of

MuSC-derived myoblasts from young and aged skeletal muscle. In order to validate these myoblasts as MuSC-derived, we first isolated myoblasts from a transgenic mouse model with MuSC lineage tracing (*Pax7-tdTomato*) where the tdTomato fluorescent protein is retained in MuSC progeny (Fig. 23A) and found that the vast majority of our cultured myoblasts were tdTomato^{+}. By comparing the oxygen flux of young and aged myoblasts following addition of various substrates (Fig. 23B), we observed decreased basal respiration (Fig. 23C), ATP production (Fig. 23D), maximal respiration (Fig. 23E), and spare capacity (Fig. 23F) in aged myoblasts relative to young. This mitochondrial dysfunction was also observed in aged mature myofibers (Fig. 23J), likely due to defective mitochondria from MuSCs permeating into the myofiber following myogenic fusion.

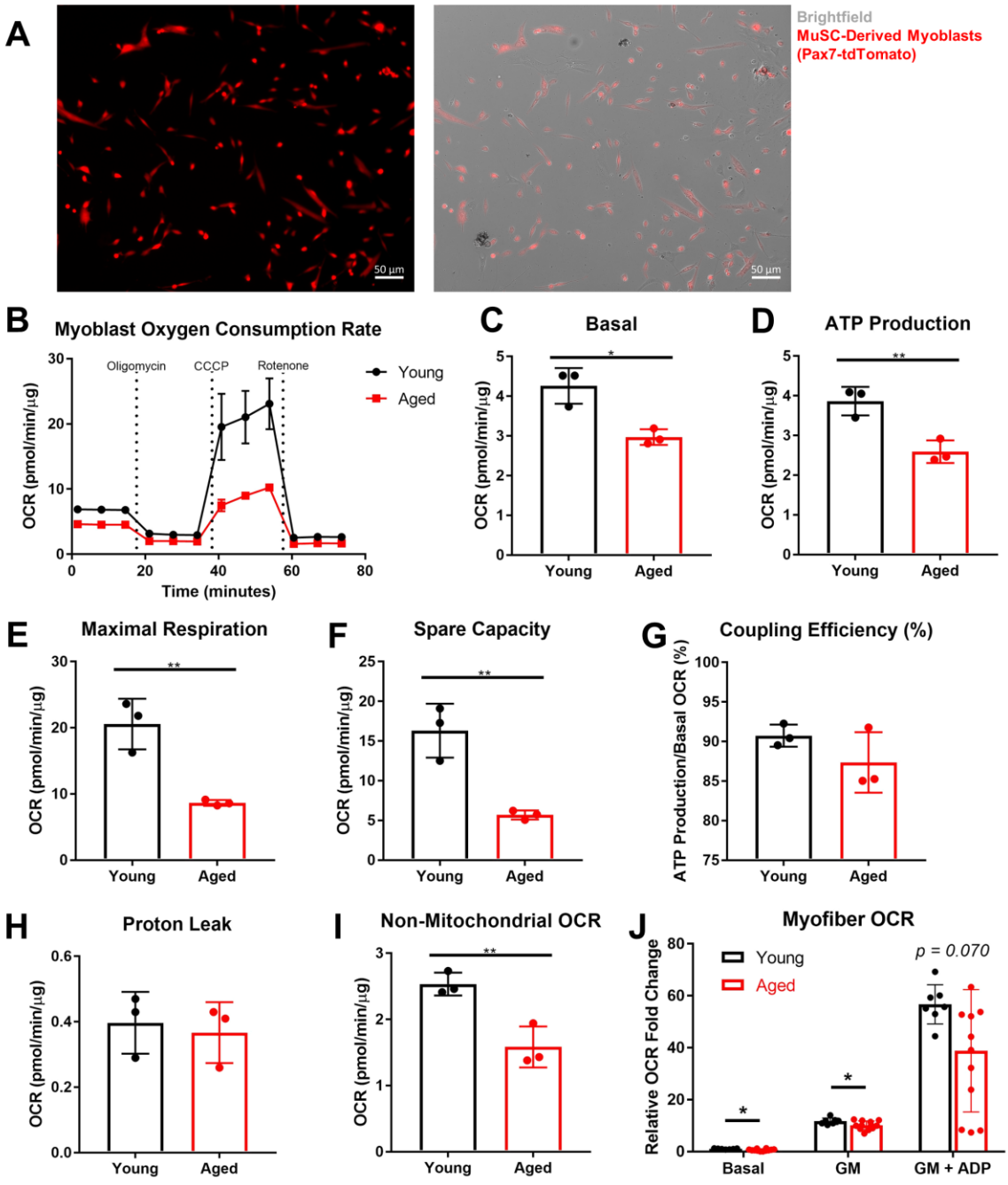

Figure 23. Characterization of aged MuSC mitochondria. (A) Image of cultured myoblasts isolated from Pax7-tdTomato (transgenic mouse line for lineage tracing of $Pax7^{+}$ MuSCs) skeletal muscle to delineate that cultured myoblasts are derived from MuSCs. (B-I) Oxygen consumption rates, ATP production, and coupling efficiency of myoblasts isolated from young (4 mos.) and aged (23 mos.) skeletal muscle using a Seahorse XFp Analyzer (n=3). (J) States 1, 2, and 3 OCR (normalized to young state 1 respiration) of permeabilized fibers from the TA of young and aged mice (n≥7). Mean ± SD, *p<0.05, **p<0.01 compared to young control using t-tests for panels C-I and multiple t-tests for panel J.

To test the effect of aged MuSCs on myofiber bioenergetic function, we transplanted GFP$^+$ aged MuSCs into *mdx* recipients (Fig. 24A) and, as anticipated, engrafted mitochondria from aged MuSCs abolished the functional improvements following transplantation despite effective aged MuSC fusion (GFP$^+$ myofibers). Following aged MuSC transplantation, no differences were observed in mtDNA copy number or PGC-1α expression compared to *mdx* control (Fig. 24B, 24C), showing that transplantation of aged MuSCs does not increase mitochondrial content. Moreover, the oxygen consumption rate on GFP$^+$ myofibers following transplantation of GFP$^+$ aged MuSCs did not show any signs of improvement (Fig. 24D), further demonstrating that MuSC-based transplantation of impaired mitochondria does not enhance the bioenergetic function of dystrophic myofibers.

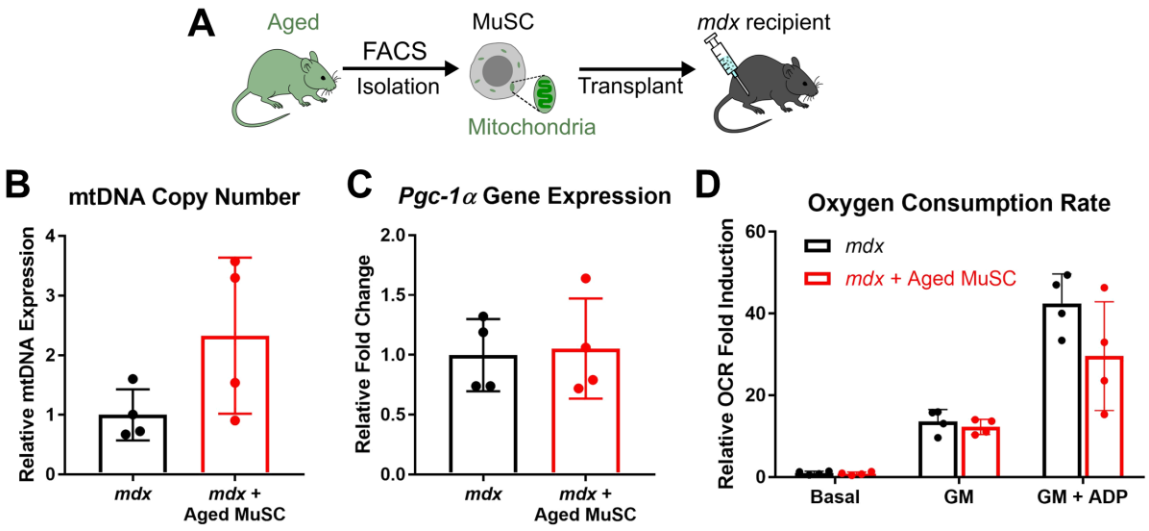

Figure 24. Transplantation of aged MuSCs does not improve bioenergetic function. (A) Schematic of aged (22 mos.) donor MuSC transplantation into *mdx* host. (B) mtDNA copy number following transplantation of aged MuSCs into *mdx* (n=4). (C) *Pgc-1α* gene expression following transplantation of aged MuSC donors into *mdx* recipients (n=4). (D) States 1, 2, and 3 OCR (normalized to *mdx* control state 1 respiration) of permeabilized fibers following transplantation of aged MuSCs into *mdx* host muscle (n=4). Mean ± SD using t-tests for panels B and C, and multiple t-tests for panel D.

To additionally examine the donor effects of MuSC mitochondrial transfer, we used MuSCs from homozygous global *Sod1* knockout (*SOD1KO*) mice, which exhibit high oxidative damage and mitochondrial myopathy due to a deficiency of this important antioxidant enzyme[117]. We first characterized the mitochondrial dysfunction of *SOD1KO* myoblasts (Fig. 25A) and found significantly decreased basal respiration (Fig. 25B), ATP production (Fig. 25C), and maximal respiration rates (Fig. 25D) compared to age-matched wildtype myoblasts. Though coupling efficiency was increased in *SOD1KO* myoblasts (Fig. 25E), like due to a compensatory response to impaired mitochondrial function, proton leak (Fig. 25F) and spare capacity (Fig. 25G) were also diminished in these knockout myoblasts. Further supporting the notion that MuSC mitochondrial dysfunction drives the myofiber mitochondrial defects, myofibers isolated from MuSC-specific *Sod1* knockout muscle exhibited high mitochondrial oxidative damage throughout the entire myofiber (Fig. 25I), suggesting that myofiber mitochondria are directly impacted by the mitochondrial quality of MuSCs. In support of previous findings[117,369], permeabilized myofibers from global *SOD1KO* muscle demonstrated significantly reduced state 2 and state 3 oxygen consumption rates compared to WT controls (Fig. 25J), again demonstrating that myofiber mitochondria directly originate from and are regulated by MuSCs and MuSC-derived myonuclei.

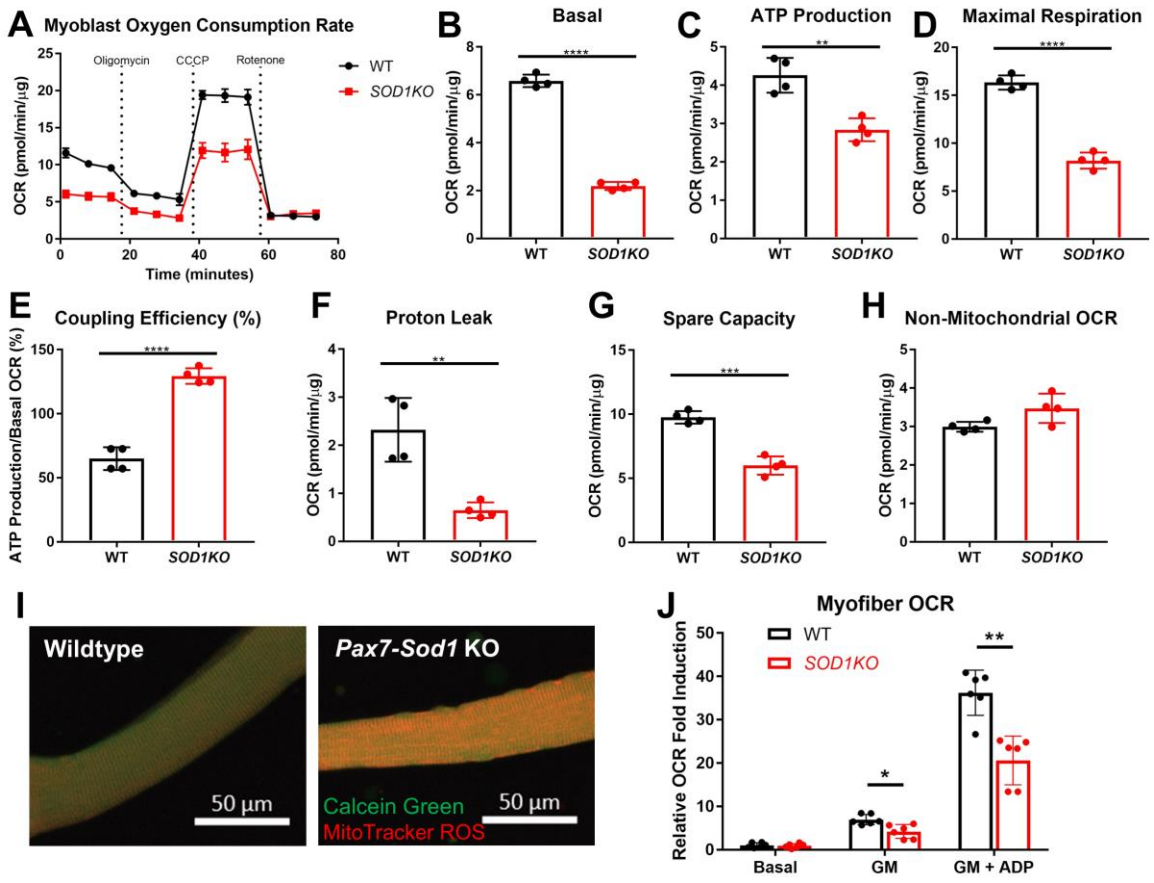

Figure 25. Characterization of *SOD1KO* MuSC mitochondria. (A-H) Oxygen consumption rates, ATP production, and coupling efficiency of myoblasts isolated from wildtype (WT) and *SOD1* knockout (*SOD1KO*) skeletal muscle using a Seahorse XFp Analyzer (n=4). (I) Confocal images of single fibers from FDB of wildtype and *Pax7-SOD1* knockout mice stained with Calcein green and Mitotracker CM-H_2XROS. (J) States 1, 2, and 3 OCR (normalized to WT state 1 respiration) of permeabilized fibers from the TA of wildtype and *SOD1* knockout mice (n=6). Mean ± SD, *p<0.05, **p<0.01, ***p<0.001, ****p<0.0001 compared to wildtype control using t-tests for panel B-H and multiple t-tests for panel J.

To further assess the impact of transplanted MuSCs with dysfunctional mitochondria, we transplanted MuSCs from global *SOD1KO* muscles into *mdx* recipients (Fig. 26A) and found abrogated accretion of functional mitochondria in the host muscle (Fig. 26B, 26C), indicating that the bioenergetically-competent donor MuSC mitochondria are vital for the enrichment of oxidative metabolism of the host myofiber. Finally, to demonstrate that the therapeutic potential for MuSC-based mitochondrial transplantation

is not restricted to DMD or dystrophic muscle, we transplanted healthy MuSC mitochondria donors to *Sod1* knockout recipient muscle (Fig. 26D). Although we did not observe an increase in mtDNA copy number (Fig. 26E) or *Pgc-1α* gene expression in the whole muscle homogenates, possibly due to the high level of mitochondrial turnover in *SOD1KO* muscles, we found significant boosts in mitochondrial bioenergetic function (Fig. 26G) of myofibers that retained mitochondria from the healthy transplanted MuSCs, illustrating the therapeutic potential of MuSC transplantation for treating numerous mitochondrial myopathies.

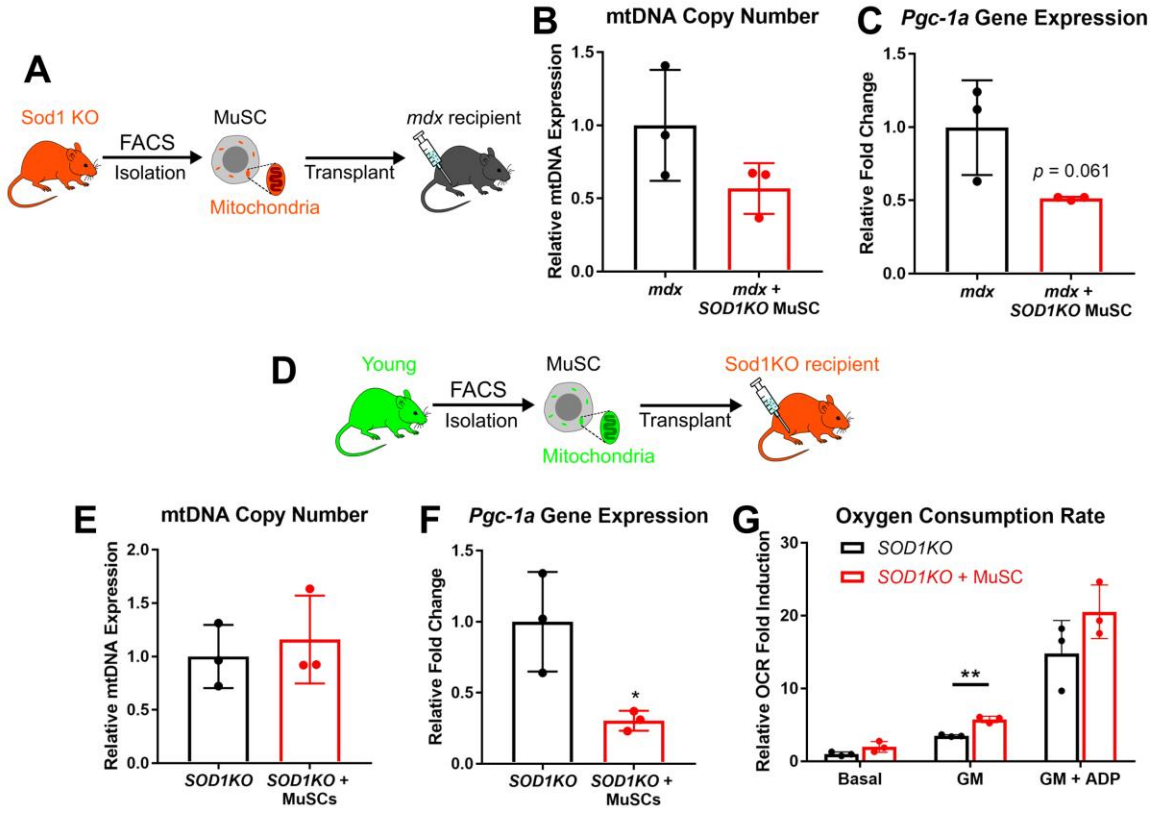

Figure 26. Transplantation of *SOD1KO* MuSCs and transplantation of healthy MuSCs into *SOD1KO* recipients. (A) Schematic diagram of *SOD1KO* MuSC donor transplantation into *mdx* recipients. (B) mtDNA copy number following transplantation of *SOD1KO* MuSCs into *mdx* (n=3). (C) *Pgc-1α* gene expression following transplantation of *SOD1KO* MuSCs into *mdx* (n=3). (D) Schematic for transplantation of young MuSCs into *Sod1*$^{-/-}$ TA. (E) mtDNA copy number following transplantation of healthy MuSCs into

SOD1KO recipient. (F) *Pgc-1α* gene expression following transplantation of healthy MuSCs into *SOD1KO* recipient. (G) State 1, 2, and 3 OCR (normalized to basal *SOD1KO* control respiration) of permeabilized fibers following transplantation of young MuSCs into *SOD1KO* (n=3). Mean ± SD, **p*<0.05, ***p*<0.01, compared to *SOD1KO* control (panels E-G) using t-tests for panels E and F, and multiple t-tests for panel G.

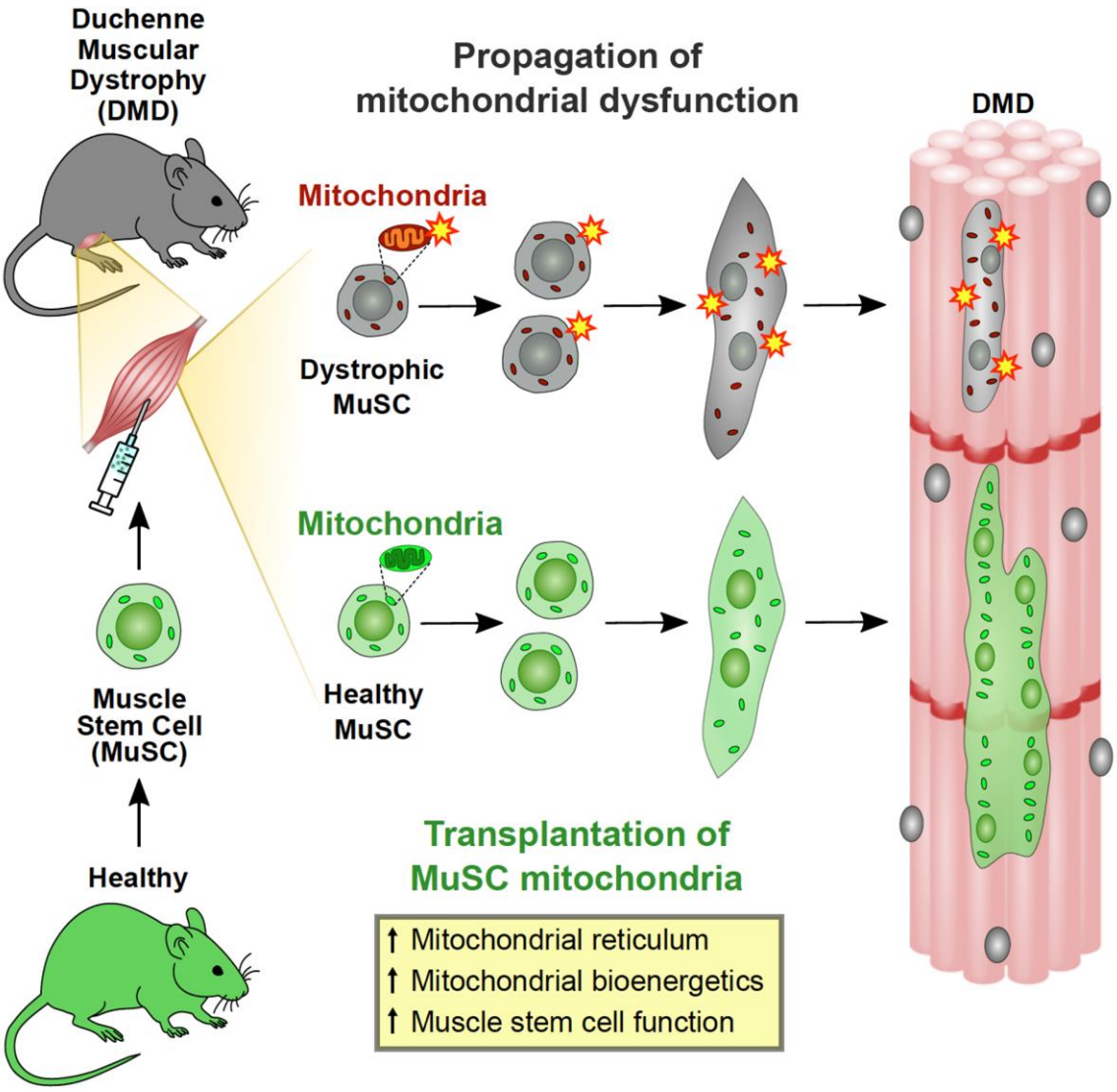

Figure 27. Graphical abstract demonstrating propagation of mitochondria from the muscle stem cell to mature myofibers.

4.5 Discussion

Here, we demonstrate the consequential role of MuSCs in maintaining myofiber mitochondria homeostasis of DMD skeletal muscle. When MuSC mitochondria are impaired, such as in dystrophic MuSCs, the dysfunctional mitochondria are transmitted to the myofiber during muscle repair. However, the bioenergetic function of dystrophin-deficient muscles can be rejuvenated via transplantation of healthy mitochondria by utilizing donor MuSCs as "delivery vehicles" to ectopically transfer new MuSC-derived mitochondria into host dystrophic myofibers (Fig. 27). Despite numerous studies reporting mitochondrial dysfunction in DMD patients and in pre-clinical models, its role in the pathogenesis of DMD has been overlooked and considered a secondary phenomenon to dystrophinopathy[205]. Intriguingly, prior to the discovery of dystrophin, DMD was in fact considered a metabolic disorder[204]. Nonetheless, a considerable amount of research has rather focused on restoring dystrophin via gene- or cell-based therapies[204,252,342], although restoration of mitochondrial function and the metabolic response has been largely ignored. Hence, in support of a recent discovery pointing towards reduced mitophagy in MuSCs as a cause of mitochondrial dysfunction in *mdx* myofibers[223], the findings from this study provide further insight into the MuSC as a source of the aberrant bioenergetic profile in dystrophic muscle and validate the ability of transplanted MuSCs to revitalize metabolic function of skeletal muscle.

MuSC transplantation will not only enhance bioenergetic function in DMD, but can also directly restore dystrophin and replenish the quiescent MuSC pool in the recipients[252,275]. Importantly, this approach can be applied in conjunction with recently developed dystrophin-targeting gene therapies (i.e., mini dystrophin, exon skipping using

CRISPR/Cas9) to simultaneously target the genetic mutations in DMD while slowing the progression of the disease[252,253]. However, clinical trials for gene therapy are mostly offered before the onset of severe symptoms and, due to several different mutant variants in the dystrophin gene that confines the pertinence of gene therapy, cell-based therapies may be a better option for many DMD patients[210,252,253]. Although MuSC availability may limit the success of translational research, significant breakthroughs in the generation of MuSCs from induced pluripotent stem cells or embryonic stem cells, combined with gene correction approaches, can improve the clinical outcomes of MuSC-based therapy by providing more transplantable cells to replenish the myogenic pool[253,275,370].

Our data demonstrate that the quality of MuSC mitochondria has a profound effect on muscle bioenergetics. In particular, this is evidenced by our studies using dystrophin-expressing aged MuSC and *SOD1KO* MuSC transplantation. Though these MuSCs are capable of replenishing dystrophin in *mdx* myofibers[252,275], and therefore restoring sarcolemmal stability and myofiber health, successfully engrafted fibers did not improve bioenergetic function due to myogenic fusion of their defective mitochondria. On the contrary, however, MuSC transplantation to treat mitochondrial myopathies can be further refined by manipulating donor MuSC mitochondria. For example, endurance-exercising donors enriches the mitochondrial content of MuSCs through PGC-1α-mediated biogenesis[267] and primes the cell to readily activate through the mTORC1 pathway[268]. Alternatively, MuSCs can also be pre-treated or co-delivered with mitochondrial-targeted small molecules or pharmacological agents to stimulate synthesis of new mitochondria or enhance mitochondrial dynamics to promote transfer of functional mitochondria into the myofiber[224,274]. In this context, other mammalian cells such as astrocytes, epithelial cells,

and mesenchymal stromal cells have been shown to transfer mitochondria intercellularly to boost the metabolic function of bioenergetically impaired tissues[371]. Yet, MuSC-based mitochondrial transfer is unique in that the MuSC-derived myonuclei that regulate mitochondrial homeostasis and myofiber repair will also fuse into the regenerating fiber. Thus, for DMD, not only does MuSC transplantation mitigate mitochondrial dysfunction, but may also repair the downstream effects of dystrophin deficiency including, but not limited to, the unstable sarcolemmal membrane, excessive Ca^{2+} influx, and exercise intolerance[341,347], thereby providing comprehensive therapeutic benefits to dystrophic muscle.

In summary, we report that the oxidative capacity of dystrophic muscle can be influenced by MuSC mitochondria via myogenic fusion. Interestingly, these findings provide a greater understanding of DMD pathophysiology and suggest that mitochondrial dysfunction is an intrinsic feature of the disease that originates in the MuSC and propagates to the myofiber. Although this mitochondrial dysfunction debilitates the myogenic program and cell fate mechanisms of dystrophic MuSCs[65], transplantation of healthy MuSCs resolves the metabolic function of DMD muscle by supplementing the engrafted myofiber with viable myonuclei and mitochondria that reestablish the crosstalk between the mitochondrial- and nuclear-genome. Overall, we provide evidence that mitochondrial transplantation through MuSC fusion revitalizes the mitochondrial function of dystrophic skeletal muscle, underscoring the value of an approach that can be used in conjunction with other modes of therapy. This study also illuminates the novel capabilities of the MuSC in muscle metabolism and its therapeutic potential for various other mitochondrial

myopathies such as hindlimb ischemia, spinal cord injury, volumetric muscle loss, and disuse atrophy.

CHAPTER 5. MUSCLE STEM CELL TRANSPLANTATION IMPROVES AGE-ASSOCIATED ISCHEMIC MITOCHONDRIAL DYSFUNCTION

5.1 Abstract

Peripheral artery disease (PAD) is a progressive, age-associated degenerative vascular disease that results in ischemia of the affected limb skeletal muscles. Although recent regenerative medicine approaches have been investigated, they have been conducted on young animals that do not capture the aging effects in the pathophysiology of PAD, such as the loss of muscle stem cells (MuSC) and impaired mitochondrial function. To determine the age-related sensitivities to ischemia, we performed a surgical hindlimb ischemia model on young and aged *C57BL/6J* mice to assess differences in regeneration and recovery. We first observed severe grades of necrosis in aged ischemic limbs due to delayed revascularization. This, in turn, led to disruptions in the mitochondrial network, bioenergetic function, myonuclear accretion, neuromuscular junction, muscle stem cell response, and redox homeostasis of the aged ischemic skeletal muscle. Due to the MuSC depletion characterized in aged muscle, we transplanted healthy MuSCs into aged ischemic muscles to replenish the MuSC pool and enhance myogenic potential. Indeed, we observed improvements in recovery in terms of the severity of necrosis. MuSC transplantation also restored the mitochondrial network and enhanced the bioenergetic function of the aged ischemic muscle. Taken together, we report drastic age-associated sensitivity and response to ischemic injury and provide a foundation for a muscle stem cell-based therapeutic that can facilitate regeneration of the aged ischemic skeletal muscle.

5.2 Introduction

Peripheral artery disease (PAD) is an age-related cardiovascular disorder in which blood vessels of the extremities are occluded by the atherosclerotic plaque and cholesterols that are built up during aging. As a result, the impaired delivery of oxygen and nutrients carried by blood leads to ischemic damage of the impacted muscles and subsequent ischemia-induced tissue necrosis. In the most severe form of PAD where blood perfusion is not sufficient to maintain tissue viability, amputation rates can reach up to 50%[147]. Although there have been recent therapeutic approaches to restore blood flow and improve muscle regeneration[200-202], these have been tested in young animals that do not represent the age-associated pathophysiology characterized in human PAD. Thus, studies that investigate the impact of age on the response to ischemia are needed to develop a clinically relevant therapy for PAD.

During aging, skeletal muscle mass and function are progressively lost, known as sarcopenia, in part due to limited protein synthesis and myokine expression[113,114,372]. As a matrix of growth factors and biomechanical support for blood vessels, skeletal muscle needs to remain viable in order to sustain the growth of new vessels and promote angiogenesis[38,373]. However, with the muscle atrophy associated with sarcopenia, aged muscles lose their capacity to support existing and newly formed blood vessels[374,375]. Moreover, angiogenesis is also impaired in old age due to diminished proliferation and migration of senescent endothelial cells[115,116], limiting the ability to form collateral vessels to bypass an ischemic occlusion. Skeletal muscles also support motor neurons, which are required for excitation-contraction of myofibers through innervation at the neuromuscular junction (NMJ). With advanced aging, however, motor neurons exhibit abnormal thinning,

distention, and sprouting while the post-synaptic endplates become fragmented and reduce in size, leading to denervation of the myofibers[118]. With an ischemic injury, motor neurons, which reside in close proximity to the vasculature, become further degenerated and the motor unit is remodeled[103]. The denervation associated with age is in part caused by high levels of oxidative stress due to mitochondrial-derived reactive oxygen species (ROS), commonly known as the mitochondrial theory of aging[119]. Through aging, the electron transport chain (ETC) of mitochondria lose their coupling efficiency, allowing leakage of electrons from the ETC that bind to oxygen and generate ROS such as superoxide[376]. Although antioxidant enzymes like superoxide dismutase (SOD) can convert the highly reactive superoxide into the more stable signaling molecule hydrogen peroxide, remaining superoxide molecules can oxidatively damage nucleic acids, proteins, and membranes of cells, or even the mitochondria themselves which then leads to the production of more ROS[377]. This vicious cycle of mitochondrial ROS generation leads to mitochondrial dysfunction and impairments in energy production that limit the energy-demanding regenerative processes of the various niche components of skeletal muscle.

In order for skeletal muscle fibers themselves to regenerate, endogenous resident muscle stem cells (MuSCs), also known as satellite cells, are required for repair of the multinucleated, post-mitotic myofiber[46]. Upon damage to the myofibers, quiescent MuSCs (marked by the expression of Pax7) activate a set of transcriptional factors to undergo asymmetric division, where the committed progenies can either form *de novo* myofibers or proliferate, differentiate, and fuse into the regenerating myofiber to increase the number of myonuclei that regulate the fiber. During this process of myogenesis, MuSCs and their progeny increase their mitochondrial content and metabolically shift from glycolysis to

oxidative phosphorylation in order to meet the energy demands of muscle regeneration[107]. With mitochondrial dysfunction that accumulates with age, however, MuSC function is debilitated and aged MuSCs are unable to properly fuse into the myofiber[124]. Furthermore, instead of generating muscle-forming progeny, MuSCs can also undergo symmetric division to self-renew and replenish the quiescent stem cell pool for future rounds of regeneration[52]. However, after many rounds of regeneration over the course of aging, the quiescent MuSC pool is eventually depleted and aged muscles lose their natural plasticity and regenerative capacity[378]. To address this phenomenon, investigators have recently explored transplantation of muscle stem cells to replenish the MuSC pool. While MuSC transplantation in models of muscular dystrophy has provided promising therapeutic outcomes[379-381], the effects of MuSC transplantation into aged ischemic muscles, and specifically its impact on mitochondrial function, has not yet been examined.

Therefore, here we demonstrate that MuSC transplantation improves the regenerative capacity and limb retention of ischemic injury in aged *C57BL/6J* mice by employing a well-characterized model of hindlimb ischemia (HLI). We first compared the sensitivity to ischemia in young and aged mice and found severe necrosis of the aged ischemic tissues. Aged myofibers also exhibited abnormal mitochondrial networks, mitochondrial dysfunction, attenuated myonuclear accretion, and impaired NMJ remodeling following ischemic injury. Transplantation of MuSCs into the ischemic tibialis anterior muscle significantly improved the level of necrosis due to restoration of the mitochondrial network, enhanced mitochondrial function, and repaired antioxidant capacity. Collectively, these findings provide insight into the age-dependent response ischemic insults and a

foundation for muscle stem cell transplantation as an effective therapeutic strategy for PAD and other muscular disorders.

5.3 Methods

5.3.1 Animal Models

All animal procedures were conducted under the approval of the Institutional Animal Care and Use Committee (IACUC) of the Georgia Institute of Technology and performed in accordance with all relevant guidelines and regulations. All mice in this study were either *C57BL/6J* genetic background or backcrossed with *C57BL/6J* for more than 6 generations and were initially purchased from Jackson Laboratory or donated by a collaborating lab. Mice were bred and maintained in pathogen-free conditions with a 12-12 light/dark cycle in the Physiological Research Laboratory (PRL) at Georgia Institute of Technology. For muscle stem/satellite cell reporter, mice expressing a tamoxifen-inducible *Cre* from the endogenous Pax7 promoter were bred with mice carrying a loxP-flanked STOP cassette followed by tdTomato in the ROSA26 locus. Other transgenic reporter mice include: *Thy1-YFP* for motor neuron[304], *mitoDendra2* for mitochondria[101,305], *S100β-EGFP* for S100β expression[382] provided by Dr. Gregario Valdez, and *β-actin-GFP* to track GFP^+ MuSCs following transplantation. Both males and females aged between 4 and 6 months, considered young adults, and between 20 and 24 months, considered aged, were used in a randomized manner for all experiments in this study.

5.3.2 Surgical Procedures

To study the effects of peripheral artery disease, we employed a well-characterized murine hindlimb ischemia (HLI) surgical ligation model, as previously described[309]. Briefly, a small unilateral incision (1 cm long) was made from the ankle to the medial thigh to expose the femoral vessels. The femoral artery and vein were then ligated with 5-0 sutures between the superficial epigastric artery and profunda femoris artery. A second ligation was made proximal to the branching of the tibial arteries, and the segment of vessels between the two ligations was excised. The skin was then closed using both sutures and wound clips. The sham surgery, where the femoral artery and vein were exposed similar to the method above without ligation or excision, was performed on the contralateral leg. Animals were maintained in single-housed cages for 3-56 days following HLI. Laser Doppler Perfusion Imaging (LDPI) was performed on a MoorLDI Imager at a scan resolution of 210x160 pixels and a height of 21 cm before euthanization by CO_2 inhalation. Perfusion was quantified in the lower hindlimb using MoorLDI Software V5.3. 28 days following HLI, hindlimbs were graded for severity of necrosis using a previously described necrosis grading scale where: grade 0 represents no necrotic tissue, grade I as necrosis in the toes only, grade II as necrotic toes and foot with loss of toes, grade III as fully necrotic foot with autoamputation of the foot up to the ankle, and grade IV as fully necrosis and autoamputation past the ankle[186,383].

To isolate and study the effects of denervation, we utilized a validated model of sciatic nerve transection (SNT). Mice were anesthetized by inhalation of 1-3% isoflurane. The hindquarter was then carefully shaved, and depilation completed with generic Nair hair removal cream. The skin was wiped 3 times with Chlorhexidine and 70% alcohol. Then a small skin incision (<10 mm) was made 1 mm posterior and parallel to the femur,

and the biceps femoris was bluntly split to expose the sciatic nerve. On the left leg, 1–2 mm sciatic nerve was then transected 5 mm proximal to its trifurcation, followed with realignment of the distal and proximal nerve ends and closure of the incision with wound clips (Autoclip, BD Clay Adams, Franklin Lakes, NJ). Sham surgery was performed on the contralateral leg where procedures were performed without nerve transection. Mice were given analgesic (0.5–1.0 mg/kg buprenorphine) and allowed to recover on a heating pad. The wound clips were removed 14 days after the SNT surgery. Sciatic nerve transections of *S100β-GFP* mice were performed at Brown University. For these experiments, young adult (6 months old), female *S100β-GFP* mice were deeply anesthetized with ketamine/xylazine intraperitoneal injection (10mg Xylazine and 90 mg Ketamine per kg body weight). After anesthesia, a small animal trimmer and depilatory cream was used to remove the fur on one leg, the surgical site was disinfected with 70% ethanol, and a small skin incision was made. The sciatic nerve from one leg was cut near the hip and the incision closed with 4-0 nonfilament sutures. Analgesia (0.5-1 mg buprenorphine per kg body weight) was administered at time of anesthesia. The contralateral leg was left unoperated for each mouse. The tibialis anterior and extensor digitorum longus muscles were harvested from injured and uninjured legs 28 days later for histological analyses.

5.3.3 Muscle Stem Cell Isolation and Transplantation

MuSCs were isolated through a cell sorting procedure as previously performed[353,354]. Briefly, hindlimb muscle tissues were harvested from young (1-3 months of age) mice, and then incubated in 20 mL of DMEM media containing 0.2% collagenase type II (Worthington Biochemical Corporation) and 2.5 U/ mL dispase (Gibco) for 90 min.

at 37 °C. After tissue digestion, the resulting media were mixed with same volume of stop media (20% FBS in F10), filtered using a cell strainer with a pore size of 70 μm, and then centrifuged (300 *g* for 5 min. at 4 °C) (Allegra X-30R Centrifuge, Beckman Coulter, USA) to obtain the myofiber-associated cell pellet. The cell pellets were washed with Hank's balanced salt solution (HBSS) containing 2% donor bovine serum (DBS), and the cells were incubated with primary antibodies. For MuSC sorting, a cocktail mixture containing the following antibodies was used: (1) APC conjugated anti-mouse CD11b (1:200; BioLegend), CD31 (1:200; BioLegend), CD45 (1:200; BioLegend), Sca-1 (1:200; BioLegend), and Ter119 (1:200; BioLegend), (2) PE conjugated anti-mouse CD29 (1:100; BioLegend), and (3) biotinylated anti-mouse CD184 (1:100; BD Biosciences). After incubation for 30 min. at 4 °C, the primary antibodies-treated cells were washed, centrifuged (300 *g* for 5 min. at 4 °C), and then treated with a secondary antibody (Streptavidin PE-Cy7) (1:50; Invitrogen) for 20 min. at 4 °C. Following propidium iodine (PI) treatment and strainer filtration (70 μm), the MuSCs (PI, CD11b, CD45, Sca-1, and Ter119; negative selection, CD29 and CD184; positive selection) were subsequently isolated by a Fluorescence activated cell sorting (FACS) (BD FACS Aria III, BD Biosciences, USA). 7 days after hindlimb ischemia, 200,000 freshly sorted MuSCs suspended in 10 µl HBSS with 2% donor bovine serum were injected intramuscularly into the TA muscle with a Hamilton syringe. Donor MuSCs were collected from *β-actin-GFP* or *mitoDendra2* mice to track transplanted cells following engraftment and myogenic fusion into the myofiber. 4 weeks following MuSC transplantation, mice were euthanized and the TAs were dissected for tissue analysis. Sham transplantation with HBSS injection without MuSCs was used as the contralateral control.

5.3.4 Histochemistry and Immunostaining

Immediately following euthanasia of animals, the tibialis anterior (TA) muscles were either snap frozen in 2-methylbutane cooled by liquid nitrogen for cryosectioning or fixed in 4% paraformaldehyde for myofiber isolation. Frozen TA muscles were sliced into 10 µm sections while fixed TA was mechanically separated into myofiber bundles for staining and then further separated into 20-30 single myofibers per sample from random areas of the muscle. Hematoxylin and eosin (H&E) and immunofluorescence were performed as previously described[310]. Materials and antibodies can be found in the appendix for dilution factors, vendors, and catalog numbers of materials. All images were taken on either Zeiss Axio Observer D1 or Zeiss 700 Laser Scanning Confocal microscopes and quantified using ImageJ. The motor units were quantified using the NMJ-morph plugin on ImageJ. Z-stack images were taken to obtain a 3D rendering of MuSCs or NMJs in Volocity. To calculate myonuclear domain, myonuclear numbers were divided by myofiber volumes approximated as volumes of a cylinder using the average radius along a 500 µm length of the myofiber.

5.3.5 Western Blot Analyses

Tibialis anterior muscles were homogenized with 25 strokes in BioMasher homogenization tubes (VWR KT749625-0030) in RIPA lysis buffer (VWR 97063-270) supplemented with Roche cOmplete Mini Protease Inhibitors (Roche 04693124001) and PhosSTOP Phosphatase Inhibitors (Roche 04906837001). Following 3 freeze-thaw cycles in liquid nitrogen and on ice, the samples were centrifuged at 18,400 *g* for 10 minutes, and the supernatants (homogenates) were normalized to total protein concentration using a

BCA protein assay kit (Thermo 23225). 50 µg of protein were run through 4-20% Criterion TGX Gels (Bio-Rad 5671093) at 150 V for 185 minutes and transferred to a PVDF membrane using a Trans-Blot Turbo System at 2.5 A for 7 minutes. Ponceau staining (Sigma P7170) was used as a loading control. Antibodies used can be found in the appendix. Membranes were imaged on Li-Cor Odyssey CLx-1050 Infrared Imaging System and bands were quantified on Li-Cor Image Studio V5.2.

5.3.6 Gene Expression Analyses

For quantitative real-time polymerase chain reaction, muscles were homogenized in a similar method to Western blot preparation with the exception of RLT buffer supplied in the RNeasy® Mini Kit (Qiagen 74104) supplemented with 1% β-mercaptoethanol to inactivate RNases rather than RIPA lysis buffer. The protocol according to Qiagen RNeasy® kit was followed for the remaining RNA isolation steps. The RNA concentration was measured by a NanoDrop One while A260/230 and A260/280 ratios were calculated for quality control. RNA content was then calculated by normalizing the RNA concentration to total muscle mass. To reverse transcribe the RNA to copy DNA, RNA concentrations were normalized to each other and the protocol according to Applied Biosystems High-Capacity cDNA Reverse Transcription Kit (Applied Biosystems 4368814) was followed, and the samples were run in a thermal cycler according to the recommended conditions. Finally, the Applied Biosystems PowerUp SYBR Green Master Mix (Applied Biosystems A25742) was used with the primers found in the appendix using an Applied Biosystems StepOnePlus Real-Time PCR system to perform the qPCR reactions. β-actin and B2M, which were found to be stably expressed following ischemia, were used housekeeping genes to quantify relative fold induction. For the PCR array data,

cDNA was mixed with PowerUp SYBR Green Master Mix, loaded into the Qiagen Mouse Mitochondria RT^2 Profiler PCR Array (330231), and run in an Applied Biosystems StepOnePlus to quantify the data.

5.3.7 Mitochondrial Respiration of Permeabilized Myofibers

Immediately following euthanasia and dissection of the tibialis anterior, fresh muscles were places in cold buffer X (7.23 mM K_2EGTA, 2.77 Ca K_2EGTA, 20 mM imidazole, 20 mM taurine, 5.7 mM ATP, 14.3 mM phosphocreatine, 6.56 mM $MgCl_2$-$6H_2O$, 50 mM K-MES) as previously described[356]. Fiber bundles with approximate wet weights of 4 mg were mechanically separated under a dissecting scope with fine forceps and permeabilized with 30 µg/ml saponin for 40 minutes. For transplanted muscles, a NIGHTSEA Stereo Microscope Fluorescence Adapter (Electron Microscopy Sciences SFA-LFS-RB, SFA-LFS-GR) was used to locate and isolate fluorescent engrafted fibers. Following permeabilization, fiber bundles were washed in cold buffer Z (105 mM K-MES, 30 mM KCl, 10 mM KH_2PO_4, 5 mM $MgCl_2$-$6H_2O$, 0.5 mg/ml BSA, 1 mM EGTA) for 15 minutes to remove any residual saponin.

Following permeabilization of fiber bundles, samples were loaded into an Oroboros O2k oxygraph with 2 mL buffer Z or buffer Z supplemented with 50 µM Amplex Red (Thermo Fisher A22188) and 0.1 U/ml horseradish peroxidase to measure oxygen consumption and hydrogen peroxide production rates. After loading samples, the chamber was equilibrated for 15 minutes to reach basal (State 1) respiration rates. Glutamate (10 mM) and malate (2 mM) were then added to the chambers for complex I-linked State 2 respiration rates, followed by the addition of ADP (5 mM) to initiate State 3 respiration to

measure various rates of oxygen consumption. For hydrogen peroxide production, the chamber was equilibrated for 15 minutes to reach basal H_2O_2 production rates, then addition of glutamate (10 mM) for complex I-linked H_2O_2 production, followed by addition of succinate (10 mM) for complex I- and II-linked H_2O_2 production, and finally addition of antimycin A (2.5 µM) for assay quality control. Oxygen consumption and H_2O_2 production rates were expressed as pmol/sec/mg fiber wet weight. All measurements were conducted at 37 °C and a working [O_2] range ~250 to 175 µM.

5.3.8 Mitochondrial Respiration of Myoblasts

For comprehensive analysis of mitochondrial respiration in myoblasts, 10,000 C2C12 cells per well in a Seahorse XFp miniplate were cultured with DMEM supplemented with 20% FBS and 1% penicillin/streptomycin until wells reached 80% confluency. Prior to running the Seahorse assay, media was changed to XF Base DMEM with 1 mM pyruvate, 2 mM glutamine, and 10 mM glucose. Sensor cartridges were loaded for sequential injections to result in final concentrations of 1 µM oligomycin, 1 µM carbonyl cyanide 3-chlorophenylhydrazone, and 0.5 µM rotenone. Myoblasts and the cartridge were placed in a Seahorse XFp Analyzer to test mitochondrial function at various stress conditions and various parameters of mitochondrial function were quantified using the Seahorse Wave software.

5.3.9 In vitro *Isolated Mitochondria Transplantation*

Mitochondria were first isolated by mincing and digesting mouse skeletal tissue with 0.1 mg/ml dispase, 1 mg/ml trypsin in Chappell-Perry buffer (100 mM KCl, 50 mM MOPS, 10 mM $MgSO_4$-$7H_2O$, 10 mM ATP, pH 7.4). Isolated mitochondria were obtained

from digested tissue through differential centrifugation and a BCA assay was performed to determine protein concentration.

During mitochondrial isolation, an *in vitro* model of ischemic injury was performed on C2C12 myoblasts as previously described[384], where cells were subjects to 3 hours of hypoxia (2% oxygen) and nutrient deprivation (replacing growth media with HBSS). Following hypoxia + nutrient deprivation (H+ND), the old growth media was restored and cells were placed back in a 20% oxygen incubator. Myoblasts were directly co-cultured with isolated mitochondria suspended in growth media at concentrations of 5 and 50 µg/ml. Co-cultures were incubated at 37°C at 20% oxygen for 24 hours to allow uptake of mitochondria, and the wells were then washed extensively with PBS to remove any mitochondria that were not internalized into the myoblasts. Cultures were then immediately prepped for the Seahorse metabolic assay.

5.3.10 Statistical Analyses

All statistical analyses were performed on GraphPad Prism 7 and data is presented as mean ± standard deviation (SD). Samples sizes were chosen using G*Power based on preliminary experiments to ensure adequate statistical power. Normality of data was tested with Shapiro-Wilk test. For experiments comparing the effects of ischemia between both young and aged mice, a two-way ANOVA with Tukey's *post hoc* test for multiple comparison was performed to assess the simple effects of uninjured vs. ischemic injury or young vs. aged. For experiments comparing a control group and injury group from the same animal (protein expression of uninjured and ischemic aged muscle, hydrogen peroxide production of uninjured and ischemic aged myofibers, quantification of $S100\beta^{+}$

cells in uninjured and denervated myofibers), multiple paired t-tests with Holm-Sidak correction was performed. *p*-value was computed without the assumption of consistent scatter (standard deviation). For experiments comparing experimental conditions to a control group (control H+ND myoblasts compared to H+ND myoblasts with co-cultured mitochondria), unpaired two-tailed t-tests assuming Gaussian distribution were used to test statistical differences. For experiments with more than 2 separate groups (uninjured aged muscle vs. ischemic muscle vs. ischemic muscle + MuSC transplantation, and control myoblasts vs. hypoxic myoblasts vs. nutrient deprived myoblasts vs. hypoxia+nutrient deprived myoblasts), ordinary one-way ANOVA was performed using Tukey's *post hoc* test for multiple comparisons. Gaussian distribution was assumed, but Geisser-Greenhouse correction was performed because sphericity was not assumed. A *p*-value of less than 0.05 was considered statistically significant for all experiments.

5.4 Results

5.4.1 Regenerative Response to Ischemic Injury is Diminished with Age

It has been previously reported that *C57BL/6J* mice recover effectively from hindlimb ischemia due to their high prevalence of collateral vessels and robust regenerative potentials for angiogenesis and myogenesis[188-190], though these studies have all been performed on young mice. Because of the diminished capacity for neovascularization and muscle growth in age, partially due to MuSC exhaustion and mitochondrial dysfunction[137,378,385], we tested the sensitivity to ischemic injury in young compared to aged *C57BL/6J* mice. We first tracked the severity of necrosis following commonly used necrosis grading scale guidelines after hindlimb ischemia where grade 0 represents no

necrotic tissue, grade I as necrosis in the toes only, grade II as necrotic toes and foot with loss of toes, grade III as fully necrotic foot with autoamputation of the foot up to the ankle, and grade IV as fully necrosis and autoamputation past the ankle[186,383] (Fig. 28A). Of the 16 young mice operated on, no ischemic leg displayed necrosis more severe than grade I by 28 days following injury (Fig. 28B), supporting the complete recovery from HLI in *C57BL/6J* mice described in literature[189]. Surprisingly, however, the majority of the 25 aged *C57BL/6J* mice with ischemia manifested necrosis at grades III and IV at day 28, with most of these foot/limb loss occurring within 10 days of ischemic injury (Fig. 28B, 28C), emphasizing the limited regenerative potential of aged muscle and manifesting a more representative animal model of severe human PAD. Interestingly, of the mice that retained their limbs, there were no differences in wet weight of the tibialis anterior (TA) muscle between control and ischemic muscles when normalizing to body weight, though control and ischemic aged muscles had consistently less relative mass compared to young mice (Fig. 28D). To assess whether this difference in sensitivity to ischemia is due to altered neovascularization, we performed laser Doppler perfusion imaging (LDPI) at various timepoints following HLI (Fig. 28E). Although blood perfusion in the ischemic limb significantly improved at day 14 compared to day 7 in both young and aged mice, the increased blood flow was significantly attenuated in aged limbs by day 28. Thus, this delayed angiogenic response to HLI likely plays a major role in the diminished recovery and limb retention observed in aged *C57BL/6J* mice.

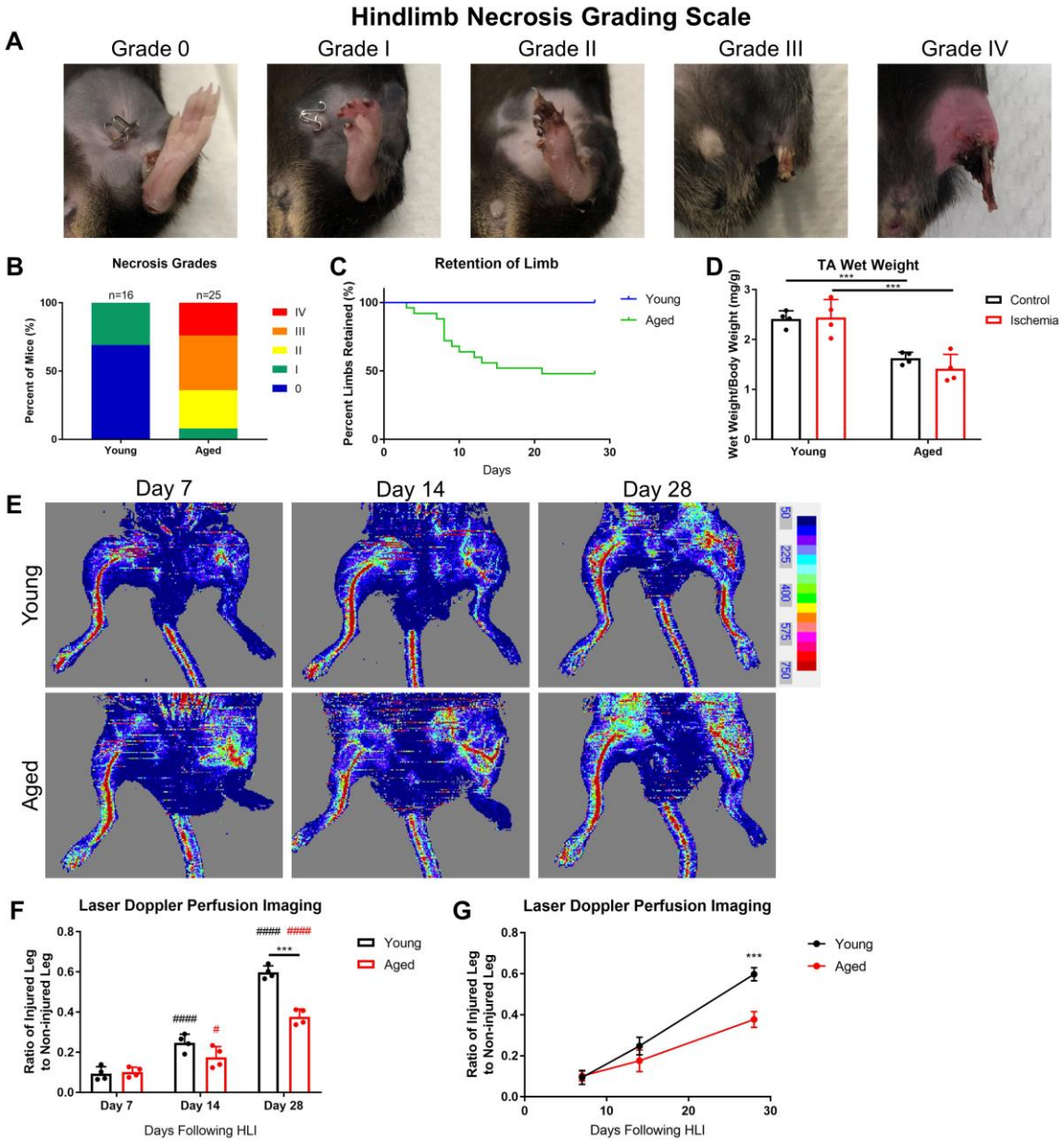

Figure 28. Diminished limb retention and reperfusion in aged mice following ischemia. (A) Representative images of hindlimb necrosis grades for grade 0 (normal), grade I (necrotic toes), grade II (necrotic foot and loss of toes), grade III (loss of foot up to ankle), and grade IV (loss of limb past ankle). (B) Percent of each necrosis grade at 28 days following ischemia in young (5 mos.) compared to aged (22 mos.) hindlimbs (n=16 young mice, n=25 aged mice). (C) Retention of foot in young and aged hindlimbs through 28 days following HLI (n=16 young mice, n=25 aged mice). (D) Wet weight of tibialis anterior (TA) muscle mass normalized to body weight in uninjured and ischemic hindlimbs from young and aged mice (n=4). (E) Representative laser Doppler perfusion images (LDPI) of the ventral side of young and aged hindlimbs at 7 days, 14 days, and 28 days following HLI. Ischemic hindlimbs shown on right of each image and contralateral control limbs

shown on left. Scale bar represents blood flow perfusion by color (n=4). (F) Mean perfusion of ischemic leg normalized to perfusion of contralateral control shown as a bar graph (n=4). (G) Mean perfusion of ischemic leg normalized to perfusion of contralateral control shown as a line graph (n=4). All data presented as mean ± SD, ***p<0.001 comparing young and aged mice, #p<0.05 compared to perfusion ratios at day 7 HLI, ####p<0.0001 compared to perfusion ratios at day 7 HLI using two-way ANOVA.

Because mitochondrial dysfunction in age has been well characterized[137], we hypothesized that defective mitochondria may contribute to the pathophysiology of aged ischemia. Consequently, we investigated differences in young and aged ischemia-induced changes to the mitochondrial morphology, a typically highly organized network of columnar reticula that can efficiently distribute metabolic intermediates and ATP to the regenerating myofiber[352]. To accomplish this, we performed HLI in young and aged *mitoDendra2* mice, where the Dendra2 fluorescent protein is targeted to the mitochondrial matrix[305] (Fig. 29A). In previous studies, we have found a significant increase in mitochondrial content and restoration of the mitochondrial network initiated by the MuSC response in young mice 28 days after HLI[103]. Similarly, single myofibers isolated from young 28 days post-HLI TA delineated a remarkable increase in mitochondrial domain, or the mitochondrial content governed by each nucleus of the myofiber, and displayed the normal reticular morphology of interfibrillar mitochondria (Fig. 29B). As observed in other studies assessing the mitochondrial network of regenerating myofibers, we also noted high densities of mitochondria in between the MuSC-derived centrally located myonuclei. In contrast, while aged myofibers also demonstrated increased mitochondrial domain and content, the highly organized architecture of mitochondria was disjointed, as seen by many mitochondrial reticula spanning several sarcomeres rather than localized into discrete columns observed in healthy myofibers (Fig. 29A, 29B). Again, we observed relatively higher densities of mitochondria between centrally located myonuclei, but these images

suggest that these newly synthesized mitochondria are unable to effectively form an organized network or integrate into the existing mitochondrial network, likely due to disrupted nuclear-mitochondrial communication.

In order to generate new myonuclei to restore nuclear-mitochondrial crosstalk, MuSCs must activate, differentiate, and fuse into the myofiber as myonuclei that can regulate myofiber mitochondria. Thus, we quantified the myonuclear number along 500 μm lengths of myofibers to determine whether altered accretion of myonuclei played a role in the inability to form a healthy mitochondrial network in aged ischemic myofibers. In young myofibers, the number of myonuclei increased dramatically following ischemia, corresponding to the restoration of the mitochondrial network. Although there was also an increase in myonuclear number of aged ischemic myofibers compared to aged control, this accretion of myonuclei was significantly attenuated compared to young ischemic myofibers (Fig. 29C). Following quantification of the myonuclear domain, or the cytoplasmic volume of myofiber governed by each myonucleus, both young and aged ischemic myofibers demonstrated similar decreases in myonuclear domain size, which may be attributed to the significant decrease in overall myofiber size from aged ischemic muscles (Fig. 29D, 29E). Together, these data show that the impaired restoration of the mitochondrial network in aged muscle parallels a reduced ability to generate new MuSC-derived myonuclei.

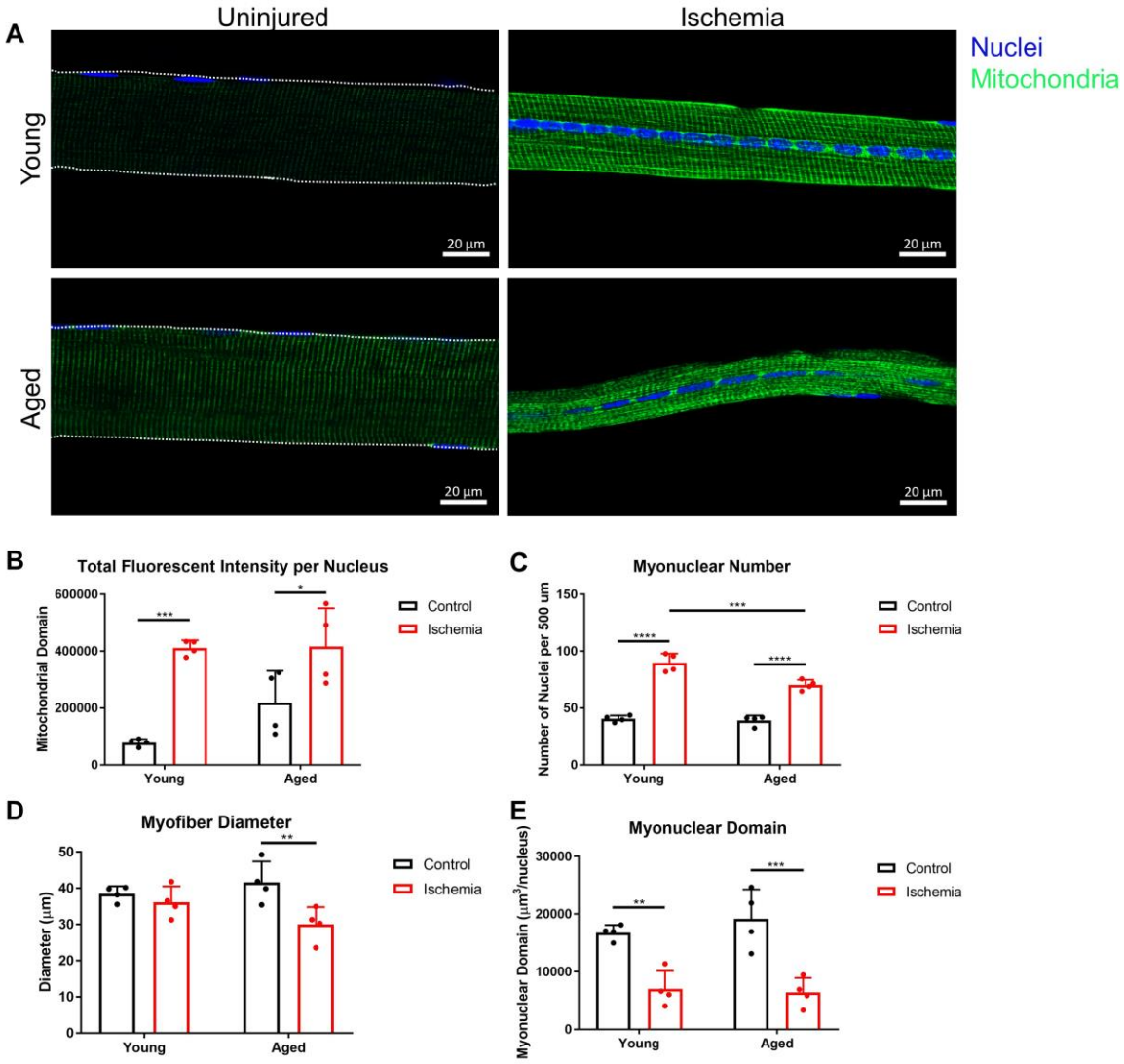

Figure 29. Impaired restoration of the mitochondrial network and accretion of myonuclei in aged ischemic myofibers. (A) Representative confocal images of interfibrillar mitochondria of single myofibers from young (5 mos.) and aged (22 mos.) TAs of *mitoDendra2* mice 28 days after HLI. Nuclei in blue, mitochondria in green. (B) Mitochondrial domain of 20 myofibers per sample in young and aged *mitoDendra2* mice 28 days after HLI. Mitochondrial domain calculated as total integrated fluorescent density of Dendra2 divided by the number of myonuclei (n=4). (C) Number of myonuclei per 500 µm of myofiber with 20 myofibers counted per sample (n=4). (D) Mean diameter of 500 µm length of 20 myofibers per sample (n=4). (E) Myonuclear domain of 20 single myofibers per sample over 500 µm of myofiber length, calculated as myofiber volume divided by number of myonuclei. Myofiber volume was approximated as the volume of a cylinder using the average radius along a 500 µm length of myofiber (n=4). All data presented as mean ± SD, *p<0.05, **p<0.01, ***p<0.001, ****p<0.0001 using 2-way ANOVA.

5.4.2 Mitochondrial Function is Reduced in Aged Ischemic Muscle

In multinucleated skeletal myofibers, the distinct morphological arrangement of mitochondrial reticula is tightly correlated with the cell's ability to generate energy[352], and so we next performed direct functional analyses of myofiber mitochondria to determine if the disrupted mitochondrial network in aged ischemia mice was associated with a loss of oxidative capacity. Following permeabilization of isolated myofiber bundles from TAs that were loaded into a high-resolution respirometers, we measured the oxygen consumption rate of the myofiber bundles normalized to wet weight at basal respiration without any exogenous substrates (state 1), mitochondrial ETC complex I-linked respiration with the addition of glutamate and malate (state 2)[365], and ATP-converting respiration with the addition of ADP (state 3). At all states of respiration, there was no significant difference between control and ischemic myofibers in young mice 28 days following HLI (Fig. 30A, 30B, 30C). However, aged ischemic myofibers demonstrated significant deficiencies in oxidative capacity at all three states of respiration compared to aged control (Fig. 30A, 30B, 30C), indicating that the altered mitochondrial morphology was indeed concomitant with a loss of bioenergetic function.

In order to elucidate the mechanism behind this mitochondrial dysfunction observed in aged ischemic muscle, we homogenized whole TAs and measured contents of proteins that play key roles in regulating oxidative stress, a characteristic of ischemic injury due to the increased levels of reactive oxygen species (ROS), such as superoxide, that are induced by rapid changes in oxygen and nutrient concentrations[140]. A key antioxidant enzyme,

superoxide dismutase (SOD), is responsible for converting the highly reactive superoxide into the hydrogen peroxide signaling molecule to maintain redox homeostasis, with the SOD1 isoform primarily localized in the cellular cytosol and mitochondrial intermembrane space while SOD2 is localized within the mitochondrial matrix. 28 days following HLI, aged ischemic muscles expressed decreased SOD content of both isoforms, suggesting an abated capability to convert superoxide into less reactive forms (Fig. 30D). Indeed, when we measured levels of aconitase, a mitochondrial matrix-localized TCA cycle enzyme with Fe-S clusters that are susceptible to ROS-induced oxidative damage and rapidly degraded by the Lon protease system[386], we found significantly reduced aconitase content in aged ischemic muscle compared to aged control (Fig. 30D), indicating that ischemia in aged muscles results in oxidative damage to cellular components within the mitochondrial matrix. To further assess the mechanism of oxidative damage in aged ischemic mitochondria with regards to the role of SOD, we loaded permeabilized fibers into a closed chamber and measured hydrogen peroxide production following addition of various substrates. At both basal respiration with no substrates and complex I-linked respiration with the addition of glutamate (G), aged ischemic myofibers generated higher levels of H_2O_2 (Fig. 30E), indicative of elevated superoxide concentration at resting state that is converted into hydrogen peroxide. With the subsequent addition of succinate, a complex II-linked substrate localized in the mitochondrial matrix, aged control myofibers generated higher levels of H_2O_2 compared to the previous two states of respiration (Fig. 30E). Conversely, the addition of succinate did not lead to an increase in H_2O_2 production in aged ischemic myofibers (Fig. 30E), indicating that the SOD system (particularly SOD2 within the matrix) is overwhelmed and unable to convert superoxide into hydrogen peroxide when

complex II (located on the matrix side of the mitochondrial inner membrane) is active. Thus, these data imply that aged ischemic myofibers harbor dysfunctional mitochondria with oxidative damage compartmentalized within the mitochondrial matrix.

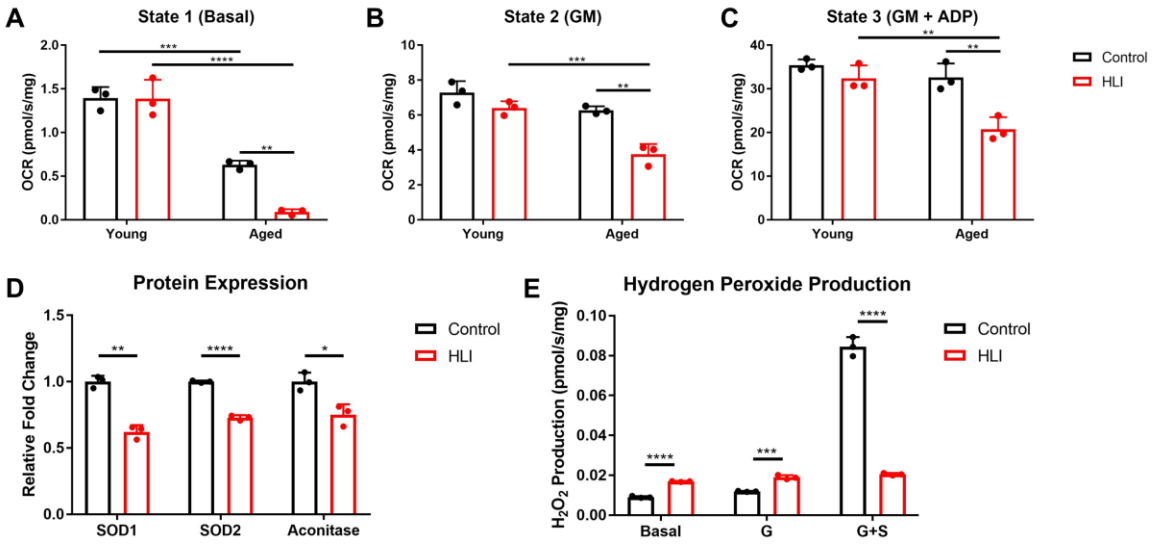

Figure 30. Oxidative damage of dysfunctional aged ischemic mitochondria is compartmentalized in the mitochondrial matrix. (A) State 1 basal oxygen consumption rate in young (4 mos.) and aged (21 mos.) control vs. ischemic myofibers (n=3). (B) State 2 complex I-linked oxygen consumption rate in young and aged control vs. ischemic myofibers with the addition of glutamate and malate (GM) (n=3). (C) State 3 ATP-producing oxygen consumption rate in young and aged control vs. ischemic myofibers with the addition of ADP (GM + ADP) (n=3). (D) Relative protein concentrations of SOD1, SOD2, and aconitase in aged control and aged ischemic (20 mos.) TA homogenate (n=3). (E) Hydrogen peroxide production from permeabilized myofiber bundles at basal activity, complex I-linked activity with the addition of glutamate (G), and complex I- and II-linked activity with the subsequent addition of succinate (G+S) (n=3). All data presented as mean ± SD, *p<0.05, **p<0.01, ***p<0.001, ****p<0.0001 using 2-way ANOVA for OCR experiments (A-C) and multiple t-tests for protein expression and H_2O_2 production experiments (D-E).

In order to test whether disrupted nuclear-mitochondrial genome communication plays a key role in the mitochondrial dysfunction of aged ischemic muscles, we next quantified the expression of various mitochondrial nuclear- and mtDNA-encoded genes through qPCR. Cox1, an mtDNA-encoded gene for a complex I subunit, was significantly

downregulated in both young and aged ischemic muscles compared to uninjured controls, though aged control and ischemic muscles had significantly decreased expression relative to young muscles (Fig. 31A). Sdha, a nuclear-encoded gene for a complex II subunit, was also significantly downregulated in both young and aged ischemic muscle compared to uninjured controls (Fig. 31B). mtDNA copy number, calculated by dividing Cox1 expression by Sdha expression, was significantly downregulated in aged muscles compared to young muscles (Fig. 31C), indicating a disturbance in the ability of the mitochondrial genome to regulate mitochondria of aged muscles. Next, we investigated the gene expression of important mitochondrial scaffolding proteins encoded by nuclear DNA. For example, prohibitin (Phb) is a multi-functional mitochondrial protein on the inner membrane that is transported from the nucleus into the mitochondria and plays a role in modulating mitochondrial autophagy following oxidative stress. While the Phb1 isoform is significantly upregulated in young muscle following ischemic injury, aged nuclei did not present a similar increase in Phb1 expression after HLI (Fig. 31D). Likewise, expression of the Phb2 isoform was also significantly decreased in uninjured and ischemic aged muscles compared to young muscles (Fig. 31E), further exemplifying the disconnect between nuclei and mitochondria in aged muscles and providing a mechanistic link for the impaired removal of defective mitochondria. Moreover, nuclear-encoded genes with mitochondrial targeting sequences that act as master regulators for mitochondrial fusion and fission, such as Opa1 and Drp1, respectively, are required for mitochondrial turnover. Gene expression analyses demonstrated that both Opa1 and Drp1 are significantly downregulated in aged muscle compared to young muscle (Fig. 31F, 31G), impairing the mitochondrial dynamics necessary to form an organized mitochondrial network. These

findings provide insight into the disrupted nuclear-mitochondrial communication that plays a role in the mitochondrial dysfunction and limited regenerative capacity of aged ischemic skeletal muscle.

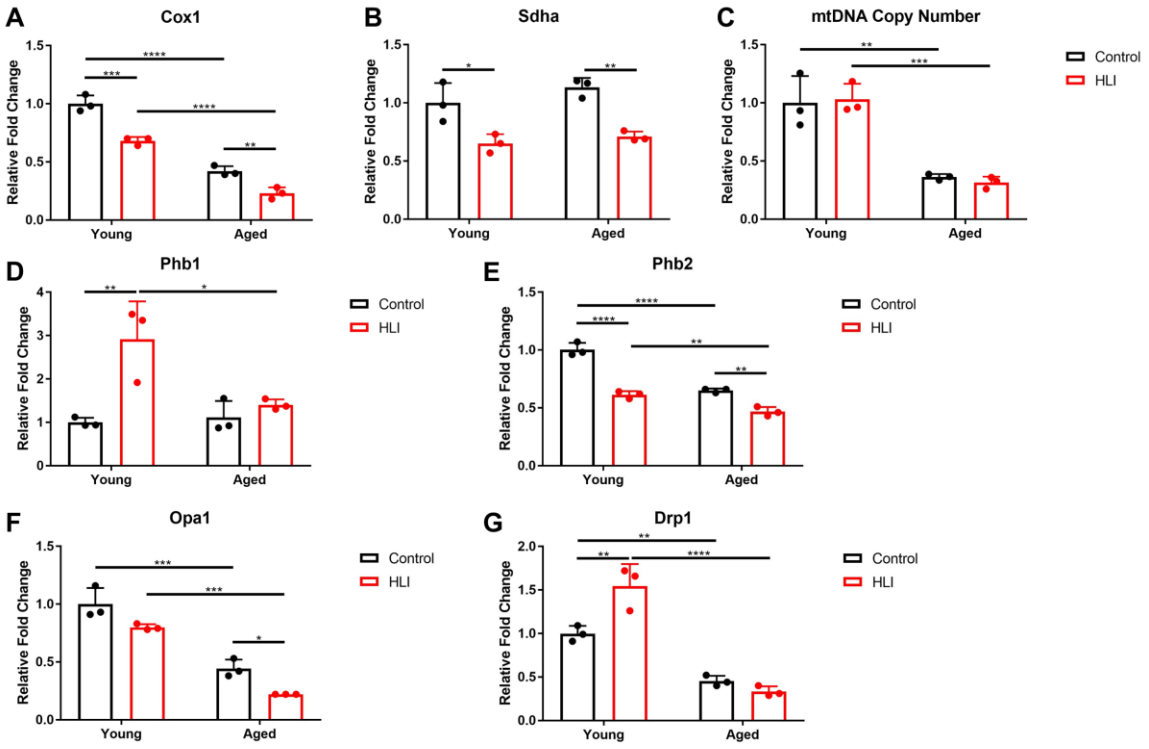

Figure 31. Disrupted mitochondrial-nuclear genome communication limits mitochondrial dynamics in aged muscles. (A) Relative gene expression of Cox1 in young (4 mos.) and aged (21 mos.) muscles following HLI (n=3). (B) Relative gene expression of Sdha in young and aged muscles following HLI (n=3). (C) Relative mtDNA copy number of young and aged muscles following HLI (n=3). (D) Relative gene expression of Phb1 in young and aged muscles following HLI (n=3). (E) Relative gene expression of Phb2 in young and aged muscles following HLI (n=3). (F) Relative gene expression of Opa1 in young and aged muscles following HLI (n=3). (G) Relative gene expression of Drp1 in young and aged muscles following HLI (n=3). All data presented as mean ± SD, *p<0.05, **p<0.01, ***p<0.001, ****p<0.0001 using 2-way ANOVA.

5.4.3 Ischemia-Induced Regeneration of the Motor Unit is Impaired in Aged Mice

Among proper mitochondrial function, innervation of muscle fibers is also necessary myofiber regeneration due to the required excitation-contraction coupling during homeostatic skeletal muscle maintenance. We have previously shown that ischemia results in degeneration of the motor neuron, denervation of the neuromuscular junction (NMJ), and remodeling of the motor unit[103]. Hence, we tested whether a decline in motor unit remodeling and reinnervation of the myofiber played roles in the age-associated limb loss following ischemia. We performed HLI on young and aged motor neuron reporter mice, in which the *Thy1* regulatory element expresses YFP (*Thy1-YFP*)[304], and imaged pre-synaptic axon terminals and post-synaptic acetylcholine receptor (AChR) endplates from extensor digitorum longus (EDL) muscles (Fig. 32A). NMJs were 3D reconstructed (Fig. 32B) and quantified using the NMJ-morph plugin on ImageJ to assess various characteristics of the motor unit. For example, area of axon terminals were significantly reduced in aged ischemic muscle due to Wallerian degeneration (Fig. 32C) while aged motor neurons displayed significantly more terminal branches following ischemia (Fig. 32D). Aged ischemic endplates were also less compact, a metric for the amount of AChR within the endplate (Fig. 32E). The area of synaptic contact as well as the percentage of overlap between the pre-synaptic axon and post-synaptic endplate were also diminished in aged muscles (Fig. 32F, 32G). Finally, aged ischemic endplates were significantly more fragmented than young counterparts (Fig. 32H) as measured by the number of AChR clusters per NMJ. These analyses signify drastic degeneration of the motor neuron and reduced reinnervation of ischemic muscles in aged mice that contribute to the diminished muscle regeneration in response to HLI.

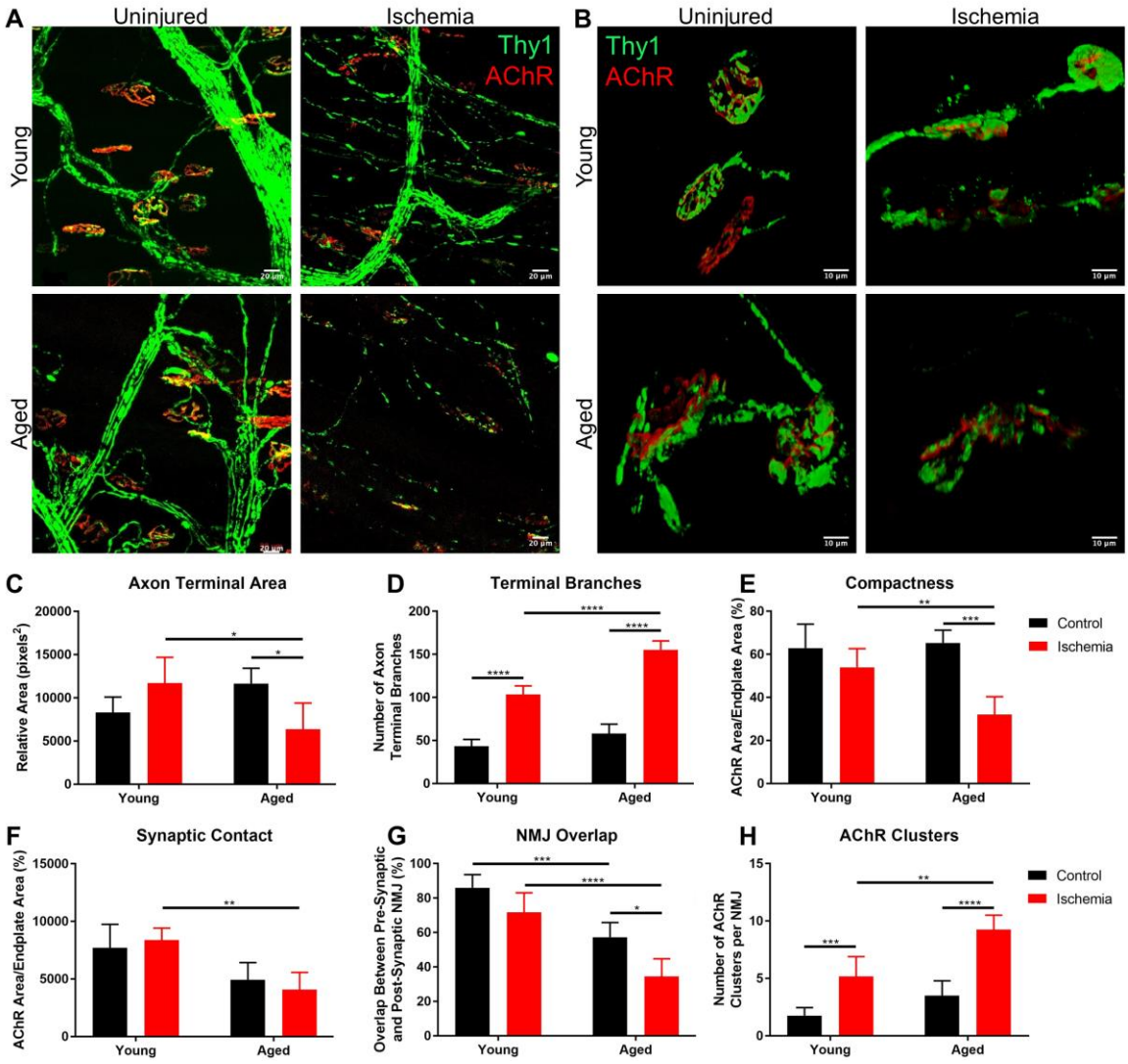

Figure 32. Aged muscles exhibit degenerated motor units following ischemia. (A) Pre-synaptic motor neuron and post-synaptic AChR endplate images from the EDL in young (6 mos.) and aged (22 mos.) control vs. ischemic limbs. α-bungarotoxin (for AChR-α subunit) in red, Thy1 (for motor neuron axon terminal) in green. Maximum intensity projections were performed from z-stacked images taken on a confocal microscope. (B) NMJs from the EDL in young and aged control vs. ischemic limbs. Z-stacked images were 3D reconstructed using Volocity. (C) Area of axon terminals from young and aged control vs. ischemic NMJs. (D) Number of axon terminal branches from young and aged control vs. ischemic NMJs. (E) Compactness of AChR endplates in young and aged control vs. ischemic NMJs. (F) Area of synaptic contact in young and aged control vs. ischemic NMJs. (G) Percent of synaptic contact area over the entire endplate area in young and aged control vs. ischemic NMJs. (H) Number of AChR clusters per endplate in young and aged control vs. ischemic NMJs. All data presented as mean ± SD, *p<0.05, **p<0.01, ***p<0.001, ****p<0.0001 using 2-way ANOVA.

During regeneration of the NMJ, subsynaptic myonuclei derived from MuSCs via myogenesis are responsible for maintaining and remodeling the NMJ following denervation. Therefore, we investigated whether the impaired reinnervation of aged myofibers was an effect of altered number of subsynaptic myonuclei (Fig. 33A). Using the *mitoDendra2* mitochondrial reporter mouse model, both young and aged myofiber bundles from the TA demonstrated increases in synaptic mitochondria required for generating energy during NMJ regeneration (Fig. 33B) and number of subsynaptic nuclei per endplate (Fig. 33C) compared to uninjured young and aged controls, respectively. However, due to the high fragmentation rate of aged ischemic NMJs, synaptic area of these NMJs were significantly larger (Fig. 33D). When we normalized the number of subsynaptic nuclei to the synaptic area, the increase in subsynaptic nuclei in aged ischemic NMJs were abolished (Fig. 33E). These data indicate that aged muscles do not generate enough myonuclei within a confined space to facilitate NMJ remodeling following an ischemic injury.

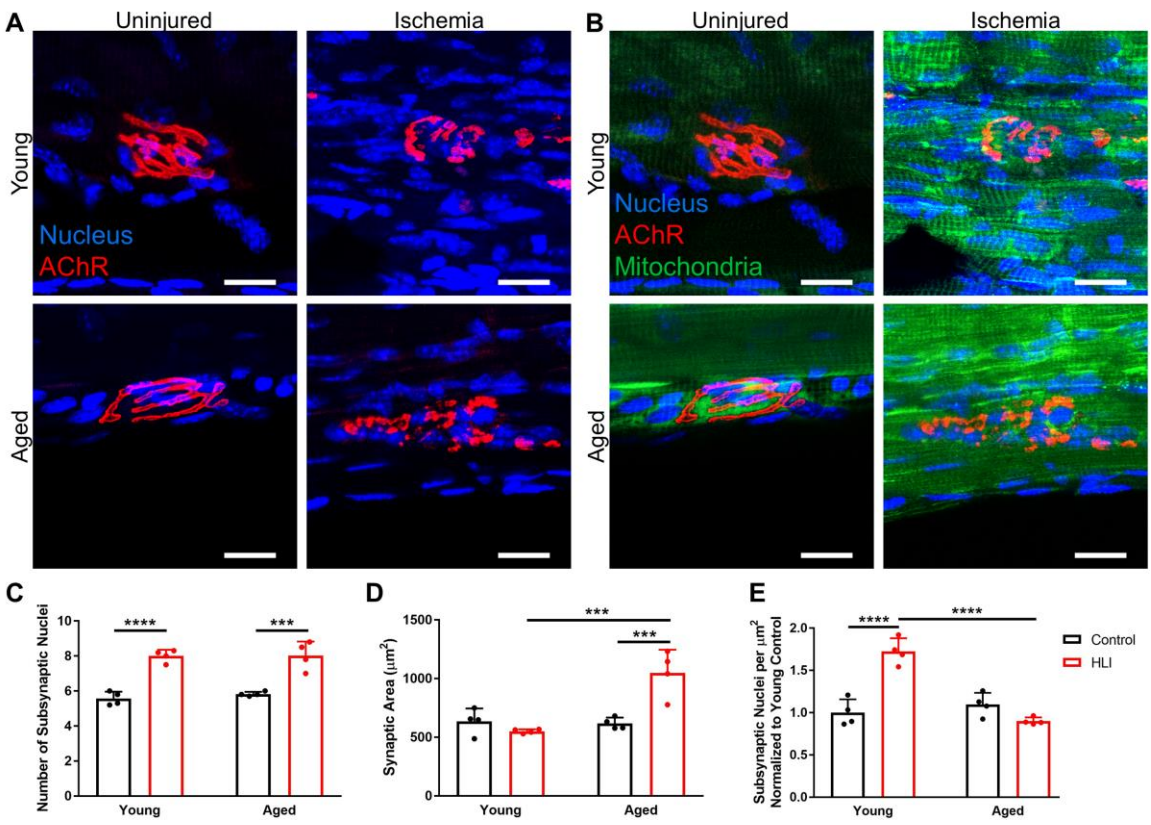

Figure 33. Aged muscles generate fewer subsynaptic nuclei per NMJ area than young muscles following ischemia. (A) NMJs from myofiber bundles from the TA in young (5 mos.) and aged (22 mos.) muscles following ischemia. Maximum intensity projection was performed on z-stacked images from confocal microscopy. Nuclei in blue, AChR-α in red. (B) NMJ mitochondria from myofiber bundles from the TA in young and aged muscles following ischemia. Maximum intensity projection was performed on z-stacked images from confocal microscopy. Nuclei in blue, AChR-α in red, mitochondria in green. (C) Number of subsynaptic nuclei in young and aged NMJs following ischemia (n=4). (D) Area of synaptic endplate (µm^2) in young and aged NMJs following ischemia (n=4). (E) Number of subsynaptic nuclei per µm^2 of synaptic area in young and aged NMJs following ischemia (n=4). At least 6 NMJs were quantified per sample for all experiments. All data presented as mean ± SD, ***p<0.001, ****p<0.0001 using 2-way ANOVA.

To directly determine the role of aged MuSCs in generating new subsynaptic nuclei that aid in the repair of the NMJ, we assessed aged MuSC myogenic potential in a mouse model of denervation through sciatic nerve transection (SNT). By crossing *Pax7-Cre*^{ER} mice with *ROSA26-tdTomato*, we generated a tamoxifen-inducible MuSC reporter mouse (*Pax7-tdTomato*) to track MuSCs at specific stages of myogenesis following injury. By

administering tamoxifen chow 14 days following SNT and isolating single myofibers at day 28, we were able to label MuSCs that expressed the canonical quiescence marker Pax7 without labeling MuSCs that have already undergone myogenesis (Fig. 34A). Interestingly, we observed a higher frequency of MuSCs in the NMJ region (within 250 μm of the NMJ) in aged denervated myofibers compared to young denervated myofibers, although this may be partially attributed to the diminished number of MuSCs per aged myofiber overall (Fig. 34B, 34C). Despite the relative increase in percent of MuSCs near the NMJ, aged NMJs gained fewer subsynaptic nuclei than young NMJs following SNT, indicating that aged MuSCs near the NMJ do not efficiently fuse into the injured myofiber as new subsynaptic nuclei. While both young and aged NMJ-associated MuSCs displayed a remarkable change in morphology by extending long projections towards the NMJ after SNT (Fig. 34E), aged denervated MuSCs were substantially larger than young denervated MuSCs (Fig. 34F), possibly due to aberrations in the ability for aged MuSCs to activate and fuse into myofiber to generate subsynaptic nuclei.

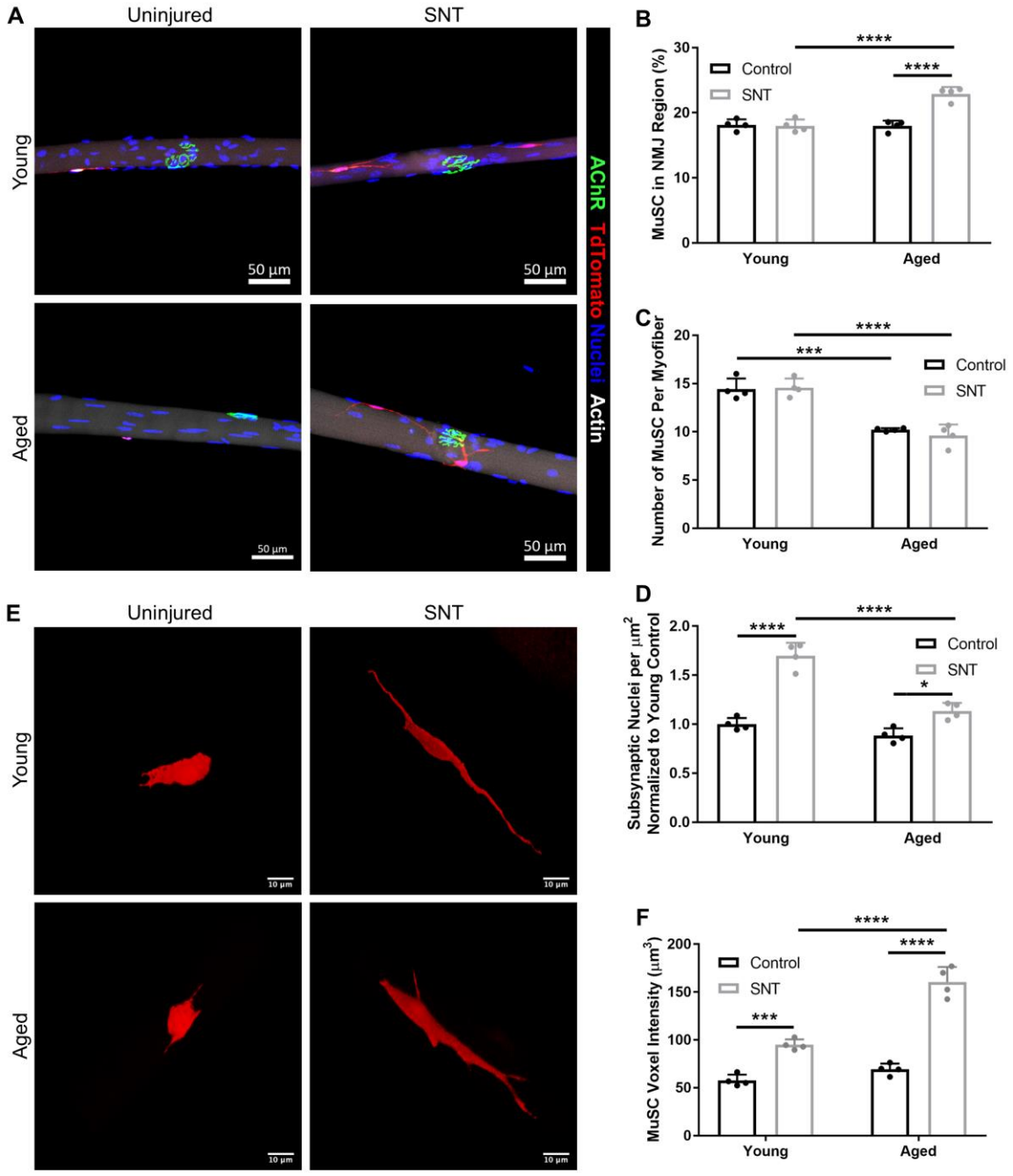

Figure 34. Aged MuSCs generate fewer subsynaptic nuclei following denervation. (A) Representative images of single TA uninjured and denervated myofibers from young (2-3 mos.) and aged (20-22 mos.) *Pax7-tdTomato* mice 28 days following SNT. AChR in green, MuSCs in red, nuclei in blue, and actin in gray. (B) Quantification of the percentage of MuSCs in the NMJ region of the myofiber out of the total number of myofiber MuSCs in uninjured contralateral control and SNT myofibers from both young and aged mice (n=4, with at least 10 myofibers quantified per sample). (C) Total number of MuSCs along the entire length of control and SNT myofibers from young and aged mice (n=4, at least 10

myofibers per sample). (D) Quantification of the number of subsynaptic nuclei per synaptic area in control and SNT myofibers from young and aged mice, normalized to the subsynaptic nuclei per area of young uninjured control (n=4, at least 10 NMJs per sample). (E) 3D reconstructed MuSCs near the NMJ in control and SNT myofibers from young and aged mice using Volocity for 3D rendering. (F) Voxel intensity of 3D reconstructed NMJ-associated MuSCs in control and SNT myofibers from young and aged mice using ImageJ for 3D quantification (n=4, 20 MuSCs per sample). All data presented as mean ± SD, ***p<0.001, ****p<0.0001 using 2-way ANOVA.

Previous research with a collaborator, Dr. Carlos Aguilar from the University of Michigan, has demonstrated through single cell RNA sequencing that a subset of MuSCs are committed to the NMJ and express S100β, a canonical marker for terminal Schwann cells that acts as a Ca^{2+} binding neurotrophic factor to induce neurite growth[387]. To ascertain whether these $S100\beta^{+}$ MuSCs facilitate the regeneration of the NMJ, we performed SNT on S100β-GFP mice donated from the Gregorio Valdez lab at Brown University and stained for Pax7 (Fig. 35A). Results portrayed $S100\beta^{+}$ cells localized at the NMJ in uninjured control with very few cells co-expressing S100β and Pax7 (Fig. 35B). However, following denervation, we observed $S100\beta^{+}$ cells distributed along the length of the myofiber and a striking increase in the number of $S100\beta^{+}/Pax7^{+}$ cells (Fig. 35B, 35C), suggesting that these S100β-expressing MuSCs play a major role in the recovery from denervation injury. While S100β typically induces cell proliferation and reduces quiescence[121,388], data from the Aguilar lab has demonstrated an increase in cells co-expressing S100β and Pax7 with age (data not shown), despite the inefficient ability of these aged NMJ-associated MuSCs to generate sufficient subsynaptic nuclei for NMJ regeneration. Thus, these findings provide a mechanistic foundation to further explore the response of aged $S100\beta^{+}$ MuSCs to NMJ injury models such as denervation and ischemia.

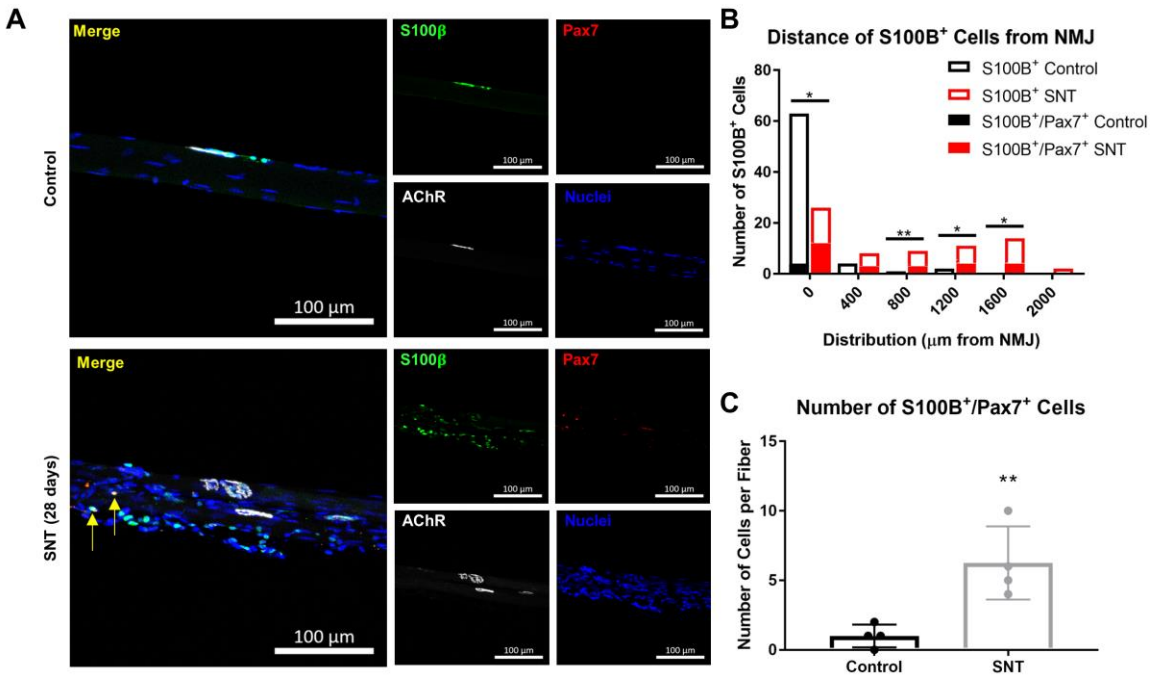

Figure 35. Denervation induces S100β expression in MuSCs. (A) Representative immunofluorescent images of isolated myofibers from young (3 mos.) uninjured and SNT S100β-GFP transgenic mice stained with Pax7, Hoechst 33342, and α-bungarotoxin. S100β in green, Pax7 in red, AChR-α in white, nuclei in blue. (B) Distance of $S100\beta^+$ and $S100\beta^+/Pax7^+$ cells from the NMJ in TA muscles from young uninjured control and young SNT muscles. A total of 70 $S100\beta^+$ cells were quantified on single myofibers from 4 different mice. *p<0.05, **p<0.01 between groups within each bin for $S100\beta^+$ cells using two-tailed T-test with Holm multiple testing corrections. No statistical significance between groups for $S100\beta^+/Pax7^+$ cells. (C) Quantification of the number of $S100\beta^+/Pax7^+$ cells per myofiber in young uninjured control and young SNT muscles (n=4). Mean ± SD, **p<0.01 between groups using two-tailed paired T-test.

5.4.4 MuSC Transplantation Improves Bioenergetic Function of Aged Ischemic Muscle

Once we characterized the satellite cell and mitochondrial deficiencies in aged skeletal muscle following ischemic injury, we tested whether transplantation of healthy, young MuSCs can improve bioenergetic function and skeletal muscle regeneration to reduce limb loss of aged ischemic mice. First, we performed a pilot study to determine the optimal timepoint to transplant MuSCs following HLI. We transplanted GFP^+ MuSCs into

the ischemic TA muscle at days 1, 3, and 7, waited 14 days after transplantation to allow sufficient time for MuSC fusion into the myofibers, and sectioned the muscles to visualize relative engraftment rates. Transplantation at day 7 post-HLI provided the most MuSC engraftment (Fig. 36A), likely due to impairments of transplanted MuSC fusion following ischemia-induced oxidative damage at earlier timepoint schedules. Therefore, for all subsequent studies, MuSCs were transplanted 7 days after ischemic injury. By appending transplantation data to necrosis grading scale and limb retention data shown in Figure 28, we noted remarkably improved grades of necrosis and retention of the foot in transplanted limbs at 28 days following injury (Fig. 36B, 36C). In fact, no limb loss was observed after 10 days of ischemia (3 days after MuSC transplant), suggesting that limb loss is prevented once transplanted MuSCs have adequate time to undergo myogenesis. To assess whether the enhanced recovery from ischemia was due to MuSC-driven improvements in perfusion, we conducted bilateral HLI surgeries and transplanted MuSCs into the TA of one limb (Fig. 36D). Although LDPI quantification did not show significant improvements in perfusion of the transplanted limb (Fig. 36E), LDPI may not be sensitive enough to detect changes in perfusion through capillaries within the TA muscle.

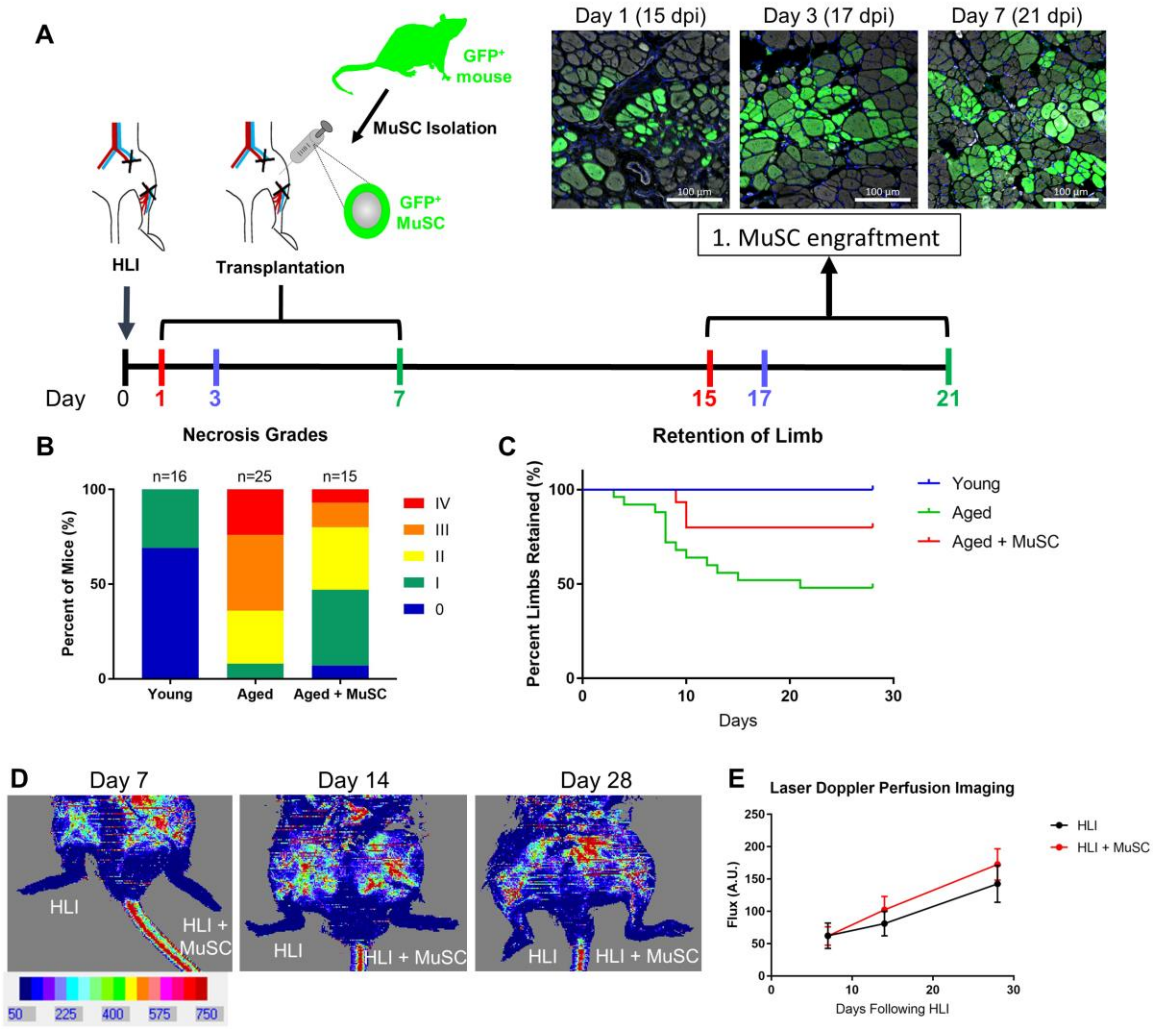

Figure 36. MuSC transplantation in aged mice improves the retention of ischemic limbs. (A) Schematic diagram of transplantation of GFP$^+$ MuSCs into the TA of ischemic hindlimbs at various timepoints and representative images of MuSC engraftment of each transplantation schedule. TAs were dissected 14 days following each transplantation regimen. (B) Percent of each necrosis grade for transplanted aged (19-22 mos.) ischemic hindlimbs at 28 days following ischemia appended to necrosis data for young (4-6 mos.) and aged (19-22 mos.) ischemic hindlimbs (n=16 young mice, n=25 aged mice, n=15 aged transplanted mice). (C) Retention of foot in transplanted ischemic hindlimbs through 28 days following HLI appended to limb retention data of young and aged ischemic hindlimbs (n=16 young mice, n=25 aged mice, n=15 aged transplanted mice). (D) Representative laser Doppler perfusion images (LDPI) of the ventral side of aged (21 mos.) hindlimbs with bilateral HLI where the TA of one hindlimb was transplanted with MuSCs and the other hindlimb served as the contralateral control. Images were taken at 7 days (immediately before transplantation), 14 days, and 28 days following HLI. Ischemic hindlimbs shown on left of each image and ischemic hindlimbs with MuSC transplantation shown on left. Scale bar represents blood flow perfusion by color. (E) Mean perfusion (flux) of ischemic

legs and ischemic legs with MuSC transplantation over 28 days following HLI (n=4). Data is presented as mean ± SD, no statistical differences were detected between perfusion of HLI and HLI with MuSC transplantation hindlimbs within each timepoint using multiple t-tests.

Because we did not find any significant differences in functional perfusion of transplanted limbs, we hypothesized that the improved limb retention outcomes were a result of enhanced bioenergetics within the muscle. Accordingly, we analyzed the network of endogenous mitochondria from uninjured aged *mitoDendra2* myofibers, ischemic aged *mitoDendra2* myofibers, and ischemic aged wildtype myofibers transplanted with *mitoDendra2* MuSCs (Fig. 37A). When measuring the fluorescent intensities of Dendra2 along the position vector of the uninjured myofiber, we observed a regular waveform along the myofiber due to the segregated architecture of mitochondrial reticula (Fig. 37B). Following ischemia, however, the fluorescent intensity plot became highly irregular with mitochondrial reticula spanning several sarcomeres (Fig. 37B). Transplanted mitochondria, on the other hand, partially restored this organized spatial configuration with distinguishable peaks and valleys in the mitochondrial fluorescent signal plot along the myofiber (Fig. 37B). Although we did not observe any statistically significant differences in the average distances between mitochondrial reticula (Fig. 37C), the variance of reticular distances within a myofiber were significantly greater in aged ischemic myofibers compared to control but was more uniform in the MuSC-derived mitochondrial network following transplantation (Fig. 37D). Because mitochondria are regulated by myonuclei, we also investigated whether the improved mitochondrial network was an effect of accreted myonuclei and indeed found elevated myonuclear number in the engrafted myofibers compared to aged control and aged ischemic myofibers (Fig. 37E). Because MuSC-engrafted myofibers also displayed larger sizes compared to ischemic myofibers (Fig. 37F),

there was no change in myonuclear domain between the two groups (Fig. 37G). Overall, these data indicate that transplantation of healthy, young MuSCs can repair the mitochondrial network of aged ischemic myofibers by increasing the number of MuSC-derived myonuclei that supervise their surrounding mitochondria.

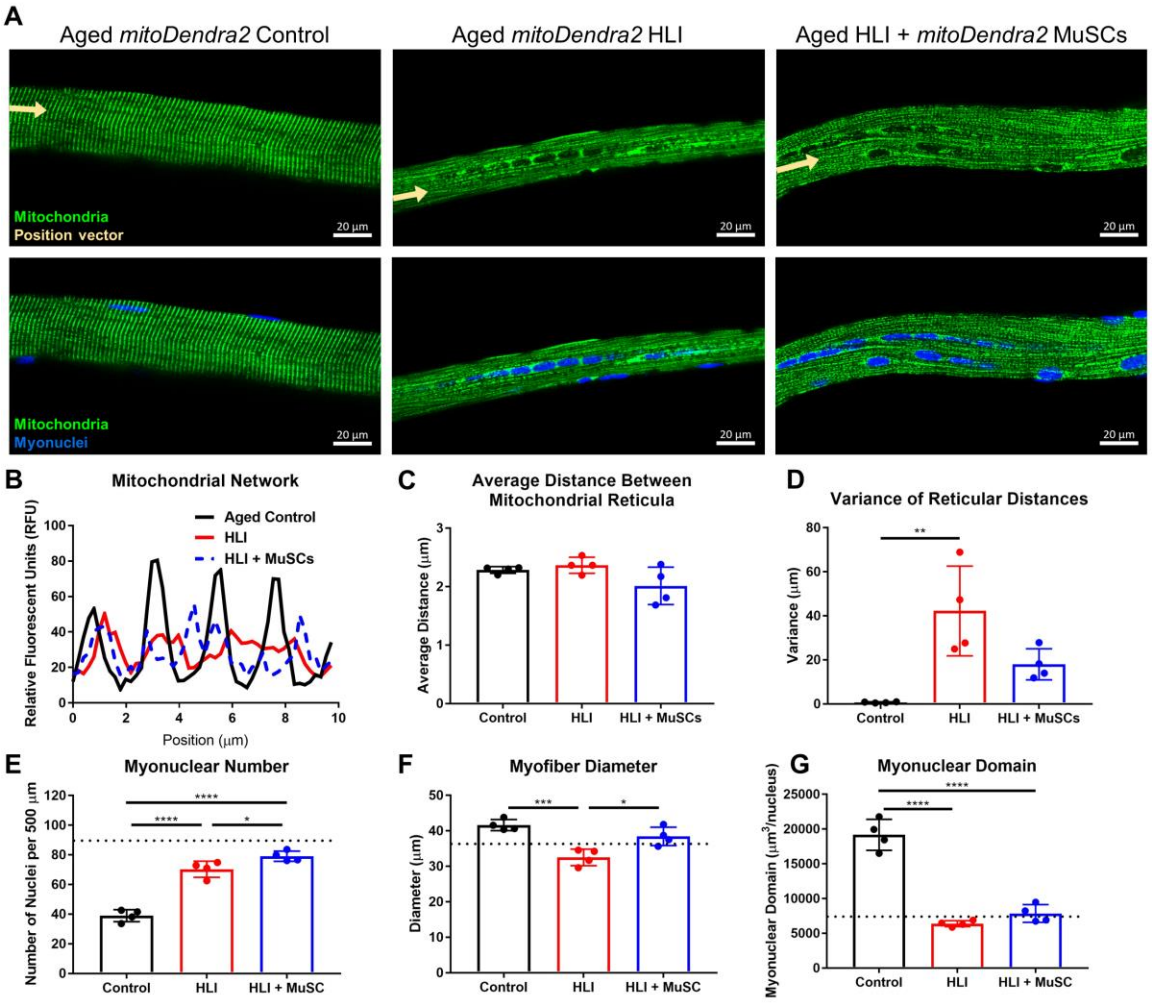

Figure 37. MuSC transplantation remodels the mitochondrial network. (A) Representative z-stacked images of single fibers from the TA of uninjured aged (22 mos.) *mitoDendra2*, ischemic aged (22 mos.) *mitoDendra2*, and ischemic aged (21 mos.) wildtype transplanted with young *mitoDendra2* MuSCs. Mitochondria in green, position vectors along the myofibers in yellow (top); mitochondria in green, nuclei in blue (bottom). (B) Representative quantification of mitochondrial network organization (relative fluorescent units) along 10 µm of fiber length (position vector) to portray segregation of mitochondrial reticula (n=4). (C) Average distance between mitochondrial reticula along

100 μm of fiber length (n=4). (D) Variance of the distances between mitochondrial reticula along 100 μm of fiber length (n=4). (E) Number of myonuclei per 500 μm of myofiber (at least 10 myofibers per sample) in aged control myofibers, ischemic aged myofibers, and MuSC-engrafted myofibers in ischemic aged muscle. Dashed line represents myonuclear number of ischemic young myofibers (n=4). (F) Average diameter of myofiber (10 myofibers per sample) along 500 μm in aged control, ischemic aged, and MuSC-engrafted myofibers in ischemic aged muscle. Dashed line represents myofiber diameter in ischemic young muscle (n=4). (G) Myonuclear domain of 10 single myofibers per sample over 500 μm, calculated as myofiber volume divided by number of myonuclei. Myofiber volume was approximated as the volume of a cylinder using the average radius along 500 μm of myofiber. Dashed line represents myonuclear domain of ischemic young myofibers. (n=4). All data is presented as mean ± SD, *p<0.05, **p<0.01, ***p<0.001, ****p<0.0001 using one-way ANOVA.

Since the highly organized mitochondrial network of myofibers is correlated to the energy production and oxidative capacity of myofibers[352], we then directly tested whether transplanted MuSC-derived mitochondria also improved mitochondrial function in terms of oxidative phosphorylation activity in permeabilized myofibers. In all three states of respiration (basal – state 1, GM – state 2, GM+ADP – state 3), aged ischemic myofibers displayed significant deficiencies in respiration compared to aged control (Fig. 38A). Following MuSC transplantation in aged ischemic muscle, engrafted myofibers impressively replenished oxidative capacity at all three states of respiration (Fig. 38A). Moreover, while ischemic myofibers did not generate increased H_2O_2 following addition of glutamate and succinate, likely due to the overwhelmed SOD2 system following ischemia in aged muscles, transplanted myofibers showed improved H_2O_2 generation (Fig. 38B), insinuating that nuclear-encoded SOD2 levels are partially restored following MuSC engraftment into the myofiber.

To investigate mechanistic changes affecting mitochondrial bioenergetics, we performed qPCR on genes related to mitochondrial-nuclear communication and mitochondrial dynamics. While gene expression of nuclear-encoded Sdha was significantly

upregulated following transplantation, expression of mitochondrial-encoded Cox1 and mtDNA copy number did not improve (Fig. 38D, 38E, 38F), implying enhanced nuclear regulation of mitochondria despite persistent deficiencies in the mitochondrial genome. Although we did not detect any changes in Phb1 expression, gene expression of the Phb2 scaffolding protein was significantly upregulated following transplantation, signifying enhanced nuclear-mitochondrial crosstalk (Fig. 38G, 38H). Finally, expression of Opa1, but not Drp1, was also upregulated in transplanted muscles (Fig. 38I, 38J), indicating enhanced mitochondrial fusion, but not fission. Taken together, these results demonstrate that transplantation of MuSCs into aged ischemic muscle restores mitochondrial oxidative function by improving communication between the mitochondrial and nuclear genomes.

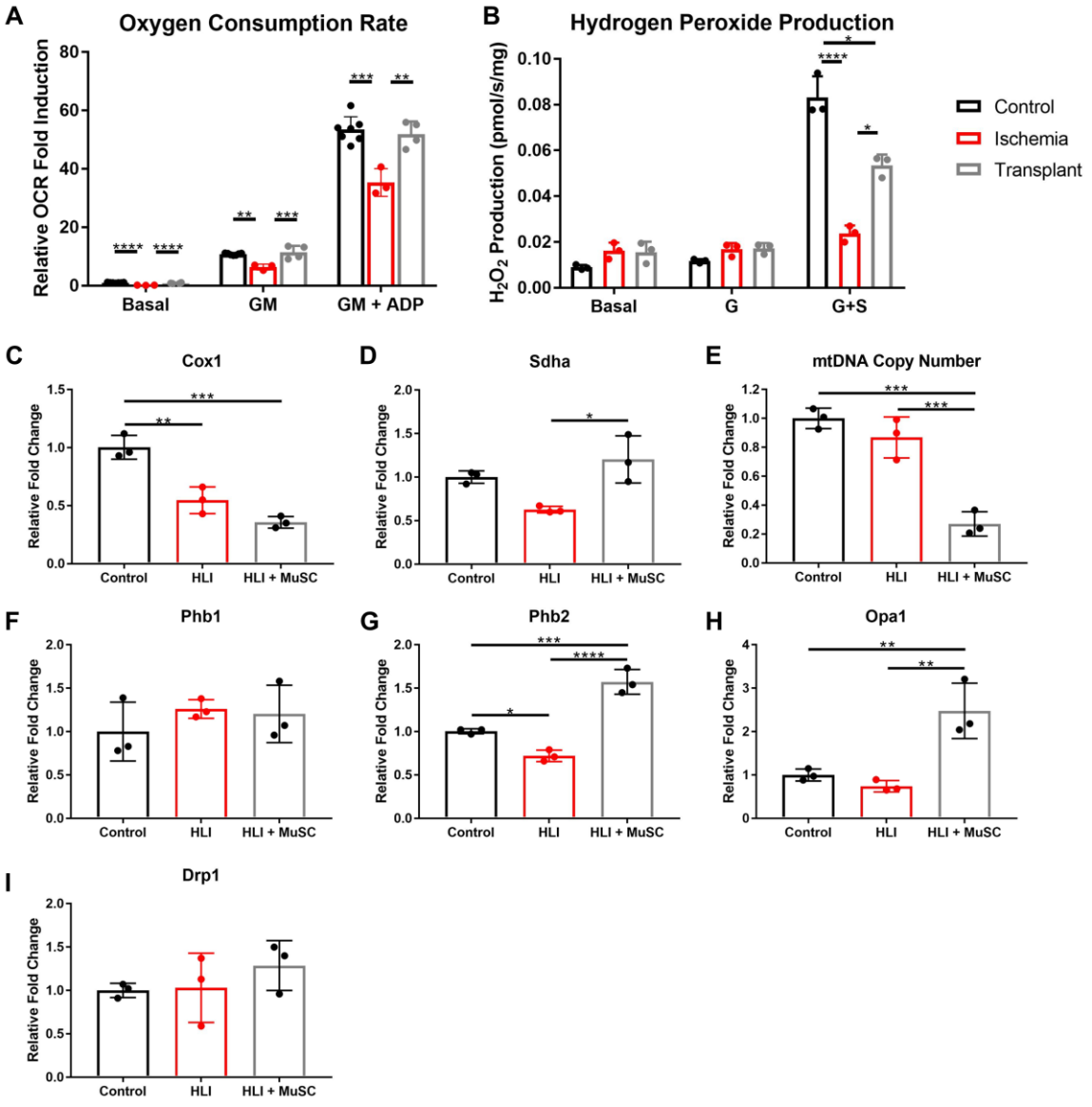

Figure 38. MuSC transplantation improves mitochondrial function and gene expression. (A) States 1 (basal), 2 (GM – complex I-linked respiration), and 3 (GM+ADP – ATP producing respiration) oxygen consumption rates (normalized to basal aged control state 1 respiration) of permeabilized myofibers from uninjured aged (23 mos.) control, aged (23 mos.) ischemia, and aged (23 mos.) ischemia with transplanted MuSCs (n≥3). (B) Hydrogen peroxide production from permeabilized myofiber bundles at basal activity, complex I-linked activity with the addition of glutamate (G), and complex I- and II-linked activity with the subsequent addition of succinate (G+S) from uninjured aged control, aged ischemia, and aged ischemia with transplanted MuSCs (n=3). (C) Relative gene expression of Cox1 in uninjured aged control TA, aged ischemic TA, and aged ischemic TA transplanted with MuSCs (n=3). (D) Relative gene expression of Sdha in uninjured aged control TA, aged ischemic TA, and aged ischemic TA transplanted with MuSCs (n=3). (E)

Relative gene expression of mtDNA copy number in uninjured aged control TA, aged ischemic TA, and aged ischemic TA transplanted with MuSCs (n=3). (F) Relative gene expression of Phb1 in uninjured aged control TA, aged ischemic TA, and aged ischemic TA transplanted with MuSCs (n=3). (G) Relative gene expression of Phb2 in uninjured aged control TA, aged ischemic TA, and aged ischemic TA transplanted with MuSCs (n=3). (H) Relative gene expression of Opa1 in uninjured aged control TA, aged ischemic TA, and aged ischemic TA transplanted with MuSCs (n=3). (I) Relative gene expression of Drp1 in uninjured aged control TA, aged ischemic TA, and aged ischemic TA transplanted with MuSCs (n=3). All data is presented as mean ± SD, *p<0.05, **p<0.01, ***p<0.001, ****p<0.0001 using one-way ANOVA for each individual state of respiration in panels A and B, and one-way ANOVA for panels C-I.

Previous studies have also shown that ischemic skeletal muscle can uptake isolated mitochondria through ectopic transplantation. To test whether or not this internalization of isolated mitochondria can lead to improved bioenergetic function in ischemic muscle, we employed an *in vitro* model of hindlimb ischemia[384] on C2C12 myoblasts by subjecting the cells to 3 hours of hypoxia (2% oxygen), 3 hours of nutrient deprivation (replacing media with HBSS buffer), or both and characterized the mitochondrial activity with a Seahorse analyzer (Fig. 39A). Although hypoxia alone did not alter basal respiration, ATP production, maximal respiration, or proton leak when normalizing to total protein within each well, hypoxia + nutrient deprivation decreased the respiration of all mitochondrial functional parameters (Fig. 39B, 39C, 39D, 39E), validating this model as an *in vitro* representation of the mitochondrial dysfunction found in ischemic muscle tissues. To test the effects of mitochondrial transplantation, we co-cultured C2C12s with isolated mitochondria derived from skeletal muscle at various concentrations for control and hypoxia + nutrient deprivation (H+ND) myoblasts. Confocal images displayed internalization of isolated mitochondria after 24 hours of co-culture at both 5 μg/ml and 50 μg/ml of mitochondria (Fig. 39F). Subsequently, we tested for functional bioenergetic improvements by subjecting myoblasts to H+ND for 3 hours, immediately co-culturing 50

μg/ml mitochondria for 24 hours, and then performing a Seahorse mitochondrial stress test (Fig. 39G). Although there were no significant improvements in basal or maximal respiration, ATP production and proton leak were enhanced following isolated mitochondrial transfer (Fig. 39H, 39I, 39J, 39K), demonstrating the therapeutic potential for mitochondrial transplantation to ischemic cells and tissues.

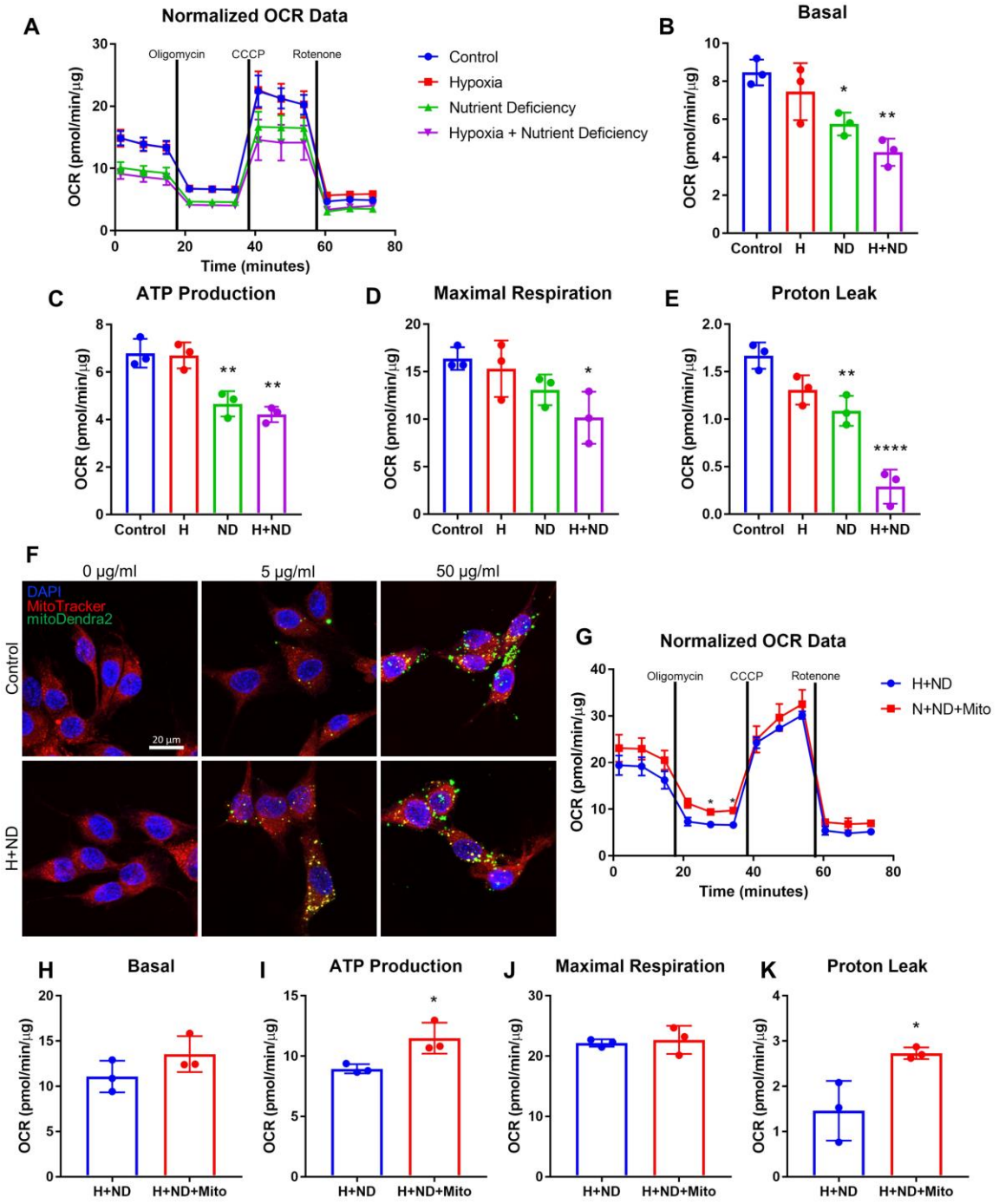

Figure 39. Isolated mitochondrial transplantation improves myoblast bioenergetic function. (A-E) Oxygen consumption rates, ATP production, and proton leak of C2C12 myoblasts using a Seahorse XFp Analyzer after hypoxia (H), nutrient deprivation (ND), or hypoxia and nutrient deprivation (H+ND) for 3 hours (n=3). (F) Representative confocal images of control and H+ND C2C12s with no mitochondria, 5 µg/ml mitochondria, and 50 µg/ml mitochondria treatments for 24 hours. (G-K) Oxygen consumption rates, ATP production, and proton leak of C2C12 myoblasts subjected to H+ND with and without 50

μg/ml treatments of mitochondria for 24 hours using a Seahorse XFp Analyzer. All data presented as mean ± SD, *p<0.05, **p<0.01, ****p<0.0001 using one-way ANOVA for H+ND characterization (panels B-E) and two-tailed t-tests for mitochondrial transplant experiments (panels H-K).

5.5 Discussion

In this chapter, we first report dramatic age-dependent changes in sensitivity to hindlimb ischemia in *C57BL/6J* mice. In young mice between 4 and 6 months of age, we observed complete recovery of ischemic tissue. At 28 days post HLI, the majority of young mice displayed normal physiology of the ischemic foot, with only some mice exhibiting necrosis at the tips of the toes. In stark contrast, aged mice between 20 and 24 months old all exhibited signs of necrosis in the ischemic hindlimb, with more than half losing the foot to autoamputation due to the impaired angiogenesis and delayed reperfusion in aged mice[115,116,185]. Because of the hindered ability to form collateral vessels, the prolonged ischemia in aged mice resulted in elevated oxidative stress that disrupted mitochondrial network formation, oxidative capacity, muscle stem cell (MuSC) myogenesis, and motor neuron regeneration, all of which rely on balanced redox homeostasis to resolve their functional capabilities[375]. Specifically, reactive oxygen species (ROS) can oxidatively damage portions of the mitochondria and diminish their oxidative capacity[140]. To selectively remove defective portions of ischemic mitochondria through autophagy (mitophagy), mitochondrial dynamics are altered to either fission off damaged segments of the mitochondria or fuse together with healthy mitochondria to dilute the effects of the dysfunction[332]. These altered dynamics, in turn, impede the ability of the myofiber to restore the distinct morphology of the mitochondrial network[101]. Furthermore, not only do these changes in mitochondrial dynamics interfere with MuSC self-renewal and fate

decisions[389], but oxidative stress also directly hampers the MuSC differentiation potential[390], both of which contribute to the aged MuSC depletion and dysfunction. Finally, motor neurons, which are high in mitochondrial content in order to generate the energy required for maintaining the membrane potential, are also susceptible to oxidative damage. It has been shown that high levels of superoxide lead to neuromuscular junction (NMJ) degeneration and impairments in motor neuron regeneration that are characteristics of sarcopenia[117].

Although we were the first to characterize these age-dependent mitochondrial and MuSC responses to ischemia in *C57BL/6J* mice, there have also been studies on strain-dependent sensitivities to hindlimb ischemia that presented a similar pathophysiology to aged mice. In particular, *BALB/c* and *129S2/Sv* mice both manifest a severe grade of necrosis following ischemic injury similar to aged *C57BL/6J* mice and have commonly been used to test therapeutic approaches for peripheral artery disease[187,391]. These exacerbated responses to ischemic insults in these different strains have been attributed to fewer pre-existing collateral vessels, diminished angiogenic potential, and reduced revascularization rates[188-190], all of which are also attributes of aging. Moreover, *BALB/c* mice exhibited 40% reductions in mitochondrial respiratory capacity following ischemic injury[191], similar to the discrepancy in respiratory capacity between young and aged *C57BL/6J* ischemic muscles. Lastly, *BALB/c* mice have demonstrated poor muscle regenerative capacity following injury due to diminished myogenesis of muscle stem cells[192], presenting another parallel to the MuSC depletion and dysfunction of aged mice. While this resemblance between the mechanisms of strain-dependent and age-dependent sensitivities to ischemia are certainly interesting, these strains rely on inherent genetic

differences rather than the pathology of aging to model severe human PAD. Testing therapeutic interventions for PAD in aged mice would provide a more clinically relevant model that directly captures the etiologies of aging that is associated with PAD.

Although several therapeutic approaches have been explored, most have focused on augmenting angiogenesis without improving the viability of ischemic muscle, which is required to physically and biochemically support newly synthesized blood vessels[38,41]. Muscle stem cell transplantation is a promising therapeutic intervention that can improve the regenerative capacity of skeletal muscle, but has not yet been investigated in ischemic injuries. Here, we report that transplantation of MuSCs to aged ischemic limbs improves the retention of the foot, partially restores the mitochondrial network, and enhances bioenergetic function. It is worth noting that these enhancements were observed with a limited number of transplantable cells, though this can be further upgraded through sourcing or manipulating the MuSCs prior to injection. For example, impressive breakthroughs in cell engineering have allowed the production of MuSCs from induced pluripotent stem cells or embryonic stem cells to maximize the number of transplantable cells to replenish the stem cell pool[275,370]. Other techniques to bioenergetically-enrich MuSCs prior to transplantation may also enhance therapeutic outcome, like the treatment of forskolin to promote MuSC proliferation and mitochondrial biogenesis in order to augment delivery of healthy mitochondria to the ischemic muscle[274,392]. Ischemic preconditioning of MuSCs has also been recently investigated to improve the tolerance to oxidative stress and boost transplant efficiency of MuSCs[106,393], allowing metabolic reprogramming of the MuSC to maximize fusion of healthy mitochondria. Other possibilities to precondition the MuSC, such as culturing MuSCs with factors to activate

the mTORC1 pathway and induce a G_{alert} cell cycle state with increased mitochondrial content[268,394], will provide investigators the ability to optimize conditions for the MuSC as a delivery vehicle to transplant mitochondria.

Alternatively, transplantation of isolated mitochondria has also recently been explored to ameliorate the impacts of ischemic injury and enhance tissue function. When isolated mitochondria were injected into injured muscles of young *C57BL/6J* mice in a non-surgical, acute form of hindlimb ischemia-reperfusion, muscle regeneration and gait patterns were significantly improved[179]. The same group, led by McCully *et al.*, also noted a reduction in infarct size and revitalization of cell viability in a young rabbit model of myocardial ischemia-reperfusion[280,395], although none of these studies tested for bioenergetic functional outcomes. Although we have reported marginal improvements the in ATP production of hypoxic/nutrient deprived myoblasts following *in vitro* mitochondrial transplantation, it is important to consider the age and severity of ischemic injury in regards to the efficacy of mitochondrial transplantation. In aged mice with surgical hindlimb ischemia, where ischemic conditions are prolonged and oxidative stress is elevated, transplanted mitochondria may become dysfunctional without having their corresponding nuclei to regulate their autophagy, dynamics, or biogenesis. Although not yet examined, it may be possible to combine MuSC transplantation with mitochondrial transplantation to restore the mitochondrial-nuclear communication by modifying MuSCs with a mitochondrial targeting peptide (KALA), incubating the modified MuSCs with isolated mitochondria, and then transplanting the mitochondria-decorated MuSCs to ischemic tissues to maximize the therapeutic impact of cell-based transplantation[396].

However, even without the *in vivo* delivery of isolated mitochondria, here we report that the age-associated decline in recovery from ischemic injury can be rescued with only MuSC transplantation. We observed delayed reperfusion in aged ischemic hindlimbs that correlated to a disorganized mitochondrial network, debilitated mitochondrial function, impaired MuSC-derived myonuclear accretion, and limited motor unit remodeling. On the basis of replenishing the MuSC population of aged mice, we transplanted healthy MuSCs and observed impressive recovery of the ischemic foot, more organized mitochondrial reticula, and enhanced mitochondrial function and signaling. Taken together, these findings provide a foundation for a MuSC-based therapeutic approach using a clinically relevant PAD animal model and further propose muscle stem cell transplantation as a candidate for treating mitochondrial myopathies.

CHAPTER 6. CONCLUSIONS AND FUTURE DIRECTIONS

6.1 Overall Conclusions

It is well established that muscle stem cells (MuSCs) are indispensable for myofiber repair and regeneration. However, the relationship between MuSCs and mitochondria of the regenerating myofiber remained unknown. The findings of this thesis provide a causal link between the mitochondria of the MuSC and mitochondria of the myofiber due to the propagation of these organelles through myogenesis and fusion into the myofiber. These results provide a foundation to develop MuSC-based therapies to treat challenging mitochondrial myopathies and establish an avenue to further optimize the MuSC as a delivery vehicle for mitochondrial transplantation.

6.1.1 Specific Aim 1: Correlate the temporal response of the muscle stem cell to remodeling of the mitochondrial network in ischemic myofibers

In chapter 3, we investigated the response and subsequent remodelling of various skeletal muscle niche components following an ischemic injury. By assessing the temporal changes of the MuSC, myonuclear number, vasculature, motor units, and mitochondria, we were able to effectively create a timeline for the regenerative responses of the niche components and provide correlative relationships between the muscle constituents. We noted concomitant increases in MuSC and myonuclear number at day 7 following hindlimb ischemia (HLI), indicating that these ischemic MuSCs are both proliferating and differentiating into myogenic progeny that fuse into the regenerating myofiber as new myonuclei. We not only observed accreted myonuclei of the whole myofiber, but also

increased subsynaptic nuclei that facilitated neuromuscular junction regeneration. These MuSC-derived myonuclei also drive mitochondrial biogenesis, as observed by the high mitochondrial densities surrounding the centrally located myonuclei stemming from MuSCs. However, due to the ischemic conditions at day 7 and 14 post-HLI, these mitochondria become dysfunctional and are removed through autophagy. After revascularization of the ischemic muscle, the increased blood flow allows the MuSC-derived mitochondria to restore their bioenergetic function. Taken together, these findings support the hypothesis that MuSCs and their downstream myonuclei play a critical role in generating and maintaining myofiber mitochondria after an ischemic injury.

6.1.2 Specific Aim 2: Demonstrate that transplanted muscle stem cells remodel the mitochondria of dystrophic host skeletal muscle

After demonstrating the correlative link between MuSCs and myofiber mitochondria, we next sought to directly test the impact of MuSC mitochondria on the bioenergetic function of the myofibers they fuse into. Though several studies have shown that dystrophic muscle harbors defective mitochondria, the origin of the mitochondrial dysfunction remained unknown. In chapter 4, we showed that dystrophic MuSCs contain dysfunctional mitochondria that impair their myogenic potential. Through differentiation, fusion into myotubes, and later fusion into mature myofibers, these MuSCs carry their mitochondria into the fused cells during myogenesis, resulting in bioenergetic deficiencies within the dystrophic myofiber. However, by transplanting MuSCs with healthy mitochondria, the myofibers generated from the exogenous MuSCs exhibit remarkably improved bioenergetic function. In contrast, by performing loss-of-function experiments by transplanting MuSCs with mitochondrial dysfunction from other disease models (aged

MuSCs, *SOD1KO* MuSCs), the improvements of MuSC transplantation on bioenergetic function were abolished, indicating that MuSC mitochondria play an important, causal role on the myofibers they fuse into.

6.1.3 Specific Aim 3: Investigate mitochondrial remodeling following muscle stem cell transplanted into aged ischemic skeletal muscle

In order to test the effects of MuSC transplantation into ischemic muscle, we first generated a mouse model of hindlimb ischemia that represented the clinical manifestation of severe human PAD. While young *C57BL/6J* mice exhibited complete recovery from surgical hindlimb ischemia, aged mice demonstrated marked reductions in the regenerative response to ischemic injury. Namely, aged mice portrayed significant proportions of limb loss following hindlimb ischemia, representative of the necrosis and subsequent amputation observed in severe human PAD. This was attributed to slower revascularization rates, impaired regeneration of the neuromuscular junction, attenuated myonuclear accretion, disorganized mitochondrial networks, and diminished bioenergetic function. Although transplantation of healthy MuSCs into aged ischemic muscles did not significantly improve revascularization, as measured by laser Doppler perfusion imaging, the mitochondrial network was notably improved in organization and bioenergetic function, likely as a result of increased myonuclear accretion that regulate these mitochondria. These findings provide even further evidence for the relationship between MuSC mitochondria and the regenerating myofiber and present a foundation for MuSCs to not only enhance skeletal muscle regeneration in mitochondrial myopathies, but also as a delivery vehicle to transfer functional mitochondria into diseased myofibers.

6.2 Future Directions

6.2.1 Biomaterial-Based MuSC Delivery

Although our MuSC transplantation model for mitochondrial myopathy shows great therapeutic potential, a limitation of this scheme is the high number of transplanted cells required to provide benefits in the bioenergetic function of the host muscle. While this may be potentially be attributed to cell death of transplanted MuSCs due to the high oxidative stress within ischemic muscle[260], this can be overcome by delivering the MuSCs in a biomimetic niche that recapitulates the stiffness of the MuSC microenvironment. Previously, we have shown that delivering MuSCs in a synthetic, biodegradable hydrogel based on a four-arm poly(ethylene glycol) (PEG) macromer functionalized with maleimide (PEG-4MAL) to both dystrophic and aged muscle remarkably increases MuSC engraftment compared to hydrogel-free delivery, even with notably fewer transplanted cells[381]. Furthermore, we have demonstrated that MuSCs can be co-delivered with recombinant proteins, such as Wnt7a to enhance myogenic potential and migration of transplanted MuSCs[262], providing a promising therapeutic avenue to optimize the hydrogel-based co-delivery of MuSCs with recombinant proteins based upon the needs of the host muscle.

For the purposes of aged ischemic muscle, we can employ other recombinant proteins to facilitate regeneration of the diseased muscles. Because aged muscles exhibited significantly slower revascularization rates following ischemic injury, VEGF recombinant protein is a favorable candidate to promote angiogenesis while simultaneously improving muscle regeneration and bioenergetic function with transplanted MuSCs. Indeed, previous

work has shown that delivery of VEGF in the engineered PEG-4MAL construct significantly improved perfusion to ischemic muscles in a murine HLI model by promoting angiogenesis[397]. By using this system to co-deliver both VEGF and MuSCs in aged ischemic muscle, transplanted MuSCs can be protected against the harsh ischemia-induced oxidative stress while concomitantly accelerating revascularization. Thus, we would expect advanced therapeutic outcomes with this co-delivery system compared to MuSCs alone.

Other biomaterial-based MuSC transplantation models may also be explored to enhance the angiogenic potential with growth factors. Various studies from the Botchwey and Temenoff groups have provided a foundation for delivery of stromal derived factor-1α (SDF-1α) in heparin-based poly(ethylene glycol) diacrylate (PEGDA) microparticles or poly(lactic-co-glycolic acid) (PLAGA) nanofibers to both modulate recruitment of pro-regenerative macrophages and improve remodelling of the microvascular network[398-400]. Although these platforms have not yet been tested in conjunction with MuSC delivery or in ischemic muscles, they offer a framework to further explore this system in other disease models where perfusion is impaired, such as in PAD.

Alternatively, beyond improving revascularization rates in ischemic muscle, mitochondria themselves can be targeted with a biomaterial-based approach. Due to the ease in manufacturing and ability to modify with peptides, liposomes have also been investigated as a delivery vehicle to enhance therapeutic outcomes in muscle cells[396]. For the purposes of MuSC delivery, transplanted MuSCs can be decorated with liposomes containing mitochondria or drugs to augment the impact of treatment. For example, giant unilamellar liposomes can be loaded with healthy mitochondria and modified with RGD

peptides that can bind to the α7β1-integrins on transplanted MuSCs so that these MuSCs transfer an extra load of functional mitochondria upon myogenic fusion into the ischemic myofiber (Fig. 40A). However, this approach may be challenging due to the high temperatures, long manufacturing times, sonication, and use of chloroform that may diminish the quality of the transplanted mitochondria. Another option may be to load the liposomes with a mitochondrial-targeted antioxidant drug, mitoTempol, which has been shown to protect muscle mitochondria against oxidative damage[401]. The smaller sizes of liposomes required for this approach would allow easier and faster manufacturing of mitoTempol-filled liposomes that decorate transplanted MuSCs that would not only protect MuSC mitochondria but also endogenous mitochondria from oxidative stress following delivery into ischemic muscles (Fig. 40B). While we have already shown proof-of-concept that MuSC transplantation can improve the bioenergetic function of the host muscles, these various biomaterial-based MuSC delivery systems would provide further enhancements to the skeletal muscle regeneration and mitochondrial function upon delivery.

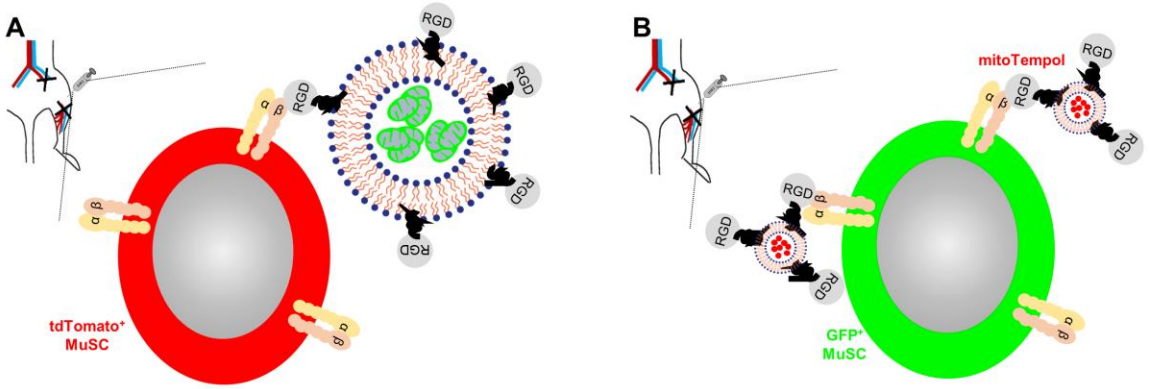

Figure 40. Transplantation of MuSCs with decorated liposomes. (A) Transplanted MuSCs decorated with large liposomes filled with mitochondria and targeted to the α7β1-integrins of the MuSC. (B) Transplanted MuSCs decorated with small liposomes filled with mitoTempol and targeted to the α7β1-integrins of the MuSC.

6.2.2 Bioenergetic Enrichment of Transplanted MuSCs

Rather than providing transplanted MuSCs with additional resources to optimize therapeutic outcomes following delivery, the exogenous MuSCs themselves can be enhanced by enriching their mitochondrial quality. Because we show that MuSC mitochondria has a consequential effect on the bioenergetic function of the engrafted myofiber, improving the mitochondrial quality of the transplanted MuSCs can provide robust bioenergetic enhancements to the host muscle. A relatively simple approach to accomplish this is by sorting MuSCs based on their mitochondrial content. Quiescent MuSCs represent a heterogeneous population dependent on various transcription factors and cell surface markers. Studies show that expression of the Pax7 transcription factor is inversely related to mitochondrial content in quiescent MuSCs[58]. MuSCs fated for self-renewal and replenishing the reserve pool express high Pax7 and maintain low levels of mitochondria while MuSCs that form myogenic progenitors express low levels of Pax7 and comprise of higher mitochondrial content. Using these distinct subpopulations to our advantage, we can fine tune the transplantation regimen based on the needs of the tissue. Ischemic muscle would likely benefit from MuSCs with high myogenic capacity and high mitochondrial content at earlier timepoints to assist in myofiber regeneration and fuse high levels of mitochondria, but after resolution of the ischemic injury, aged ischemic muscles can be transplanted with MuSCs with low mitochondria to repopulate the stem cell pool.

Due to the highly adaptive nature of muscle stem cells, another option to enrich transplanted MuSCs is through preconditioning. In chapter 4, we demonstrated that MuSCs

isolated from exercise preconditioned mice rejuvenated the bioenergetic function of dystrophic muscle following transplantation, which we attributed to mitochondrial enrichment of the donor MuSCs following exercise-induced PGC-1α-mediated biogenesis and mTORC1 activation[267,268]. In the context of transplantation for ischemic muscle, it is also possible to prime MuSCs for ischemic injury prior to delivery. The adaptive stress response, known as hormesis, of MuSCs allows the cells to undergo epigenetic changes of various transcription factors or growth factors in the presence of mild stress so they can maintain their functions and respond strongly when exposed to a more severe stress of a similar nature[402]. Taking advantage of this phenomenon, donor muscles can be preconditioned to mild ischemia by regular yet transient applications of a tourniquet. Ischemia preconditioned MuSCs can then be isolated and transplanted into severe ischemic muscle following surgical hindlimb ischemia to respond more effectively to the ischemic environment and regenerate the myofibers more robustly. Preliminary data shows that muscles exposed to ischemia preconditioning for 4 weeks quickly restored muscle morphology after surgical HLI (Fig. 41A, 41B) and attenuated the need to deposit as many myonuclei into the regenerating myofiber compared to non-preconditioned muscles (Fig. 41C, 41D). However, it is currently unclear if this protective effect of ischemia preconditioning is a result of an adaptive response of the MuSC or if preconditioned muscles form more collateral vessels that allow more efficient revascularization following severe ischemic injury. Further testing is required to elucidate the mechanism behind ischemic preconditioning and determine whether ischemia preconditioned MuSCs can provide superior therapeutic benefits following transplantation into ischemic muscles.

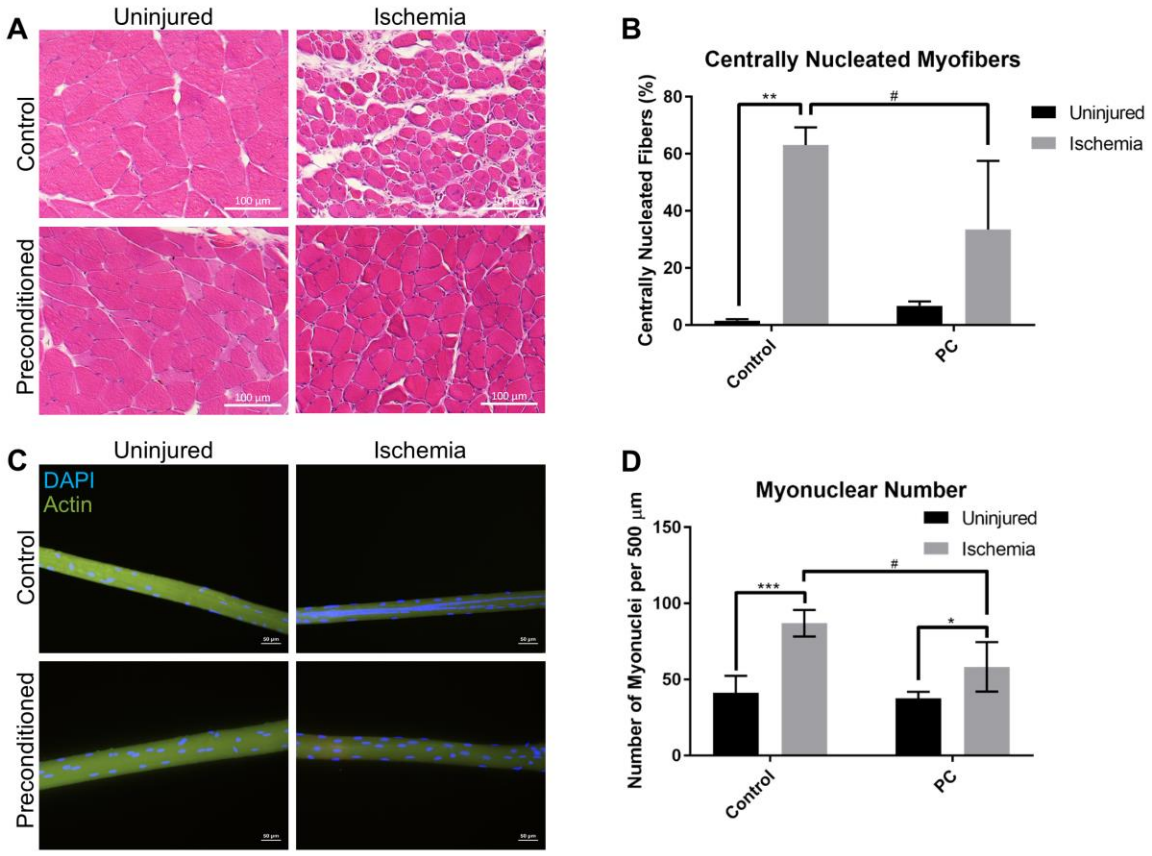

Figure 41. Ischemia preconditioned muscles are protected against severe ischemic injury. (A) H&E staining of control and ischemia preconditioned (4 weeks preconditioning) TA muscles 14 days after surgical hindlimb ischemia. (B) Percentage of centrally nucleated myofibers in control and preconditioned muscles from uninjured and surgical HLI TA muscles. (C) Representative images of single myofibers isolated from the TA muscle of control and preconditioned muscles following surgical HLI and uninjured contralateral control. Nuclei in blue, actin in green. (D) Myonuclear number along a 500 µm length of myofiber isolated from the TA of control and preconditioned muscles following surgical HLI or uninjured contralateral muscle. All data presented as mean ± SD, $*p<0.05$, $**p<0.01$, $***p<0.001$ between uninjured and surgical hindlimb ischemia, and $^{\#}p<0.05$ between control and preconditioned muscles using one-way ANOVA.

Muscle stem cells can also be preconditioned prior to transplantation by exposing the cells to various culture conditions or pharmacological agents. For example, MuSCs that were subjected to hypoxic culture (1% oxygen tension) for 48 hours demonstrated marked improvements in engraftment efficiency and self-renewal following transplantation into ischemic tissue[106], which can be beneficial to replenish the stem cell pool in diseased aged

muscles. However, because the primary objective of our transplantation models is to transplant myogenic progenitors to facilitate muscle regeneration, other approaches using pharmacological agents may be more applicable. One particular case is the use of forskolin, which increases MuSC proliferation by enriching the mitochondrial content[274]. This would not only provide a higher number of transplantable cells, but would also provide the recipient muscles with more healthy mitochondria to vastly improve bioenergetic function. Interestingly, in a pilot experiment where we treated wildtype and dystrophic MuSCs with forskolin *in vitro*, wildtype MuSCs exhibited astonishing increases in mitochondrial content and shifted their growth toward proliferation rather than myogenic fusion (Fig. 42). Due to the high mitochondrial content, we anticipate that these MuSCs will switch to a myogenic lineage following transplantation, but direct testing is still needed. In contrast, dystrophic MuSCs did not display a similar increase in mitochondrial content (Fig. 42), possibly due to intrinsic defects in the ability to synthesize mitochondria. This preliminary data indicates that *mdx* MuSCs do not respond effectively to forskolin treatment and administration of the drug into dystrophic muscles may not result in the desired effect. Rather, forskolin treatment of healthy MuSCs that can then be transplanted into dystrophic muscles may provide the therapeutic benefits of MuSC-dependent mitochondrial transfer into the regenerating myofibers, based upon the findings of this thesis. While the purpose of this thesis is to provide a foundation for the improvements in bioenergetic function following transplantation of healthy MuSCs, there are several avenues to further enhance this transplantation model to maximize the effects of muscle stem cell transplantation.

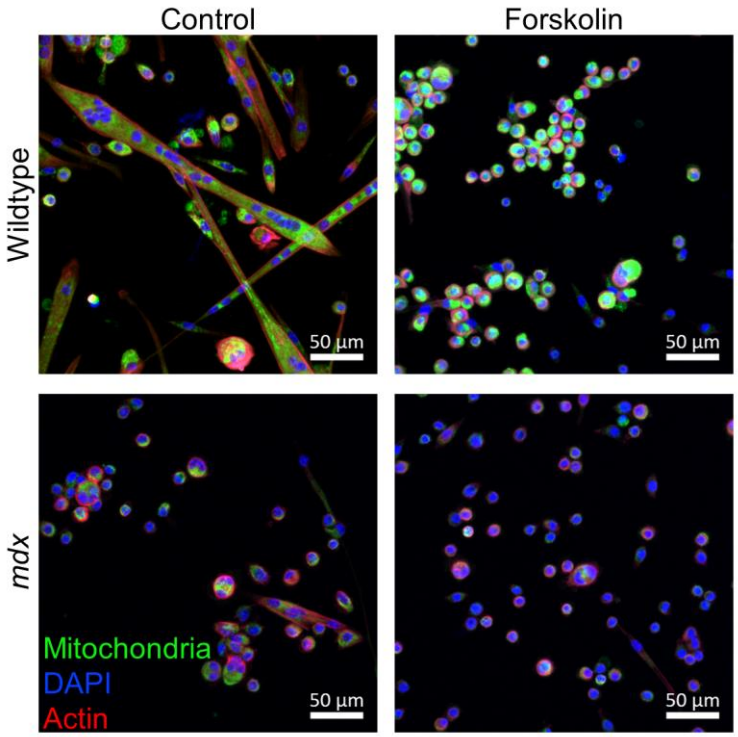

Figure 42. Forskolin treatment increases proliferation and mitochondrial content of wildtype, but not dystrophic, MuSCs. Cultured MuSCs isolated from wildtype/mitoDendra2 and *mdx*/mitoDendra2 muscles. Control MuSCs were cultured for 10 days in growth media while forskolin MuSCs were cultured for 10 days in growth media supplemented with 50 µm forskolin, with daily 25 ng/µl bFGF for all groups for the first 4 days of culture. At day 10 of culture, cells were fixed with 4% PFA and imaged with a confocal microscope. Mitochondria (mitoDendra2) shown in green, nuclei in blue, and actin in red.

APPENDIX A. SUPPLEMENTARY INFORMATION

A.1 qPCR Primer Sequences

Gene	Sequence (5' → 3')	PrimerBank ID
β-actin (forward)	GATCTGGCACCACACCTTCT	N/A
β-actin (reverse)	GGGGTGTTGAAGGTCTCAAA	
B2m (forward)	TTCTGGTGCTTGTCTCACTGA	31981890a1
B2m (reverse)	CAGTATGTTCGGCTTCCCATTC	
mt-Co1 (forward)	ATCACTACCAGTGCTAGCCG	N/A
mt-Co1 (reverse)	CCTCCAGCGGGATCAAAGAA	
Sdha (forward)	GGAACACTCCAAAAACAGACCT	15030102a1
Sdha (reverse)	CCACCACTGGGTATTGAGTAGAA	
Pgc-1α (forward)	TATGGAGTGACATAGAGTGTGCT	6679433a1
Pgc-1α (reverse)	CCACTTCAATCCACCCAGAAAG	
Phb1 (forward)	ACCCATTCACTTATGAGGACCC	27734098a1
Phb1 (reverse)	CTGCTCCGATGACCTCTTCA	
Phb2 (forward)	ATCCGTGTTCACCGTGGAAG	6671622a1
Phb2 (reverse)	CCCGAATGTCATAGATGATGGG	
Opa1 (forward)	TGGAAAATGGTTCGAGAGTCAG	19526960a1
Opa1 (reverse)	CATTCCGTCTCTAGGTTAAAGCG	
Drp1 (forward)	ATGCCAGCAAGTCCACAGAA	N/A
Drp1 (reverse)	TGTTCTCGGGCAGACAGTTT	

A.2 Buffer Formulations

Buffer	Components
Chappel-Perry Buffer, pH 7.4	100 mM KCl 50 mM MOPS 5 mM $MgSO_4$-$7H_2O$ 6.06 mg/mL ATP
Chappel-Perry Buffer II, pH 7.4	100 mM KCl 50 mM MOPS 5 mM $MgSO_4$-$7H_2O$ 1 mM EGTA 2 mg/mL bovine serum albumin
Mitochondrial Respiration Buffer, pH 7.4	100 mM KCl 50 mM MOPS 0.5 mM EGTA
Buffer X (BIOPS), pH 7.1	7.23 mM K_2EGTA 2.77 mM Ca K_2EGTA 20 mM Imidazole 20 mM Taurine 5.7 mM ATP 14.3 mM PCr 6.56 mM $MgCl_2$-$6H_2O$ 50 mM K-MES
Buffer Z (Respiration Buffer), pH 7.1	105 mM K-MES 30 mM KCl 10 mM KH_2PO_4 5 mM $MgCl_2$-$6H_2O$ 0.5 mg/mL bovine serum albumin 1 mM EGTA (added fresh)

REFERENCES

1 Hermansen, L., Hultman, E. & Saltin, B. Muscle glycogen during prolonged severe exercise. *Acta physiologica Scandinavica* **71**, 129-139, doi:10.1111/j.1748-1716.1967.tb03719.x (1967).

2 Romijn, J. A. *et al.* Regulation of endogenous fat and carbohydrate metabolism in relation to exercise intensity and duration. *The American journal of physiology* **265**, E380-391, doi:10.1152/ajpendo.1993.265.3.E380 (1993).

3 Shulman, G. I. *et al.* Quantitation of muscle glycogen synthesis in normal subjects and subjects with non-insulin-dependent diabetes by 13C nuclear magnetic resonance spectroscopy. *The New England journal of medicine* **322**, 223-228, doi:10.1056/nejm199001253220403 (1990).

4 Jensen, J., Aslesen, R., Ivy, J. L. & Brørs, O. Role of glycogen concentration and epinephrine on glucose uptake in rat epitrochlearis muscle. *The American journal of physiology* **272**, E649-655, doi:10.1152/ajpendo.1997.272.4.E649 (1997).

5 Felig, P., Owen, O. E., Wahren, J. & Cahill, G. F., Jr. Amino acid metabolism during prolonged starvation. *J Clin Invest* **48**, 584-594, doi:10.1172/jci106017 (1969).

6 Biolo, G., Zhang, X. J. & Wolfe, R. R. Role of membrane transport in interorgan amino acid flow between muscle and small intestine. *Metabolism* **44**, 719-724, doi:10.1016/0026-0495(95)90183-3 (1995).

7 Cahill, G. F., Jr. Starvation in man. *The New England journal of medicine* **282**, 668-675, doi:10.1056/nejm197003192821209 (1970).

8 Febbraio, M. A. & Pedersen, B. K. Contraction-induced myokine production and release: is skeletal muscle an endocrine organ? *Exercise and sport sciences reviews* **33**, 114-119, doi:10.1097/00003677-200507000-00003 (2005).

9 Pedersen, B. K. Muscles and their myokines. *Journal of Experimental Biology* **214**, 337-346, doi:10.1242/jeb.048074 (2011).

10 Handschin, C., Rhee, J., Lin, J., Tarr, P. T. & Spiegelman, B. M. An autoregulatory loop controls peroxisome proliferator-activated receptor gamma coactivator 1alpha expression in muscle. *Proceedings of the National Academy of Sciences of the United States of America* **100**, 7111-7116, doi:10.1073/pnas.1232352100 (2003).

11 Schnyder, S. & Handschin, C. Skeletal muscle as an endocrine organ: PGC-1α, myokines and exercise. *Bone* **80**, 115-125, doi:10.1016/j.bone.2015.02.008 (2015).

12 Miura, P., Amirouche, A., Clow, C., Bélanger, G. & Jasmin, B. J. Brain-derived neurotrophic factor expression is repressed during myogenic differentiation by

miR-206. *Journal of neurochemistry* **120**, 230-238, doi:10.1111/j.1471-4159.2011.07583.x (2012).

13 Jensen, L., Schjerling, P. & Hellsten, Y. Regulation of VEGF and bFGF mRNA expression and other proliferative compounds in skeletal muscle cells. *Angiogenesis* **7**, 255-267, doi:10.1007/s10456-004-4184-4 (2004).

14 Hojman, P. *et al.* Fibroblast growth factor-21 is induced in human skeletal muscles by hyperinsulinemia. *Diabetes* **58**, 2797-2801, doi:10.2337/db09-0713 (2009).

15 Steensberg, A. *et al.* Production of interleukin-6 in contracting human skeletal muscles can account for the exercise-induced increase in plasma interleukin-6. *The Journal of physiology* **529 Pt 1**, 237-242, doi:10.1111/j.1469-7793.2000.00237.x (2000).

16 Frontera, W. R. & Ochala, J. Skeletal Muscle: A Brief Review of Structure and Function. *Calcified Tissue International* **96**, 183-195, doi:10.1007/s00223-014-9915-y (2015).

17 Ottenheijm, C. A. & Granzier, H. Lifting the nebula: novel insights into skeletal muscle contractility. *Physiology (Bethesda, Md.)* **25**, 304-310, doi:10.1152/physiol.00016.2010 (2010).

18 van Wessel, T., de Haan, A., van der Laarse, W. J. & Jaspers, R. T. The muscle fiber type–fiber size paradox: hypertrophy or oxidative metabolism? *European Journal of Applied Physiology* **110**, 665-694, doi:10.1007/s00421-010-1545-0 (2010).

19 Burkholder, T. J., Fingado, B., Baron, S. & Lieber, R. L. Relationship between muscle fiber types and sizes and muscle architectural properties in the mouse hindlimb. *Journal of Morphology* **221**, 177-190, doi:doi:10.1002/jmor.1052210207 (1994).

20 Ausoni, S., Gorza, L., Schiaffino, S., Gundersen, K. & Lømo, T. Expression of myosin heavy chain isoforms in stimulated fast and slow rat muscles. *The Journal of neuroscience : the official journal of the Society for Neuroscience* **10**, 153-160, doi:10.1523/jneurosci.10-01-00153.1990 (1990).

21 Tintignac, L. A., Brenner, H.-R. & Rüegg, M. A. Mechanisms Regulating Neuromuscular Junction Development and Function and Causes of Muscle Wasting. *Physiological Reviews* **95**, 809-852, doi:10.1152/physrev.00033.2014 (2015).

22 Perez, V. J. & Moore, B. W. Wallerian degeneration in rabbit tibial nerve: changes in amounts of the S-100 protein. *Journal of neurochemistry* **15**, 971-977, doi:10.1111/j.1471-4159.1968.tb11640.x (1968).

23 Shen, J., Tareste, D. C., Paumet, F., Rothman, J. E. & Melia, T. J. Selective activation of cognate SNAREpins by Sec1/Munc18 proteins. *Cell* **128**, 183-195, doi:10.1016/j.cell.2006.12.016 (2007).

24 Maximov, A., Tang, J., Yang, X., Pang, Z. P. & Südhof, T. C. Complexin controls the force transfer from SNARE complexes to membranes in fusion. *Science (New York, N.Y.)* **323**, 516-521, doi:10.1126/science.1166505 (2009).

25 Owens, G. C. & Walcott, E. C. Extensive Fusion of Mitochondria in Spinal Cord Motor Neurons. *PLOS ONE* **7**, e38435, doi:10.1371/journal.pone.0038435 (2012).

26 Buller, A. J., Eccles, J. C. & Eccles, R. M. Interactions between motoneurones and muscles in respect of the characteristic speeds of their responses. *The Journal of physiology* **150**, 417-439 (1960).

27 Chakkalakal, J. V., Nishimune, H., Ruas, J. L., Spiegelman, B. M. & Sanes, J. R. Retrograde influence of muscle fibers on their innervation revealed by a novel marker for slow motoneurons. *Development (Cambridge, England)* **137**, 3489-3499, doi:10.1242/dev.053348 (2010).

28 Grinnell, A. D. Dynamics of nerve-muscle interaction in developing and mature neuromuscular junctions. *Physiological Reviews* **75**, 789-834, doi:10.1152/physrev.1995.75.4.789 (1995).

29 Wu, H., Xiong, W. C. & Mei, L. To build a synapse: signaling pathways in neuromuscular junction assembly. *Development (Cambridge, England)* **137**, 1017-1033, doi:10.1242/dev.038711 (2010).

30 Nishizawa, T., Tamaki, H., Kasuga, N. & Takekura, H. Degeneration and regeneration of neuromuscular junction architecture in rat skeletal muscle fibers damaged by bupivacaine hydrochloride. *Journal of muscle research and cell motility* **24**, 527-537, doi:10.1023/b:jure.0000009905.89618.33 (2003).

31 Nitkin, R. M. *et al.* Identification of agrin, a synaptic organizing protein from Torpedo electric organ. *The Journal of cell biology* **105**, 2471-2478, doi:10.1083/jcb.105.6.2471 (1987).

32 Falls, D. L., Rosen, K. M., Corfas, G., Lane, W. S. & Fischbach, G. D. ARIA, a protein that stimulates acetylcholine receptor synthesis, is a member of the neu ligand family. *Cell* **72**, 801-813, doi:https://doi.org/10.1016/0092-8674(93)90407-H (1993).

33 Zhang, B. *et al.* Wnt proteins regulate acetylcholine receptor clustering in muscle cells. *Molecular Brain* **5**, 7, doi:10.1186/1756-6606-5-7 (2012).

34 Martin, P. & Lewis, J. Origins of the neurovascular bundle: interactions between developing nerves and blood vessels in embryonic chick skin. *The International journal of developmental biology* **33**, 379-387 (1989).

35 Bagher, P. & Segal, S. S. Regulation of blood flow in the microcirculation: role of conducted vasodilation. *Acta physiologica (Oxford, England)* **202**, 271-284, doi:10.1111/j.1748-1716.2010.02244.x (2011).

36 Andersen, P. & Kroese, A. J. Capillary supply in soleus and gastrocnemius muscles of man. *Pflugers Archiv : European journal of physiology* **375**, 245-249, doi:10.1007/bf00582437 (1978).

37 Folkow, B. & Halicka, H. D. A comparison between "red" and "white" muscle with respect to blood supply, capillary surface area and oxygen uptake during rest and exercise. *Microvascular Research* **1**, 1-14, doi:https://doi.org/10.1016/0026-2862(68)90002-2 (1968).

38 Kilarski, W. W., Samolov, B., Petersson, L., Kvanta, A. & Gerwins, P. Biomechanical regulation of blood vessel growth during tissue vascularization. *Nature medicine* **15**, 657-664, doi:10.1038/nm.1985 (2009).

39 Davis, C. M., Danehower, S. C., Laurenza, A. & Molony, J. L. Identification of a role of the vitronectin receptor and protein kinase C in the induction of endothelial cell vascular formation. *Journal of cellular biochemistry* **51**, 206-218 (1993).

40 Yang, J. T., Rayburn, H. & Hynes, R. O. Embryonic mesodermal defects in alpha 5 integrin-deficient mice. *Development (Cambridge, England)* **119**, 1093-1105 (1993).

41 Brooks, P. C. Role of integrins in angiogenesis. *European Journal of Cancer* **32**, 2423-2429, doi:10.1016/S0959-8049(96)00381-4 (1996).

42 Grant, D. S. *et al.* Two different laminin domains mediate the differentiation of human endothelial cells into capillary-like structures in vitro. *Cell* **58**, 933-943, doi:https://doi.org/10.1016/0092-8674(89)90945-8 (1989).

43 Schnaper, H. W., Kleinman, H. K. & Grant, D. S. Role of laminin in endothelial cell recognition and differentiation. *Kidney International* **43**, 20-25, doi:https://doi.org/10.1038/ki.1993.5 (1993).

44 Richardson, R. S. *et al.* Human VEGF gene expression in skeletal muscle: effect of acute normoxic and hypoxic exercise. *The American journal of physiology* **277**, H2247-2252, doi:10.1152/ajpheart.1999.277.6.H2247 (1999).

45 Jain, R. K. *et al.* Angiogenesis in brain tumours. *Nature Reviews Neuroscience* **8**, 610-622 (2007).

46 Charge, S. B. & Rudnicki, M. A. Cellular and molecular regulation of muscle regeneration. *Physiol Rev* **84**, 209-238, doi:10.1152/physrev.00019.2003 (2004).

47 Lander, A. D. *et al.* What does the concept of the stem cell niche really mean today? *BMC Biol* **10**, 19, doi:10.1186/1741-7007-10-19 (2012).

48 Liu, W., Wei-LaPierre, L., Klose, A., Dirksen, R. T. & Chakkalakal, J. V. Inducible depletion of adult skeletal muscle stem cells impairs the regeneration of neuromuscular junctions. *Elife* **4**, doi:10.7554/eLife.09221 (2015).

49 Verma, M. *et al.* Muscle Satellite Cell Cross-Talk with a Vascular Niche Maintains Quiescence via VEGF and Notch Signaling. *Cell Stem Cell* **23**, 530-543.e539, doi:10.1016/j.stem.2018.09.007 (2018).

50 Williams, R. S. & Annex, B. H. Plasticity of myocytes and capillaries: a possible coordinating role for VEGF. *Circ Res* **95**, 7-8, doi:10.1161/01.res.0000136345.81719.37 (2004).

51 Christov, C. *et al.* Muscle satellite cells and endothelial cells: close neighbors and privileged partners. *Molecular biology of the cell* **18**, 1397-1409, doi:10.1091/mbc.e06-08-0693 (2007).

52 Hart, C. A., Tsui, J., Khanna, A., Abraham, D. J. & Baker, D. M. Stem cells of the lower limb: their role and potential in management of critical limb ischemia. *Experimental biology and medicine (Maywood, N.J.)* **238**, 1118-1126, doi:10.1177/1535370213503275 (2013).

53 Yin, H., Price, F. & Rudnicki, M. A. Satellite cells and the muscle stem cell niche. *Physiological reviews* **93**, 23-67, doi:10.1152/physrev.00043.2011 (2013).

54 Sheehan, S. M. & Allen, R. E. Skeletal muscle satellite cell proliferation in response to members of the fibroblast growth factor family and hepatocyte growth factor. *J Cell Physiol* **181**, 499-506, doi:10.1002/(sici)1097-4652(199912)181:3<499::aid-jcp14>3.0.co;2-1 (1999).

55 Allen, R. E. & Boxhorn, L. K. Regulation of skeletal muscle satellite cell proliferation and differentiation by transforming growth factor-beta, insulin-like growth factor I, and fibroblast growth factor. *J Cell Physiol* **138**, 311-315, doi:10.1002/jcp.1041380213 (1989).

56 Lotze, M. T. *et al.* The grateful dead: damage-associated molecular pattern molecules and reduction/oxidation regulate immunity. *Immunological reviews* **220**, 60-81, doi:10.1111/j.1600-065X.2007.00579.x (2007).

57 Li, Y. P. TNF-alpha is a mitogen in skeletal muscle. *Am J Physiol Cell Physiol* **285**, C370-376, doi:10.1152/ajpcell.00453.2002 (2003).

58 Rocheteau, P., Gayraud-Morel, B., Siegl-Cachedenier, I., Blasco, M. A. & Tajbakhsh, S. A subpopulation of adult skeletal muscle stem cells retains all template DNA strands after cell division. *Cell* **148**, 112-125, doi:10.1016/j.cell.2011.11.049 (2012).

59 Wu, R. *et al.* MicroRNA-431 accelerates muscle regeneration and ameliorates muscular dystrophy by targeting Pax7 in mice. *Nature Communications* **6**, 7713, doi:10.1038/ncomms8713 (2015).

60 Wüst, S. *et al.* Metabolic Maturation during Muscle Stem Cell Differentiation Is Achieved by miR-1/133a-Mediated Inhibition of the Dlk1-Dio3 Mega Gene Cluster. *Cell metabolism* **27**, 1026-1039.e1026, doi:https://doi.org/10.1016/j.cmet.2018.02.022 (2018).

61 Beauchamp, J. R. *et al.* Expression of CD34 and Myf5 defines the majority of quiescent adult skeletal muscle satellite cells. *The Journal of cell biology* **151**, 1221-1234, doi:10.1083/jcb.151.6.1221 (2000).

62 García-Prat, L. *et al.* FoxO maintains a genuine muscle stem-cell quiescent state until geriatric age. *Nature Cell Biology* **22**, 1307-1318, doi:10.1038/s41556-020-00593-7 (2020).

63 Ono, Y. *et al.* Muscle Stem Cell Fate Is Controlled by the Cell-Polarity Protein Scrib. *Cell Reports* **10**, 1135-1148, doi:https://doi.org/10.1016/j.celrep.2015.01.045 (2015).

64 Yennek, S., Burute, M., Théry, M. & Tajbakhsh, S. Cell adhesion geometry regulates non-random DNA segregation and asymmetric cell fates in mouse skeletal muscle stem cells. *Cell Rep* **7**, 961-970, doi:10.1016/j.celrep.2014.04.016 (2014).

65 Dumont, N. A. *et al.* Dystrophin expression in muscle stem cells regulates their polarity and asymmetric division. *Nature medicine* **21**, 1455-1463, doi:10.1038/nm.3990 (2015).

66 Liu, Y. *et al.* Splicing Factor SRSF1 Is Essential for Satellite Cell Proliferation and Postnatal Maturation of Neuromuscular Junctions in Mice. *Stem Cell Reports* **15**, 941-954, doi:https://doi.org/10.1016/j.stemcr.2020.08.004 (2020).

67 Hall, Z. W. & Ralston, E. Nuclear domains in muscle cells. *Cell (Cambridge)* **59**, 771-772 (1989).

68 Pavlath, G. K., Rich, K., Webster, S. G. & Blau, H. M. Localization of muscle gene products in nuclear domains. *Nature* **337**, 570-573, doi:10.1038/337570a0 (1989).

69 Mantilla, C. B., Sill, R. V., Aravamudan, B., Zhan, W.-Z. & Sieck, G. C. Developmental effects on myonuclear domain size of rat diaphragm fibers. *Journal of Applied Physiology* **104**, 787-794, doi:10.1152/japplphysiol.00347.2007 (2008).

70 Hansson, K.-A. *et al.* Myonuclear content regulates cell size with similar scaling properties in mice and humans. *Nature Communications* **11**, 6288, doi:10.1038/s41467-020-20057-8 (2020).

71 Murach, K. A., Englund, D. A., Dupont-Versteegden, E. E., McCarthy, J. J. & Peterson, C. A. Myonuclear Domain Flexibility Challenges Rigid Assumptions on Satellite Cell Contribution to Skeletal Muscle Fiber Hypertrophy. *Frontiers in Physiology* **9**, doi:10.3389/fphys.2018.00635 (2018).

72 Itoh, M. *et al.* Alterations of biochemical marker levels and myonuclear numbers in rat skeletal muscle after ischemia-reperfusion. *Molecular and cellular biochemistry* **373**, 11-18, doi:10.1007/s11010-012-1470-0 (2013).

73 Matsuba, Y. *et al.* Gravitational unloading inhibits the regenerative potential of atrophied soleus muscle in mice. *Acta physiologica (Oxford, England)* **196**, 329-339, doi:10.1111/j.1748-1716.2008.01943.x (2009).

74 Gundersen, K. *et al.* No change in myonuclear number during muscle. *J Appl Physiol* **113**, 290-296 (2012).

75 Bruusgaard, J. C. & Gundersen, K. In vivo time-lapse microscopy reveals no loss of murine myonuclei during weeks of muscle atrophy. *The Journal of clinical investigation* **118**, 1450-1457 (2008).

76 Sandonà, D. *et al.* Adaptation of mouse skeletal muscle to long-term microgravity in the MDS mission. *PloS one* **7**, e33232 (2012).

77 Mitchell, P. O. & Pavlath, G. K. A muscle precursor cell-dependent pathway contributes to muscle growth after atrophy. *American Journal of Physiology-Cell Physiology* **281**, C1706-C1715 (2001).

78 Conceição, M. S. *et al.* Muscle Fiber Hypertrophy and Myonuclei Addition: A Systematic Review and Meta-analysis. *Med Sci Sports Exerc* **50**, 1385-1393, doi:10.1249/mss.0000000000001593 (2018).

79 Sinha-Hikim, I., Roth, S. M., Lee, M. I. & Bhasin, S. Testosterone-induced muscle hypertrophy is associated with an increase in satellite cell number in healthy, young men. *American Journal of Physiology-Endocrinology and Metabolism* **285**, E197-E205, doi:10.1152/ajpendo.00370.2002 (2003).

80 Egner, I. M., Bruusgaard, J. C. & Gundersen, K. Satellite cell depletion prevents fiber hypertrophy in skeletal muscle. *Development (Cambridge, England)* **143**, 2898-2906, doi:10.1242/dev.134411 (2016).

81 van der Meer, S. F. T., Jaspers, R. T., Jones, D. A. & Degens, H. The time course of myonuclear accretion during hypertrophy in young adult and older rat plantaris muscle. *Annals of Anatomy - Anatomischer Anzeiger* **193**, 56-63, doi:https://doi.org/10.1016/j.aanat.2010.08.004 (2011).

82 Kadi, F. *et al.* The effects of heavy resistance training and detraining on satellite cells in human skeletal muscles. *The Journal of physiology* **558**, 1005-1012, doi:https://doi.org/10.1113/jphysiol.2004.065904 (2004).

83 Kirby, T. J. *et al.* Myonuclear transcription is responsive to mechanical load and DNA content but uncoupled from cell size during hypertrophy. *Molecular biology of the cell* **27**, 788-798, doi:10.1091/mbc.E15-08-0585 (2016).

84 Bruusgaard, J. C., Johansen, I. B., Egner, I. M., Rana, Z. A. & Gundersen, K. Myonuclei acquired by overload exercise precede hypertrophy and are not lost on detraining. *Proceedings of the National Academy of Sciences* **107**, 15111-15116, doi:10.1073/pnas.0913935107 (2010).

85 Psilander, N. *et al.* Effects of training, detraining, and retraining on strength, hypertrophy, and myonuclear number in human skeletal muscle. *Journal of Applied Physiology* **126**, 1636-1645, doi:10.1152/japplphysiol.00917.2018 (2019).

86 Egner, I. M., Bruusgaard, J. C., Eftestøl, E. & Gundersen, K. A cellular memory mechanism aids overload hypertrophy in muscle long after an episodic exposure to anabolic steroids. *The Journal of physiology* **591**, 6221-6230, doi:10.1113/jphysiol.2013.264457 (2013).

87 Boengler, K., Heusch, G. & Schulz, R. Nuclear-encoded mitochondrial proteins and their role in cardioprotection. *Biochimica et biophysica acta* **1813**, 1286-1294, doi:10.1016/j.bbamcr.2011.01.009 (2011).

88 Remels, A. H. *et al.* Regulation of mitochondrial biogenesis during myogenesis. *Molecular and cellular endocrinology* **315**, 113-120, doi:10.1016/j.mce.2009.09.029 (2010).

89 Brenmoehl, J. & Hoeflich, A. Dual control of mitochondrial biogenesis by sirtuin 1 and sirtuin 3. *Mitochondrion* **13**, 755-761, doi:https://doi.org/10.1016/j.mito.2013.04.002 (2013).

90 Jager, S., Handschin, C., St-Pierre, J. & Spiegelman, B. M. AMP-activated protein kinase (AMPK) action in skeletal muscle via direct phosphorylation of PGC-1alpha. *Proceedings of the National Academy of Sciences of the United States of America* **104**, 12017-12022, doi:10.1073/pnas.0705070104 (2007).

91 Youle, R. J. & van der Bliek, A. M. Mitochondrial fission, fusion, and stress. *Science (New York, N.Y.)* **337**, 1062-1065, doi:10.1126/science.1219855 (2012).

92 Merkwirth, C. *et al.* Prohibitins control cell proliferation and apoptosis by regulating OPA1-dependent cristae morphogenesis in mitochondria. *Genes & development* **22**, 476-488, doi:10.1101/gad.460708 (2008).

93 Fusaro, G., Dasgupta, P., Rastogi, S., Joshi, B. & Chellappan, S. Prohibitin induces the transcriptional activity of p53 and is exported from the nucleus upon apoptotic signaling. *The Journal of biological chemistry* **278**, 47853-47861, doi:10.1074/jbc.M305171200 (2003).

94 Kasashima, K., Ohta, E., Kagawa, Y. & Endo, H. Mitochondrial functions and estrogen receptor-dependent nuclear translocation of pleiotropic human prohibitin 2. *The Journal of biological chemistry* **281**, 36401-36410, doi:10.1074/jbc.M605260200 (2006).

95 Tigano, M., Vargas, D. C., Tremblay-Belzile, S., Fu, Y. & Sfeir, A. Nuclear sensing of breaks in mitochondrial DNA enhances immune surveillance. *Nature* **591**, 477-481, doi:10.1038/s41586-021-03269-w (2021).

96 Cardamone, M. D. *et al.* Mitochondrial Retrograde Signaling in Mammals Is Mediated by the Transcriptional Cofactor GPS2 via Direct Mitochondria-to-Nucleus Translocation. *Molecular Cell* **69**, 757-772.e757, doi:10.1016/j.molcel.2018.01.037 (2018).

97 Janssen, J. J. E., Grefte, S., Keijer, J. & de Boer, V. C. J. Mito-Nuclear Communication by Mitochondrial Metabolites and Its Regulation by B-Vitamins. *Frontiers in Physiology* **10**, doi:10.3389/fphys.2019.00078 (2019).

98 Lee, C. *et al.* The mitochondrial-derived peptide MOTS-c promotes metabolic homeostasis and reduces obesity and insulin resistance. *Cell metabolism* **21**, 443-454, doi:10.1016/j.cmet.2015.02.009 (2015).

99 Wallace, D. C. Mitochondria as Chi. *Genetics* **179**, 727-735, doi:10.1534/genetics.104.91769 (2008).

100 Chen, Z. *et al.* Mitochondrial DNA segregation and replication restrict the transmission of detrimental mutation. *Journal of Cell Biology* **219**, doi:10.1083/jcb.201905160 (2020).

101 Mishra, P., Varuzhanyan, G., Pham, A. H. & Chan, D. C. Mitochondrial dynamics is a distinguishing feature of skeletal muscle fiber types and regulates organellar compartmentalization. *Cell metabolism* **22**, 1033-1044, doi:10.1016/j.cmet.2015.09.027 (2015).

102 Ferreira, R. *et al.* Subsarcolemmal and intermyofibrillar mitochondria proteome differences disclose functional specializations in skeletal muscle. *Proteomics* **10**, 3142-3154, doi:10.1002/pmic.201000173 (2010).

103 Mohiuddin, M. *et al.* Critical Limb Ischemia Induces Remodeling of Skeletal Muscle Motor Unit, Myonuclear-, and Mitochondrial-Domains. *Scientific Reports* **9**, 9551, doi:10.1038/s41598-019-45923-4 (2019).

104 Twig, G. *et al.* Fission and selective fusion govern mitochondrial segregation and elimination by autophagy. *The EMBO journal* **27**, 433-446 (2008).

105 Jin, S. M. & Youle, R. J. PINK1- and Parkin-mediated mitophagy at a glance. *Journal of cell science* **125**, 795-799, doi:10.1242/jcs.093849 (2012).

106 Liu, W. *et al.* Hypoxia promotes satellite cell self-renewal and enhances the efficiency of myoblast transplantation. *Development (Cambridge, England)* **139**, 2857-2865, doi:10.1242/dev.079665 (2012).

107 Ryall, J. G. Metabolic reprogramming as a novel regulator of skeletal muscle development and regeneration. *The FEBS journal* **280**, 4004-4013, doi:10.1111/febs.12189 (2013).

108 Pala, F. *et al.* Distinct metabolic states govern skeletal muscle stem cell fates during prenatal and postnatal myogenesis. *Journal of cell science* **131**, jcs212977, doi:10.1242/jcs.212977 (2018).

109 Wagatsuma, A. & Sakuma, K. Mitochondria as a Potential Regulator of Myogenesis. *The Scientific World Journal* **2013**, 9, doi:10.1155/2013/593267 (2013).

110 Pavlidou, T. *et al.* Metformin Delays Satellite Cell Activation and Maintains Quiescence. *Stem Cells International* **2019**, 19, doi:10.1155/2019/5980465 (2019).

111 Chaillou, T. & Lanner, J. T. Regulation of myogenesis and skeletal muscle regeneration: effects of oxygen levels on satellite cell activity. *FASEB journal : official publication of the Federation of American Societies for Experimental Biology* **30**, 3929-3941, doi:10.1096/fj.201600757R (2016).

112 Duvall, C. L. *et al.* The role of osteopontin in recovery from hind limb ischemia. *Arteriosclerosis, thrombosis, and vascular biology* **28**, 290-295, doi:10.1161/atvbaha.107.158485 (2008).

113 Mosoni, L. *et al.* Altered response of protein synthesis to nutritional state and endurance training in old rats. *The American journal of physiology* **268**, E328-335, doi:10.1152/ajpendo.1995.268.2.E328 (1995).

114 Han, L., Wu, S. & Hu, P. The functions of sarcopenia related myokines. *Translational Medicine of Aging* **2**, 38-41, doi:https://doi.org/10.1016/j.tma.2018.08.001 (2018).

115 Swift, M. E., Kleinman, H. K. & DiPietro, L. A. Impaired wound repair and delayed angiogenesis in aged mice. *Laboratory investigation; a journal of technical methods and pathology* **79**, 1479-1487 (1999).

116 Sadoun, E. & Reed, M. J. Impaired angiogenesis in aging is associated with alterations in vessel density, matrix composition, inflammatory response, and growth factor expression. *The journal of histochemistry and cytochemistry : official journal of the Histochemistry Society* **51**, 1119-1130, doi:10.1177/002215540305100902 (2003).

117 Jang, Y. C. *et al.* Increased superoxide in vivo accelerates age-associated muscle atrophy through mitochondrial dysfunction and neuromuscular junction

degeneration. *The FASEB Journal* **24**, 1376-1390, doi:10.1096/fj.09-146308 (2010).

118 Jang, Y. C. & Van Remmen, H. Age-associated alterations of the neuromuscular junction. *Experimental gerontology* **46**, 193-198, doi:10.1016/j.exger.2010.08.029 (2011).

119 Muller, F. L. *et al.* Denervation-induced skeletal muscle atrophy is associated with increased mitochondrial ROS production. *American Journal of Physiology-Regulatory, Integrative and Comparative Physiology* **293**, R1159-R1168, doi:10.1152/ajpregu.00767.2006 (2007).

120 Day, K., Shefer, G., Shearer, A. & Yablonka-Reuveni, Z. The depletion of skeletal muscle satellite cells with age is concomitant with reduced capacity of single progenitors to produce reserve progeny. *Developmental biology* **340**, 330-343, doi:10.1016/j.ydbio.2010.01.006 (2010).

121 Chakkalakal, J. V., Jones, K. M., Basson, M. A. & Brack, A. S. The aged niche disrupts muscle stem cell quiescence. *Nature* **490**, 355-360, doi:10.1038/nature11438 (2012).

122 Shefer, G., Van de Mark, D. P., Richardson, J. B. & Yablonka-Reuveni, Z. Satellite-cell pool size does matter: defining the myogenic potency of aging skeletal muscle. *Developmental biology* **294**, 50-66 (2006).

123 Carlson, B. M., Dedkov, E. I., Borisov, A. B. & Faulkner, J. A. Skeletal muscle regeneration in very old rats. *The Journals of Gerontology Series A: Biological Sciences and Medical Sciences* **56**, B224-B233 (2001).

124 Sousa-Victor, P. *et al.* Geriatric muscle stem cells switch reversible quiescence into senescence. *Nature* **506**, 316-321, doi:10.1038/nature13013 (2014).

125 Fry, C. S. *et al.* Inducible depletion of satellite cells in adult, sedentary mice impairs muscle regenerative capacity without affecting sarcopenia. *Nature medicine* **21**, 76-80 (2015).

126 Brack, A. S., Bildsoe, H. & Hughes, S. M. Evidence that satellite cell decrement contributes to preferential decline in nuclear number from large fibres during murine age-related muscle atrophy. *Journal of cell science* **118**, 4813-4821, doi:10.1242/jcs.02602 (2005).

127 Liu, W. *et al.* Loss of adult skeletal muscle stem cells drives age-related neuromuscular junction degeneration. *Elife* **6**, e26464 (2017).

128 Rhoads, R. P. *et al.* Satellite cells isolated from aged or dystrophic muscle exhibit a reduced capacity to promote angiogenesis in vitro. *Biochemical and Biophysical Research Communications* **440**, 399-404, doi:https://doi.org/10.1016/j.bbrc.2013.09.085 (2013).

129 Brack, A. S. *et al.* Increased Wnt signaling during aging alters muscle stem cell fate and increases fibrosis. *Science (New York, N.Y.)* **317**, 807-810 (2007).

130 Carey, K. A., Farnfield, M. M., Tarquinio, S. D. & Cameron-Smith, D. Impaired expression of Notch signaling genes in aged human skeletal muscle. *The Journals of Gerontology Series A: Biological Sciences and Medical Sciences* **62**, 9-17 (2007).

131 Florian, M. C. *et al.* A canonical to non-canonical Wnt signalling switch in haematopoietic stem-cell ageing. *Nature* **503**, 392-396 (2013).

132 Raue, U., Slivka, D., Jemiolo, B., Hollon, C. & Trappe, S. Myogenic gene expression at rest and after a bout of resistance exercise in young (18–30 yr) and old (80–89 yr) women. *Journal of Applied Physiology* **101**, 53-59 (2006).

133 Verdijk, L. B. *et al.* Satellite cells in human skeletal muscle; from birth to old age. *Age* **36**, 545-557 (2014).

134 Mookerjee, S. A., Gerencser, A. A., Nicholls, D. G. & Brand, M. D. Quantifying intracellular rates of glycolytic and oxidative ATP production and consumption using extracellular flux measurements. *The Journal of biological chemistry* **292**, 7189-7207, doi:10.1074/jbc.M116.774471 (2017).

135 Li, Z. & Graham, B. H. Measurement of mitochondrial oxygen consumption using a Clark electrode. *Methods Mol Biol* **837**, 63-72, doi:10.1007/978-1-61779-504-6_5 (2012).

136 Chistiakov, D. A., Sobenin, I. A., Revin, V. V., Orekhov, A. N. & Bobryshev, Y. V. Mitochondrial Aging and Age-Related Dysfunction of Mitochondria. *BioMed Research International* **2014**, 238463, doi:10.1155/2014/238463 (2014).

137 Sun, N., Youle, R. J. & Finkel, T. The Mitochondrial Basis of Aging. *Molecular cell* **61**, 654-666, doi:10.1016/j.molcel.2016.01.028 (2016).

138 Gouspillou, G. *et al.* Increased sensitivity to mitochondrial permeability transition and myonuclear translocation of endonuclease G in atrophied muscle of physically active older humans. *The FASEB Journal* **28**, 1621-1633 (2014).

139 Drummond, M. J. *et al.* Downregulation of E3 ubiquitin ligases and mitophagy-related genes in skeletal muscle of physically inactive, frail older women: a cross-sectional comparison. *Journals of Gerontology Series A: Biomedical Sciences and Medical Sciences* **69**, 1040-1048 (2014).

140 Pipinos, II *et al.* Mitochondrial defects and oxidative damage in patients with peripheral arterial disease. *Free radical biology & medicine* **41**, 262-269, doi:10.1016/j.freeradbiomed.2006.04.003 (2006).

141 Raghupathi, W. & Raghupathi, V. An Empirical Study of Chronic Diseases in the United States: A Visual Analytics Approach. *Int J Environ Res Public Health* **15**, 431, doi:10.3390/ijerph15030431 (2018).

142 Comlossy, M. in *National Conference of State Legislatures.* 1-16.

143 Collaboration, G. B. o. C. D. The Burden of Cardiovascular Diseases Among US States, 1990-2016. *JAMA Cardiology* **3**, 375-389, doi:10.1001/jamacardio.2018.0385 (2018).

144 Raghupathi, W. & Raghupathi, V. An overview of health analytics. *J Health Med Informat* **4**, 2 (2013).

145 Mohler III, E. R. Peripheral Arterial Disease: Identification and Implications. *JAMA Internal Medicine* **163**, 2306-2314, doi:10.1001/archinte.163.19.2306 (2003).

146 Allison, M. A. *et al.* Ethnic-specific prevalence of peripheral arterial disease in the United States. *American journal of preventive medicine* **32**, 328-333, doi:10.1016/j.amepre.2006.12.010 (2007).

147 Swaminathan, A., Vemulapalli, S., Patel, M. R. & Jones, W. S. Lower extremity amputation in peripheral artery disease: improving patient outcomes. *Vasc Health Risk Manag* **10**, 417-424, doi:10.2147/VHRM.S50588 (2014).

148 Hardman, R. L., Jazaeri, O., Yi, J., Smith, M. & Gupta, R. Overview of classification systems in peripheral artery disease. *Semin Intervent Radiol* **31**, 378-388, doi:10.1055/s-0034-1393976 (2014).

149 Gardner, A. W. & Afaq, A. Management of lower extremity peripheral arterial disease. *J Cardiopulm Rehabil Prev* **28**, 349-357, doi:10.1097/HCR.0b013e31818c3b96 (2008).

150 Vignaud, A. *et al.* Impaired Skeletal Muscle Repair after Ischemia-Reperfusion Injury in Mice. *Journal of Biomedicine and Biotechnology* **2010**, 724914, doi:10.1155/2010/724914 (2010).

151 Wilson, R. J. *et al.* Mitochondrial protein S-nitrosation protects against ischemia reperfusion-induced denervation at neuromuscular junction in skeletal muscle. *Free radical biology & medicine* **117**, 180-190, doi:10.1016/j.freeradbiomed.2018.02.006 (2018).

152 Brevetti, G., Oliva, G., Silvestro, A., Scopacasa, F. & Chiariello, M. Prevalence, risk factors and cardiovascular comorbidity of symptomatic peripheral arterial disease in Italy. *Atherosclerosis* **175**, 131-138, doi:10.1016/j.atherosclerosis.2004.03.009 (2004).

153 Shvartsman, D. *et al.* Sustained Delivery of VEGF Maintains Innervation and Promotes Reperfusion in Ischemic Skeletal Muscles Via NGF/GDNF Signaling. *Molecular Therapy* **22**, 1243-1253, doi:10.1038/mt.2014.76 (2014).

154 Gardner, A. W., Montgomery, P. S. & Parker, D. E. Physical activity is a predictor of all-cause mortality in patients with intermittent claudication. *J Vasc Surg* **47**, 117-122, doi:10.1016/j.jvs.2007.09.033 (2008).

155 Singh, N. *et al.* Leg strength predicts mortality in men but not in women with peripheral arterial disease. *J Vasc Surg* **52**, 624-631, doi:10.1016/j.jvs.2010.03.066 (2010).

156 McDermott, M. M. *et al.* Decline in functional performance predicts later increased mobility loss and mortality in peripheral arterial disease. *J Am Coll Cardiol* **57**, 962-970, doi:10.1016/j.jacc.2010.09.053 (2011).

157 Jain, A. *et al.* The Walking Impairment Questionnaire stair-climbing score predicts mortality in men and women with peripheral arterial disease. *J Vasc Surg* **55**, 1662-1673 e1662, doi:10.1016/j.jvs.2011.12.010 (2012).

158 McDermott, M. M. *et al.* Calf muscle characteristics, strength measures, and mortality in peripheral arterial disease: a longitudinal study. *J Am Coll Cardiol* **59**, 1159-1167, doi:10.1016/j.jacc.2011.12.019 (2012).

159 Jain, A. *et al.* Declining walking impairment questionnaire scores are associated with subsequent increased mortality in peripheral artery disease. *J Am Coll Cardiol* **61**, 1820-1829, doi:10.1016/j.jacc.2013.01.060 (2013).

160 Leeper, N. J. *et al.* Exercise capacity is the strongest predictor of mortality in patients with peripheral arterial disease. *J Vasc Surg* **57**, 728-733, doi:10.1016/j.jvs.2012.07.051 (2013).

161 Rissanen, T. T. *et al.* Expression of vascular endothelial growth factor and vascular endothelial growth factor receptor-2 (KDR/Flk-1) in ischemic skeletal muscle and its regeneration. *The American journal of pathology* **160**, 1393-1403, doi:10.1016/S0002-9440(10)62566-7 (2002).

162 Pipinos, II *et al.* The myopathy of peripheral arterial occlusive disease: Part 2. Oxidative stress, neuropathy, and shift in muscle fiber type. *Vasc Endovascular Surg* **42**, 101-112, doi:10.1177/1538574408315995 (2008).

163 Ryan, T. E. *et al.* Mitochondrial therapy improves limb perfusion and myopathy following hindlimb ischemia. *J Mol Cell Cardiol* **97**, 191-196, doi:10.1016/j.yjmcc.2016.05.015 (2016).

164 Ryan, T. E. *et al.* Targeted Expression of Catalase to Mitochondria Protects Against Ischemic Myopathy in High-Fat Diet-Fed Mice. *Diabetes* **65**, 2553-2568, doi:10.2337/db16-0387 (2016).

165 McClung, J. M. *et al.* BAG3 (Bcl-2-Associated Athanogene-3) Coding Variant in Mice Determines Susceptibility to Ischemic Limb Muscle Myopathy by Directing Autophagy. *Circulation* **136**, 281-296, doi:10.1161/CIRCULATIONAHA.116.024873 (2017).

166 Ryan, T. E. *et al.* Extensive skeletal muscle cell mitochondriopathy distinguishes critical limb ischemia patients from claudicants. *JCI insight* **3**, doi:10.1172/jci.insight.123235 (2018).

167 Bhat, H. K., Hiatt, W. R., Hoppel, C. L. & Brass, E. P. Skeletal muscle mitochondrial DNA injury in patients with unilateral peripheral arterial disease. *Circulation* **99**, 807-812 (1999).

168 Brass, E. P., Wang, H. & Hiatt, W. R. Multiple skeletal muscle mitochondrial DNA deletions in patients with unilateral peripheral arterial disease. *Vasc Med* **5**, 225-230 (2000).

169 Brass, E. P., Hiatt, W. R., Gardner, A. W. & Hoppel, C. L. Decreased NADH dehydrogenase and ubiquinol-cytochrome c oxidoreductase in peripheral arterial disease. *Am J Physiol Heart Circ Physiol* **280**, H603-609 (2001).

170 Pipinos, II *et al.* Abnormal mitochondrial respiration in skeletal muscle in patients with peripheral arterial disease. *J Vasc Surg* **38**, 827-832 (2003).

171 Weiss, D. J. *et al.* Oxidative damage and myofiber degeneration in the gastrocnemius of patients with peripheral arterial disease. *Journal of translational medicine* **11**, 230, doi:10.1186/1479-5876-11-230 (2013).

172 AlGhatrif, M. *et al.* Lower Mitochondrial Energy Production of the Thigh Muscles in Patients With Low-Normal Ankle-Brachial Index. *Journal of the American Heart Association* **6**, doi:10.1161/JAHA.117.006604 (2017).

173 Hart, C. R. *et al.* Increased skeletal muscle mitochondrial free radical production in peripheral arterial disease despite preserved mitochondrial respiratory capacity. *Exp Physiol*, doi:10.1113/EP086905 (2018).

174 McDermott, M. M. *et al.* Peripheral artery disease, calf skeletal muscle mitochondrial DNA copy number, and functional performance. *Vasc Med*, 1358863X18765667, doi:10.1177/1358863X18765667 (2018).

175 Renault, V., Thornell, L. E., Eriksson, P. O., Butler-Browne, G. & Mouly, V. Regenerative potential of human skeletal muscle during aging. *Aging cell* **1**, 132-139, doi:10.1046/j.1474-9728.2002.00017.x (2002).

176 Renault, V., Thornell, L. E., Butler-Browne, G. & Mouly, V. Human skeletal muscle satellite cells: aging, oxidative stress and the mitotic clock. *Experimental gerontology* **37**, 1229-1236, doi:10.1016/s0531-5565(02)00129-8 (2002).

177 Gomes, M. J. *et al.* Skeletal muscle aging: influence of oxidative stress and physical exercise. *Oncotarget* **8**, 20428-20440, doi:10.18632/oncotarget.14670 (2017).

178 Waters, R. E., Terjung, R. L., Peters, K. G. & Annex, B. H. Preclinical models of human peripheral arterial occlusive disease: implications for investigation of therapeutic agents. *Journal of Applied Physiology* **97**, 773-780, doi:10.1152/japplphysiol.00107.2004 (2004).

179 Orfany, A. *et al.* Mitochondrial transplantation ameliorates acute limb ischemia. *J Vasc Surg*, doi:10.1016/j.jvs.2019.03.079 (2019).

180 Charles, A. L. *et al.* Muscles Susceptibility to Ischemia-Reperfusion Injuries Depends on Fiber Type Specific Antioxidant Level. *Front Physiol* **8**, 52, doi:10.3389/fphys.2017.00052 (2017).

181 Gillani, S., Cao, J., Suzuki, T. & Hak, D. J. The effect of ischemia reperfusion injury on skeletal muscle. *Injury* **43**, 670-675, doi:https://doi.org/10.1016/j.injury.2011.03.008 (2012).

182 Hidalgo, A. *et al.* Modelling ischemia-reperfusion injury (IRI) in vitro using metabolically matured induced pluripotent stem cell-derived cardiomyocytes. *APL Bioengineering* **2**, 026102, doi:10.1063/1.5000746 (2018).

183 Chouchani, E. T. *et al.* Ischaemic accumulation of succinate controls reperfusion injury through mitochondrial ROS. *Nature* **515**, 431-435, doi:10.1038/nature13909 (2014).

184 Padgett, M. E., McCord, T. J., McClung, J. M. & Kontos, C. D. Methods for Acute and Subacute Murine Hindlimb Ischemia. *Journal of visualized experiments : JoVE*, doi:10.3791/54166 (2016).

185 Brenes, R. A. *et al.* Toward a mouse model of hind limb ischemia to test therapeutic angiogenesis. *Journal of vascular surgery* **56**, 1669-1679, doi:10.1016/j.jvs.2012.04.067 (2012).

186 Goto, T. *et al.* Search for appropriate experimental methods to create stable hind-limb ischemia in mouse. *The Tokai journal of experimental and clinical medicine* **31**, 128-132 (2006).

187 Ryan, T. E. *et al.* Mitochondrial therapy improves limb perfusion and myopathy following hindlimb ischemia. *J Mol Cell Cardiol* **97**, 191-196, doi:10.1016/j.yjmcc.2016.05.015 (2016).

188 Schmidt, C. A. *et al.* Strain-Dependent Variation in Acute Ischemic Muscle Injury. *The American journal of pathology* **188**, 1246-1262, doi:10.1016/j.ajpath.2018.01.008 (2018).

189 McClung, J. M. *et al.* Skeletal muscle-specific genetic determinants contribute to the differential strain-dependent effects of hindlimb ischemia in mice. *Am J Pathol* **180**, 2156-2169, doi:10.1016/j.ajpath.2012.01.032 (2012).

190 Helisch, A. *et al.* Impact of mouse strain differences in innate hindlimb collateral vasculature. *Arteriosclerosis, thrombosis, and vascular biology* **26**, 520-526, doi:10.1161/01.ATV.0000202677.55012.a0 (2006).

191 Schmidt, C. A. *et al.* Diminished force production and mitochondrial respiratory deficits are strain-dependent myopathies of subacute limb ischemia. *J Vasc Surg* **65**, 1504-1514.e1511, doi:10.1016/j.jvs.2016.04.041 (2017).

192 Grounds, M. D. & McGeachie, J. K. A comparison of muscle precursor replication in crush-injured skeletal muscle of Swiss and BALBc mice. *Cell and tissue research* **255**, 385-391 (1989).

193 Couffinhal, T. *et al.* Impaired collateral vessel development associated with reduced expression of vascular endothelial growth factor in ApoE−/− mice. *Circulation* **99**, 3188-3198 (1999).

194 Rivard, A. *et al.* Rescue of diabetes-related impairment of angiogenesis by intramuscular gene therapy with adeno-VEGF. *The American journal of pathology* **154**, 355-363 (1999).

195 Hughes, G. C., Post, M. J., Simons, M. & Annex, B. H. Translational physiology: porcine models of human coronary artery disease: implications for preclinical trials of therapeutic angiogenesis. *Journal of Applied Physiology* **94**, 1689-1701 (2003).

196 Seifert, F., Banker, M., Lane, B., Bagge, U. & Anagnostopoulos, C. An evaluation of resting arterial ischemia models in the rat hind limb. *The Journal of cardiovascular surgery* **26**, 502-508 (1985).

197 Sunder-Plassmann, L., Gandolfo, A. & Utz, C. Effectiveness of buflomedil in arterial occlusive disease. Modification of transcutaneous oxygen pressure in a placebo-controlled double-blind study. *MMW, Munchener medizinische Wochenschrift* **126**, 247-248 (1984).

198 Walsworth, M. K., de Bie, R., Figoni, S. F. & O'Connell, J. B. Peripheral Artery Disease: What You Need to Know. *Journal of Orthopaedic & Sports Physical Therapy* **47**, 957-964, doi:10.2519/jospt.2017.7442 (2017).

199 Norgren, L. TASC II Working Group. Inter-society consensus for the management of peripheral arterial disease. *Int Angiol* **26**, 81-157 (2007).

200 Cooke, J. P. & Losordo, D. W. Modulating the vascular response to limb ischemia: angiogenic and cell therapies. *Circulation research* **116**, 1561-1578, doi:10.1161/CIRCRESAHA.115.303565 (2015).

201 Olea, F. D. *et al.* Vascular Endothelial Growth Factor Overexpression Does Not Enhance Adipose Stromal Cell–Induced Protection on Muscle Damage in Critical Limb Ischemia. *Arteriosclerosis, thrombosis, and vascular biology* **35**, 184-188, doi:doi:10.1161/ATVBAHA.114.304348 (2015).

202 Borselli, C. *et al.* Functional muscle regeneration with combined delivery of angiogenesis and myogenesis factors. *Proceedings of the National Academy of Sciences of the United States of America* **107**, 3287-3292, doi:10.1073/pnas.0903875106 (2010).

203 Matzke, S. & Lepantalo, M. Claudication does not always precede critical leg ischemia. *Vascular medicine (London, England)* **6**, 77-80 (2001).

204 Timpani, C. A., Hayes, A. & Rybalka, E. Revisiting the dystrophin-ATP connection: How half a century of research still implicates mitochondrial dysfunction in Duchenne Muscular Dystrophy aetiology. *Medical Hypotheses* **85**, 1021-1033, doi:https://doi.org/10.1016/j.mehy.2015.08.015 (2015).

205 Tabebordbar, M., Wang, E. T. & Wagers, A. J. Skeletal muscle degenerative diseases and strategies for therapeutic muscle repair. *Annual review of pathology* **8**, 441-475, doi:10.1146/annurev-pathol-011811-132450 (2013).

206 Kelly-Worden, M. & Thomas, E. Mitochondrial Dysfunction in Duchenne Muscular Dystrophy. *Open Journal of Endocrine and Metabolic Diseases* **Vol.04No.08**, 8, doi:10.4236/ojemd.2014.48020 (2014).

207 Honeycombe, J. & Anand, R. Molecular analysis of the Duchenne muscular dystrophy locus. *Comparative biochemistry and physiology. A, Comparative physiology* **93**, 125-131, doi:10.1016/0300-9629(89)90199-0 (1989).

208 Millay, D. P. *et al.* Genetic and pharmacologic inhibition of mitochondrial-dependent necrosis attenuates muscular dystrophy. *Nature medicine* **14**, 442-447, doi:10.1038/nm1736 (2008).

209 Perumal, A. R., Rajeswaran, J. & Nalini, A. Neuropsychological profile of duchenne muscular dystrophy. *Applied neuropsychology. Child* **4**, 49-57, doi:10.1080/21622965.2013.802649 (2015).

210 Campbell, K. P. Three muscular dystrophies: loss of cytoskeleton-extracellular matrix linkage. *Cell* **80**, 675-679 (1995).

211 Koenig, M. *et al.* Complete cloning of the duchenne muscular dystrophy (DMD) cDNA and preliminary genomic organization of the DMD gene in normal and affected individuals. *Cell* **50**, 509-517, doi:https://doi.org/10.1016/0092-8674(87)90504-6 (1987).

212 Deconinck, N. & Dan, B. Pathophysiology of duchenne muscular dystrophy: current hypotheses. *Pediatric neurology* **36**, 1-7, doi:10.1016/j.pediatrneurol.2006.09.016 (2007).

213 Bernardi, P. The mitochondrial permeability transition pore: a mystery solved? *Front Physiol* **4**, 95, doi:10.3389/fphys.2013.00095 (2013).

214 Marchi, S. & Pinton, P. The mitochondrial calcium uniporter complex: molecular components, structure and physiopathological implications. *The Journal of physiology* **592**, 829-839, doi:10.1113/jphysiol.2013.268235 (2014).

215 Dubinin, M. V. *et al.* Duchenne muscular dystrophy is associated with the inhibition of calcium uniport in mitochondria and an increased sensitivity of the organelles to the calcium-induced permeability transition. *Biochimica et Biophysica Acta (BBA) - Molecular Basis of Disease* **1866**, 165674, doi:https://doi.org/10.1016/j.bbadis.2020.165674 (2020).

216 Onopiuk, M. *et al.* Mutation in dystrophin-encoding gene affects energy metabolism in mouse myoblasts. *Biochemical and biophysical research communications* **386 3**, 463-466 (2009).

217 Pinton, P., Giorgi, C., Siviero, R., Zecchini, E. & Rizzuto, R. Calcium and apoptosis: ER-mitochondria Ca2+ transfer in the control of apoptosis. *Oncogene* **27**, 6407-6418, doi:10.1038/onc.2008.308 (2008).

218 Kavanagh, N. I., Ainscow, E. K. & Brand, M. D. Calcium regulation of oxidative phosphorylation in rat skeletal muscle mitochondria. *Biochimica et Biophysica Acta (BBA) - Bioenergetics* **1457**, 57-70, doi:https://doi.org/10.1016/S0005-2728(00)00054-2 (2000).

219 Sharma, U., Atri, S., Sharma, M. C., Sarkar, C. & Jagannathan, N. R. Skeletal muscle metabolism in Duchenne muscular dystrophy (DMD): an in-vitro proton NMR spectroscopy study. *Magnetic resonance imaging* **21**, 145-153, doi:10.1016/s0730-725x(02)00646-x (2003).

220 Griffin, J. L. *et al.* Metabolic Profiling of Genetic Disorders: A Multitissue 1H Nuclear Magnetic Resonance Spectroscopic and Pattern Recognition Study into Dystrophic Tissue. *Analytical Biochemistry* **293**, 16-21, doi:https://doi.org/10.1006/abio.2001.5096 (2001).

221 Kuznetsov, A. V. *et al.* Impaired mitochondrial oxidative phosphorylation in skeletal muscle of the dystrophin-deficient mdx mouse. *Molecular and cellular biochemistry* **183**, 87-96, doi:10.1023/A:1006868130002 (1998).

222 Pant, M. *et al.* Metabolic dysfunction and altered mitochondrial dynamics in the utrophin-dystrophin deficient mouse model of duchenne muscular dystrophy. *PLoS One* **10**, e0123875, doi:10.1371/journal.pone.0123875 (2015).

223 Luan, P. *et al.* Urolithin A improves muscle function by inducing mitophagy in muscular dystrophy. *Science translational medicine* **13**, eabb0319, doi:10.1126/scitranslmed.abb0319 (2021).

224 Pauly, M. *et al.* AMPK activation stimulates autophagy and ameliorates muscular dystrophy in the mdx mouse diaphragm. *The American journal of pathology* **181**, 583-592 (2012).

225 Pellegrini, C. *et al.* Melanocytes--a novel tool to study mitochondrial dysfunction in Duchenne muscular dystrophy. *Journal of cellular physiology* **228**, 1323-1331, doi:10.1002/jcp.24290 (2013).

226 Moore, T. M. *et al.* Mitochondrial Dysfunction Is an Early Consequence of Partial or Complete Dystrophin Loss in mdx Mice. *Frontiers in physiology* **11**, 690-690, doi:10.3389/fphys.2020.00690 (2020).

227 Blau, H. M., Webster, C. & Pavlath, G. K. Defective myoblasts identified in Duchenne muscular dystrophy. *Proceedings of the National Academy of Sciences* **80**, 4856-4860, doi:10.1073/pnas.80.15.4856 (1983).

228 Wong, L. J. C., Wladyka, C. & Mardach-Verdon, R. A mitochondrial DNA mutation in a patient with an extensive family history of Duchenne muscular dystrophy. *Muscle & Nerve: Official Journal of the American Association of Electrodiagnostic Medicine* **30**, 118-122 (2004).

229 Chang, N. C., Chevalier, F. P. & Rudnicki, M. A. Satellite Cells in Muscular Dystrophy - Lost in Polarity. *Trends Mol Med* **22**, 479-496, doi:10.1016/j.molmed.2016.04.002 (2016).

230 Sacco, A. *et al.* Short Telomeres and Stem Cell Exhaustion Model Duchenne Muscular Dystrophy in mdx/mTR Mice. *Cell* **143**, 1059-1071, doi:https://doi.org/10.1016/j.cell.2010.11.039 (2010).

231 Fukada, S.-i. *et al.* Genetic Background Affects Properties of Satellite Cells and mdx Phenotypes. *The American Journal of Pathology* **176**, 2414-2424, doi:https://doi.org/10.2353/ajpath.2010.090887 (2010).

232 Smith, C. A. *et al.* aPKC-mediated phosphorylation regulates asymmetric membrane localization of the cell fate determinant Numb. *The EMBO journal* **26**, 468-480, doi:https://doi.org/10.1038/sj.emboj.7601495 (2007).

233 Knoblich, J. A. Asymmetric cell division: recent developments and their implications for tumour biology. *Nature Reviews Molecular Cell Biology* **11**, 849-860, doi:10.1038/nrm3010 (2010).

234 Wirtz-Peitz, F., Nishimura, T. & Knoblich, J. A. Linking Cell Cycle to Asymmetric Division: Aurora-A Phosphorylates the Par Complex to Regulate Numb

Localization. *Cell* **135**, 161-173, doi:https://doi.org/10.1016/j.cell.2008.07.049 (2008).

235 Benton, R. & Johnston, D. S. Drosophila PAR-1 and 14-3-3 Inhibit Bazooka/PAR-3 to Establish Complementary Cortical Domains in Polarized Cells. *Cell* **115**, 691-704, doi:https://doi.org/10.1016/S0092-8674(03)00938-3 (2003).

236 Suzuki, A. *et al.* aPKC Acts Upstream of PAR-1b in Both the Establishment and Maintenance of Mammalian Epithelial Polarity. *Current Biology* **14**, 1425-1435, doi:https://doi.org/10.1016/j.cub.2004.08.021 (2004).

237 Boldrin, L., Zammit, P. S. & Morgan, J. E. Satellite cells from dystrophic muscle retain regenerative capacity. *Stem Cell Res* **14**, 20-29, doi:10.1016/j.scr.2014.10.007 (2015).

238 Ribeiro, A. F. *et al.* Muscle satellite cells and impaired late stage regeneration in different murine models for muscular dystrophies. *Scientific Reports* **9**, 11842, doi:10.1038/s41598-019-48156-7 (2019).

239 McGreevy, J. W., Hakim, C. H., McIntosh, M. A. & Duan, D. Animal models of Duchenne muscular dystrophy: from basic mechanisms to gene therapy. *Dis Model Mech* **8**, 195-213, doi:10.1242/dmm.018424 (2015).

240 Bulfield, G., Siller, W. G., Wight, P. A. & Moore, K. J. X chromosome-linked muscular dystrophy (mdx) in the mouse. *Proceedings of the National Academy of Sciences of the United States of America* **81**, 1189-1192, doi:10.1073/pnas.81.4.1189 (1984).

241 Sicinski, P. *et al.* The molecular basis of muscular dystrophy in the mdx mouse: a point mutation. *Science (New York, N.Y.)* **244**, 1578-1580, doi:10.1126/science.2662404 (1989).

242 Cox, G. A., Phelps, S. F., Chapman, V. M. & Chamberlain, J. S. New mdx mutation disrupts expression of muscle and nonmuscle isoforms of dystrophin. *Nature genetics* **4**, 87-93 (1993).

243 Im, W. B. *et al.* Differential expression of dystrophin isoforms in strains of mdx mice with different mutations. *Human molecular genetics* **5**, 1149-1153 (1996).

244 Chapman, V. M., Miller, D. R., Armstrong, D. & Caskey, C. T. Recovery of induced mutations for X chromosome-linked muscular dystrophy in mice. *Proceedings of the National Academy of Sciences* **86**, 1292-1296 (1989).

245 Yucel, N., Chang, A. C., Day, J. W., Rosenthal, N. & Blau, H. M. Humanizing the mdx mouse model of DMD: the long and the short of it. *NPJ Regen Med* **3**, 4, doi:10.1038/s41536-018-0045-4 (2018).

246 Deconinck, A. E. *et al.* Utrophin-dystrophin-deficient mice as a model for Duchenne muscular dystrophy. *Cell* **90**, 717-727 (1997).

247 Grady, R. M. *et al.* Skeletal and cardiac myopathies in mice lacking utrophin and dystrophin: a model for Duchenne muscular dystrophy. *Cell* **90**, 729-738 (1997).

248 Guo, C. *et al.* Absence of α7 integrin in dystrophin-deficient mice causes a myopathy similar to Duchenne muscular dystrophy. *Human molecular genetics* **15**, 989-998 (2006).

249 Rooney, J. E. *et al.* Severe muscular dystrophy in mice that lack dystrophin and α7 integrin. *Journal of cell science* **119**, 2185-2195 (2006).

250 Mourkioti, F. *et al.* Role of telomere dysfunction in cardiac failure in Duchenne muscular dystrophy. *Nature cell biology* **15**, 895-904 (2013).

251 Young, C. S. & Pyle, A. D. Exon skipping therapy. *Cell* **167**, 1144 (2016).

252 Konieczny, P., Swiderski, K. & Chamberlain, J. S. Gene and cell-mediated therapies for muscular dystrophy. *Muscle Nerve* **47**, 649-663, doi:10.1002/mus.23738 (2013).

253 Min, Y. L. *et al.* CRISPR-Cas9 corrects Duchenne muscular dystrophy exon 44 deletion mutations in mice and human cells. *Sci Adv* **5**, eaav4324, doi:10.1126/sciadv.aav4324 (2019).

254 Tabebordbar, M. *et al.* In vivo gene editing in dystrophic mouse muscle and muscle stem cells. *Science (New York, N.Y.)* **351**, 407-411 (2016).

255 Nelson, C. E. *et al.* In vivo genome editing improves muscle function in a mouse model of Duchenne muscular dystrophy. *Science (New York, N.Y.)* **351**, 403-407 (2016).

256 Kimura, E., Li, S., Gregorevic, P., Fall, B. M. & Chamberlain, J. S. Dystrophin delivery to muscles of mdx mice using lentiviral vectors leads to myogenic progenitor targeting and stable gene expression. *Molecular Therapy* **18**, 206-213 (2010).

257 Quarta, M. *et al.* An artificial niche preserves the quiescence of muscle stem cells and enhances their therapeutic efficacy. *Nature biotechnology* **34**, 752-759, doi:10.1038/nbt.3576 (2016).

258 Sacco, A., Doyonnas, R., Kraft, P., Vitorovic, S. & Blau, H. M. Self-renewal and expansion of single transplanted muscle stem cells. *Nature* **456**, 502-506, doi:10.1038/nature07384 (2008).

259 Günther, S. *et al.* Myf5-positive satellite cells contribute to Pax7-dependent long-term maintenance of adult muscle stem cells. *Cell stem cell* **13**, 590-601, doi:10.1016/j.stem.2013.07.016 (2013).

260 Bouchentouf, M. *et al.* Vascular endothelial growth factor reduced hypoxia-induced death of human myoblasts and improved their engraftment in mouse muscles. *Gene therapy* **15**, 404-414, doi:10.1038/sj.gt.3303059 (2008).

261 Gilbert, P. M. *et al.* Substrate elasticity regulates skeletal muscle stem cell self-renewal in culture. *Science (New York, N.Y.)* **329**, 1078-1081, doi:10.1126/science.1191035 (2010).

262 Han, W. M., Mohiuddin, M., Anderson, S. E., García, A. J. & Jang, Y. C. Co-delivery of Wnt7a and muscle stem cells using synthetic bioadhesive hydrogel enhances murine muscle regeneration and cell migration during engraftment. *Acta Biomaterialia* **94**, 243-252, doi:https://doi.org/10.1016/j.actbio.2019.06.025 (2019).

263 Moresi, V., Marroncelli, N. & Adamo, S. New insights into the epigenetic control of satellite cells. *World J Stem Cells* **7**, 945-955, doi:10.4252/wjsc.v7.i6.945 (2015).

264 Leroux, L. *et al.* Hypoxia Preconditioned Mesenchymal Stem Cells Improve Vascular and Skeletal Muscle Fiber Regeneration After Ischemia Through a Wnt4-dependent Pathway. *Molecular Therapy* **18**, 1545-1552, doi:10.1038/mt.2010.108 (2010).

265 Sart, S., Ma, T. & Li, Y. Preconditioning stem cells for in vivo delivery. *Biores Open Access* **3**, 137-149, doi:10.1089/biores.2014.0012 (2014).

266 Yu, S. P., Wei, Z. & Wei, L. Preconditioning strategy in stem cell transplantation therapy. *Transl Stroke Res* **4**, 76-88, doi:10.1007/s12975-012-0251-0 (2013).

267 Baar, K. *et al.* Adaptations of skeletal muscle to exercise: rapid increase in the transcriptional coactivator PGC-1. *The FASEB journal* **16**, 1879-1886 (2002).

268 Rodgers, J. T. *et al.* mTORC1 controls the adaptive transition of quiescent stem cells from G0 to GAlert. *Nature* **510**, 393-396, doi:10.1038/nature13255 (2014).

269 Dirnagl, U. & Meisel, A. Endogenous neuroprotection: mitochondria as gateways to cerebral preconditioning? *Neuropharmacology* **55**, 334-344, doi:10.1016/j.neuropharm.2008.02.017 (2008).

270 Ravati, A., Ahlemeyer, B., Becker, A., Klumpp, S. & Krieglstein, J. Preconditioning-induced neuroprotection is mediated by reactive oxygen species and activation of the transcription factor nuclear factor-kappaB. *Journal of neurochemistry* **78**, 909-919, doi:10.1046/j.1471-4159.2001.00463.x (2001).

271 Aly, A., Peterson, K. M., Lerman, A., Lerman, L. O. & Rodriguez-Porcel, M. Role of oxidative stress in hypoxia pre-conditioning of cells transplanted to the myocardium: a molecular imaging study. *The Journal of cardiovascular surgery* **52**, 579 (2011).

272 Peterson, K. M., Aly, A., Lerman, A., Lerman, L. O. & Rodriguez-Porcel, M. Improved survival of mesenchymal stromal cell after hypoxia preconditioning: role of oxidative stress. *Life sciences* **88**, 65-73, doi:10.1016/j.lfs.2010.10.023 (2011).

273 Lerner, R. G. *et al.* Targeting a Plk1-Controlled Polarity Checkpoint in Therapy-Resistant Glioblastoma-Propagating Cells. *Cancer research* **75**, 5355-5366, doi:10.1158/0008-5472.can-14-3689 (2015).

274 Xu, C. *et al.* A Zebrafish Embryo Culture System Defines Factors that Promote Vertebrate Myogenesis across Species. *Cell* **155**, 909-921, doi:10.1016/j.cell.2013.10.023 (2013).

275 Darabi, R. *et al.* Human ES- and iPS-derived myogenic progenitors restore DYSTROPHIN and improve contractility upon transplantation in dystrophic mice. *Cell Stem Cell* **10**, 610-619, doi:10.1016/j.stem.2012.02.015 (2012).

276 Darabi, R. *et al.* Assessment of the myogenic stem cell compartment following transplantation of Pax3/Pax7-induced embryonic stem cell-derived progenitors. *Stem cells (Dayton, Ohio)* **29**, 777-790 (2011).

277 Clark, M. A. & Shay, J. W. Mitochondrial transformation of mammalian cells. *Nature* **295**, 605-607, doi:10.1038/295605a0 (1982).

278 Roushandeh, A. M., Kuwahara, Y. & Roudkenar, M. H. Mitochondrial transplantation as a potential and novel master key for treatment of various incurable diseases. *Cytotechnology* **71**, 647-663, doi:10.1007/s10616-019-00302-9 (2019).

279 Kitani, T., Kami, D., Matoba, S. & Gojo, S. Internalization of isolated functional mitochondria: involvement of macropinocytosis. *Journal of cellular and molecular medicine* **18**, 1694-1703, doi:10.1111/jcmm.12316 (2014).

280 Masuzawa, A. *et al.* Transplantation of autologously derived mitochondria protects the heart from ischemia-reperfusion injury. *American journal of physiology. Heart and circulatory physiology* **304**, H966-982, doi:10.1152/ajpheart.00883.2012 (2013).

281 Bertero, E., Maack, C. & O'Rourke, B. Mitochondrial transplantation in humans: "magical" cure or cause for concern? *The Journal of Clinical Investigation* **128**, 5191-5194, doi:10.1172/JCI124944 (2018).

282 Berridge, M. V. *et al.* Horizontal transfer of mitochondria between mammalian cells: beyond co-culture approaches. *Current Opinion in Genetics & Development* **38**, 75-82, doi:https://doi.org/10.1016/j.gde.2016.04.003 (2016).

283 Acquistapace, A. *et al.* Human mesenchymal stem cells reprogram adult cardiomyocytes toward a progenitor-like state through partial cell fusion and mitochondria transfer. *Stem cells (Dayton, Ohio)* **29**, 812-824 (2011).

284 Önfelt, B. *et al.* Structurally distinct membrane nanotubes between human macrophages support long-distance vesicular traffic or surfing of bacteria. *The Journal of Immunology* **177**, 8476-8483 (2006).

285 Astanina, K., Koch, M., Jüngst, C., Zumbusch, A. & Kiemer, A. K. Lipid droplets as a novel cargo of tunnelling nanotubes in endothelial cells. *Scientific reports* **5**, 11453 (2015).

286 Koyanagi, M., Brandes, R. P., Haendeler, J., Zeiher, A. M. & Dimmeler, S. Cell-to-cell connection of endothelial progenitor cells with cardiac myocytes by nanotubes: a novel mechanism for cell fate changes? *Circulation research* **96**, 1039-1041 (2005).

287 Tavi, P. *et al.* Myogenic skeletal muscle satellite cells communicate by tunnelling nanotubes. *Journal of cellular physiology* **223**, 376-383 (2010).

288 Swaminathan, A., Vemulapalli, S., Patel, M. R. & Jones, W. S. Lower extremity amputation in peripheral artery disease: improving patient outcomes. *Vasc Health Risk Manag* **10**, 417-424, doi:10.2147/VHRM.S50588 (2014).

289 Olea, F. D. *et al.* Vascular endothelial growth factor overexpression does not enhance adipose stromal cell-induced protection on muscle damage in critical limb ischemia. *Arteriosclerosis, thrombosis, and vascular biology* **35**, 184-188, doi:10.1161/atvbaha.114.304348 (2015).

290 Cooke, J. P. & Losordo, D. W. Modulating the Vascular Response to Limb Ischemia Angiogenic and Cell Therapies. *Circulation research* **116**, 1561-1578, doi:10.1161/CIRCRESAHA.115.303565 (2015).

291 Kilarski, W. W., Samolov, B., Petersson, L., Kvanta, A. & Gerwins, P. Biomechanical regulation of blood vessel growth during tissue vascularization. *Nature Medicine* **15**, 657, doi:10.1038/nm.1985

https://www.nature.com/articles/nm.1985#supplementary-information (2009).

292 Mandal, S., Lindgren, A. G., Srivastava, A. S., Clark, A. T. & Banerjee, U. Mitochondrial function controls proliferation and early differentiation potential of embryonic stem cells. *Stem cells (Dayton, Ohio)* **29**, 486-495, doi:10.1002/stem.590 (2011).

293 Richter, C. *et al.* Oxidants in mitochondria: from physiology to diseases. *Biochimica et Biophysica Acta (BBA) - Molecular Basis of Disease* **1271**, 67-74, doi:https://doi.org/10.1016/0925-4439(95)00012-S (1995).

294 Latroche, C. *et al.* Skeletal Muscle Microvasculature: A Highly Dynamic Lifeline. *Physiology* **30**, 417-427, doi:10.1152/physiol.00026.2015 (2015).

295 Sciorati, C., Rigamonti, E., Manfredi, A. A. & Rovere-Querini, P. Cell death, clearance and immunity in the skeletal muscle. *Cell Death and Differentiation* **23**, 927-937, doi:10.1038/cdd.2015.171 (2016).

296 Yang, X. *et al.* Patterning of Muscle Acetylcholine Receptor Gene Expression in the Absence of Motor Innervation. *Neuron* **30**, 399-410, doi:https://doi.org/10.1016/S0896-6273(01)00287-2 (2001).

297 Rowan, S. L. *et al.* Denervation Causes Fiber Atrophy and Myosin Heavy Chain Co-Expression in Senescent Skeletal Muscle. *PLOS ONE* **7**, e29082, doi:10.1371/journal.pone.0029082 (2012).

298 Holloszy, J. O. & Larsson, L. Motor Units: Remodeling in Aged Animals. *The Journals of Gerontology: Series A* **50A**, 91-95, doi:10.1093/gerona/50A.Special_Issue.91 (1995).

299 Eichmann, A., Makinen, T. & Alitalo, K. Neural guidance molecules regulate vascular remodeling and vessel navigation. *Genes & development* **19**, 1013-1021, doi:10.1101/gad.1305405 (2005).

300 Cattin, A.-L. *et al.* Macrophage-Induced Blood Vessels Guide Schwann Cell-Mediated Regeneration of Peripheral Nerves. *Cell* **162**, 1127-1139, doi:10.1016/j.cell.2015.07.021 (2015).

301 Schultz, E. Changes in the satellite cells of growing muscle following denervation. *The Anatomical record* **190**, 299-311, doi:10.1002/ar.1091900212 (1978).

302 Alnaes, E. & Rahamimoff, R. On the role of mitochondria in transmitter release from motor nerve terminals. *The Journal of physiology* **248**, 285-306 (1975).

303 Verstreken, P. *et al.* Synaptic mitochondria are critical for mobilization of reserve pool vesicles at Drosophila neuromuscular junctions. *Neuron* **47**, 365-378, doi:10.1016/j.neuron.2005.06.018 (2005).

304 Feng, G. *et al.* Imaging neuronal subsets in transgenic mice expressing multiple spectral variants of GFP. *Neuron* **28**, 41-51 (2000).

305 Pham, A. H., McCaffery, J. M. & Chan, D. C. Mouse lines with photo-activatable mitochondria to study mitochondrial dynamics. *Genesis* **50**, 833-843, doi:10.1002/dvg.22050 (2012).

306 Sun, N. *et al.* Measuring In Vivo Mitophagy. *Molecular Cell* **60**, 685-696, doi:10.1016/j.molcel.2015.10.009 (2015).

307 Sun, N. *et al.* A fluorescence-based imaging method to measure in vitro and in vivo mitophagy using mt-Keima. *Nature protocols* **12**, 1576-1587, doi:10.1038/nprot.2017.060 (2017).

308 Chakkalakal, J. V., Kuang, S., Buffelli, M., Lichtman, J. W. & Sanes, J. R. Mouse transgenic lines that selectively label type I, type IIa, and types IIX+B skeletal muscle fibers. *genesis* **50**, 50-58, doi:doi:10.1002/dvg.20794 (2012).

309 Couffinhal, T. *et al.* Mouse model of angiogenesis. *The American Journal of Pathology* **152**, 1667-1679 (1998).

310 Anderson, S. E. *et al.* Determination of a Critical Size Threshold for Volumetric Muscle Loss in the Mouse Quadriceps. *Tissue Engineering Part C: Methods* **25**, 59-70, doi:10.1089/ten.tec.2018.0324 (2019).

311 Karsch-Mizrachi, I., Travis, M., Blau, H. & Leinwand, L. A. Expression and DNA sequence analysis of a human embryonic skeletal muscle myosin heavy chain gene. *Nucleic acids research* **17**, 6167-6179, doi:10.1093/nar/17.15.6167 (1989).

312 Mahdy, M. A. A., Lei, H. Y., Wakamatsu, J.-I., Hosaka, Y. Z. & Nishimura, T. Comparative study of muscle regeneration following cardiotoxin and glycerol injury. *Annals of Anatomy - Anatomischer Anzeiger* **202**, 18-27, doi:https://doi.org/10.1016/j.aanat.2015.07.002 (2015).

313 Hardy, D. *et al.* Comparative Study of Injury Models for Studying Muscle Regeneration in Mice. *PLoS One* **11**, e0147198, doi:10.1371/journal.pone.0147198 (2016).

314 Cadot, B. *et al.* Nuclear movement during myotube formation is microtubule and dynein dependent and is regulated by Cdc42, Par6 and Par3. *EMBO reports* **13**, 741-749, doi:10.1038/embor.2012.89 (2012).

315 Rochard, P. *et al.* Mitochondrial activity is involved in the regulation of myoblast differentiation through myogenin expression and activity of myogenic factors. *The Journal of biological chemistry* **275**, 2733-2744 (2000).

316 Moyes, C. D., Mathieu-Costello, O. A., Tsuchiya, N., Filburn, C. & Hansford, R. G. Mitochondrial biogenesis during cellular differentiation. *The American journal of physiology* **272**, C1345-1351, doi:10.1152/ajpcell.1997.272.4.C1345 (1997).

317 Duguez, S., Feasson, L., Denis, C. & Freyssenet, D. Mitochondrial biogenesis during skeletal muscle regeneration. *American journal of physiology. Endocrinology and metabolism* **282**, E802-809, doi:10.1152/ajpendo.00343.2001 (2002).

318 Wu, H. *et al.* Regulation of mitochondrial biogenesis in skeletal muscle by CaMK. *Science (New York, N.Y.)* **296**, 349-352, doi:10.1126/science.1071163 (2002).

319 Quiros, P. M., Goyal, A., Jha, P. & Auwerx, J. Analysis of mtDNA/nDNA Ratio in Mice. *Current protocols in mouse biology* **7**, 47-54, doi:10.1002/cpmo.21 (2017).

320 Rooney, J. P. *et al.* PCR based determination of mitochondrial DNA copy number in multiple species. *Methods in molecular biology (Clifton, N.J.)* **1241**, 23-38, doi:10.1007/978-1-4939-1875-1_3 (2015).

321 Taanman, J.-W. The mitochondrial genome: structure, transcription, translation and replication. *Biochimica et Biophysica Acta (BBA) - Bioenergetics* **1410**, 103-123, doi:https://doi.org/10.1016/S0005-2728(98)00161-3 (1999).

322 Bayraktar, E. C. *et al.* MITO-Tag Mice enable rapid isolation and multimodal profiling of mitochondria from specific cell types in vivo. *Proceedings of the National Academy of Sciences* **116**, 303, doi:10.1073/pnas.1816656115 (2019).

323 Meeusen, S. *et al.* Mitochondrial inner-membrane fusion and crista maintenance requires the dynamin-related GTPase Mgm1. *Cell* **127**, 383-395, doi:10.1016/j.cell.2006.09.021 (2006).

324 Song, Z., Ghochani, M., McCaffery, J. M., Frey, T. G. & Chan, D. C. Mitofusins and OPA1 mediate sequential steps in mitochondrial membrane fusion. *Molecular biology of the cell* **20**, 3525-3532, doi:10.1091/mbc.E09-03-0252 (2009).

325 Frezza, C. *et al.* OPA1 controls apoptotic cristae remodeling independently from mitochondrial fusion. *Cell* **126**, 177-189, doi:10.1016/j.cell.2006.06.025 (2006).

326 Ishihara, N., Fujita, Y., Oka, T. & Mihara, K. Regulation of mitochondrial morphology through proteolytic cleavage of OPA1. *The EMBO journal* **25**, 2966-2977, doi:10.1038/sj.emboj.7601184 (2006).

327 DeVay, R. M. *et al.* Coassembly of Mgm1 isoforms requires cardiolipin and mediates mitochondrial inner membrane fusion. *The Journal of cell biology* **186**, 793-803, doi:10.1083/jcb.200906098 (2009).

328 Song, Z., Chen, H., Fiket, M., Alexander, C. & Chan, D. C. OPA1 processing controls mitochondrial fusion and is regulated by mRNA splicing, membrane potential, and Yme1L. *The Journal of cell biology* **178**, 749-755, doi:10.1083/jcb.200704110 (2007).

329 Kathiria, A. S. *et al.* Prohibitin 1 Modulates Mitochondrial Stress-Related Autophagy in Human Colonic Epithelial Cells. *PLOS ONE* **7**, e31231, doi:10.1371/journal.pone.0031231 (2012).

330 Norton, M. *et al.* ROMO1 is an essential redox-dependent regulator of mitochondrial dynamics. *Science signaling* **7**, ra10, doi:10.1126/scisignal.2004374 (2014).

331 Yamada, T. *et al.* Interaction between myoglobin and mitochondria in rat skeletal muscle. *Journal of applied physiology (Bethesda, Md. : 1985)* **114**, 490-497, doi:10.1152/japplphysiol.00789.2012 (2013).

332 Miranda, S., Foncea, R., Guerrero, J. & Leighton, F. Oxidative Stress and Upregulation of Mitochondrial Biogenesis Genes in Mitochondrial DNA-Depleted HeLa Cells. *Biochemical and Biophysical Research Communications* **258**, 44-49, doi:https://doi.org/10.1006/bbrc.1999.0580 (1999).

333 Pipinos, I. I. *et al.* Abnormal mitochondrial respiration in skeletal muscle in patients with peripheral arterial disease. *Journal of Vascular Surgery* **38**, 827-832, doi:https://doi.org/10.1016/S0741-5214(03)00602-5 (2003).

334 Berendse, M., Grounds, M. D. & Lloyd, C. M. Myoblast structure affects subsequent skeletal myotube morphology and sarcomere assembly. *Experimental cell research* **291**, 435-450 (2003).

335 LeBleu, V. S. *et al.* PGC-1alpha mediates mitochondrial biogenesis and oxidative phosphorylation in cancer cells to promote metastasis. *Nat Cell Biol* **16**, 992-1003, 1001-1015, doi:10.1038/ncb3039 (2014).

336 Canto, C. *et al.* AMPK regulates energy expenditure by modulating NAD+ metabolism and SIRT1 activity. *Nature* **458**, 1056-1060, doi:10.1038/nature07813 (2009).

337 Marinho, H. S., Real, C., Cyrne, L., Soares, H. & Antunes, F. Hydrogen peroxide sensing, signaling and regulation of transcription factors. *Redox Biology* **2**, 535-562, doi:https://doi.org/10.1016/j.redox.2014.02.006 (2014).

338 Muller, F. L., Liu, Y. & Van Remmen, H. Complex III releases superoxide to both sides of the inner mitochondrial membrane. *Journal of Biological Chemistry* (2004).

339 Ryan, T. E. *et al.* Mitochondrial Regulation of the Muscle Microenvironment in Critical Limb Ischemia. *Frontiers in Physiology* **6**, doi:10.3389/fphys.2015.00336 (2015).

340 Hoffman, E. P., Brown, R. H., Jr. & Kunkel, L. M. Dystrophin: the protein product of the Duchenne muscular dystrophy locus. *Cell* **51**, 919-928, doi:10.1016/0092-8674(87)90579-4 (1987).

341 Hamer, P., McGeachie, J., Davies, M. & Grounds, M. Evans Blue Dye as an in vivo marker of myofibre damage: optimising parameters for detecting initial myofibre membrane permeability. *Journal of anatomy* **200**, 69-79 (2002).

342 Sun, C., Serra, C., Lee, G. & Wagner, K. R. Stem cell-based therapies for Duchenne muscular dystrophy. *Exp Neurol* **323**, 113086, doi:10.1016/j.expneurol.2019.113086 (2020).

343 Hughes, M. C. *et al.* Early myopathy in Duchenne muscular dystrophy is associated with elevated mitochondrial H2O2 emission during impaired oxidative phosphorylation. *Journal of Cachexia, Sarcopenia and Muscle* **10**, 643-661, doi:10.1002/jcsm.12405 (2019).

344 Schuh, R. A., Jackson, K. C., Khairallah, R. J., Ward, C. W. & Spangenburg, E. E. Measuring mitochondrial respiration in intact single muscle fibers. *American journal of physiology. Regulatory, integrative and comparative physiology* **302**, R712-719, doi:10.1152/ajpregu.00229.2011 (2012).

345 Timpani, C. A., Hayes, A. & Rybalka, E. Revisiting the dystrophin-ATP connection: How half a century of research still implicates mitochondrial dysfunction in Duchenne Muscular Dystrophy aetiology. *Med Hypotheses* **85**, 1021-1033, doi:10.1016/j.mehy.2015.08.015 (2015).

346 Ryu, D. *et al.* NAD+ repletion improves muscle function in muscular dystrophy and counters global PARylation. *Science translational medicine* **8**, 361ra139, doi:10.1126/scitranslmed.aaf5504 (2016).

347 Franco, A. & Lansman, J. B. Calcium entry through stretch-inactivated ion channels in mdx myotubes. *Nature* **344**, 670-673 (1990).

348 Vila, M. C. *et al.* Mitochondria mediate cell membrane repair and contribute to Duchenne muscular dystrophy. *Cell Death & Differentiation* **24**, 330-342, doi:10.1038/cdd.2016.127 (2017).

349 Laker, R. C. *et al.* A Novel MitoTimer Reporter Gene for Mitochondrial Content, Structure, Stress, and Damage in Vivo*. *Journal of Biological Chemistry* **289**, 12005-12015, doi:https://doi.org/10.1074/jbc.M113.530527 (2014).

350 Ryan, M. T. & Hoogenraad, N. J. Mitochondrial-nuclear communications. *Annual review of biochemistry* **76**, 701-722, doi:10.1146/annurev.biochem.76.052305.091720 (2007).

351 Murach, K. A., Englund, D. A., Dupont-Versteegden, E. E., McCarthy, J. J. & Peterson, C. A. Myonuclear Domain Flexibility Challenges Rigid Assumptions on Satellite Cell Contribution to Skeletal Muscle Fiber Hypertrophy. *Front Physiol* **9**, 635, doi:10.3389/fphys.2018.00635 (2018).

352 Glancy, B. *et al.* Mitochondrial reticulum for cellular energy distribution in muscle. *Nature* **523**, 617-620, doi:10.1038/nature14614 (2015).

353 Cerletti, M. *et al.* Highly efficient, functional engraftment of skeletal muscle stem cells in dystrophic muscles. *Cell* **134**, 37-47, doi:10.1016/j.cell.2008.05.049 (2008).

354 Han, W. M. *et al.* Synthetic matrix enhances transplanted satellite cell engraftment in dystrophic and aged skeletal muscle with comorbid trauma. *Sci Adv* **4**, eaar4008, doi:10.1126/sciadv.aar4008 (2018).

355 Yoshioka, K. *et al.* A Modified Pre-plating Method for High-Yield and High-Purity Muscle Stem Cell Isolation From Human/Mouse Skeletal Muscle Tissues. *Frontiers in Cell and Developmental Biology* **8**, doi:10.3389/fcell.2020.00793 (2020).

356 Berru, F. N. *et al.* Chronic kidney disease exacerbates ischemic limb myopathy in mice via altered mitochondrial energetics. *Scientific Reports* **9**, 15547, doi:10.1038/s41598-019-52107-7 (2019).

357 Aguilar, C. A. *et al.* Transcriptional and Chromatin Dynamics of Muscle Regeneration after Severe Trauma. *Stem Cell Reports* **7**, 983-997, doi:10.1016/j.stemcr.2016.09.009 (2016).

358 Bolger, A. M., Lohse, M. & Usadel, B. Trimmomatic: a flexible trimmer for Illumina sequence data. *Bioinformatics (Oxford, England)* **30**, 2114-2120, doi:10.1093/bioinformatics/btu170 (2014).

359 Li, B. & Dewey, C. N. RSEM: accurate transcript quantification from RNA-Seq data with or without a reference genome. *BMC Bioinformatics* **12**, 323, doi:10.1186/1471-2105-12-323 (2011).

360 Love, M. I., Huber, W. & Anders, S. Moderated estimation of fold change and dispersion for RNA-seq data with DESeq2. *Genome Biology* **15**, 550, doi:10.1186/s13059-014-0550-8 (2014).

361 Subramanian, A. *et al.* Gene set enrichment analysis: A knowledge-based approach for interpreting genome-wide expression profiles. *Proceedings of the National Academy of Sciences* **102**, 15545-15550, doi:10.1073/pnas.0506580102 (2005).

362 Kholmukhamedov, A., Schwartz, J. M. & Lemasters, J. J. Isolated mitochondria infusion mitigates ischemia-reperfusion injury of the liver in rats: mitotracker probes and mitochondrial membrane potential. *Shock* **39**, 543-543, doi:10.1097/SHK.0b013e318292300d (2013).

363 Rozo, M., Li, L. & Fan, C. M. Targeting beta1-integrin signaling enhances regeneration in aged and dystrophic muscle in mice. *Nature medicine* **22**, 889-896, doi:10.1038/nm.4116 (2016).

364 Nagasawa, T. The chemokine CXCL12 and regulation of HSC and B lymphocyte development in the bone marrow niche. *Advances in experimental medicine and biology* **602**, 69-75, doi:10.1007/978-0-387-72009-8_9 (2007).

365 Gnaiger, E. Capacity of oxidative phosphorylation in human skeletal muscle: new perspectives of mitochondrial physiology. *Int J Biochem Cell Biol* **41**, 1837-1845, doi:10.1016/j.biocel.2009.03.013 (2009).

366 Lexell, J. & Downham, D. Y. The occurrence of fibre-type grouping in healthy human muscle: a quantitative study of cross-sections of whole vastus lateralis from men between 15 and 83 years. *Acta neuropathologica* **81**, 377-381, doi:10.1007/bf00293457 (1991).

367 Palmieri, F. The mitochondrial transporter family SLC25: identification, properties and physiopathology. *Molecular aspects of medicine* **34**, 465-484, doi:10.1016/j.mam.2012.05.005 (2013).

368 Shefer, G., Rauner, G., Yablonka-Reuveni, Z. & Benayahu, D. Reduced satellite cell numbers and myogenic capacity in aging can be alleviated by endurance exercise. *PLoS One* **5**, e13307, doi:10.1371/journal.pone.0013307 (2010).

369 Muller, F. L. *et al.* Absence of CuZn superoxide dismutase leads to elevated oxidative stress and acceleration of age-dependent skeletal muscle atrophy. *Free Radic Biol Med* **40**, 1993-2004, doi:10.1016/j.freeradbiomed.2006.01.036 (2006).

370 Pouzet, B. *et al.* Factors affecting functional outcome after autologous skeletal myoblast transplantation. *The Annals of thoracic surgery* **71**, 844-851 (2001).

371 Torralba, D., Baixauli, F. & Sánchez-Madrid, F. Mitochondria Know No Boundaries: Mechanisms and Functions of Intercellular Mitochondrial Transfer. *Frontiers in cell and developmental biology* **4**, 107-107, doi:10.3389/fcell.2016.00107 (2016).

372 Cuthbertson, D. *et al.* Anabolic signaling deficits underlie amino acid resistance of wasting, aging muscle. *FASEB journal : official publication of the Federation of American Societies for Experimental Biology* **19**, 422-424, doi:10.1096/fj.04-2640fje (2005).

373 Wagner, P. D. The critical role of VEGF in skeletal muscle angiogenesis and blood flow. *Biochemical Society Transactions* **39**, 1556-1559, doi:10.1042/bst20110646 (2011).

374 Wagatsuma, A. Effect of aging on expression of angiogenesis-related factors in mouse skeletal muscle. *Experimental gerontology* **41**, 49-54, doi:10.1016/j.exger.2005.10.003 (2006).

375 Rivard, A. *et al.* Age-dependent impairment of angiogenesis. *Circulation* **99**, 111-120, doi:10.1161/01.cir.99.1.111 (1999).

376 Jastroch, M., Divakaruni, A. S., Mookerjee, S., Treberg, J. R. & Brand, M. D. Mitochondrial proton and electron leaks. *Essays Biochem* **47**, 53-67, doi:10.1042/bse0470053 (2010).

377 Fukai, T. & Ushio-Fukai, M. Superoxide dismutases: role in redox signaling, vascular function, and diseases. *Antioxid Redox Signal* **15**, 1583-1606, doi:10.1089/ars.2011.3999 (2011).

378 Snow, M. H. The effects of aging on satellite cells in skeletal muscles of mice and rats. *Cell and tissue research* **185**, 399-408, doi:10.1007/BF00220299 (1977).

379 Benchaouir, R. *et al.* Restoration of human dystrophin following transplantation of exon-skipping-engineered DMD patient stem cells into dystrophic mice. *Cell stem cell* **1**, 646-657 (2007).

380 Gussoni, E. *et al.* Dystrophin expression in the mdx mouse restored by stem cell transplantation. *Nature* **401**, 390-394, doi:10.1038/43919 (1999).

381 Han, W. M. *et al.* Synthetic matrix enhances transplanted satellite cell engraftment in dystrophic and aged skeletal muscle with comorbid trauma. *Science Advances* **4**, eaar4008, doi:10.1126/sciadv.aar4008 (2018).

382 Zuo, Y. *et al.* Fluorescent Proteins Expressed in Mouse Transgenic Lines Mark Subsets of Glia, Neurons, Macrophages, and Dendritic Cells for Vital Examination. *The Journal of Neuroscience* **24**, 10999-11009, doi:10.1523/jneurosci.3934-04.2004 (2004).

383 Vu, N. *et al.* Adipose derived stem cell transplantation is better than bone marrow mesenchymal stem cell transplantation in treating hindlimb ischemia in mice. *Biomedical Research and Therapy* **3**, doi:10.7603/s40730-016-0046-0 (2016).

384 Arany, Z. *et al.* HIF-independent regulation of VEGF and angiogenesis by the transcriptional coactivator PGC-1α. *Nature* **451**, 1008-1012, doi:10.1038/nature06613 (2008).

385 Chen, Y. *et al.* Aging Reprograms the Hematopoietic-Vascular Niche to Impede Regeneration and Promote Fibrosis. *Cell metabolism*, doi:https://doi.org/10.1016/j.cmet.2020.11.019 (2020).

386 Bota, D. A. & Davies, K. J. A. Lon protease preferentially degrades oxidized mitochondrial aconitase by an ATP-stimulated mechanism. *Nature Cell Biology* **4**, 674-680, doi:10.1038/ncb836 (2002).

387 Winningham-Major, F., Staecker, J. L., Barger, S. W., Coats, S. & Van Eldik, L. J. Neurite extension and neuronal survival activities of recombinant S100 beta proteins that differ in the content and position of cysteine residues. *The Journal of cell biology* **109**, 3063-3071, doi:10.1083/jcb.109.6.3063 (1989).

388 Riuzzi, F. *et al.* Cellular and molecular mechanisms of sarcopenia: the S100B perspective. *J Cachexia Sarcopenia Muscle* **9**, 1255-1268, doi:10.1002/jcsm.12363 (2018).

389 Khacho, M. *et al.* Mitochondrial Dynamics Impacts Stem Cell Identity and Fate Decisions by Regulating a Nuclear Transcriptional Program. *Cell Stem Cell* **19**, 232-247, doi:10.1016/j.stem.2016.04.015 (2016).

390 Zaccagnini, G. *et al.* p66(ShcA) and oxidative stress modulate myogenic differentiation and skeletal muscle regeneration after hind limb ischemia. *The Journal of biological chemistry* **282**, 31453-31459, doi:10.1074/jbc.M702511200 (2007).

391 Heil, M. *et al.* Blood monocyte concentration is critical for enhancement of collateral artery growth. *American journal of physiology. Heart and circulatory physiology* **283**, H2411-2419, doi:10.1152/ajpheart.01098.2001 (2002).

392 Bogacka, I., Ukropcova, B., McNeil, M., Gimble, J. M. & Smith, S. R. Structural and Functional Consequences of Mitochondrial Biogenesis in Human Adipocytes in Vitro. *The Journal of Clinical Endocrinology & Metabolism* **90**, 6650-6656, doi:10.1210/jc.2005-1024 (2005).

393 Jain, I. H. *et al.* Hypoxia as a therapy for mitochondrial disease. *Science (New York, N.Y.)* **352**, 54-61, doi:10.1126/science.aad9642 (2016).

394 Malam, Z. & Cohn, R. D. Stem cells on alert: priming quiescent stem cells after remote injury. *Cell Stem Cell* **15**, 7-8, doi:10.1016/j.stem.2014.06.012 (2014).

395 McCully, J. D. *et al.* Injection of isolated mitochondria during early reperfusion for cardioprotection. *American journal of physiology. Heart and circulatory physiology* **296**, H94-h105, doi:10.1152/ajpheart.00567.2008 (2009).

396 Katayama, T. *et al.* A mitochondrial delivery system using liposome-based nanocarriers that target myoblast cells. *Mitochondrion* **49**, 66-72, doi:https://doi.org/10.1016/j.mito.2019.07.005 (2019).

397 Phelps, E. A., Landázuri, N., Thulé, P. M., Taylor, W. R. & García, A. J. Bioartificial matrices for therapeutic vascularization. *Proceedings of the National Academy of Sciences* **107**, 3323-3328, doi:10.1073/pnas.0905447107 (2010).

398 Tellier, L. E. *et al.* Localized SDF-1α Delivery Increases Pro-Healing Bone Marrow-Derived Cells in the Supraspinatus Muscle Following Severe Rotator Cuff Injury. *Regenerative Engineering and Translational Medicine* **4**, 92-103, doi:10.1007/s40883-018-0052-4 (2018).

399 Krieger, J. R. *et al.* Spatially localized recruitment of anti-inflammatory monocytes by SDF-1α-releasing hydrogels enhances microvascular network remodeling. *Biomaterials* **77**, 280-290, doi:10.1016/j.biomaterials.2015.10.045 (2016).

400 Das, A., Segar, C. E., Hughley, B. B., Bowers, D. T. & Botchwey, E. A. The promotion of mandibular defect healing by the targeting of S1P receptors and the recruitment of alternatively activated macrophages. *Biomaterials* **34**, 9853-9862, doi:10.1016/j.biomaterials.2013.08.015 (2013).

401 Supinski, G. S., Wang, L., Schroder, E. A. & Callahan, L. A. P. MitoTEMPOL, a mitochondrial targeted antioxidant, prevents sepsis-induced diaphragm dysfunction. *American journal of physiology. Lung cellular and molecular physiology* **319**, L228-l238, doi:10.1152/ajplung.00473.2019 (2020).

402 Mattson, M. P. Hormesis defined. *Ageing Res Rev* **7**, 1-7, doi:10.1016/j.arr.2007.08.007 (2008).